Bi and Mn nanostructures on the Si(001) surface

Christopher James Kirkham, UCL, Physics

In loving memory of Raymond Kirkham

I, Christopher James Kirkham confirm that the work presented in this thesis is my own. Where information has been derived from other sources, I confirm that this has been indicated in the thesis.

Acknowledgments

This work would not have been possible without the contributions of many people. First of all, my primary supervisor David Bowler who has provided guidance, ideas and support throughout my PhD. Next is Veronika Brázdová, who helped me learn how to use VASP in the early stages of my research. Andrew Fisher, my second supervisor, must also be thanked for general support, and help making sure my ideas make sense. A large amount of the work could not have been done without the help of Christoph Renner and his colleagues Sigrun Köster and Maria Longobardi. Without their experimental results, and the related discussions, progress could not have been made on the Bi nanoline or Mn nanowire. There are two other people who also have to be thanked for their contributions to the Mn nanowire research. James Owen, for discussions and ideas throughout, bringing in his experience from the search for the structure of the Bi nanoline, and Andrew Morris, for his help with the AIRSS work. There are two further experimentalists who have to be thanked for their contributions. Koichi Murata for the new results for buried Bi nanolines and Kazushi Miki for discussion on Bi deposition. I acknowledge the use of the UCL Legion High Performance Computing Facility (Legion@UCL), and associated support services, in the completion of this work. Without the many months and years of computing time that I have no doubt used, completion of this work would not have been possible. Jmol, the open-source Java viewer for chemical structures in 3D, has also been a vital tool for analysing structures and producing images of them. Finally I have to thank Nami Kusumoto for her love and support throughout the past 3 years, and putting up with all the physics talk.

Publications

The work presented in Chapter 5 contributed to the paper *Bi on the Si(001) surface* [1].

The work presented in Chapter 6 is contributing to the paper *Engineering the H:Si(001) surface to place Bi atoms with atomic precision*, which is currently in preparation.

The work presented in Chapter 7 is contributing to the paper *Electronic Structure of the Bi nanoline*, which is currently in preparation.

The work presented in Chapter 9 is contributing to the paper *Structure of the Mn nanowire*, which is currently in preparation.

Abstract

With the increasing miniaturisation of electronics, it is becoming important to study nanoscale systems, down to the control and manipulation of individual atoms. This work focuses on several different structures, all on the technologically important Si(001) surface, including individual spin active Bi adatoms, the Bi nanoline and the Mn nanowire. Research in this area is guided by both experimental results and theoretical simulations. Here I explore the latter, via Density Functional Theory, with a particular focus on simulated STM images, demonstrating both the successes and limitations of these techniques. This work aims to both explain experimental results and suggest new experimental avenues.

Adsorption of individual Bi atoms on Si(001) shows promise for quantum computing applications, due to the existence of spin active adsorption sites. However, rapid diffusion makes them unsuitable for real world applications. Selective depassivation of the H:Si(001) surface is shown to be a viable technique for trapping spin active Bi atoms, and offers the possibility of targeted Bi incorporation.

Nanolines of Bi, which spontaneously form on Si(001) have been extensively studied, both experimentally and theoretically. Recent experimental STM results have shown a strong bias dependence to the appearance of the nanolines, and here I present simulations which successfully explain these results. I also present further studies into defects on the nanoline.

I also studied nanowires that form when Mn is adsorbed on Si(001), which offer the possibility of magnetic nanowires. However, at present their physical structure is still unknown, despite prior efforts to address this. Here I present a thorough investigation into potential models for the Mn nanowire, encompassing prior models, their extensions and other surface or subsurface Mn arrangements. This remains an open problem, although identification of specific features in the experimental images, and deficiencies in previous models, has furthered our understanding of the problem.

Contents

Chapter 1

Introduction

With increasing computing power it is becoming routine in the field of materials science to use simulations as a complement to experimental results. Simulations can be applied to a variety of different scenarios including those that are difficult or impossible to assess experimentally, and where experiments alone are not enough to explain observations. Simulations can be used to explain new results for known structures, but they can also be used to determine structures which are not clear based on experiment alone. Beyond this, structures or ideas can be assessed for suitability in simulations before being implemented experimentally.

In this work I have used Density Functional Theory (DFT) to investigate a variety of nanostructures on the Si(001) surface, with potential applications in nanoelectronics. Silicon is an important material in the semiconductor industry, with its properties relying on the careful control of dopants. One class of dopants used are Group V atoms, which add an extra valence electron to the system, making it an n-type semiconductor. Traditionally the lighter elements, such as phosphorus, have been favoured over the heavier ones, such as bismuth, but in recent years there has been an increased interest, both experimentally and theoretically, in the latter. With the increasing miniaturisation of electronic circuits there has been growing interest in the use of Group V atoms as qubits for quantum computing [2], specifically in spintronics. Here Bi is of particular interest due to its long electron spin coherence times [3].

Spintronics is one of the most exciting branches of quantum computing currently being studied, which aims to use the spins of individual electrons to encode information. Electrons can exist in spin up or spin down states, which can be mapped to the 1s or 0s of traditional computing. They can also exist in states which are a superposition of the two, essentially making them a 1 and a 0 at the same time. These quantum bits, or qubits, can then be used to perform calculations that would either be impossible on a classical machine, or simply too time consuming. At the forefront of this research are efforts to develop a Silicon based quantum computer. This has the advantage of being compatible with current technology, and benefiting from existing technology for nanoscale manufacturing, in addition to the favourable properties offered by dopants in Si. For example, it has been shown that it is possible to perform coherent manipulation of an individual electron spin qubit [4] in P doped Si, and that in isotopically pure Si the coherence times of Bi atoms can be extended to upwards of 30 minutes [5]. On top of this, developments in Scanning Tunneling Microscopy now allow for the deterministic placement of single dopants [6]. Many issues still

remain, including how to scale up these systems, and which of the many suggested schemes to use.

More detailed background information on both the structures studied here and the theoretical underpinning of the work will be covered in Chapters 2 and 3 respectively, providing an understanding of the context within which the work covered here can be placed. Details of the methodologies used throughout this work are also provided in Chapter 4.

The work presented here has direct links into COMPASSS (Coherent Optical Microwave Physics for Atomic-Scale Spintronics in Silicon), which is an ESPRC programme grant, which aims to fabricate new, single impurity derived devices in silicon, based on the ability of quantum objects to be in two states at once. COMPASSS is looking to implement the Stoneham quantum computing scheme [7], whereby two Bi qubits are mediated by a control P atom placed between them. Michelle Simmon's group at the University of New South Wales, have demonstrated the capability of making single atom transistors by placing P atoms with near atomic precision, via careful H lithography and deposition of a PH_3 precursor [6]. However there is no equivalent Bi precursor, meaning that it is not yet possible to precisely place all three units needed for the Stoneham quantum computing scheme. In this work Bi adsorption on or incorporation in the Si(001) (Chapter 5) and H passivated Si(001) (Chapter 6) surface are investigated, partly with the aim of addressing this problem. Aside from this it also fills in the current gaps in our knowledge of Bi adsorption on the Si(001) surface, with the aim of using adsorbed Bi atoms as qubits themselves. Previous studies of single Bi atoms on the Si(001) surface have not modelled the Si(001) surface accurately, have not considered the spin properties of the Bi and have not looked at the diffusion of individual Bi adatoms.

Another area of interest is that of nanolines or nanowires which will be needed as interconnects in solid state quantum computing. A nanoline is a structure which is confined to a few nanometres in two dimensions, but is elongated in the third, hence forming a line. The distinction between nanolines and nanowires is their electrical conductance. The former only satisfy the geometric constraint given above, whilst the latter are also conducting or semiconducting [8]. As well as the electrical properties of these wires the assembly process must be considered. Accurate deposition or lithography is either impossible or incredibly labour intensive, whilst self-assembly is much less labour intensive, but offers less control over the final structures. From a manufacturing point of view, self-assembly is preferred, however few structures offer the atomic perfection of the Bi nanoline, although the electronic properties do not appear to be ideal [9]. The Bi nanolines could however be used to template nanowires of other elements, which is a potential avenue for future research. New experimental results from Christoph Renner's group in Geneva have revealed an interesting new bias dependence to the appearance of the Bi nanolines, which will be tackled in Chapter 7, in addition to attempts to identify a new feature observed along the nanolines in Chapter 8.

Mn nanowires are promising new structures, since they can be self-assembled on the Si(001) surface, and given the magnetic nature of Mn atoms offer the potential for a ferromagnetic semiconductor [10]. However there is as yet no agreed structure for the Mn nanowires and none of the current suggestions adequately explain all the experimental observations. Without a proper

understanding of the structure of the nanolines their suitability for nanoscale electronics cannot be assessed. In Chapter 9 details of the search for the structure of the Mn nanowire are given, re-assessing old models, extending them and exploring new ideas.

Finally, all of the work will be drawn together in Chapter 10, with some looks towards future work.

Chapter 2

Literature Review

2.1 The Si(001) surface

The Si(001) surface has been studied both experimentally [11] and theoretically [12] in order to understand its structure and the reconstructions which can occur. Several different possible reconstructions exist, but only those with direct relevance to this work will be recounted here. The simplest, known as the (2×1) reconstruction consists of rows of flat Si dimers aligned along the (110) direction, with a trench running between them. If these Si dimers are buckled, such as in the p(2×2) and c(4×2) reconstructions, the energy of the system is reduced. The p(2×2) reconstruction consists of neighbouring dimer rows buckled in parallel, whilst the c(4×2) reconstruction consists of neighbouring dimers rows with alternate buckling. Structural models for both of these structures are shown in Figure 2.1 to demonstrate these differences. Of these two reconstructions the c(4×2) is marginally more energetically favourable, by about 3 meV per dimer [12], but this energetic similarity means that both types of reconstruction have been observed experimentally [11]. These are the main two reconstructions that will be used throughout this work.

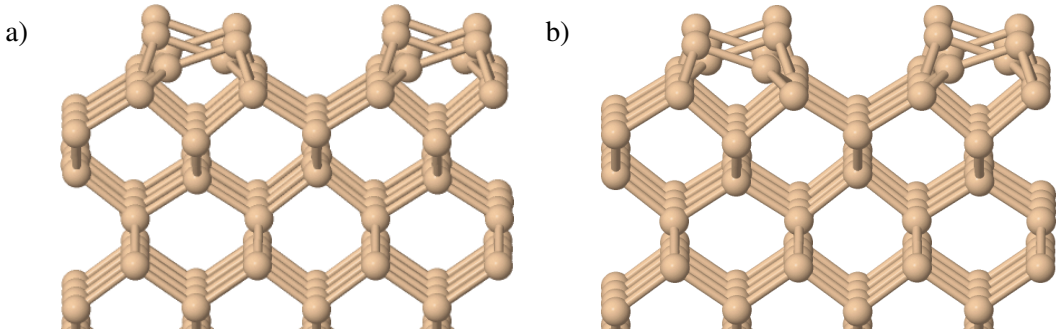

Figure 2.1: Models of the Si(001) surface, showing both a) the p(2×2) and b) the c(4×2) reconstructions.

2.2 Group V atoms on and in the Si(001) surface

There have been many studies of Group V atoms on the Si(001) surface, both from an experimental and a theoretical perspective. Experimental studies using atomically resolved Scanning Tunneling Microscopy (STM) have shown that regardless of atom type, all of the Group V atoms

will preferentially adsorb as ad-dimers located above the Si dimers and lying perpendicular to the Si dimer rows [13, 14, 15, 16, 17].

The adsorption of single Group V atoms has been covered in detail in theoretical studies [18, 19, 20] up to Sb with the most complete work done on P. Group V atoms can initially adsorb to the Si(001) surface as isolated adatoms and at a variety of sites before forming dimers. For P it was found that isolated adatoms preferentially adsorb either at the M site, or near the D site (see Figure 2.2 for labels), the former being more energetically favourable [20]. Theoretical calculations [21] confirmed experimental results showing that multiple adatoms favour adsorption as ad-dimers. For As and Sb, theoretical studies found preferential adsorption near the D site [19] and that adsorption as ad-dimers was favoured over two isolated adatoms [22], once again confirming experimental results. There has been limited theoretical work on Bi adatoms so far [23], usually focusing on dimers or larger structures, such as nanolines [9, 24].

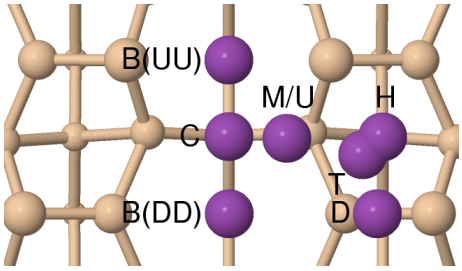

Figure 2.2: Top view of positions of adatom sites investigated on the c(4×2) surface. The letters indicate the label given to the sites in this section. The M and U sites cannot be easily distinguished from a top view. Silicon is shown in beige and bismuth in purple. Atom sizes are scaled with height and only the first 4 layers are shown for clarity.

Previous theoretical work on Bi adatoms [23] looked at the flat Si(001) 2×1 surface using a molecular cluster model. However this is not the correct surface reconstruction. These results supported adsorption as ad-dimers and suggested the D site as a preferential adatom site. Later theoretical work determined these ad-dimers to lie perpendicular to the Si dimers [25]. Experimental observations confirmed on-row adsorption perpendicular to the Si dimer rows as the preferred configuration for Bi ad-dimers [16]. The parallel configuration and in-trench ad-dimers were also observed as well as transitions from these to the perpendicular configuration. Theoretical calculations later confirmed these results [26].

This work will address adsorption of Bi adatoms on the reconstructed c(4×2) and p(2×2) Si(001) surfaces, rather than the flat 2×1 used previously, revealing new adsorption sites which cannot be found using an unbuckled model. The spin properites of the individual Bi adatoms, and the diffusion processes which can occur on the surface will also be explored, neither of which has been done before.

Incorporation of Group V atoms into the Si(001) surface to form X-Si heterodimers (where X = P, As, Sb or Bi) has also received considerable attention, both experimentally and theoretically [27, 28, 29, 30, 20], with the bulk of this research focused on P-Si heterodimers. As-Si heterodimers have been studied theoretically [30], but to the best of my knowledge, Sb-Si and Bi-Si heterodimers have thus far not been studied in detail.

P-Si heterodimers are formed via the deposition of PH_3 onto the Si(001) surface, and a subsequent thermal anneal [27, 29]. During the initial stages of deposition, both PH_3 and PH_2 can be found adsorbed to the Si(001) surface, due to the fact that the adsorption process is partly dissociative. Annealing to 350 °C will result in the full disocciation of the PH_3/PH_2 into P and H, with the former incorporating into the surface to form P-Si heterodimers, and the latter leading to the formation of monohydride structures on the surface [29]. In addition, the ejected Si from the incorporation process will form 1D Si dimer chains along the surface.

The exact location in the surface of the P-Si heterodimers can be found via the use of an STM, although this becomes more difficult for larger PH_3 doses. In filled states the heterodimer appears as a zigzag, due to the static dimer buckling of neighbouring Si dimers, induced by the heterodimer [29]. In the case of higher coverages, the presence of monohydride structures removes the Si dimer buckling, meaning that this zigzag is no longer visible. In empty states, regardless of coverage, the heterodimer will appear as a bright spot, allowing for easy identification.

Theoretical simulations examining the P-Si heterodimers and their surrounding environment revealed further intricacies to the structure [30]. There are two competing structures for the P-Si heterodimers, known as HD1 and HD2, based on the relative orientations of the neighbouring Si dimers to the heterodimer, which under normal circumstances has the P atom buckled upwards. In the HD1 structure the Si dimers buckle in the same direction as the heterodimer, whilst for the HD2 structure the buckling alternates, just like for the clean surface. Of these two the HD2 structure is lower in energy by 0.14 eV, a result which is repeated for As-Si heterodimers.

If these structures are subsequently charged they behave differently, with only the HD1 structure showing a change in buckling. As charge accumulates on the HD1 structure the buckling of the structure reverses, until the Si atom is buckled upwards. This is once again repeated for As-Si dimers. Given that the HD2 structure is lower in energy, it might be expected that it would be observed experimentally, however the structural changes observed when the HD1 structure is charged more closely match to the experimental STM results. Unfortunately, it is not possible to make a meaningful comparison of the energies of the charged structures to test whether the energy ordering is reversed under these circumstances.

Details of the incorporation process were elucidated by Bennett *et al* [20], who studied the pathways and energetic barriers for P incorporation into the Si(001) surface, and the subsequent diffusion of the ejected Si. Incorporation of P into the surface results in a P-Si heterodimer, with the ejected Si adsorbed at a nearby M-like site, still bonded to the P atom.

To reach this point, two different pathways were considered, starting with P at the M and D adatom adsorption sites respectively. The activation energy for the former was found to be 1.55 eV, whilst the latter has a smaller activation energy of 1.24 eV, meaning that incorporation from the D site is more likely to occur. However, the end structure is 0.39 eV worse in energy than the starting M position, suggesting that the process would be quickly reversed, unless the ejected Si could diffuse to a more favourable position.

Subsequent calculations showed that when the ejected Si is adsorbed at certain sites, such as M sites which are not directly next to the P atom, the energy of the system is lower than for the adsorbed P atom. In addition, it was found that diffusion of the Si atom is practically the

same as on the clean surface, barring some minor changes in the immediate vicinity of the P-Si heterodimer. These two results taken together mean that once P has incorporated into the surface, it is more likely that the ejected Si will diffuse out into the rest of the surface than reverse the incorporation process.

In this work similar structures and processes will be investigated for the Bi-Si heterodimer, both on the clean and H passivated Si(001) surface.

2.3 Hydrogen lithography

Hydrogen Lithography is a technique whereby an STM is used to selectively desorb H from an Ultra High Vacuum (UHV) H passivated Si(001) surface, with the remaining H acting as a mask, allowing for atomic scale patterning [31].

There are two possible regimes in which H depassivation can occur, high bias and low bias. In the high bias regime there is a direct excitation of the Si-H bond from the σ bonding state to the σ^* antibonding state, leading to the breaking of the Si-H bond [31]. This method shows no temperature dependence [32] and has a higher yield and is thus faster. However it only offers a resolution of $40 - 50$ Å [31], making it unsuitable for atomic scale patterning.

In the low bias regime there is some disagreement over the exact process that takes place. One suggestion is a vibrational heating model [33], whereby the accumulation of more than ten tunnel electrons from the STM tip produces the excitation of a single vibrational quantum of energy, thus breaking the Si-H bond. Another possibility is a more complicated process involving highly dissipative inelastically scattered tunnel electrons [34], where as few as two electrons can break the Si-H bond. This method has better resolution due to reduced beam divergence since the tip is closer to the surface [31], and as such is better for atomic scale patterning.

A technique known as Feedback Controlled Lithography (FCL) was developed by Hersam *et al.* [35], which allows for the controllable removal of a single H at a time. Whilst patterning, a feedback loop monitors the changes in the current and tip sample spacing. When the H is desorbed there is an increase in tunneling current due to the newly formed Si dangling bond. The feedback loop compensates for this by retracting the tip from the surface. This will terminate the patterning process so that only 1 H is removed. This enables the fabrication of well controlled arrays of isolated dangling bonds [36].

More recently Randall *et al.* [37, 38] have made steps towards making this a reproducible automated process. They have identified important matters that need addressing, such as an optimised tip structure and image analysis techniques. The tip structure is important for ensuring the process is reproducible. A sharper tip, such as a single atom tip, has better resolution, but will be less robust to degradation. However, atomic scale resolution might not be needed, with dimer row resolution possibly sufficient. Image analysis can automate processes such as drift correction [37] or feature identification [38], although the latter will need further development.

One example where H lithography can be useful is the atomically precise placement of dopant atoms such as P [28, 6]. In this technique H atoms are desorbed from an area of 3 Si dimers before being dosed with PH_3. The sample is then annealed to allow for the incorporation of a P

atom. This can occur because the rest of the H layer blocks P diffusion and the P incorporation temperature is below that for H desorption. The remaining H is then removed and the dopant encapsulated in Si. This allows for the placement of P dopants to within ± 1 lattice site (3.8 Å). Applying this same technique to other Group V atoms, such as Bi, is not quite so simple though because a PH_3 equivalent is not currently known. In this work the idea of combining H lithography and the subsequent deposition of atomic Bi is explored as a method for precisely placing Bi atoms.

2.4 Bismuth nanolines on Si(001)

2.4.1 Structure, properties and growth

Bismuth nanolines have been of interest since their accidental discovery in 1995, and the first publication on the subject by Naitoh *et al.* [39]. They are atomically straight structures which lie perpendicular to the Si dimer rows and can grow up to 1 μm in length. Examples are shown in Figure 2.3. They only form under specific conditions, either by exposing the surface to Bi below the desorption temperature, and then annealing within the desorption window, or by exposing the surface to a large amount of Bi within the desorption window [9].

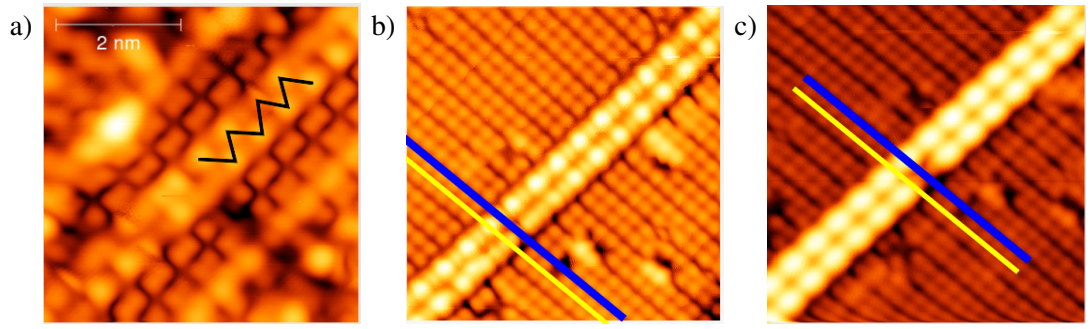

Figure 2.3: STM images of the Bi nanoline at a) +1.2 V, b) +1.5 V and c) +2.0 V. This shows a shift in appearance of the Bi nanoline from a zigzag pattern, to bright spots between the Bi dimer rows, to bright spots on the dimer rows. Images are courtesy of Sigrun Köster from Christoph Renner's group in Geneva.

Bi nanolines appear to nucleate spontaneously on the Si(001) surface and a nanoline will not stop growing unless it runs out of Bi or meets another perpendicular line. If the nanoline approaches a lower step edge it can overgrow the edge, with Si surrounding it to form a peninsula, leaving holes in the surface. Examples of this behaviour are shown in Figure 2.4. It has been suggested [40] that this is due to fluctuations of the Si step edges [41]. When the step edge moves the Bi nanoline can grow further, thus preventing the step edge from moving back. This process can repeat allowing the Bi nanoline to overgrow a step edge. The same process can take place when a Bi nanoline approaches a higher step edge, forming an inlet. The excess Si removed from this can add to other areas of the step edge or form islands. The fact the nanoline will only stop at other lines suggests that the activation barrier for a dimer in a line to diffuse out of the way is very large.

The lines have an internal structure which shows two dimer shaped features in phase with the

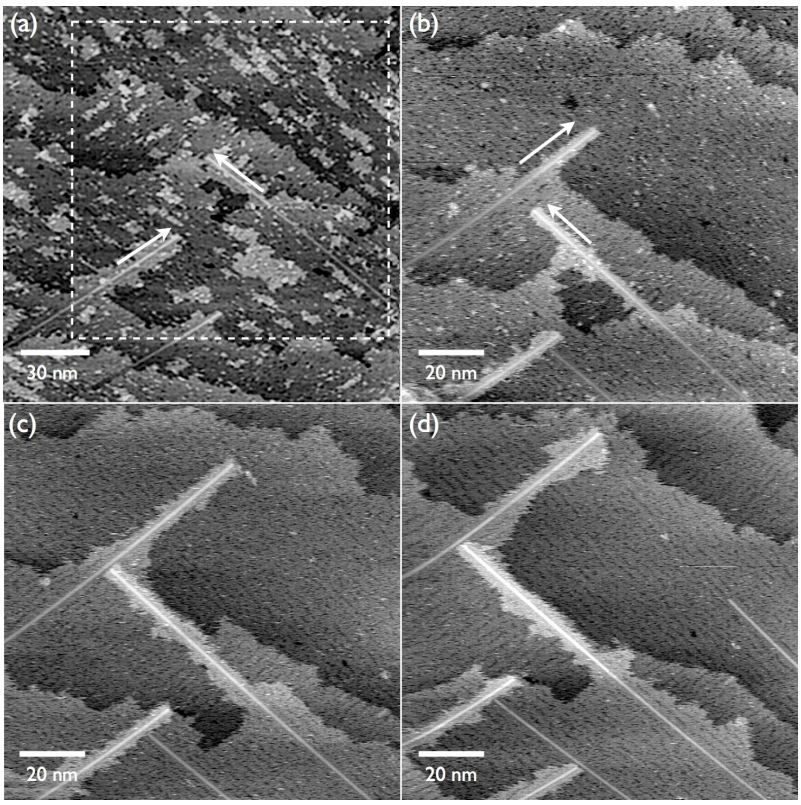

Figure 2.4: Subsequent STM images of the same region of the Si(001) surface, showing Bi nanolines overgrowing step edges. Images (c) and (d) also show one Bi nanoline blocking the growth of another. Reproduced from [40] with the permission of David Bowler.

surrounding Si dimers. The spacing between these features was measured to be 6.3 Å . It was originally believed that the nanolines took up a width equivalent to 3 Si dimers, but it was later shown to be 4 Si dimers wide [42]. Several different structures have been suggested for the Bi nanoline, such as the Miki [9], Naitoh [42] and Haiku [43] structures, all of which are shown in Figure 2.5. The Miki structure involves the substitution of two Si dimers with Bi dimers and the creation of a missing dimer defect between them [9]. This replicated some of the electronic features of the real line, however this model was built when the nanoline was still believed to be 3 dimers wide. The Naitoh structure was suggested as an alternative which took account of this. It involves the substitution of two adjacent Si dimers with Bi dimers and the creation of missing dimer defects either side of them [42]. Again this replicated some of the electronic behaviour, but failed to match the Bi dimer spacing, being too narrow at 5 Å. Both of these models also lacked a mechanism to explain the lack of observed kinking along the nanolines. The Haiku structure consists of two adjacent Bi ad-dimers sitting on top of the dimer rows and a reconstruction of the Si below the Bi dimers into 5- and 7-membered rings [43]. This structure matches all experimental observations and is lower in energy than the other structures, however it was not immediately accepted due to the difficulty of observing the reconstructed Si. This has recently become possible by removing the Bi nanolines with a dedicated hydrogen cracker [44], further details of which will be supplied in subsection 2.4.3.

They are the only currently known example of atomically perfect, straight, self assembled 1D nanostructures on the Si(001) surface [40], which would make them ideal for nanoelectronics,

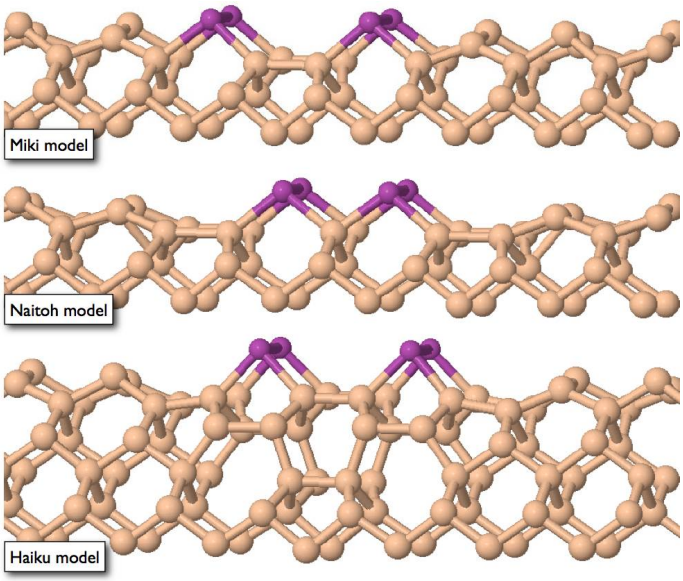

Figure 2.5: Suggested structures for the Bi nanoline. Bi atoms are in purple, Si atoms in beige. The dimer rows run from left to right across the image. Reproduced from [40] with the permission of James Owen.

were it not for the fact that they appear to not be metallic. However they could still be used as a template for growing nanowires of other elements, more details of which can be found in a recent review [45].

As of yet, there has not been a full characterisation of the electronic structure of the Bi nanoline with varying bias voltages, although partial results have been reported [46, 47, 48]. In general these results have merely distinguished between a low bias region, where the Bi lines are darker than the surrounding Si, and a high bias regime, where they are brighter. Prior results suggested that at a bias of -0.6 V to 0.6 V the nanoline appears as a trench [9], implying a density of states lower than that of the surrounding Si. However, the results which will be presented here reveal a more complicated appearance over this bias range. This work will further explore the electronic structure of the Bi nanolines, looking in greater detail than all previous studies.

2.4.2 Burying the Bi nanoline

Burying Bi nanolines in a layer of epitaxial Si is an important step in using them for nanoelectronic applications, such as connections, or for packaging them and protecting them from atmospheric attack. The Bi nanolines can also be used as a precisely controlled source of Bi atoms in the bulk, whose depth can be controlled to near atomic layer precision.

However the burial process is not as simple as just overgrowing Si on top of the Bi nanolines. This is because the Bi will segregate to the surface and destroy the nanoline structures. To prevent this a further Bi surfactant layer can be deposited first [49, 50] before overgrowing with Si. The additional Bi layer prevents the segregation of the nanoline Bi to the surface, with the surfactant layer doing so instead.

Care must be taken with the subsequent removal of this layer. A simple thermal anneal will remove the surfactant Bi, but will also disrupt the nanoline structure trying to be preserved. Instead

a wet chemical etch can be used without affecting the buried nanolines [49].

If instead an Sb surfactant layer is used exchange occurs between the surfactant and the Bi nanolines, resulting in the burial of a layer of Sb atoms [50]. This offers the opportunity to place other Group V atoms with the same precision as the Bi nanoline, although this does not appear to have been attempted with either P or As yet.

Since it is impossible to view the incorporated structure directly like with the surface nanolines, alternative techniques must be used to study the structure. X-ray scattering suggest that the 1D character and Bi dimerisation can be maintained [51], however the exact structure cannot be deduced from this alone. Previous DFT simulations from the same study suggest that the Bi dimers will bond to the Si overlayer, instead of the Haiku core, leaving a large vacancy within which the Haiku core will reconstruct. This is because it is energetically prohibitive to maintain the Haiku reconstruction after encapsulation. This new structure is more energetically favourable than other simple models for Bi defects, such as substitution, however it is by no means a definitive result. In this work Bi in bulk Si will be briefly explored to aid in characterising the buried nanolines.

2.4.3 Haiku stripe

Recent experiments [44, 52, 53] have shown that it is possible to remove the Bi nanoline from the Si(001) surface, whilst still retaining the underlying Haiku core. This structure is known as the Haiku stripe and provides conclusive evidence for the Haiku reconstruction, since it is only ever observed after the removal of Bi nanolines. Haiku stripes share lots of properties with the Bi nanolines, such as lengths of over 1 μm and the fact they are atomically perfect straight lines with a constant width of exactly 4 Si dimers (1.54 nm). This paves the way for Si dangling bond wire structures or the templating of other nanowires [53].

The Bi nanolines are removed via the use of a H cracker which supplies H_2 at about 1600 $^\circ$ C and $5\times\ 10^{-7}$ mbar for 5 minutes resulting in a dose of 120 L [44, 52, 53]. These hot, high kinetic energy H passivate the surface Si dangling bonds, before stripping away the Bi to reveal the Haiku stripe. The end result of which is sensitive to the sample temperature. If the sample is kept at 300 $^\circ C$, the H will passivate the entirety of the Haiku stripe [44, 52], whereas if the sample is kept at 420 $^\circ C$, in the desorption window for H, a row of single dimer wide Si dangling bonds will remain down the centre of the Haiku stripe [53]. The reason for this difference is that H bind more strongly to the Si on the surface or at the edges of the Haiku structure, than those in the middle. These weaker bonds also suggests the possibility of using Scanning Probe Lithography (SPL) to depassivate an entire Haiku stripe leaving the rest of the surface unaffected. This could be used as a scaleable process for nanoline construction, but currently it is only possible to control the density of these lines [53] and not their location.

The Haiku stripe consists of Si dimers which are aligned perpendicular to the rest of the surface dimers, and display a variety of arrangements, some of which are not observed for regular surface dimers. By comparison between experimental and simulated STM images it has been possible to identify several arrangements including buckled dimers, flat dimers and H terminated dimers [53]. Of these the flat dimers are a new result, because they are not normally stable on the clean Si(001) surface. In addition these results suggest the existence of flat Si dimers which alternate in height,

a matter which will be investigated in this work.

2.5 Mn Nanowires on Si(001)

The deposition of low coverages (0.05 ML to 0.5 ML) of Mn onto the Si(001) surface at room temperature results in the formation of Mn nanowires oriented perpendicular to the Si dimer rows [54, 55], examples of which are shown in Figure 2.6. At higher coverages Mn clusters begin to form instead. The wires are usually 2-17 units long, measured in units of the distance between centres of the Si dimers, perpendicular to the dimer rows, since it is harder to resolve the distance between individual Mn atoms [54]. This length can be increased by deposition in the vicinity of Bi nanolines, such as shown in Figure 2.7. The height of the nanowire is approximately 1.3 Å. The majority of the nanowires are straight, with only a few displaying kinks. In the region around the Mn nanowires the Si(001) surface buckles to form a p(2×2) reconstruction.

The Mn nanowire offers the potential for a self-assembled magnetic nanowire, but currently there is no adequate model for the structure of the nanowire which accurately reproduces all of the experimental results. Without an accurate structure for the Mn nanowire it is difficult to make a proper assessment of its properties, or future applications for the structure. Experimental STM images of the Mn nanowires reveal many detail about their structure, but there is relatively little published data on this, and the results are not always of the highest quality. The nanowire appears as a protrusion in STM images, however a single study has reported that it appears as a depression in empty state images at about 0.7 V [55]. The Mn nanowire shows a series of interesting features which vary with bias voltage, making reproduction in simulation difficult. Figure 2.6 shows some of the important features which have been observed experimentally and must be addressed in any successful model. These features include:

- A sawtooth appearance at negative biases where one side of the nanoline appears flat and the other serrated, as shown in a) and b).
- A diagonal tilt to the individual units of the nanowire at negative biases, as indicated by the arrows in a).
- A series of bright round spots centred in the trench between dimer rows at positive biases, as demonstrated in c). Since the whole of the Si dimer row undergoes a phase shift at higher positive biases the feature looks like it is on the dimer rows, rather than between them.
- At lower positive biases, such as in Figure 2.7, the Si dimers directly next to the Mn nanowire show a phase shift relative to the rest of the Si dimer row, in exactly the same manner as is observed next to the Bi nanoline.

Of these the most striking is the sawtooth appearance of the nanoline, which appears to be a result of the internal structure of the nanowire, rather than an interplay between the nanowire and the surrounding Si. The clearest evidence for this is shown in Figure 2.6.b), where there is a defect or region of otherwise missing Si directly next to the flat side of the nanowire, but the nanowire appearance remains constant along its full length.

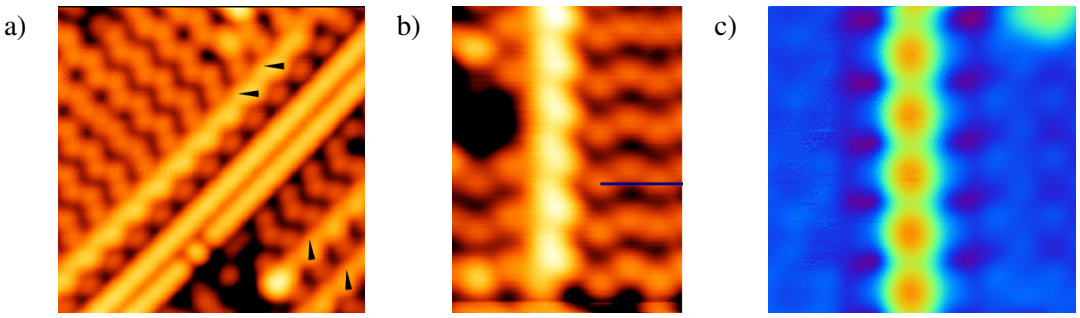

Figure 2.6: Experimental STM images of the Mn nanowire at a variety of bias voltages. a) Mn nanowire at -2.0 V. Arrows indicate a diagonal tilt to individual units of the Mn nanowire. b) Mn nanowire at -2.5 V, showing the Mn nanowire with a sawtooth appearance, regardless of the surrounding Si. c) Mn nanowire at +1.8 V. The Mn nanowire appears as a series of bright spots centred in the trench between dimer rows. Images are courtesy of Sigrun Sigrun Köster from Christoph Renner's group in Geneva.

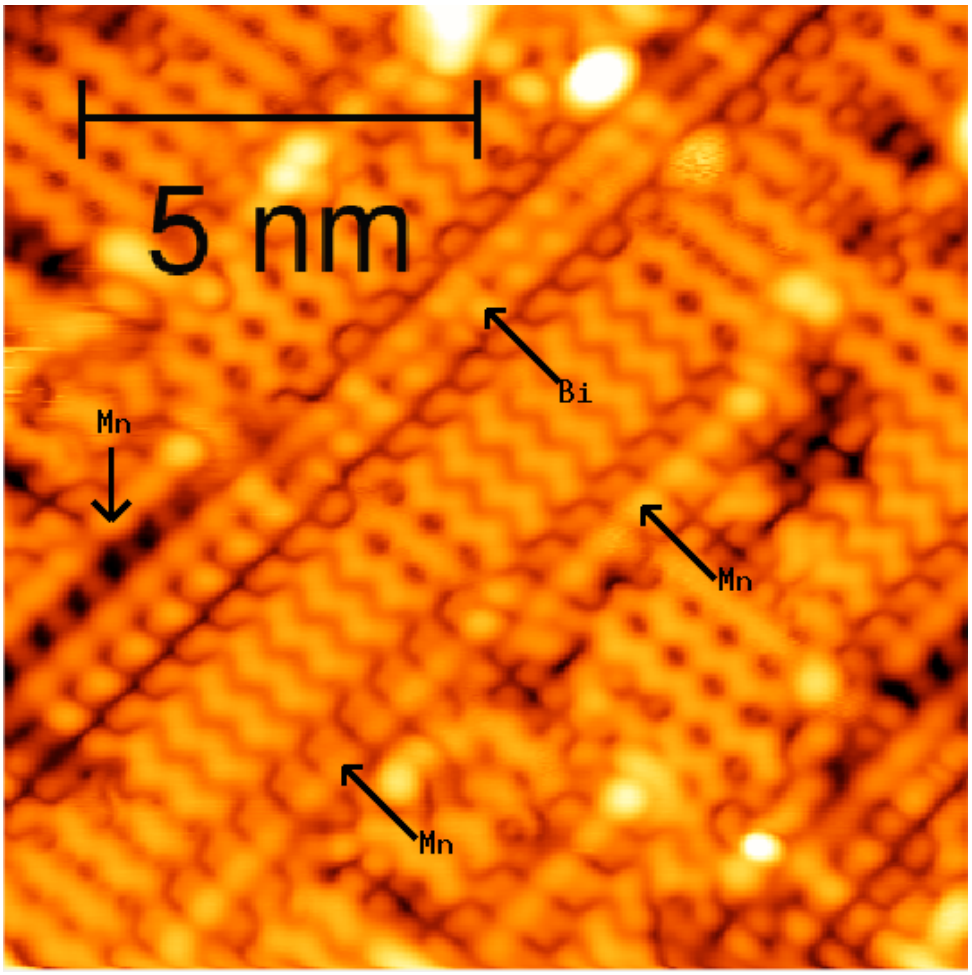

Figure 2.7: Experimental STM image at +1.2 V containing both the Mn nanowire and the Bi nanoline. The Si directly next to both types of nanostructure show a phase shift relative to the Si dimer rows. Image courtesy of Sigrun Sigrun Köster from Christoph Renner's group in Geneva.

There have been several attempts to characterise the Mn nanowire via DFT, but none have successfully reproduced all of the experimental features. Comparison of experimental results and

earlier theoretical studies on Mn adatoms [56] suggested Mn atoms in the centre of the trench between Si dimers as a potential model [54], which will henceforth be known as the C chain. This was later highlighted in a more detailed study of Mn structures where the similarities between simulated and experimental STM images were noted [57]. It however fails to reproduce all the experimental features, most notably the sawtooth appearance. Full details of this model and comparisons to experiment will be made later in Chapter 9, when the model is revisited.

The current favoured model is a structure known as the Wang trimer [58], which consists of a repeated trimer unit containing a buckled Mn dimer lying across the trench. Full details of this model will be provided when revisited in Chapter 9. When originally suggested it was claimed to reproduce the experimental STM results better than all other models, despite providing no simulated STM images to support this claim. Later work by Fuhrer $et\ al.$ [59] re-examined the Wang trimer, making direct comparisons between experiment and theory. They provide an argument for the sawtooth appearance, based on the evidence available to them, attributing it to the relative orientations of the buckled Si dimers and the Wang trimer. Newer experimental results, which were not available at the time of their paper, such as those shown in Figure 2.6.b), suggest this is not a valid model. This will be covered in more detail later. In addition to this, the model fails to explain all of the experimental features, and provides a bad match at positive biases, with Fuhrer $et\ al.$ admitting that further work on the Mn nanowire still needs to be done. At this time I do not believe a convincing structure has been found.

Chapter 3

Theory

3.1 Density Functional Theory

Density Functional Theory (DFT) [60, 61] is a quantum mechanical theory used in physics and chemistry to investigate the electronic structure of many-body systems, such as atoms, molecules and condensed phases. In principle all of the properties of a system, including ground and excited states, can be determined by using a functional (function of another function) of the ground state electron density $n_0(\mathbf{r})$, hence the name. Throughout this work DFT is implemented using the Vienna *Ab initio* Simulation Package (VASP) [62, 63] version 4.6.34. The explanations provided here for DFT and its various complexities draw heavily from Richard Martin's book on the subject [64].

DFT is an exact theory of many body systems, which applies to any interacting particles in an external potential $V_{ext}(\mathbf{r})$, where the Hamiltonian can be written as

$$\hat{H} = -\frac{\hbar^2}{2m_e}\sum_i {\nabla_i}^2 + \sum_i V_{ext}(\mathbf{r}_i) + \frac{1}{2}\sum_{i\neq j}\frac{e^2}{|\mathbf{r}_i - \mathbf{r}_j|}. \tag{3.1}$$

The basis for DFT comes from two theorems first proven by Hohenberg and Kohn [60], which are as follows.

Firstly, for any system of interacting particles in an external potential $V_{ext}(\mathbf{r})$, this potential is determined uniquely, bar a constant, by the ground state particle density $n_0(\mathbf{r})$. This means that the Hamiltonian is fully determined, and thus so too are the many-body wavefunctions for all states. Thus given only $n_0(\mathbf{r})$, all of the properties of the system are determined. However, this theorem gives no method for how to actually solve the many-body problem in the presence of $V_{ext}(\mathbf{r})$.

Secondly, a universal functional for the energy, $E[n]$, in terms of the density $n(\mathbf{r})$ can be defined, which is valid for any $V_{ext}(\mathbf{r})$. This energy functional is as follows

$$E[n] = T[n] + E_{int}[n] + \int V_{ext}(\mathbf{r})n(\mathbf{r})d^3r, \tag{3.2}$$

where $T[n]$ is the kinetic energy, E_{int} is the internal energies of the system and $V_{ext}(\mathbf{r})$ is an external potential. For any particular $V_{ext}(\mathbf{r})$, the exact ground state of this system is the global minimum value of the functional $E[n]$. The density $n(\mathbf{r})$ which minimises this functional is the

exact ground state density $n_0(\mathbf{r})$. Thus, with just the functional $E[n]$ it is possible to determine the exact ground state energy and density. However, in general this cannot be used to determine the excited states.

These theorems put forward by Hohenberg and Kohn show that it is possible to determine all of the properties of a system based on $n(\mathbf{r})$, but it does not provide the methods with which to do this. The first problem is how to find n(r), since the functional is not known. Secondly, in principle $n(\mathbf{r})$ is sufficient to understand all of the properties of a system, however at present it is only understood how to relate some properties of a system to $n(\mathbf{r})$. No one has yet found a way to extract all of the general properties from it.

In order to make the difficult interacting many-body problem of the Hohenberg-Kohn formulation solvable, Kohn and Sham [61] reformulated it in terms of an auxiliary independent particle problem. In principle this allows the use of independent particle methods for exact calculations of the properties of many-body systems. In practice this has produced remarkably successful approximate formulations.

The Kohn-Sham *ansatz* states that there is a fictitious non-interacting system, which moves in an effective potential, whose density is equal to that of the original interacting system. There is no rigorous proof that this assumption holds for all cases, but the great successes of this method would suggest it to be true. The independent particle equations for this non-interacting system are then solvable, with the many-body terms included in an exchange-correlation functional of the density. By solving these equations it is then possible to extract the ground state density and energy for the interacting problem, with the accuracy of this result only limited by approximations made in the exchange-correlation functional. These approximations have proven very successful for studying wide-band systems, with moderate success for some systems which show the effects of correlations, but fail for strongly correlated systems.

This auxiliary Kohn-Sham Hamiltonian can be written as

$$\hat{H}^{\sigma}_{aux} = -\frac{1}{2}\nabla^2 + V^{\sigma}_{eff}(\mathbf{r}), \tag{3.3}$$

which consists of a kinetic energy operator and an effective local potential, $V^{\sigma}_{eff}(\mathbf{r})$, which acts on an electron of spin σ at point $\mathbf{r}$. The effective potential can be written as

$$V^{\sigma}_{eff}(\mathbf{r}) = V_{ext}(\mathbf{r}) + V_H[n] + V^{\sigma}_{xc}[n^{\uparrow}, n^{\downarrow}], \tag{3.4}$$

where $V_{ext}(\mathbf{r})$ is an external potential due to the nuclei and any other external fields, $V_H[n]$ is the Hartree potential and $V^{\sigma}_{xc}[n^{\uparrow}, n^{\downarrow}]$ is the exchange-correlation potential. Here arrows are used to indicate spins. For a system of $N = N^{\uparrow} + N^{\downarrow}$ independent electrons which obeys the above Hamiltonian, the ground state has one electron in each of the N^{σ} orbitals $\psi^{\sigma}_i(\mathbf{r})$ with the lowest eigenvalues of Eq. 3.3. The density of this auxiliary system is then given by the sums of squares of the orbitals for each spin

$$n(\mathbf{r}) = \sum_{\sigma} n(\mathbf{r}, \sigma) = \sum_{\sigma} \sum_{i=1}^{N^{\sigma}} |\psi^{\sigma}_i(\mathbf{r})|^2. \tag{3.5}$$

The energy of this auxiliary system is given by

$$E_{KS} = T_S[n] + E_H[n] + E_{xc}[n] + \int V_{ext}(\mathbf{r})n(\mathbf{r})d\mathbf{r}. \tag{3.6}$$

Where T_S, the independent particle kinetic energy, is given by

$$T_S = -\frac{1}{2}\sum_{\sigma}\sum_{i=1}^{N^\sigma}\langle\psi_i^\sigma(\mathbf{r})|\nabla^2|\psi_i^\sigma(\mathbf{r})\rangle \tag{3.7}$$

and E_H, the classical Coulomb interaction energy of the electron density $n(\mathbf{r})$ interacting with itself, also known as the Hartree energy, is given by

$$E_H[n] = \frac{1}{2}\int d^3r d^3r' \frac{n(\mathbf{r})n(\mathbf{r'})}{|\mathbf{r}-\mathbf{r'}|}. \tag{3.8}$$

V_{ext} and E_H are well defined, and T_S is given explicitly as a functional of the orbitals.

All of the many-body effects of exchange and correlation are included in exchange correlation energy E_{xc}, which is the difference of the kinetic and internal interaction energies of the true many-body system from those of the fictitious independent particle system which has replaced electron-electron interactions with E_H. If the universal form of E_{xc} were known, then it would be possible to find the exact ground state density and energy for the many-body problem by solving the Kohn-Sham equations. At present, only approximate forms of E_{xc} are known, but this still makes it possible to calculate the ground state properties of many-body systems.

Examples of these approximations include the Local Density Approximation (LDA) [61], the Generalised Gradient Approximation (GGA) and their extensions.

LDA is a density only approximation where the functional E_{xc} at each point in the system is the same as that of a homogeneous electron gas of the same local density

$$E_{xc}^{LDA}[n] = \int \epsilon_{xc}[n(\mathbf{r})]n(\mathbf{r})d^3r, \tag{3.9}$$

where $\epsilon_{xc}[n(\mathbf{r})]$ is the exchange-correlation energy density of a homogeneous electron gas with the local density $n(\mathbf{r})$. This can be extended to include spin by the local spin-density approximation (LSDA)

$$E_{xc}^{LSDA}[n_\uparrow, n_\downarrow] = \int \epsilon_{xc}(n_\uparrow, n_\downarrow)n(\mathbf{r})d^3r, \tag{3.10}$$

where the arrows refer to spins.

The local approximation is used because for densities typical of solids, the range of exchange and correlation effects is small. The approximation works best for systems closest to a homogeneous electron gas, and badly for inhomogeneous cases like atoms. This is because of a spurious self interaction term which is not cancelled by the exchange terms in this approximation. The effect of this is negligible for the homogeneous electron gas, but has a large effect for atoms. In spite of this, LSDA has been shown to work remarkably well, even for atoms.

GGAs are a family of functionals which also considers the gradient of the electron density, and offer a marked improvement over the LSDA

$$E_{xc}^{GGA}[n_\uparrow, n_\downarrow] = \int \epsilon_{xc}(n_\uparrow, n_\downarrow, \nabla n_\uparrow, \nabla n_\downarrow)n(\mathbf{r})d^3r. \tag{3.11}$$

Whilst there is only one LDA there are several possible parameterisations of the GGA. Some of which are semi-empirical with some parameters derived from experimental observations, whilst others have parameters set to *ab initio* limits.

The semi-empirical parameterisations are less accurate but come at a smaller computational cost compared to the *ab initio* methods. One of the most popular is the gradient-corrected Perdew-Burke-Ernzerhof (PBE) [65] exchange-correlation functional, which has been employed here when studying Bi on the Si(001) surface, and in bulk Si. Another commonly used functional is the PW91 [66] functional, which has been applied to the Bi nanoline and the Mn nanowire.

Given an expression for $E_{xc}[n]$ and the Kohn Sham equation (Eq. 3.3), it is possible to find the ground state density and energy via a self-consistent loop. From an initial guess for the density $n(\mathbf{r})$ it is possible to calculate an effective potential $V^{\sigma}_{eff}(\mathbf{r})$, which can then be used to solve the Kohn Sham equation. From this it is then possible to calculate a new density via Eq. 3.5, which can then be used to repeat the process again. This will be repeated until self consistency is reached. Of all of these steps the most computationally expensive is solving the Kohn Sham equation.

In order to make solving the self-consistent Kohn-Sham equation more tractable, pseudopotentials (PPs) were introduced, which replace the strong Coulomb potential of the nucleus and the effects of tightly bound core electrons by an effective ionic potential acting on the valence electrons. Inside this core region pseudopotentials will differ from the all-electron potentials, but the two will match outside of a core radius R_c. Pseudopotentials are not unique, meaning there are multiple different pseudopotentials which can all reproduce the all-electron potentials outside of the core radius. This means it is possible to choose a form which simplifies the calculations and the interpretation of the results. Additionally, there is no best pseudopotential for any specific atomic species, with different pseudopotentials suited to different purposes.

Most modern PPs are based on *ab initio* Norm-Conserving pseudopotentials (NC-PPs), developed by Hamann, Schluter and Chiang [67]. Norm conservation is key for making the pseudopotentials accurate and transferable, which means that pseudopotentials generated for one environment, such as atoms, can be used in another, such as condensed matter. In addition, they constructed a list of requirements for good *ab initio* pseudopotentials, which is as follows [67]:

1. The all-electron and pseudo valence eigenvalues agree for the chosen atomic reference configuration.
2. The all-electron and pseudo valence wavefunctions agree outside of a core radius R_c.
3. The logarithmic derivatives of the all-electron and pseudo valence wavefunctions agree at R_c.
4. The integrated charge inside R_c agrees for the all-electron and pseudo wavefunctions. This is norm conservation.
5. The first energy derivative of the logarithmic derivatives of the all-electron and pseudo wavefunctions agree at R_c.

Points 1 and 2 mean that the NC-PP will be equal to the atomic potential outside of the cut off radius R_c. These follow onto point 3, since the wavefunction and its derivative are continuous

at R_c for a smooth potential. The conservation of charge in point 4 ensures that both the pseudo-orbital and the potential outside R_c is correct. Point 5 is crucial for constructing a pseudopotential which can be generated in a simple atomic enviroment, but also applied to more complex systems. In molecules and solids the wavefunctions and eigenvalues will change, and a pseudopotential which satisfied point 5 will reproduce these changes to the first order in the self-consistent potential.

When constructing pseudopotentials there are competing issues between their accuracy and transferability, against the cost of calculations. The latter is often referred to in terms of the "smoothness" of the pseudopotential, with the "smoother" a potential, the lower its computational cost. Achieving accuracy and transferability leads to a small R_c and hard potentials, because one wants to describe the wavefunction near the atom as well as possible. Smoothness leads to a choice of a larger R_c and soft potentials, because one wants to describe the wavefunction with as few basis functions as possible. It is desireable to have pseudopotentials which are as smooth as possible, but also accurate. NC-PPs for example achieve accuracy, but have to sacrifice smoothness.

Ultrasoft pseudopotentials (US-PPs) [68] achieve accurate results by expressing the pseudo function as a sum of a smooth part and a more rapidly varying function localised around each ionic core. US-PPs have improved accuracy over NC-PPs and are less costly, but the programs needed to handle them have to be more complicated. The radial wavefunctions for US-PPs are nodeless and extend into the core region, whereas NC-PPs require that they are only moderately smoother than the all-electron wavefunction. US-PPs relax the requirement for norm conservation, which allows the use of a much larger R_c, whilst still retaining accuracy.

Another alternative is projector augmented waves (PAWs) [69, 70], which express valence wavefunctions as a sum of smooth functions and core functions. They retain the full set of all electron core functions, along with the smooth part of the valence functions. The PAW method composes basis functions out of atom-like partial waves in the core region and envelope functions appropriate for the bonding in between. These parts are then matched at the boundary of the two regions. PAWs are useful for total energy and force calculations.

DFT is not without its failings, some of which can be attributed to the approximate nature of current exchange-correlation functionals, others which are more fundamental problems. One of the most well known failings is the fact that DFT fails to reproduce the band gap of semiconductors and insulators. This is because the Kohn-Sham gap is not the same as the fundamental gap, even if the correct exchange-correlation functional were found. For example for semiconducting solids the Kohn-Sham gap will often be much smaller than the fundamental gap. Hybrid functionals can be used to address this problem for specific systems, but there is as yet no universal solution.

The delocalisation error of approximate functionals, whereby DFT artificially spreads out the electrons, can lead to many errors, such as underestimating the barriers of chemical reactions, the energies of dissociating molecular ions, and charge transfer excitation energies, as well as overestimating the binding energies of charge transfer complexes and the response to an electric field in molecules and materials. This error is due to the dominating Coulomb term that pushes electrons apart. As a result approximate functionals tend to spread out the electron density artificially.

The delocalisation error also manifests itself in the fact DFT gets the derivatives of energy

with respect to fractional charge wrong. The energy of an atom as a function of charge should be a straight line between integers, due to the discrete nature of electrons. However approximate functionals are convex between integers, leading to predictions of lower energies for fractional charges. This leads to incorrect ionisation energies and electron affinity and an underestimation of the band gap. If a functional instead shows concave behaviour between integers this results in a localisation problem. Some hybrid functionals contain both types of errors, which can lead to cancellations and an improvement of predictions of properties like the band gap, but do not provide a general solution [71].

In addition DFT calculations fail to describe degenerate or near degenerate states, such as those which arise in transition metal systems, the breaking of chemical bonds and strongly correlated materials. All these problems are a consequence of the static correlation error of the functionals. This problem is due to the difficulty in using electron density to describe the interaction of degenerate states.

Another issue is the self interaction problem, which is the spurious interaction of an electron with itself. If the exact exchange correlation functional was known this would be cancelled. Some techniques have been developed to deal with this such as self-interaction correction (SIC) [72] and the optimised effective potential method (OEP) [73].

DFT often fails to describe strongly correlated d and f electrons, due to an inadequate description of the strong Coulomb repulsion between electrons localised on metal ions. This can be remedied by introducing a strong intra-atomic interaction in a screened HF like manner, as an on-site replacement of the LSDA, such as in the DFT+U method [74, 75]. This describes the strongly correlated electrons by the Hubbard model, introducing the Hubbard U, which is the Coulomb energy cost to place 2 electrons at the same site. The rest of the valence electrons are treated in the standard way. The energy is thus calculated according to:

$$E_{DFT+U} = E_{DFT} + E_{Hub} - E_{dc}. \tag{3.12}$$

Where E_{Hub} is the Hubbard Hamiltonian for modelling correlated systems and E_{dc} is the double counting energy, which must be subtracted. This is to remove the part of the interaction energy which is being modelled by E_{Hub}.

3.2 Transition State Theory and the Nudged Elastic Band method

Transition State Theory (TST) [76, 77] is primarily used to understand how chemical reactions take place, but can also be used to understand the diffusion or rearrangement of particles on surfaces, as in this work. One of the basic ideas behind TST is that progress of a chemical reaction can be described as a point on a potential energy surface (PES). By finding the minimum energy path (MEP) between a pair of stable states on the PES it is possible to determine the activation energy for the process. For diffusion of particles this pair of states will be the initial and final positions of the particles in question. An MEP passes through at least one first order saddle point and the energy difference between this and either of the stable states is the activation energy for the process in that direction. From this the rate of diffusion can be calculated. For the purposes of this work a

simple Arrhenius relation is assumed

$$R = A \exp\left(\frac{-E_A}{k_b T}\right), \tag{3.13}$$

where A is the attempt frequency, here assumed to be $10^{13}\ s^{-1}$, k_b is the Boltzmann constant, T is the temperature in Kelvin and E_A is the activation energy.

There are several methods for calculating MEPs and hence diffusion rates. These include the Dewar, Healy and Stewart (DHS) method [78] and its extensions [79], the dimer method [80], the constrained optimisation (CO) method [81], the activation-relaxation technique (ART) method [82], the one-side growing string (OGS) method [79], the Nudged Elastic Band (NEB) method [83] and a variation known as the Climbing Image Nudged Elastic Band (CINEB) method [84]. In this work the CINEB method is used because it is fast, converges to the TS and is generally considered the superior method. The ART, CO and OGS methods can give unsatisfactory results, whilst the performance of the dimer method varies. Some variations of the DHS method can approach the CINEB method for speed and accuracy.

The NEB method is a variation of a chain-of-states method [85], a method which connect several states, or images, of the system, creating a path between end points. These states are connected together with spring forces similar to elastic bands. The intermediate states are often straight-line interpolations in Cartesian coordinates [86], but in some cases more care must be taken. If the reaction involves rotation, interpolation of internal coordinates can be more suitable. If an intermediate is already known this can be incorporated into the path. If multiple MEPs are possible, the initial guess will influence which MEP is found, so several guesses should be made.

In the simplest version, known as the Plain Elastic Band (PEB) method, the force on image i is

$$\mathbf{F}_i = -\nabla V(\mathbf{R}_i) + \mathbf{F}_i^S, \tag{3.14}$$

where $\nabla V(\mathbf{R}_i)$ is the true force and

$$\mathbf{F}_i^S = k(|\mathbf{R}_{i+1} - \mathbf{R}_i| - |\mathbf{R}_i - \mathbf{R}_{i-1}|) \tag{3.15}$$

is the spring force, where k is a spring constant, assumed to be the same for each image.

This method has some shortcomings. If the elastic band is too stiff the path misses the saddle point by cutting corners, because the component of the spring force perpendicular to the path pulls images off the MEP. If the spring constant is smaller the path is closer to the saddle point, but images slide down and avoid the barrier region. This is because the component of the true force in the direction of the path causes the distance between the images to become uneven [83].

In the NEB method the perpendicular component of the spring force and the parallel component of the true force are projected out, and the force on image i becomes

$$\mathbf{F}_i^0 = -\nabla V(\mathbf{R}_i)\ |_\perp + \mathbf{F}_i^S \cdot \hat{\tau}_\parallel \hat{\tau}_\parallel. \tag{3.16}$$

Here $\hat{\tau}_\parallel$ is defined as normalised local tangent to the elastic band at image i, and $\nabla V(\mathbf{R}_i)\ |_\perp = \nabla V(\mathbf{R}_i) - \nabla V(\mathbf{R}_i) \cdot \hat{\tau}_\parallel \hat{\tau}_\parallel$ [83]. This projection of the forces is known as nudging. Doing so decouples the dynamics of the path from the distribution of images on the path, which is essential to

converging to the MEP. The spring force does not interfere with the relaxation of the images perpendicular to the path, and the relaxed configuration of the images satisfies $\nabla V(\mathbf{R}_i) \mid_\perp = 0$ such that they lie on the MEP. Since the spring force only affects the distribution of the images within the path, its choice is fairly arbitrary. Unfortunately to determine the saddle point from the NEB method requires interpolation, which can be inaccurate when the energy barrier is narrow compared to the length of the MEP. To remedy this problem the CINEB method was introduced [84].

The CINEB method is a slight modification to the NEB method, which retains the information about the shape of the MEP, but rigorously converges to the saddle point. This comes at no additional computational cost. After a few iterations with the NEB the image with the highest energy i_{max} is identified, henceforth known as the climbing image, and the force acting on it is modified to

$$\mathbf{F}_{i_{max}} = -\nabla V(\mathbf{R}_{i_{max}}) + 2\nabla V(\mathbf{R}_{i_{max}}) \mid_\parallel . \tag{3.17}$$

This is the full force due to the potential with the component along the band inverted. The climbing image is unaffected by the spring forces, so the spacing of the images either side of the climbing image will be different. On one side they will be compressed, on the other more spread out. If there are multiple maxima in the MEP it is possible to specify multiple climbing images, provided there are enough images close to the climbing image. The climbing image moves up the PES along the elastic band and down the potential surface perpendicular to the band. Provided the CINEB method converges, the climbing image will converge to the saddle point [84]. The energy and gradient for each image in the elastic band must be evaluated using a description of the energetics of the system. For each image the coordinates of adjacent images are required to estimate the local tangent to the path, project out the perpendicular component of the gradient and add the parallel component of the spring force [83]. It has been shown that for accurate energy barriers only a single intermediate image is sufficient [79].

3.3 Density of States

The density of states (DOS) of a system describes the number of electronic states occupied, or free to be occupied in a system. States with energies that lie lower than the Fermi level are occupied, whilst those above the Fermi level are unoccupied at zero temperature. The greater the density of states at a given energy level the more states can be occupied, with a density of zero meaning no states can be occupied. The density of states can be split into spin majority and spin minority components, indicating which spin there is more of in the system. The local density of states (LDOS) describes this for a single atom in the system.

In VASP the wavefunction character and local partial DOS are calculated by projecting the wavefunctions onto spherical harmonics that are non zero within spheres of the Wigner Seitz radius (specified by RWIGS in VASP) around each ion. When PAWs are used, this radius is taken instead from the radius of the PAWs. This information can be used to construct for example partial DOS projected onto molecular orbitals. These results are qualitative, since there is no unambiguous way to determine the location of an electron. Quantitative results can only be obtained by comparison to a reference system.

3.4 Scanning Tunneling Microscopy

Scanning Tunneling Microscopy (STM) [87, 88] is a method for imaging atomic scale surfaces based on the concept of quantum tunelling. When a sharp conducting tip is brought very close to the surface to be examined and a bias is applied between the two, it is possible for electrons to tunnel through the vacuum between them. The resulting tunelling current is a function of the tip position, the applied voltage and LDOS of the sample. Information about the sample can be gained by scanning the tip across the surface. This scanning can be done at either a constant height or a constant current, although the latter is much more common. In constant current mode, the tip scans across a sample using piezoelectric elements to control the x and y positions, and a feedback loop to adjust the tip height and thus maintain a constant current. These changes in height can then be used to gain both topographic and electronic information about the surface. Occupied states can be imaged by applying a negative bias to the sample, whilst unoccupied states can be imaged by applying a positive bias. To achieve atomic resolution, a tip with a single atom at its apex is needed, however this is also very unstable. In order to properly understand STM images it is important for experiment and theory to work together.

In an STM a tunnel junction is formed between the tip and the sample. The current measured across this junction is due to an electron tunneling from the tip to sample, or vice versa. There are many different factors which can influence this process, such as the tip-sample distance, the chemical composition of the tip and sample, the electronic structure of both, the chemical interactions between surface and tip atoms, and the electrostatic interactions of the sample and tip [89].

Usually the tunneling current is set to a fixed value, with the position of the tip relative to sample varied via distorting a piezocrystal to keep the current constant. This sensitivity of current to the tip-sample distance is the basis of vertical resolution in STM. If a square potential barrier is assumed for the vacuum region between the tip and sample, the tunelling current can be approximated by

$$I(z) \propto e^{-k\sqrt{2\Phi}z}, \tag{3.18}$$

where k is a constant, Φ is the work function of the two surfaces, and z is the tip-sample distance. In reality the work functions of the tip and sample will not usually be the same, the decay of electron states is not constant, and the density of states above the surface is typically varied. It is also problematic to estimate the tip-sample distance accurately.

When the bias voltage applied to the sample is changed, this has two effects. Firstly it shifts the Fermi level of one lead relative to the other, and secondly it creates a surface dipole which compensates for the first effect. Both of these processes are understood in principle, but they lack detailed simulations. If the electron density of surface and tip are fairly smooth, then the current will increase approximately linearly with applied voltage. This is due to the energy difference between the E_F of the sample and the tip, which increases the number of electron states provided by one lead, increases the number of empty states provided by the other, and leads to the condition of resonant tunneling [89].

Electrostatic effects are introduced at the interface, due to the applied bias voltage and the

general differences in E_F between the sample and tip, however these do not substantially alter the electronic surface structure, and can be neglected for metal and semiconductor surfaces.

The chemical forces between the tip and surface are important to understand, because if a chemical bond forms between the two, this can lead to changes in the tunneling current, or changes to the structure of the tip-sample system. Chemical forces will only have an effect if the tip and sample are brought within a certain distance, which will vary with the system being studied. For example, for Au(111) this was determined to be 4.6-4.7 Å [90]. If the separation is reduced further, for example to about 4.0-4.1 Åin the case of Au(111), the forces between the tip and sample will grow rapidly and the stability of the system will be destroyed as ions jump back and forth between the tip and sample. Between these two regions there is an increase in tunneling current beyond exponential growth and an increase in surface corrugation by a factor of two to three. High resolution STM can operate within this range.

Magnetic forces between the tip and sample are only important if both are magnetic. Magnetism influences the tunneling current due to the magnetic moment and electronic structure of different spins, and the orientation of the magentic axis.

In order to produce simulated STM images it is necessary to model both the surface and the tip, and the interactions between them, before calculating the current under these conditions. These results can then be compared to experiment.

Modeling the surface accurately requires knowing the surface structure, which can be derived from previous experimental and theoretical studies. When the exact structure of the system being studied is not known, such as in some of the work here, it becomes necessary to try many structures to find the correct one, guided by comparisons to experiment. The surface can then be modelled using DFT software such as VASP.

Due to computational costs and the complexity of modeling real tips, simpler models assuming idealised tips are often used instead. The most widely used is the Tersoff-Hamman approximation [91, 92], which in this work is implemented in bSKAN33 [93, 94, 95]. In this approximation it is assumed that a single tip orbital is responsible for the image contrast. It used to be unclear whether this tip orbital was s-like or d-like [96, 97] in nature, but detailed simulations of the tip apex revealed it to be d-like [98]. Due to these simplifications, tip effects are essentially neglected. For more accurate simulations the effect of the tip must be included, such as in the Bardeen approach [99], however this is not used here.

The Tersoff-Hamman approximation is reliable if there are no substantial chemical interactions between the surface and tip, and if the feature size of the surface structures being studied is above that of the length scale of electron states of an STM tip. The former is hard to quantify properly, because it varies with the system being studied and the experimental set up. In general for semiconductors the tip-surface interactions can be neglected. For the latter, the tip state is typically half the interatomic distance of the metal in the tip (1-2 Å). This means that for feature sizes above this, the exact geometry of the tip states does not matter. Whilst this is not fulfilled for high resolution scans with atomic precision, it is otherwise okay to ignore the structure of the tip during simulations.

If the above conditions hold true, then the constant current contour can be related to the charge

density contour of the surface. The tunneling current is proportional to the LDOS at the position of the STM tip [89]. In many standard simulations this provides a reliable qualitative picture of the surface topography, even though it does not generally reproduce the observed corrugation values.

Chapter 4

Methodologies

4.1 General

In this work a variety of different techniques have been employed, and whilst the generalities and methods stay the same throughout, the specific details change with the structures studied. DFT [60, 61] as implemented in the Vienna *Ab initio* Simulation Package (VASP) [62, 63] version 4.6.34 was used throughout to perform these calculations. In all cases the core electrons were described by the projector augmented wave (PAW) method [69, 70]. The choice of exchange correlation functional varies with structure, so will be specified individually.

The Si(001) surface was represented by a periodically repeated eight to ten layer slab model, with a reconstructed surface layer consisting of buckled Si dimers with either c(4×2) or p(2×2) periodicity. In some cases the (2×1) reconstruction was used, often referred to in the text as flat. In this context, a layer is defined as Si atoms which are at the same height in z, assuming a structural reconstruction is not present. The first layer for example will usually have Si atoms at two different heights due to the buckling of the surface Si dimers, whilst the sixth layer will all be at the same height. The exact number of layers for each model and the surface or subsurface reconstructions used, will be specified for each structure in their respective Sections. The choice of Si lattice constant for these structures depends on the exchange correlation functional used, so will be specified for each structure.

The extent of the simulation cell was varied depending on the needs of the calculation, with the surface consisting of between one and three dimer rows, which could be up to eleven Si-Si dimers in length. In general the size was chosen to prevent interaction between periodic images of adsorbates. In some cases larger cells were necessary to properly represent the periodicity of the structure being studied.

In all of the models used, the bottom Si layer was terminated by H atoms in a dihydride structure. To create this dihydride structure, H atoms were placed along the bulk Si-Si bond direction, with the Si-H distance chosen to match literature value for Silane [100]. Prior to the full structural relaxations the bottom two Si layers and the H atoms were allowed to relax whilst keeping all other Si atoms fixed, to optimise the Si-H bond lengths. For all subsequent calculations both the H atoms and the bottom two layers of Si atoms were fixed, in order to simulate a bulk like environment. The studied adsorbates or nanostructures were placed atop the first layer of Si

atoms, and all but the bottom two Si layers and their terminating H atoms were fully optimised.

The periodic images of the cell were separated by large vacuum gaps in the z direction, in order to prevent interaction between the top and bottom of the slab model. The size of vacuum gap varied with structure, so will be specified for each structure.

For bulk Si, matters such as the vacuum gap, the surface reconstruction, and the fixing of certain layers do not need to be considered.

For many calculations the energy cut off was set to 1.25 times the default specified in the POTCAR file, due to using the high precision settings in VASP. This was to converge adsorption energies to within 0.01 eV, and allow more accurate comparisons of structures containing the same number of adsorbates. In many cases this meant an energy cut off of 250 eV was used, due to the 200 eV default for H, however this can vary with atom choice. It will be noted in the text when values which do not follow these criteria are used. In some cases the precision was set to normal, hence lowering the energy cut off, in order to speed up calculations on problematic structures.

The choice of k-points varied with model size, but in general the greatest number of k-points were along the direction of features like the Bi nanoline or Mn nanowire. Specific details will be given in each Section.

Unless stated otherwise, for all calculations, geometry optimisations were performed with a 0.02 eV/Å convergence condition for the forces on each atom. All calculations were spin polarised and unless specified otherwise, no restrictions were placed on the spins in the system.

Adsorption energies per atom were calculated using

$$E_{ads} = \frac{E_{system+X} - E_{system} - nE_X}{n}, \tag{4.1}$$

where $E_{system+X}$ is the energy of the adsorbed structure, E_{system} is the energy of the structure being studied without adsorbates, E_X is the energy of a single atom of the species being studied calculated in the same unit cell and n is the number of adsorbate atoms. This equation can only be used when all energy values are obtained under the same conditions, such as cut off energy and choice of k-points. This means that when an adsorbate atom with a higher default cut off energy than H is used, for example O, the original calculation without the adsorbate must be repeated at this new higher cut off. It is also important that the number of atoms for each species remains constant throughout, i.e. $n_{adsorbates}$+n_{system}=$n_{syst+ads}$, otherwise meaningful comparisons cannot be made. This means that substituted structures cannot be compared to those without substitutions, unless the replaced atom is still kept within the model.

The CINEB method [84] was used to calculate the diffusion barriers and pathways between the different adatom sites and to study incorporation processes. Most calculations used 3 intermediate images between end points, but when there were considerably smaller or larger separations between these end points, 1 or 5 images were used respectively. The CINEB method can converge to the transition state only using a single intermediate image [79], but when the separation of initial and final states were larger, a greater number of images were used to ensure that any intermediate transition states were not missed. The rates of diffusion were calculated using eq. 3.13.

Much of the work presented here makes use of simulated STM images produced using the Tersoff-Hamman method, as implemented in bSKAN33 [93, 94, 95]. In most cases, simulated

STM images were produced for biases ranging between $\pm$ 3.0 V, in intervals of 0.1 V. Such narrow intervals were chosen because some details of the electronic structure only appear over very narrow bias ranges, which would have been missed otherwise. For values greater than $\pm$2.0 V, intervals of 0.5 V were used.

I will now address the specific details unique to each Chapter.

4.2 Bi on and in the Si(001) surface

To study Bi on and in the Si(001) surface (Chapter 5) the gradient-corrected Perdew-Burke-Ernzerhof (PBE) [65] exchange-correlation functional was used. For Bi the $6s^2 6p^3$ electrons were treated as valence, the rest as core.

The Si(001) surface was represented by a 10 layer slab model with either c(4$\times$2) or p(2$\times$2) periodicity. The bulk lattice constant for Si was calculated to be $a_0 = 5.469$ Å in very good agreement with the experimental value of 5.4306 Å [101]. The surface consisted of two rows of four Si-Si dimers. The periodic images of the cell were separated by a vacuum gap of 12.84 Å when no Bi was present.

An energy cutoff of 300 eV was used to converge the adsorption energies to within 0.01 eV. A (2$\times$2$\times$1) Monkhorst-Pack k-mesh is adequate for coarse grained simulations but a (3$\times$3$\times$1) k-mesh was required to converge adsorption energies to within 0.01 eV for some sites. Structures with overall spins of 0 and $\frac{1}{2}$ were both tested.

The CINEB method was used to study diffusion of Bi on the Si(001) surface, and incorporation of Bi into the Si(001) surface.

4.3 Bi on and in the H passivated Si(001) surface

The methodology used to study Bi on and in the H passivated Si(001) surface (Chapter 6 and Appendix A) was largely the same as described in Section 4.2, with the main difference being that the surface Si dimers were H passivated, rather than clean. This removes the dimer buckling, leaving the surface dimers flat. In some cases larger cells were used, with two rows of eight dimers, rather than the four used previously. In these cases a 1$\times$2$\times$1 k-point mesh was used. Calculations this was used for included, incorporation, the Bi-vacancy structure, checks of diffusion calculations and the additional tests on the 2$\times$D structure.

4.4 Bi nanoline and related structures

Investigations into the electronic structure of the Bi nanoline (Chapter 7), the nature of features along the Bi nanoline (Chapter 8) and the Haiku stripe (Appendix D) all followed roughly the same methodology with a few modifications relevant to each specific problem. Throughout, the PW91 exchange-correlation functional [66] was used. For Bi the $6s^2 6p^3$ electrons were treated as valence, the rest as core. The energy cut off used for calculations depended on the species of adsorbate being studied, but followed the criteria set out earlier.

For these calculations the experimental bulk lattice constant of $a_o = 5.4306$ Å was used. A 10 layer slab model was used, with in most cases the p(2×2) surface reconstruction. This is because the experimental results show this to be the more common surface configuration around the Bi nanoline. Results discussed later suggest why this might be the case, rather than the normally more energetically favourable c(4×2) reconstruction. When other reconstructions, such as the c(4×2), have been used this is noted in the text. The periodic images of the surface were separated by a vacuum gap of 12.73 Å to prevent interaction between repeated images.

Depending on the needs of the simulation, cells with between one and three rows of Si dimers were used. The majority of the calculations were done with the double row structure to make visualisation easier, with the single row structure generally only used to reduce calculation times, or for studying the Haiku stripe. In some cases, such as the c(4×2) surface reconstruction, it is not possible to represent the system with fewer than two rows. For some of the larger nanoline variants it became necessary to increase the structure to three rows to be able to include the whole repeated unit.

For most calculations the dimer rows are the equivalent of ten dimers long, consisting of four regular dimers, the Haiku reconstructed region, which occupies another four rows, and then two more regular dimers. The Bi nanoline then sits atop the Haiku core, consisting of a pair of Bi dimers per dimer row. Where noted, this was extended to eleven dimers to allow for a periodicity mismatch between the Si on either side of the Bi nanoline. Ten and eleven dimer versions of the Si surface without the Haiku core were also constructed, to test how this would alter the bias dependence of the Bi nanolines.

Any adsorbates or modifications to the line were made based on this structure. When studying adsorbates they were placed above the Bi dimers of the Bi nanoline. When studying the Haiku stripe the Bi dimers were removed from the Haiku core, leaving the central Si dimers clean. In addition all of the other surface Si were H terminated. The two Si dimers down the centre of the Haiku stripe were placed at alternating heights prior to relaxation.

For most calculations a (2×1×1) Monkhorst-Pack k-mesh was used, however for more detailed band structure and electronic structure calculations, up to a (10×1×1) k-mesh was used. In all cases the largest number of k-points was along the direction of the Bi nanoline. Geometry optimisations were performed with a 0.02 eV/Å convergence condition for the forces on each atom, but this was sometimes relaxed to 0.03 or 0.04 eV/Å. In some cases geometry optimisations were stopped early to make a preliminary assessment of suitability. These cases will be noted later in the text.

All calculations were spin polarised with in most cases no restrictions placed on the spins, the only exception to this being when studying the Haiku stripe. The Haiku stripe with Si dimers at alternating heights was allowed to relax for a variety of different spin arrangements. Since there are four surface Si which are not H passivated there are potentially four unpaired electrons, so structures with an overall spin of between 0 and +2 were used in steps of 1/2.

Simulated STM images were generated using bSKAN33.

To gain further insight into the changing appearance of the Bi nanoline, band decomposed charge densities were examined for individual and all k-points and compared to the experimental

and simulated STM results.

4.5 Bi in bulk Si

For studying Bi in bulk Si (Appendix C) the PBE [65] exchange-correlation functional was used. For Bi the $6s^2 6p^3$ electrons were treated as valence, the rest as core. A cut off energy of 300 eV was used with a 2×2×2 k-point mesh. A 512 atom bulk Si cell was used, with a lattice constant of 5.469 Å, the previously calculated theoretical lattice constant. It has previously been shown that using a cell of this size is important for defect calculations [102].

Three different sets of calculations were performed based on the number of Bi atoms in the cell, ranging from zero to two. For the cells with just bulk Si several different vacancy structures were examined including the mono-,di- [102, 103] and tri-vacancies [104, 105]. These have all been studied extensively before, although only the simplest versions were replicated here. For cells with just a single Bi defect the number of associated vacancies was varied from zero to two. Finally for cells with two Bi atoms the distance between the defects was varied from nearest to next next nearest neighbour.

4.6 Mn nanowire

When studying the Mn nanowire (Chapter 9 and Appendix E) the PW91 exchange-correlation functional [66] was used, with a plane wave cut off of 320 eV. The valence state $3p^6 3d^5 4s^2$ for Mn was used.

For these calculations a lattice constant of $a_o = 5.47$ Å was used, which is the PW91 lattice constant, in line with the work on the Wang trimer [58]. The Si(001) surface was represented by an eight layer slab model with p(2×2) surface periodicity and two rows of eight Si dimers. This is because the experimental results show this to be the more common surface configuration around the Mn nanowire. The periodic images of the surface were separated by a vacuum gap of 17.32 Å to prevent interaction between repeated images.

For these calculations a (2×1×1) Monkhorst-Pack k-mesh was used, with the largest number of k-points along the direction of the Mn nanowire. All calculations were spin polarised and usually with no restrictions placed on the system. In some cases the relative spins of neighbouring Mn atoms were set to ferromagnetic or anti-ferromagnetic arrangements. The details of these arrangements will be given later in Chapter 9.

DFT+U [74, 75] calculations were performed using the Dudarev formulation [106], using Coulomb and exchange parameters of U=4.2 eV and J=1 eV, following the methods of Sena *et al.* [57] when studying the C chain previously.

Simulated STM images were generated using bSKAN33.

Chapter 5

Bi on the Si(001) surface

Here I present an investigation of the adsorption, incorporation and diffusion of single Bi adatoms on the Si(001) surface for both the c(4×2) and p(2×2) reconstructions. For individual adatoms their energetics and properties were examined, with the aim of determining the most energetically favourable adsorption site and whether or not the Bi adatom had a single unpaired electron at any of these sites, for use in spintronics. The study of diffusion is important to determine whether the individual adatom sites are stable or not, and to explain why they have yet to be observed in experiment. I also consider formation of ad-dimers, and a comparison to P and As adatoms. Studying ad-dimers serves as a check of whether previous results stating ad-dimers to be more energetically favourable than adatoms holds true for these calculations. Comparisons to P and As are to check whether the properties observed for individual Bi adatoms are exclusive to Bi, or if smaller Group V atoms display similar properties. Incorporation was compared to adsorption, both in terms of the energetics of the structures and the barriers to their formation, because the two processes will be competing against each other. In addition, the effect of charging the resulting Bi-Si heterodimers has been investigated, in a similar manner to the work performed by Radny *et al.* [30]. Subsurface interstitial Bi were also briefly studied, but only preliminary results will be presented here.

5.1 Results and Discussion

5.1.1 Adatoms

The adsorption sites for a single Bi adatom on the Si(001) c(4×2) and p(2×2) reconstructions have been investigated by optimising the atomic structure of the system for multiple different starting geometries. Seven adsorption sites were found as shown in Figure 5.1. Five of these correspond to structures from previous work for single Bi adsorbates on the Si(001) surface, namely B, D, H, M [19, 107] and C [57]. The remaining two, T and U, were identified in this work. Adsorption energies have been calculated for each site and are shown in Table 5.1, which will be discussed in more detail later.

These sites can be split into two types, the on-row sites and the in-trench sites. The former includes the D, H, M, T and U sites, the latter the B and C sites. The energies for all these structures are presented later in Table 5.1. Since the c(4×2) and p(2×2) reconstructions are identical when

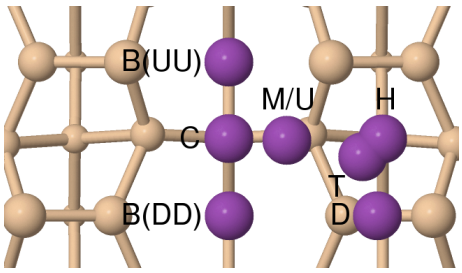

Figure 5.1: Top view of positions of adatom sites investigated on the c(4×2) surface. The letters indicate the label given to the sites in this section. The M and U sites cannot be easily distinguished from a top view. Silicon is shown in beige and bismuth in purple. Atom sizes are scaled with height and only the first 4 layers are shown for clarity.

looking at a single row, the on-row sites will be the same for both reconstructions, which was confirmed by initial calculations, whereas the in-trench sites will be affected by the different dimer arrangements across the rows. For the p(2×2) reconstruction the dimer ends are always paired as an up and a down atom across the trench, whereas for the c(4×2) reconstruction they can either be two up atoms or two down atoms. At all sites the Bi adatom only had a significant effect on the geometry of the dimers it was directly bonded to. I now discuss the structure, properties and energetics of these adsorption sites in detail, looking at the in-trench sites, the on-row sites, their energies, spin, and the local density of states (LDOS) for the Bi adatom. Comparisons are later drawn with similar, but smaller, Group V atoms, such as P and As.

In-trench sites

Site B is the bridge site between the ends of two dimers across the trench between rows, as shown in Figure 5.2. Both B sites are identical for the p(2×2) reconstruction, but for the c(4×2) reconstruction there are two types, which have been labelled B(UU) and B(DD) due to the pairing of the surrounding Si dimer atoms. In these two cases the Bi bonds to two Si atoms, but look significantly different due to the position of the Si atoms. The Bi-Si bond lengths are very similar (2.88 Å and 2.86 Å respectively) but the B(UU) site has a much sharper Si-Bi-Si bond angle of 107.3°, whereas at the B(DD) site it is nearly flat from one Si to the other with a bond angle of 170.4°. For the B(DD) structure both Si dimers which are bonded to the Bi are lengthened by 0.04 Å, whereas for the B(UU) they are lengthened by 0.08 Å. On the p(2×2) surface the Bi atom lies closer to the down atom (2.63 Å) than the up atom (3.18 Å), and lengthens the former Si dimer by 0.05 Å without changing the length of the latter. The bond to the up atom is only very weak. The Si-Bi-Si bond angle lies between those for the c(4×2) reconstruction structures at 133.8°.

Site C (not illustrated due to smaller adsorption energies) is the centre site in the middle of the trench, which bonds weakly to the two surrounding up atoms. Due to the differences in buckling of the surface dimers the C site looks different for the two surface reconstructions. For the p(2×2) reconstruction the up Si lie diagonally across from one another, meaning the Bi bonds in a diagonal line across the trench. For the c(4×2) reconstruction, the Si pair up across the trench in either down or up pairs, with the Bi bonding to the up pair, and thus lying slightly off centre. In both cases the four surrounding Si dimers are lengthened, those the Bi is bonded to by 0.06 Å, those it does not

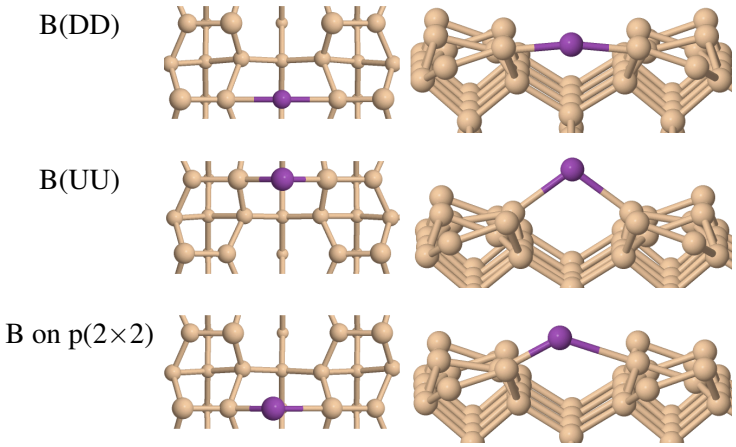

Figure 5.2: Top and side views of the B(DD) and B(UU) sites for the c(4×2) reconstruction and the B site for the p(2×2) reconstruction.

bond to by 0.09 Å.

On-row sites

Site D is located above a Si dimer, as shown in Figure 5.3. The Bi is bonded to both Si atoms in the dimer, nearly flattening it and lengthening it by 0.01 Å. Since the dimer is not completely flat the bonds to the formerly up atoms are slightly shorter (2.69 Å) than those to the formerly down atoms (2.71 Å). At site T the Bi is three-fold coordinated, bonding to three surrounding Si atoms, as shown in Figure 5.3, which has also been identified via calculations for Group III adatoms [19]. The Bi bonds with two up atoms (2.94 Å and 2.86 Å respectively), and one down atom (2.75 Å). The surrounding dimers were flattened slightly, but their bond lengths were unchanged to within 0.01 Å.

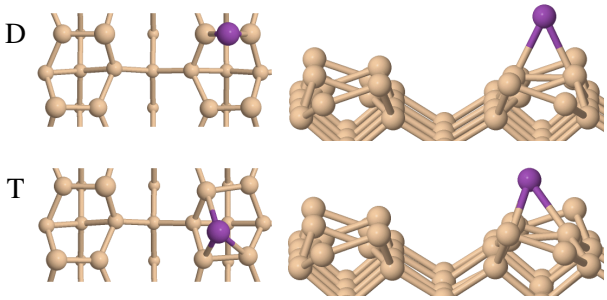

Figure 5.3: Top and side views of the D and T sites.

Site H is the pedestal site located between two dimers within a row. Here the Bi bonds to four surrounding Si atoms and partly flattens both surrounding dimers, as shown in Figure 5.4. As with the D site, bonds with the formerly up atoms are shorter (2.88 Å compared to 2.94 Å). The Si dimers directly attached to the Bi are lengthened by 0.05 Å.

Sites M and U are very similar to each other, both being inter-dimer sites located above a second layer Si and between the ends of dimers within a row as shown in Figure 5.5. The main difference between the two is the height at which the Bi lies above the surface. The M site lies 2.77 Å above the second layer Si, whereas the U site is 3.26 Å above it. At the M site the Bi bonds

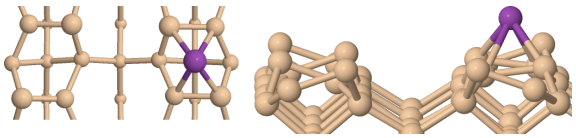

Figure 5.4: Top and side views of the H site.

to three Si atoms, two dimer ends and the second layer Si directly below it, whereas at the U site the Bi only bonds to the two dimer ends. This conclusion was drawn by making a comparison between the charge densities of the two structures, imaged at the same isosurface values, as shown in Figure 5.6. For the U structure there is a small region of no charge density between the Bi and the subsurface Si, suggesting no bonding, whereas this is not true for the M site. A similar conclusion could be drawn from the fact that the U site is spin active, with one unpaired electron, and thus can only be forming two bonds, as opposed to the M site where this is not the case. This will be explored properly in the next section. At both sites the bond to the formerly up atom is shorter than that to the formerly down atom and at the M site the bond to the second layer Si is the longest. At the M site the Si dimer at the down end is shortened by 0.02 Å and the dimer at the up end is lengthened by 0.04 Å, whereas for the U site the former dimer is unchanged, whilst the latter is lengthened by 0.07 Å. The U site is similar to the elevated end bridge structure seen during P diffusion on the same surface [20].

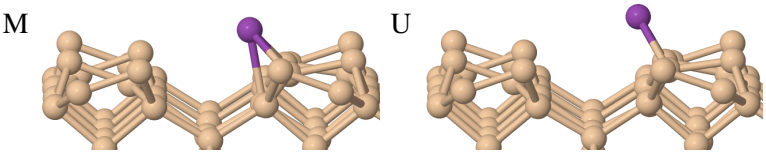

Figure 5.5: Side view of the M and U sites.

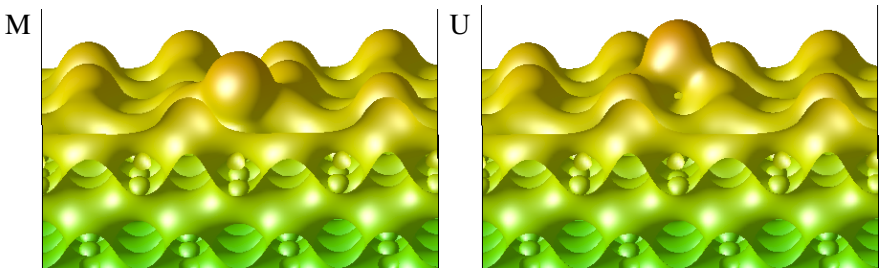

Figure 5.6: Charge density for M and U sites, where the raised feature is the Bi adatom. For the U site there is a slight gap in the charge density between the Bi adatom and the Si atom directly below it, which is not present for the M site. The charge densities are generated for an isosurface value of 0.18 e^{-}/Å^{3}.

Adsorption energies and spin

Results where the overall spin on the adsorbed system is fixed to either zero or $\frac{1}{2}$ are presented in Table 5.1. Given that there are an odd number of electrons in the system, it would be expected that all of the structures should have an overall spin of $\frac{1}{2}$, localised on either the Bi atom or one of the

surface Si atoms. However, when no restrictions were placed on the overall spin of the system, results with an overall spin of either 0 or $\frac{1}{2}$ were found, depending on the structure being studied. For example, with Bi at the D site, the overall spin would be $\frac{1}{2}$, whilst if the Bi was at the H site it would be zero. A possible explanation for this behaviour is that when calculations indicated a net spin of zero, VASP has delocalised the final electron over the entire system. Forcing an overall spin of $\frac{1}{2}$ on all of the structures was done to obtain results with the expected overall spin. Zero overall spin results were obtained for all of the structures to allow a proper comparison between the two spin configurations. In both cases E_{ads} is calculated with regards to the same E_{system} and E_{Bi}. The p(2×2) on-row structures are the same as the c(4×2) structures, and therefore they are not shown.

Table 5.1: Adsorption energies of the different Bi adsorption sites on both the c(4×2) and p(2×2) reconstructed surfaces, with overall spin fixed to 0 and $\frac{1}{2}$.

	Spin (μ_B)	
	0	$\frac{1}{2}$
Site	E_{ads} (eV)	E_{ads} (eV)
c(4×2)		
B(DD)	-1.23	-1.20
B(UU)	-1.76	-1.84
C	-1.31	-1.30
D	-2.45	-2.61
H	-2.44	-2.40
M	-2.53	-2.49
T	-2.62	-2.59
U	-2.24	-2.38
p(2×2)		
B	-1.40	-1.55
C	-1.43	-1.47

On-row sites have a larger adsorption energy than the in-trench sites, by more than 1 eV in some cases. Spin makes little difference to the geometries of the different structures, but plays an important role in determining the energies. For the B(UU), D, U and p(2×2) B and C sites, having an overall spin of $\frac{1}{2}$ is more energetically favourable. For every other adsorption site, forcing a spin of $\frac{1}{2}$ on the system reduces the adsorption energy compared to no overall spin. As Figure 5.7 shows, for the B(UU), D and U sites there is a localised spin on the Bi adatom, whereas some of the other structures displayed a localised spin on one of the Si atoms, if at all. The behaviour of the B(UU), D and U sites is of interest for spintronics. The common feature for these three sites is the fact that the Bi is twofold coordinated, whereas for most other sites the Bi is threefold coordinated or more. Bi has three 6p electrons which could participate in bonding, so it makes sense that sites where the Bi is twofold coordinated would show spin on the Bi atom itself, due to the one remaining unpaired 6p electron. This is supported by the shape of the spin difference density in Figure 5.7, which resemble p-orbitals. It would therefore make sense that in cases where the Bi is

threefold coordinated, such as the T site, that there would be no spin on the Bi atom.

Structures where the Bi is twofold coordinated with bond angles near 90° show spin, and this arises due to the natural Bi bonding being p^3 rather than sp^3 [24]. The importance of the bond angle is demonstrated by the B(DD) structure where no spin is more energetically favourable than $\frac{1}{2}$ spin, despite being twofold coordinated. In the latter case the spin is split between the Bi atom and the two Si atoms it is directly bonded to. This change in electronic structure can be explained by the change in hybridisation due to the much larger Si-Bi-Si bond angle of 170.4°. The D site is unusual in that the bond angle is only 52.2° and yet it shows spin on the Bi.

Using the D site as a test case I determined that spin-orbit coupling does not have a significant impact on the energetics of these structures. This was done by including the LSORBIT and SAXIS tags in the VASP input files, which allow the inclusion of spin-orbit coupling, and set the quantisation axes for spin respectively. The largest energy difference observed was only 3 meV, comparing the field aligned along the x direction and the z direction.

There is little agreement between the results of this work and those previously obtained [23]. The previous work used an atomic cluster model featuring flat dimers, which do not represent the real structure, and most of the differences can be attributed to this fact. There is disagreement in the ordering of the sites in terms of adsorption energy and significant quantitative differences in calculated adsorption energies for all but the H site. The difference in geometries between the flat and buckled surfaces alters how favourable certain sites are, especially for those bridging the trench. This may explain the large differences seen for the B and C sites and why the structures such as the T site were not investigated previously.

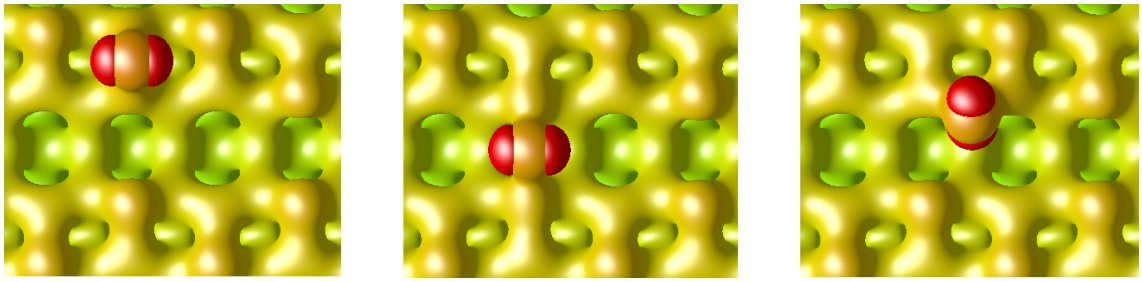

Figure 5.7: Spin density difference and charge density for a Bi at the D (left), B(UU) (middle) and U (right) sites, showing an unpaired electron on the Bi atom. Spin up is indicated in red, with the charge density shown in green/yellow, with the colour difference due to height. The dimer rows run from left to right. The charge densities are generated for an isosurface values of 0.18 e^-/Å^3, and spin density differences for isosurface values of $\pm$0.028 e^-/Å^3. The same settings are used throughout this work.

DFT is likely to predict the sites where a single unpaired electron is on the Bi to be less stable than they actually are due to the self interaction problem. There are several methods for addressing this problem, such as including exact exchange, using DFT+U or SIC. However all of these solutions require some degree of empiricism and the only effect that these would have would be to make these structures even more stable.

Local Density of States for the Bi atom

By analysing the spd-orbital decomposed density of states (DOS) for the Bi adatoms at the different sites, as demonstrated in Figures 5.8 and 5.9, information on the nature of their bonding can be obtained. These were obtained by the standard VASP projection based on PAWs. There are some general trends in Bi bonding shared across all adsorption sites, but there are also some striking differences between sites with and without an unpaired electron, such as the D and H sites respectively. The s states are mostly populated at energies 10 to 12 eV below the Fermi energy (E_F) with only small populations close to or above E_F. This shows that the s states of the Bi play little role in the bonding process. For structures without an unpaired electron these s states are sharper and deeper, lying closer to 12 eV below E_F, whilst those with an unpaired electron are usually more spread out and closer to 11 eV below E_F.

For the p states the largest populations are around E_F, showing that it is mainly the p electrons that participate in bonding. For those structures where there is an unpaired electron on the Bi atom there is a sharp peak in the spin majority DOS just below E_F, and a sharp peak in the spin minority DOS just above E_F, indicating that the unpaired electron is in a p orbital. As such the B(UU), D and U sites all have a similar DOS. For the D site specifically, the splitting between these peaks is about 0.7 eV as demonstrated in Figure 5.10. The difference between the spin components indicates a split state, with an empty state that could be tunelled into. If the majority spin is assumed to be up, then this empty state is for the down spin electron that would be paired with the currently unpaired electron on the Bi atom. The spin splitting seen in the D site DOS indicates that there is a single p orbital that cannot be involved in bonding, meaning the bonding is either sp^2 or p^3. Given the depth of the s orbital, p^3 bonding is likely to be stronger. Since the H site Bi does not have an unpaired electron, the spin majority and minority DOS are the same, with no signs of the spin splitting observed for the D site.

A similar difference is observed between the M and U site DOS, despite the fact that the main structural difference between the two is the height of the Bi adatom above the surface. This confirms the assessment made earlier that the two structures have different bonding. The M site has s states that are 1 eV deeper, whilst the U site has more populated p states around E_F and shows the spin splitting characteristic of an unpaired electron.

Comparison to P and As

Given that for some adsorption sites Bi adatoms have an unpaired spin, it would be interesting to know if the same is true for lighter Group V atoms such as P or As. Rather than repeat the entire investigation, only those adsorption sites where the Bi had an unpaired electron and large adsorption energies were chosen, namely the D and U sites. The B sites were excluded due to lower adsorption energies. Structures such as the T or H sites, which did not show an unpaired electron on the Bi atom were not investigated, due to the expectation that this would still be true for smaller atoms. There were difficulties obtaining the U site, with the structures always relaxing to the M site instead. This meant that structures with an unpaired electron on the P or As could not be found on this region of the surface. As with the Bi, both spin zero and spin $\frac{1}{2}$ configurations were investigated, with the energy differences presented in Table 5.2.

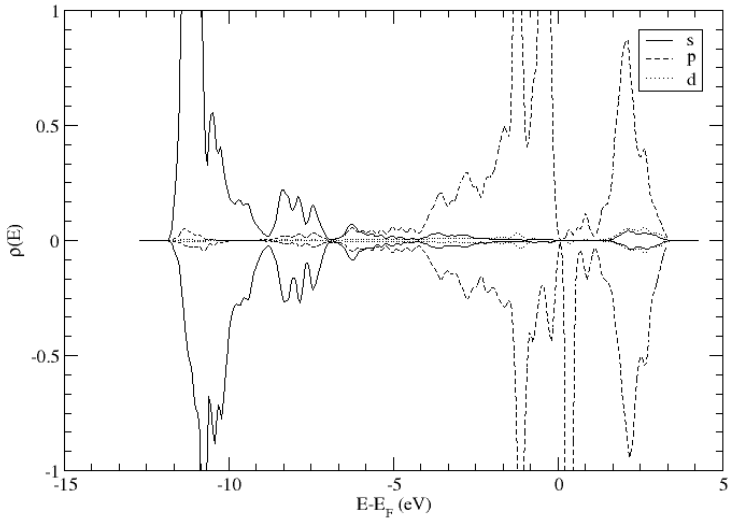

Figure 5.8: spd-orbital decomposed density of states (DOS) plots for the D site Bi atom, with an unpaired electron on the Bi atom. Plots are scaled to the same height to allow for direct comparison between this and Figure 5.9. The unbroken lines are s orbitals, dashed are p orbitals and dotted are d orbitals. The spin majority DOS are plotted on the positive $\rho(E)$ axis, the spin minority on the negative. The energy scale given along the x axis is in terms of E-E_F, such that the zero of the x axis is at E_F.

Table 5.2: Energy difference (ΔE) between spin 0 and spin $\frac{1}{2}$ configurations for Group V adatoms on the Si(001) surface at the D and M sites. A negative ΔE indicates that the spin $\frac{1}{2}$ configuration is lower in energy, whilst a positive energy indicates that the spin 0 configuration is lower in energy.

Adatom species	Site	ΔE (eV)
P	D	-0.007
	M	+0.014
As	D	-0.100
	M	+0.032
Bi	D	-0.158
	M	+0.040

For P there is very little difference in energies between the structures without any overall spin and those with. For the D site the energies are practically indistinguishable, although with spin is marginally more energetically favourable by 7 meV. For the M site no overall spin is most energetically favourable by 14 meV. Neither of these values are significant in DFT terms. At the D site there is some spin on the P atom, but it also appears to be shared with some of the subsurface Si. In addition, the two p-orbital like shapes seen in the spin difference density for the Bi adatoms are not present. Examining the spin population reveals several partly occupied bands for both

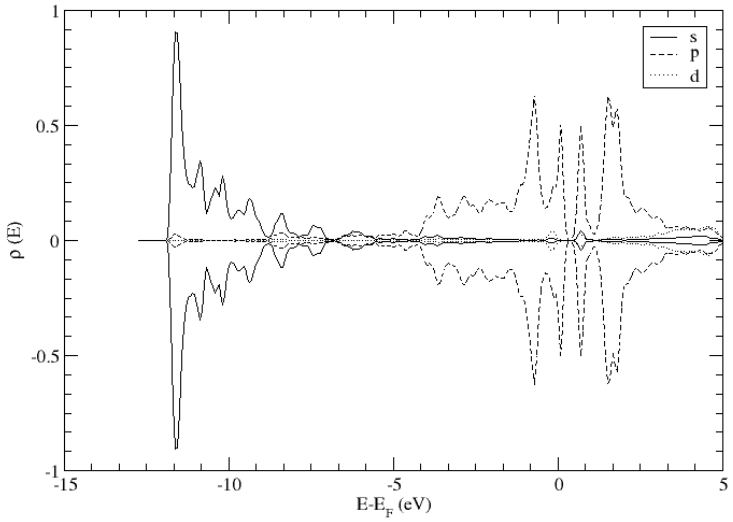

Figure 5.9: spd-orbital decomposed density of states (DOS) plots for the H site Bi atom. Plots are scaled to the same height to allow for direct comparison between this and Figure 5.8. The unbroken lines are s orbitals, dashed are p orbitals and dotted are d orbitals. The spin majority DOS are plotted on the positive $\rho(E)$ axis, the spin minority on the negative. The energy scale given along the x axis is in terms of E-E$_F$, such that the zero of the x axis is at E$_F$.

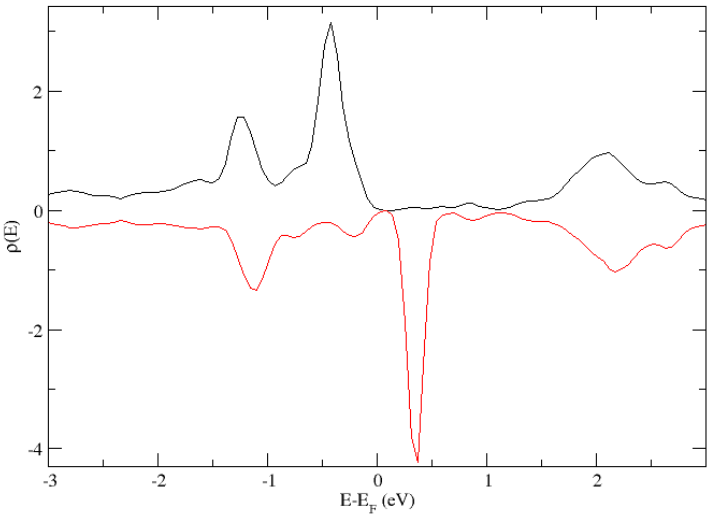

Figure 5.10: LDOS for a Bi adatom at the D site. The black line represents the majority spin channel and the red line represents the minority spin channel. The energy scale given along the x axis is in terms of E-E$_F$, such that the zero of the x axis is at E$_F$.

the spin up and down components, in comparison to the Bi structure where there are no partly occupied bands. This may explain why the spin is not localised on the P atom. At the M site,

when there is spin, it is located on the down Si atom at the other end of the dimers the P bonds to, and not the P atom itself.

For As there is a greater energy difference between those structures with and without spin. At the D site the structure with spin is 0.1 eV more energetically favourable than without, whilst at the M site the structure without spin is more energetically favourable by 0.03 eV. At the D site the spin difference density shows a p-orbital like shape on the As atom in the same manner as on the Bi atom, and as with Bi there are no partly occupied bands. At the M site, when there is spin, it is located on a down Si atom.

These results show that the U site is even harder to obtain with smaller Group V atoms, narrowing the choices of potential adsorption sites with spin localised on the adsorbate atom. If it is assumed that the energy differences between the in-trench and on-row sites is similar to the Bi case, this leaves only the D site as a suitable candidate. Given the difficulties with obtaining the U site, even for Bi, it is probably not worth the effort to pursue this further. These results also show that adatoms smaller than Bi still have a localised spin when adsorbed at the D site, however this behaviour is different for P, where it appears to be delocalised over the P atom and several Si.

5.1.2 Diffusion

Diffusion of the Bi atoms can either occur on the dimer rows or in the trench. In both cases the Bi can either diffuse parallel or perpendicular to the direction of the dimer row. For diffusion on the rows, both reconstructions are considered the same, so only the c(4×2) reconstruction is investigated. For diffusion through the trench both the c(4×2) and p(2×2) reconstructions are investigated. A brief discussion of diffusion rates is presented at the end.

Diffusion on the dimer rows

The route from one D site to another involves diffusion from a D site to the nearest T site, through the H site to the opposite T site before reaching the next D site along the row, as shown in Figure 5.11. The activation energy for diffusion from a D site to a T site is 0.07 eV and 0.09 eV in the reverse direction. The H site was revealed to be a metastable intermediate between two T sites, as such an activation energy of 0.18 eV is required to move between T sites. The limiting step for diffusion along the rows is therefore diffusing between the T sites.

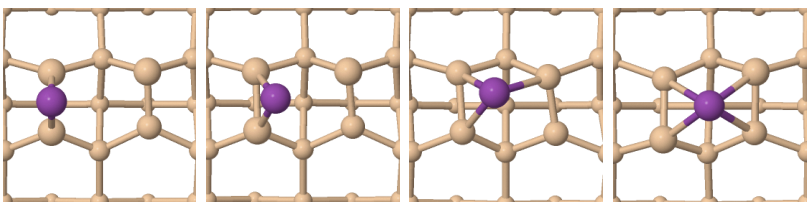

D Site	Transition State	T Site	H Site
0.00 eV	+0.07 eV	-0.02 eV	+0.16 eV

Figure 5.11: Diffusion pathway from the D site (far left) to the H (far right). The energies given are relative to the D site. The H site is a transition state between two T sites on opposite corners of the 2 dimer block. The dimer row runs from left to right.

Diffusion across the rows, between the sites which lie on the edge of the row and those in the centre, as shown in Figure 5.12, was investigated to find out whether the Bi was more likely to move towards the trench or stay in the middle of the dimer rows. Diffusion from the M site to the T site showed subtleties related to spin. The U site with zero magnetic moment appeared as an intermediate on the path, which is 0.13 eV less stable than the U site with spin $\frac{1}{2}$. Clearly small changes in bonding can have a strong effect on the spin state of the Bi. There was a 0.29 eV activation energy for moving from M to T and a 0.37 eV activation energy moving in the reverse direction. Diffusion away from the trench is therefore easier than diffusion towards the trench. Diffusion to all other on-row sites had to go via the T site first.

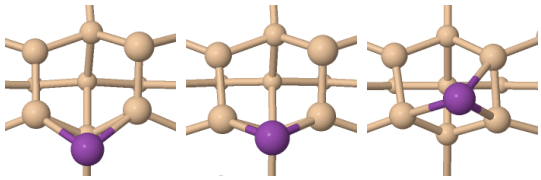

M Site	U Site	T Site
0.00 eV	+0.29 eV	-0.08 eV

Figure 5.12: Diffusion pathway from the M site (left) to the T site (right). The energies given are relative to the M site. The intermediate U site does not have spin on the Bi atom. The dimer row runs from left to right.

Diffusion through the trench

Diffusion in the trench can either occur across or along the trench. For diffusion across the trench several different routes were considered. The starting point was either taken to be a D or M site and the end point was considered to be a B, C or M site, with the M site on the opposite end of the trench. Since the B site is not symmetric on the p(2×2) reconstruction, diffusion from both sides of the trench must be considered.

For the c(4×2) reconstruction diffusion from a D site to a B(UU) site is in a straight line between the two sites, with the Bi moving through intermediate structures where it is only bonded to a single Si. This has an activation energy of 1.32 eV whereas the reverse process has an activation energy of 0.55 eV. Diffusion between the D and B(DD) sites goes via an M site first. The B(DD) site was revealed to be a metastable intermediate between two M sites, as such an activation energy of 1.30 eV is required to reach the B(DD) site. Diffusion between the M site and the B(UU), as shown in Figure 5.13, is via an intermediate minimum with nearly the same energy as the B(UU) site. Here, the Bi is out of line with the up atoms, parallel to the direction of the trench. The activation energy for the first step is 0.71 eV, whereas the reverse is only 0.04 eV. The activation energy for diffusion between the intermediate and the B(UU) site is only 0.02 eV. Finally, the C site is shown to be a metastable intermediate with an activation energy of 1.22 eV coming from the M site. These activation energies show that for diffusion between the rows the route between two M sites via the B(UU) site would be most favourable due to its lower activation energy, and that diffusion out of the trench is more favourable than diffusion into the trench. A calculation of the full M to M diffusion path confirmed this, and found the Bi to diffuse via the intermediate

minimum in Figure 5.13, bypassing the B(UU) site.

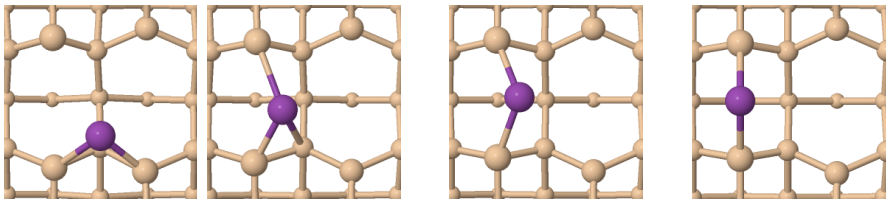

M Site	Transition State	Intermediate Minimum	B(UU) Site
0.00 eV	+0.71 eV	+0.67 eV	+0.69 eV

Figure 5.13: Diffusion pathway across the trench from an M site (left) to the B(UU) site (right). The trench runs from left to right. The energies given are relative to the M site. The route up to the third image also serves as the diffusion pathway across the trench between two M sites.

For the p(2×2) reconstruction, diffusion between the rows is complicated by the fact the in-trench sites are asymmetric, however this has little overall effect on the diffusion pathways across the trench. As with the c(4×2) reconstruction the pathway with the lowest activation barrier lies between the B and C sites, and is higher in energy at 0.84 eV.

Diffusion along the trench will occur in a similar manner to across the trench, going via the M and B sites. This is because the C site lies higher in energy than the intermediate on the M to B path, so diffusion down the centre of the trench will have a higher energy barrier than diffusion between adjacent M sites.

Diffusion rates

Diffusion along the rows is much faster than diffusion between the rows. For example, at 300 K diffusion between the on-row sites have rates ranging from $10^{6}\ s^{-1}$ to $10^{11}\ s^{-1}$ whereas the diffusion rate for the most favourable route across the trench is only of order 10 s^{-1}. To observe Bi adatoms, diffusion would need to be suppressed. Cooling to below 20 K would be required to reduce all diffusion rates to at least $10^{-5}\ s^{-1}$ (of the order of 1 per day) and allow the use of these structures experimentally, with further cooling needed for use in devices.

5.1.3 Ad-dimers

Most observations of high coverages of Bi on Si(001) show dimers [9]. The relative stabilities of dimers compared to adatoms was therefore calculated. Four different ad-dimer structures were studied, here labelled DD, UU, BB and MM, as shown in Figure 5.14, indicating the location of the two adatoms in relation to the adatom sites used. Other configurations were not considered on the basis of stability and in light of experimental observations. The adsorption energy per Bi atom for each structure is presented in Table 5.3. In all cases the structures had no overall spin, because both Bi atoms are threefold coordinated.

In line with experimental observations, and following chemical intuition, ad-dimer structures were found to be more energetically favourable than two adatoms at equivalent sites. The DD ad-dimer is the most energetically favourable, as found previously [23, 24]. The diffusion rates for Bi adatoms indicate that dimers would preferentially form on rows, though MM dimers might

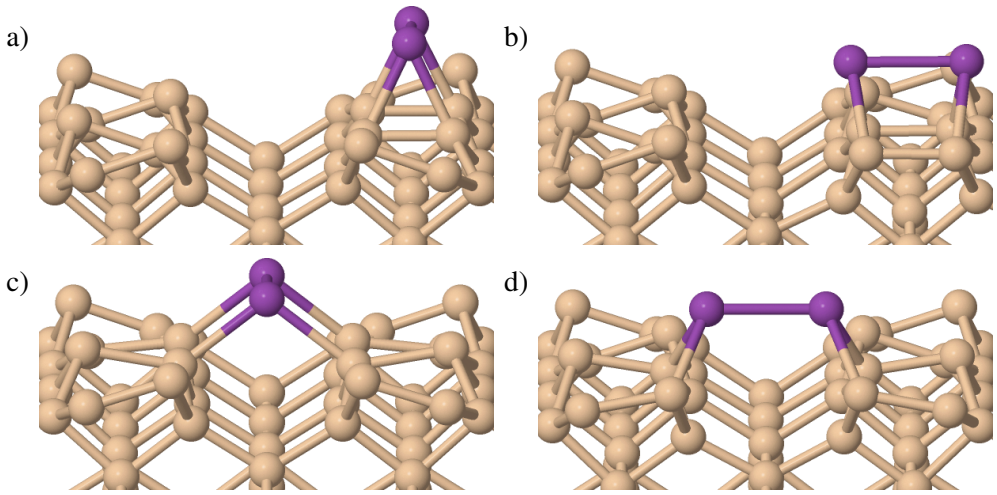

Figure 5.14: Bi ad-dimers on the Si(001) c(4×2) surface, a) dimer at DD position, b) dimer at UU position, c) dimer at BB position, d) dimer at MM position.

Table 5.3: Adsorption energies per Bi atom for Bi ad-dimers on the c(4×2) Si(001) surface, labelled as in figure 5.14.

Ad-dimer	E_{ads}/Bi atom(eV)
DD	-3.38
UU	-3.24
MM	-2.88
BB	-2.85

form if two Bi atoms on adjacent rows bonded. This means that two Bi adatoms on the Si(001) surface would form an ad-dimer rather than remain as two separated adatoms, given temperatures above 20 K and enough time. Given the improvements in adsorption energy compared to single adatoms, and the very low energy barriers for diffusion of single adatoms on the clean surface, it was decided that investigation into this process was not necessary. Energy barriers to formation are expected to be lower, or at worst the same, as diffusion on the surface. For example, the DD dimer formed spontaneously from two Bi adatoms placed at neighbouring D sites.

5.1.4 Substitution

One way for Bi to incorporate into the surface is via substitution into the Si dimers, forming Bi-Si heterodimers. The different possible structures for these heterodimers, and the effect of charge accumulation on them has been investigated, in a similar manner to work that has already been performed for P and As heterodimers [30]. Following on from this, the energy barriers to their formation have been investigated, alongside studying the energetics of the Si that will be ejected during the incorporation process.

Structures

When Bi substitutes into the Si surface it can form one of two structures, depending on the buckling of the Bi-Si heterodimer relative to the Si dimers directly neighbouring it. These two structures

are known as HD1, where the heterodimer is in phase with the Si dimers, and HD2, where it is out of phase with the Si dimers. Examples of both of these structures are shown in Figure 5.15. For now, the ejected Si will be treated as completely removed from the surface, in order to simplify studying the heterodimers.

For both types of heterodimer, the Bi atom is up buckled, with the Si atom down buckled. The same behaviour has been observed for other Group V heterodimers [30], and is attributed to the fact that the Bi atom retains a lone pair. Comparing the energetics of the two structures reveals that the HD2 structure is 0.08 eV more energetically favourable than the HD1 structure. This is in general agreement with results seen for P and As heterodimers, however the energy difference observed here is smaller. Radny *et al.* [30] found that for both P and As, the HD2 structure was 0.14 eV more energetically favourable, and that even with regular Si dimers this difference was 0.09 eV. Given the small energy differences involved the slightly lower value for the Bi-Si heterodimers should not be of too much concern, since all the values are of the same order of magnitude. The reason that the HD1 structure is higher in energy than the HD2 structure is because it breaks the pattern of alternately buckled surface dimers.

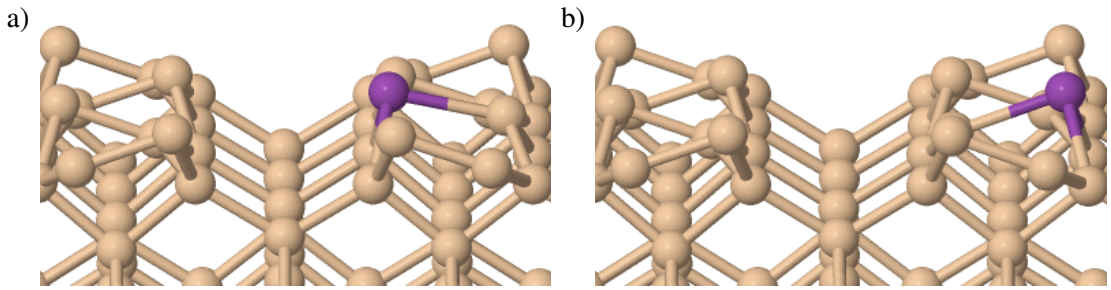

Figure 5.15: Structural models where a Bi atom has substituted for a surface Si atom, forming a Bi-Si heterodimer. a) HD1 structure, with the heterodimer in phase with the neighbouring Si dimers. b) HD2 structure, with the heterodimer out of phase with the neighbouring Si dimers. For the HD1 structure, the alternating buckling pattern of the surface dimers has been broken.

It has previously been shown that charge accumulation on the surface, such as could happen when imaging it with an STM tip, has a significant effect on the buckling of the heterodimer in the HD1 structure, but relatively little effect on the HD2 structure [30]. With increased charge accumulation, the HD1 heterodimer will invert its buckling, such that the Si atom becomes up buckled and the Group V atom down buckled, thus restoring the regular buckling pattern of the surface. The HD2 heterodimer barely changes. To test whether this still held true for the Bi-Si heterodimer, calculations for the HD1 and HD2 structures were repeated, but with one or two added electrons. The results of these calculations are presented in Table 5.4, alongside those for P and As for comparison. Energies produced in VASP for charged systems are not meaningful, so energy comparisons of the two arrangements cannot be made.

The HD2 Bi-Si heterodimer is barely affected by charge accumulation, a result which is consistent with the other Group V heterodimers. When a single electron is added to the HD1 structure the buckling angle of the heterodimer is greatly reduced, such that it is almost flat. This replicates results seen for both the P- and As-Si heterodimers. However, the Bi-Si results differ from previous results when a second electron is added. Whereas the P- and As-Si heterodimers show a

Table 5.4: Bond lengths (L) and buckling angles (θ) for Group V-Si heterodimers in cells with additional electrons. N_e indicates the regular cell, whilst N_e+1 and N_e+2 are 1 and 2 additional electrons respectively. The data for P and As is from [30]. It should be noted that charged HD2 structures could not be fully relaxed for Bi, so the results are presented for forces of 0.05 eV/Å (N_e+1) and 0.06 eV/Å (N_e+2). Where θ is negative this means that the orientation of the buckling has reversed compared to the uncharged system.

		N_e		N_e+1		N_e+2	
Atom species	Structure	L (Å)	θ (°)	L (Å)	θ (°)	L (Å)	θ (°)
P	HD1	2.26	14.6	2.33	3.2	2.42	-5.7
	HD2	2.30	15.5	2.30	15.7	2.29	15.8
As	HD1	2.40	17.6	2.46	6.4	2.56	-2.5
	HD2	2.44	18.4	2.43	18.3	2.42	18.0
Bi	HD1	2.76	11.7	2.83	4.3	2.84	4.0
	HD2	2.73	19.4	2.71	20.3	2.70	18.5

reversal of the dimer buckling, with the Si atom very slightly buckled upwards compared to the Group V atom, the Bi-Si heterodimer remains in its original orientation, and barely changes from the result for a single added electron. This difference could be explained by the relative size of the Bi atom compared to the smaller P and As atoms. Due to its large size there will be a more significant energy barrier to pushing the Bi atom down relative to the Si atom.

In order to make meaningful comparisons between the energies of the heterodimer structures and the adatom structures, it is necessary to consider cells with the same number of atoms. To do this, the ejected Si was then treated as an adatom near the Bi-Si heterodimer, as if it had only just been removed from the dimer. The ejected Si was considered to stay adsorbed at the M site near the Bi, as shown in Figure 5.16, since this is the most energetically favourable position for a Si adatom on the clean Si(001) surface [108] and is close to its original position within the Si dimer. These structures will also be important for studying the incorporation process for the Bi atom, because the start and end points will need to have the same number of atoms.

Surprisingly the HD1 structure with Si at a nearby M site was found to be 0.07 eV more energetically favourable than the HD2 structure, which could be due to how the ejected Si affects the surrounding Si dimers. The HD2 and HD1 substitutions were -1.96 eV and -2.03 eV lower in energy than the Si(001) surface and an atomic Bi, which is worse than all of the on-row adatom sites, such as the T site, with an energy difference of -2.62 eV, but better than the in-trench sites. In many cases Bi atoms will preferably adsorb on, rather than incorporate into the Si(001) surface.

Energy barriers

Having determined that it is possible for Bi to substitute into the Si(001) surface, the energy barriers to forming these structures were examined, for comparison to surface diffusion. Based on the energies of the end structures alone, the substituted structures are less likely than the adatom structures, but the barriers would give a proper measure of how less likely. Bi adatoms at either the D or M sites were considered as starting points for the substitution whilst the structures from

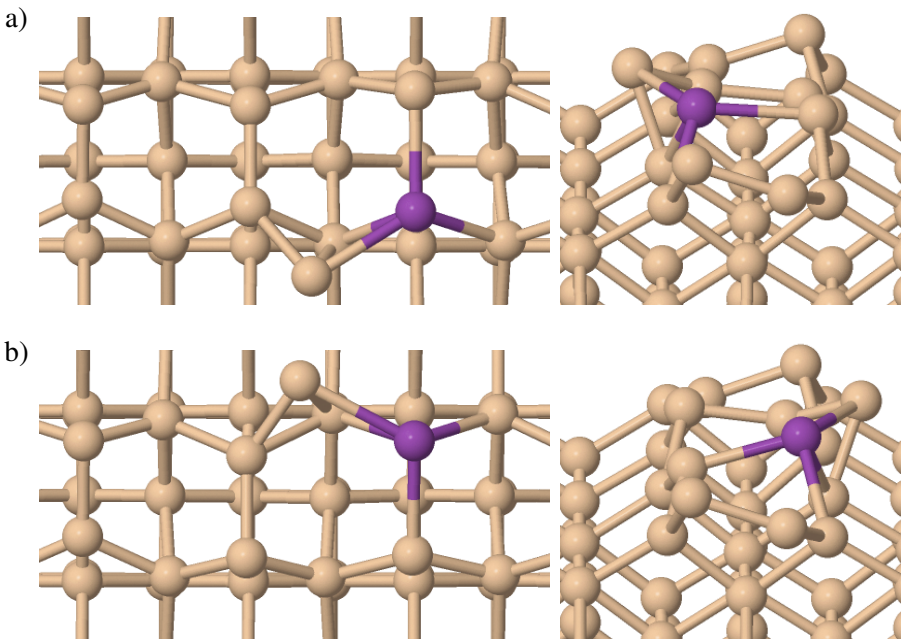

Figure 5.16: Structural models of Bi substituted into the Si(001) surface, with the ejected Si adsorbed at a nearby M site. a) HD1. b) HD2.

Figure 5.16 were chosen as end points. Using these structures and the CINEB method the energy barriers for substitution were investigated. Activation energies for the respective routes are given in Table 5.5.

Table 5.5: Activation energies for substitution of a Bi adatom for either an up or a down Si dimer atom from both D and M adsorption sites

Heterodimer	Starting site	$E_A(eV)$
HD1	D	1.65
	M	1.33
HD2	D	1.58
	M	1.44

Regardless of the end structure, substitution from the M site has a lower activation energy than substitution from the D site, making this a better starting position for substitution. In addition, the energy difference between these two routes is greater than the energy difference between the two starting structures, indicating that the two routes do not have a common intermediate. When looking at substitution from the M or D sites individually, the end point has an effect on the barrier heights. Substitution from the D site has a lower barrier for the HD2 structure, whereas substitution from the M site has a lower barrier for the HD1 structure. All of these barriers are larger than those for diffusion of the adatoms on the surface, and significantly so compared to the on-row diffusion. Bi adatoms are much more likely to diffuse along the surface than incorporate into it.

This process has previously been studied for P [20], so it is helpful to compare the two results. Since P incorporation was considered for flat Si dimers, a distinction between the HD1 and HD2

structures was not made. To allow for the comparisons made here, it is assumed that the dimer buckling will have relatively little effect on the activation energies for incorporation, at least compared to their magnitude. For P, it was found that incorporation from the M site had an activation energy of 1.55 eV, whilst for the D site it was 1.24 eV. Thus meaning the D site is a better starting position for incorporation than the M site, the opposite of what is observed here for Bi. This difference is likely attributed to the fact that for P, the M site is lower in energy than the D site, whilst for Bi the D site is lower in energy. Whilst the competing incorporation processes do not have a common intermediate it is to be expected that incorporation from the lower energy starting point would require more energy.

Despite the difference in starting position, the lowest energy barriers that must be overcome to incorporate into the surface are remarkably similar for P and Bi. There is only a 0.09 eV difference between the lowest incorporation barriers for P and Bi, with the barrier for Bi being slightly larger. Bi and P are thus expected to incorporate at roughly the same rate.

Further studies of the ejected Si atom

Since the final structures are all higher in energy than the initial structures, the barriers for the Si atoms to substitute back into the surface will be lower than those for the initial Bi substitution, suggesting that process will be quickly reversed. However, the Si atom could instead diffuse out into the rest of the surface, to more energetically favourable positions. With this in mind, and following the ideas put forward by Bennett *et al.* [20] when studying the P-Si heterodimer, a variety of different adsorption sites for the ejected Si were investigated as shown in Figure 5.17. The energetics of these structures are presented in Table 5.6. Primarily the D and M sites were investigated because these are favourable sites for Si adatoms on the Si(001) surface. A complete analysis of adsorption sites for the ejected Si was not deemed necessary.

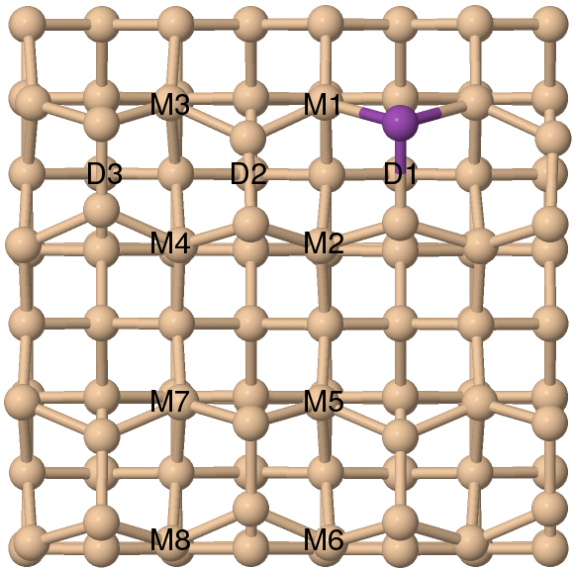

Figure 5.17: Adsorption sites for ejected Si after Bi substitution. Here the HD2 heterodimer is shown, but labelling is the same for the HD1 heterodimer, just the position of the Bi changes.

Comparing these energies to those in Table 5.1 shows that in most cases the Bi adatom struc-

Table 5.6: Energies of structures with a Bi-Si heterodimer and the ejected Si as an adatom. These are compared to the clean Si(001) surface and an atomic Bismuth (ΔE). The sites are labelled as in Figure 5.17.

Site of ejected Si	ΔE (eV)	ΔE (eV)
	HD2	HD1
M1	-1.96	-2.64
M2	-2.02	-2.03
M3	-2.65	-2.45
M4	-2.54	-2.52
M5	-2.60	-2.48
M6	-2.59	-2.45
M7	-2.56	-2.45
M8	-2.58	-2.45
D1	-1.61	-1.62
D2	-2.05	-
D3	-1.98	-1.93
Off-D3	-2.28	-

tures are lower in energy, but for some, such as the M3 site near the HD2 heterodimer or the M1 site near the HD1 heterodimer, the substituted structures are lower in energy. This is in line with results for the P-Si heterodimer, which also show an improvement in energy when the ejected Si was adsorbed at M sites which are not directly bonded to the P atom [20].

The M5-8 sites, which lie on the adjacent dimer row, show relatively small changes with position, suggesting that once the Si atom gets far enough away from the heterodimer it will no longer feel its influence, instead behaving as if on the clean Si(001) surface. From here it will likely diffuse into the rest of the surface, since Si atoms are very mobile on the Si(001) surface [108].

If substitution takes place, the ejected Si can either substitute back into the Bi-Si heterodimer or diffuse to one of the other more energetically favourable sites, and from here into the rest of the surface. The energy barriers to the former process are about 0.8-0.9 eV, whereas the latter has not been determined in this work. On clean Si(001) the activation energy for diffusion along the row is 0.6 eV [108], so unless the presence of the Bi raises this by a significant amount the barriers to the Si diffusion will be lower than for Si substitution back into the Bi-Si heterodimer. If this is assumed to be true, then it is more likely that the ejected Si will diffuse away from the Bi-Si heterodimer, towards more stable adsorption sites, rather than incorporating back into the surface. Due to the low probability of substitution happening in the first place, compared to diffusion and dimer formation, and the computational cost of investigating this matter, no further work has been performed. It is not expected that the diffusion barriers will differ significantly from those on the clean surface.

5.1.5 Subsurface

Another way for Bi to incorporate into the surface is to go into subsurface interstitial sites. Results obtained so far show subsurface interstitial Bi to have a much higher energy than Bi adatoms or substitutional Bi. In all cases they were significantly worse (1 to 4 eV) than the energies of the surface and the Bi atom separated. The deeper the Bi was in the surface the less energetically favourable the structure was. This sort of behaviour can be attributed to the size of the Bi, with the region surrounding the Bi being significantly distorted. In some cases a few of the Si-Si bonds appear to have been broken as a result. For subsurface Bi which lie closer to the surface, it can also have an effect on the surface dimers. Based on these results alone it can be concluded that subsurface interstitial Bi are unlikely compared to other structures and any further work is just likely to confirm this.

5.2 Conclusions

It has been shown that Bi adatoms will preferentially adsorb on the Si dimer rows, rather than in the trench between them. The most energetically favourable sites are the D and T sites. For the T site, this can be explained by the fact that the Bi atom is threefold coordinated. Despite only being twofold coordinated, the D site is nearly as energetically stable, and additionally has an unpaired electron on the Bi atom. Other examples of sites with unpaired electrons include the U and B(UU) sites. Diffusion of the Bi atoms on the Si(001) surface was found to be fast in all directions, with diffusion along the Si dimer rows ($10^6\ s^{-1}$ to $10^{11}\ s^{-1}$) several orders of magnitude faster than diffusion between rows ($10\ s^{-1}$). Finally two adatoms will preferentially form an ad-dimer.

The D, U and B(UU) sites are all potential qubit candidates due to the unpaired electron on their Bi atoms. Of these the D site is the most promising due to its large adsorption energy. However, the low activation energies for diffusion and the preference for forming ad-dimers means that experimental observation of these structures would prove extremely difficult. The Bi would either diffuse away quickly into rest of the surface, or pair up with other Bi atoms moving around the surface to form ad-dimers. This explains the lack of reported experimental observations of Bi adatoms on Si(001) even at low coverages ($\sim$0.05 ML) [16], since very low coverages and temperatures would be required to prevent dimer formation. Even if low enough temperatures and coverages were used there is no guarantee that the Bi would adsorb at the desired sites, rather than getting stuck at sites which are not spin active.

Smaller Group V atoms, such as P and As, were also investigated for similar uses, but results so far suggest they will be less suitable than Bi. In both cases, the U site was not observed, with the structure always relaxing instead to the M site, which does not display an unpaired spin on the Group V atom. This reduces the number of possible spin active sites, essentially just leaving the D site. At the D site, As behaved in the same way as Bi, showing a localised spin on the adsorbate atom, whereas for P, it appeared delocalised between the adsorbate atom and several Si atoms. Group V atoms other than Bi could be used as qubits on the Si(001) surface, however P appears unsuitable.

An alternative to adsorption on the surface is incorporation into the surface, and these results

show that the latter process cannot compete with the former. It is much more likely that Bi adatoms will diffuse along the surface and pair up to form ad-dimers than substitute into a Si dimer or move subsurface. However, if incorporation does occur, the ejected Si is more likely to diffuse into the rest of the surface than substitute back for the Bi atom, making the heterodimer stable. As with smaller Group V heterodimers the arrangement of the neighbouring Si dimers is important, with the HD2 structure, which maintains the surface buckling pattern, being preferred. Similar to the P and As heterodimers, the buckling of the HD1 structure can be altered due to charge accumulation in the system, however due to the size of the Bi atom the buckling angle cannot be completely reversed. These incorporated structures would only be found in very small quantities, if at all.

To utilise Bi for quantum information purposes, either as qubits on the surface, or as precisely placed dopants in the surface, would require modifications to the surface, such as H passivation and subsequent patterning, as will be discussed in Chapter 6.

Chapter 6

Engineering the H:Si(001) surface to capture spin active Bi adatoms

As shown in Chapter 5 single Bi adatoms can have a single unpaired electron but are very mobile. To perform experiments to test these structures or build devices based on them, the mobility issue must be overcome. The simplest method would involve cooling the system down to a low enough temperature to prevent the diffusion of individual Bi adatoms, which comes with its own set of problems. There is no guarantee that the Bi adatoms would adsorb at the desired D or U sites. If the Bi adatoms adsorb at other sites they would become stuck in configurations without spin, which is undesirable. In addition the cooling would need to be achieved before all the Bi starts pairing up to form ad-dimers, which would also become stuck at low temperatures and do not display spin on the Bi atoms.

An alternative method of preventing diffusion is to modify the Si(001) surface prior to Bi deposition, thus introducing obstacles to the diffusion of the Bi adatoms. The method considered here involves selective depassivation of a hydrogen passivated Si(001) surface in order to create traps for the Bi atoms. H passivation of the Si(001) surface results in a structure where all the Si dimer atoms are terminated with H, leaving no dangling bonds. The subsequent removal of H atoms from specific positions, by the use of an STM tip, can reveal the underlying Si again, and provide an adsorption site for a Bi adatom. If the surrounding Si dimers remain H terminated this should prevent the diffusion of the Bi adatoms, and thus allow for the capture of spin active Bi adatoms.

There are many matters that need to be examined in order to determine the suitability of this method. It is important to know the behaviour of Bi on the regular H:Si(001) surface (Sec. 6.1), to check whether the Bi atoms will be mobile enough to reach the depassivated regions. The adsorption of Bi in the depassivated region (Sec. 6.2) is important to determine whether or not the Bi are still spin active, and the energetics of these systems. This is necessary for spintronics applications, but the method could also be applied to placing Bi atoms with atomic precision. The LDOS for the Bi adatoms was also compared to those for clean Si(001) surface to check whether the H passivation has any significant effect. Comparisons to similar P and As structures were also made to determine whether these properties are exclusive to Bi or not.

One of the most important matters to consider is the diffusion processes for the Bi to move

into and out of the depassivated region (Sec. 6.3). The barriers to diffusion out of the adsorption sites must be significantly greater than the barriers to diffusion in, for this to be a suitable method for capturing the Bi adatoms.

For spintronics applications, an array of spin active Bi adatoms would be useful and thus what happens when multiple Bi adatoms are adsorbed (Sec. 6.4) was investigated. Just like on the clean Si(001) surface, the formation of Bi dimers (Sec. 6.5) would get rid of the desired spin properties and this must be accounted for.

This method could offer a route towards Bi incorporation at specific positions (Sec. 6.6), which would be useful for fabricating atomic scale devices, or for specific purposes, such as the Stoneham quantum computing proposal [7]. Thus potential routes to incorporation, and their associated barriers were investigated, and compared to those for diffusion out of the depassivated region. Incorporation is only a reasonable prospect if the barriers to incorporation are smaller than, or of a similar order as, those for diffusion.

6.1 Bi on the H:Si(001) surface

To start, a completely hydrogen covered surface was considered, with a single Bi atom placed on top of it and allowed to relax. Adsorption energies for several structures can be found in Table 6.1, with notation retained from Figure 5.1 for the clean surface. These labels are only used to identify the position of the Bi atoms relative to the underlying Si(001) surface. Due to the presence of the H atoms, the Bi cannot bond to the surface in the same manner as the clean surface. Instead the Bi is physisorbed and is only very loosely bound to the surface.

These results show that it is possible for the Bi atoms to adsorb both on the dimer rows and in the trench region between them, however the adsorption energies are significantly worse than for the clean surface. This is to be expected, because the Bi can no longer directly bond to the surface Si atoms. Adsorption in the trench is slightly better than adsorption on the row, likely due to the fact the Bi will not be in as close proximity to the H atoms whilst in the trench. Some sites, such as D, are unlikely to be found at all, due to positive adsorption energies from trying to adsorb in such close proximity to the H passivated Si dimers.

Table 6.1: Adsorption energies for Bi atoms on the H:Si(001) surface. Sites are labelled as per adsorption sites on the clean surface.

Site	E_{ads}(eV)	Spin
H	-0.07	3/2
C	-0.10	3/2
D	+0.46	1/2
B	-0.18	1/2
B	+0.28	3/2

Given the possible adsorption sites for the Bi atoms, it is important to know whether diffusion between them is possible or not. If the deposited Bi cannot diffuse around the surface, then the Bi can never reach the depassivated region. Only diffusion along the trench was shown to be a

feasible route, with a 0.12 eV barrier moving from C to B, and 0.20 eV going in reverse. One potential problem with this route is that the intermediate maximum has an adsorption energy of +0.02 eV, which would suggest it is more energetically favourable for the Bi to desorb from the surface, rather than diffuse along the surface. Given the small energy difference involved it should still be possible for the Bi to diffuse along the trench, however some of the Bi atoms might instead leave the surface.

Simulations failed to find reasonable routes for diffusion along the rows, or into and out of the trench. Diffusion along the rows would involve passing through or near the energetically unfavourable D site. Calculations for diffusion between the trench and the dimer rows could not relax to reasonable intermediate structures, suggesting that there is a significant barrier to entering or leaving the trench. Overall, this means that for the regular H:Si(001) surface, Bi is only likely to be able to diffuse along the trench. If Bi manages to adsorb at an H site it will likely become fixed at that position, because diffusion either along or out of the row is highly unlikely. Alternatively, it could simply desorb from the surface.

6.2 Bi adatoms in the depassivated region of the H:Si(001) surface

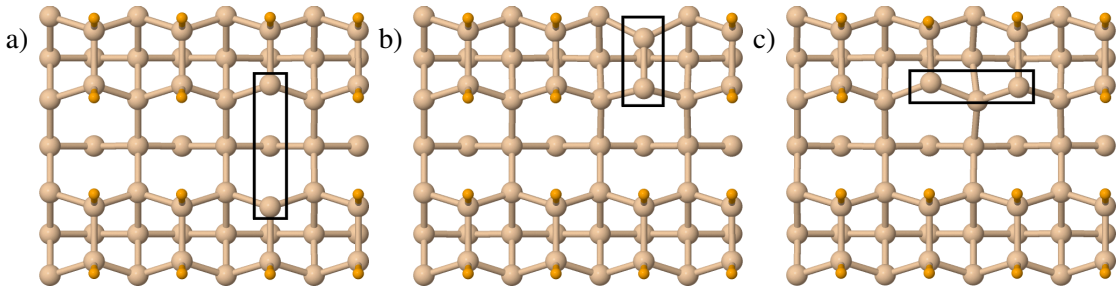

Figure 6.1: H:Si(001) surface with small depassivated regions to allow for the adsorption of Bi adatoms. Structures shown have H removed from a) ends of Si dimers separated by the trench, b) above a Si dimer, and c) ends of adjacent Si dimers in the same row. H atoms are shown in orange, rather than the usual white, to make identification easier. The black boxes are used to highlight the depassivated region. For clarity, only the first four Si layers are shown.

In order for the Bi to adsorb directly to the Si(001) surface some of the H atoms were removed revealing the underlying Si atoms as shown in Figure 6.1. A Bi adatom was then placed at the B, D or U sites as shown in Figure 6.2. These structures were chosen for their spin properties on the clean Si(001) surface, and to determine whether this still held true on the H:Si(001) surface. Structures such as the T and H were not studied, due to the lack of an unpaired electron on the Bi atom. The energetics and spin of these structures are given in Table 6.2. In all cases the spin listed is localised on the Bi atom, and were obtained by running calculations with no restrictions placed on the overall or individual spins in the system. The final two structures detailed in the Table, with a single H replaced by a Bi, and the Bi in a dimer vacancy will be covered in detail later. Unlike on the clean surface where both M and U sites are observed across adjacent dimer ends, the Bi would only relax to the U site in the depassivated region. It is possible that the presence of the additional H atoms is restricting the possible bonding configurations for the Bi adatom. This

raises the possibility of building an atomic scale switch, where the Bi can be switched between a U site and an M site, and thus spin and no spin, by the adsorption and desorption of H atoms. This idea is explored further in Appendix A.

Table 6.2: Adsorption energies for Bi adsorbed at different sites in the H:Si(001) surface. Energies on the clean surface are also provided for comparison.

Location of Bi atom	E_{ads} (eV)	Spin
B site between 2 revealed dimer ends	-2.67	1/2
B(UU) on clean	-1.84	1/2
D site on revealed Si dimer	-2.68	1/2
D on clean	-2.61	1/2
U site across revealed ends of 2 dimers	-3.02	1/2
U site on clean	-2.38	1/2
Replacing a single H atom	-1.97	-1
Bi in a dimer vacancy	-2.85	1/2

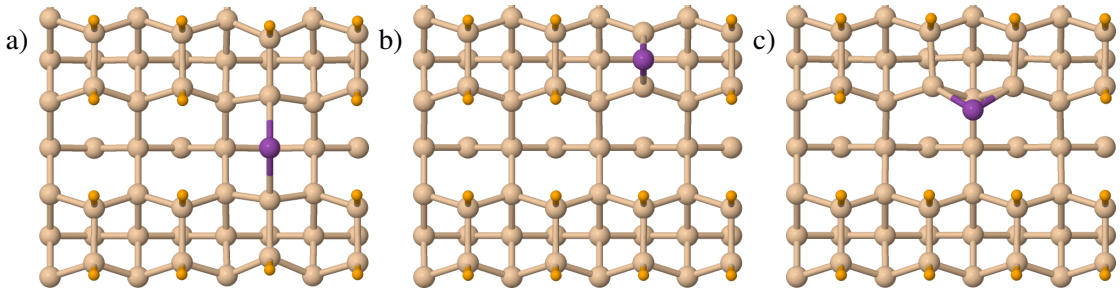

Figure 6.2: Top view of the a) B site, b) D site and c) U site in the depassivated region of the H:Si(001) surface.

All of these sites have a greater adsorption energy than the equivalent sites on the clean surface, with significant improvements seen for the B and U sites. It is important to note that these values are calculated relative to different starting structures, whereas on the clean surface they are all calculated relative to the same structure. Thus is it also instructive to look at absolute energies, as presented in Table 6.3, in order to explain some of the differences observed.

Table 6.3: Absolute energies for Bi adsorption sites on the H:Si(001) surface and the associated structures without Bi. These numbers are provided as a means of comparing the relative energies of these structures, and do not have meaning on their own.

Site	E_{system} (eV)	$E_{system+Bi}$ (eV)	E_{ads} (eV)
B	-1009.730	-1013.723	-2.67
D	-1010.043	-1014.056	-2.68
U	-1009.721	-1014.067	-3.02

In terms of absolute energy, the D and U sites are approximately the same, but are differentiated by considering their respective starting points. The B site by comparison is higher in energy, but due to the higher energy of its starting position, its adsorption energy is approximately the

same as that of the D site.

The energy differences observed for the structures with just the gaps can be explained by the nature of the dangling bonds on the H:Si(001) surface. For the D gap, an entire Si dimer is exposed, which is relatively stable. However for the B and U gaps, there are two holes, each with half a dimer exposed. A clean dimer is better than two separate dangling bonds, which is reflected in the fact that the D gap is 0.3 eV better than either the B or U gaps, which have nearly the same energy.

Filling either of the B or U gaps thus removes a relatively unstable gap, and partly explains the large adsorption energies observed. The remaining differences arise due to nature of the final adsorbed structures. Both the D and U sites are good because the Bi is relatively unstrained, something reflected in the fact that they are approximately the same energy. The B site on the other hand is a relatively poor position, so filling in the gap is not ideal, and the energy gain will be less.

The adsorption energy of the D site most closely resembles the value on the clean surface because a single revealed dimer is closer the clean surface than two separted dangling bonds.

Another important difference to remember with these adsorption sites, is that unlike the clean surface, they will not be competing with each other, and the Bi cannot move from one site to another. This means they can be treated in isolation, and that their own adsorption energy is the most important detail for determining their stability, and not their energies relative to each other.

In addition all 3 structures have a spin on the Bi as shown in Figure 6.3, which resembles a p-orbital, in the same manner as on the clean surface. This can be attributed to the unpaired electron on the Bi atom, due to the fact it is forming two bonds with the exposed Si atoms. In all cases the direction of the p-orbital is perpendicular to the direction of the Bi-Si bonds.

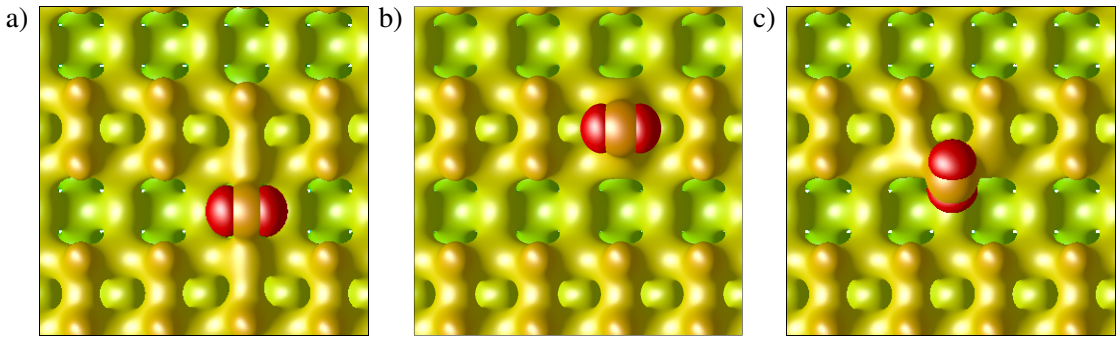

Figure 6.3: Spin density difference and charge density for the a) B site, b) D site, and c) U site in the depassivated region of the H:Si(001) surface. All three structures have an unpaired electron on the Bi atom. Red indicates spin up and other colours charge density coloured by height.

The H:Si(001) surface also offers the opportunity to study other structures, which are completely inaccessible on the clean surface, which may also have interesting spin properties. One such example is the case where a single H atom has been removed, allowing the Bi adatom to bond to a single Si atom, as shown in Figure 6.4. On the clean surface this structure would spontaneously relax to one of the more familiar sites, such as the D site. Whilst this structure does not have as favourable an adsorption energy as the B, D or U sites, at only -1.97 eV, it is still significantly better than remaining on the fully H passivated surface. Since the Bi only makes one

bond to Si, this means the structure has an overall spin of 1, due to the two unpaired electrons on the Bi atom. This manifests itself in a ring around the Bi atom, due to the superposition of p_x and p_y orbitals. This might prove to be an interesting structure for future investigations related to spin.

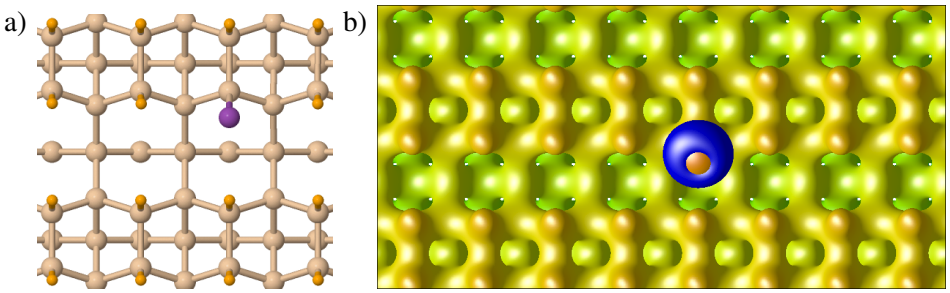

Figure 6.4: a) Top view and b) spin density difference and charge density for a structure where a single H atom on the H:Si(001) surface has been replaced with a Bi adatom. In the latter image, blue indicates spin down.

Another possibility relates to defects in the surface, such as missing dimers, which can lead to interesting features like the Bi-vacancy (Bi-V) structure [109], which displays spin on the Bi atom in a similar manner to the adatom sites. In a real sample the H:Si(001) surface will not be perfect, but will instead contain defects, such as missing dimers. These defects will not be H terminated during H passivation of the surface, leaving small regions of the surface without H, into which deposited Bi could adsorb.

To test whether Bi adsorbed in these defects would behave the same as on the clean surface, the Bi-V structure was replicated in the middle of the H:Si(001) surface as shown in Figure 6.5. The spin behaviour remains the same as previously reported, and the adsorption energy is comparable to that for the regular adatom sites, at -2.85 eV, with only the U site being better.

These results suggest the Bi-V structure can be used as an alternative spin active site, rather than those studied earlier, like the D site. However, the location of the Bi-V structure cannot be controlled, because the position of the missing dimer defects cannot be controlled. This is a distinct disadvantage compared to the adatom sites, where the depassivated region can be controlled, and thus too the location of the Bi atom. One advantage this structure does offer is the fact that it does not require a depassivation step. Once the surface has been H passivated it would be expected that some missing dimer defects will exist, into which Bi can then adsorb. This should mean it is easier to realise the Bi-V structure experimentally, and study it, however it would not be suitable for atomic scale devices.

6.2.1 Local Density of States for the Bi atom

The LDOS was calculated for the D and U site Bi adatoms on the H:Si(001) surface, as shown in Figure 6.6. For the D site the LDOS is nearly the same as for the D site on the clean surface, shown before in Figure 5.10. The sharp peak in the majority spin just below the Fermi energy, and the sharp peak in the minority spin just above the Fermi energy still remain, with a splitting of about 0.7 eV. The LDOS here appears smoother and flatter, which could be because any hybridisation with the Si dangling bonds has been removed, since there are none. From the Fermi energy to 1 eV

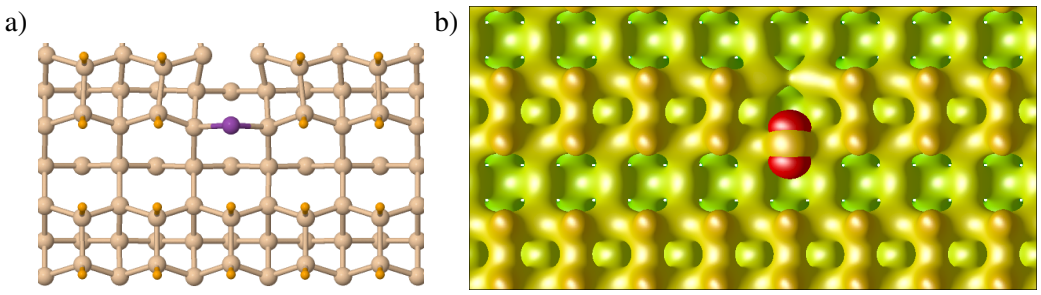

Figure 6.5: a) Top view and b) spin density difference and charge density for the Bi-V structure on H:Si(001).

above the Fermi energy the spin majority component is completely flat with a population of zero, and the same is true for the spin minority component outside of the peak at about 0.3 eV above the Fermi energy. On the clean surface there were small but non-zero populations in this region. This shows that the presence of nearby H atoms has little effect on the LDOS, if anything the regions of zero population around the Fermi energy are an improvement.

At the U site there is a peak in the majority spin component about 0.2 eV below the Fermi energy, and a peak in the minority spin component about 0.4 eV above the Fermi energy. The splitting between peaks is 0.6 eV, which is smaller than for the D site. The population of these two peaks is also smaller than the equivalent peaks at the D site. At the D site for both spin components there are secondary peaks at about 1 eV below the Fermi energy, these peaks shift about 0.5 eV closer to the Fermi level at the U site, and have a greater population. For the majority spin channel this approaches the same value as the primary peak. All this suggests the D site is more suitable for use in spintronics.

6.2.2 Comparison to P and As adatoms

Table 6.4: Energy difference (ΔE) between spin 0 and spin $\frac{1}{2}$ configurations for P and As adsorbed at gaps in H:Si(001) surface at the D and M sites. In all cases the sites with spin are lower in energy.

Adatom species	Site	ΔE (eV)
P	D	-0.08
	M	-0.01
As	D	-0.13
	M	-0.04

Just like with the clean Si(001) surface, comparisons were made to P and As adatoms to determine whether some of these properties were exclusive to Bi or not. For both species, adsorption at the D and U sites was possible, however the spin structures were not the same as for Bi adatoms. As on the clean surface, structures with overall spins of zero and $\frac{1}{2}$ were compared, even though it was expected that only the spin $\frac{1}{2}$ results would properly represent reality. The energy differences for these configurations are presented in Table 6.4.

At the D site, structures with spin on the Group V atom were more energetically favourable than those without, as expected. In both cases there was an unpaired electron on the Group V

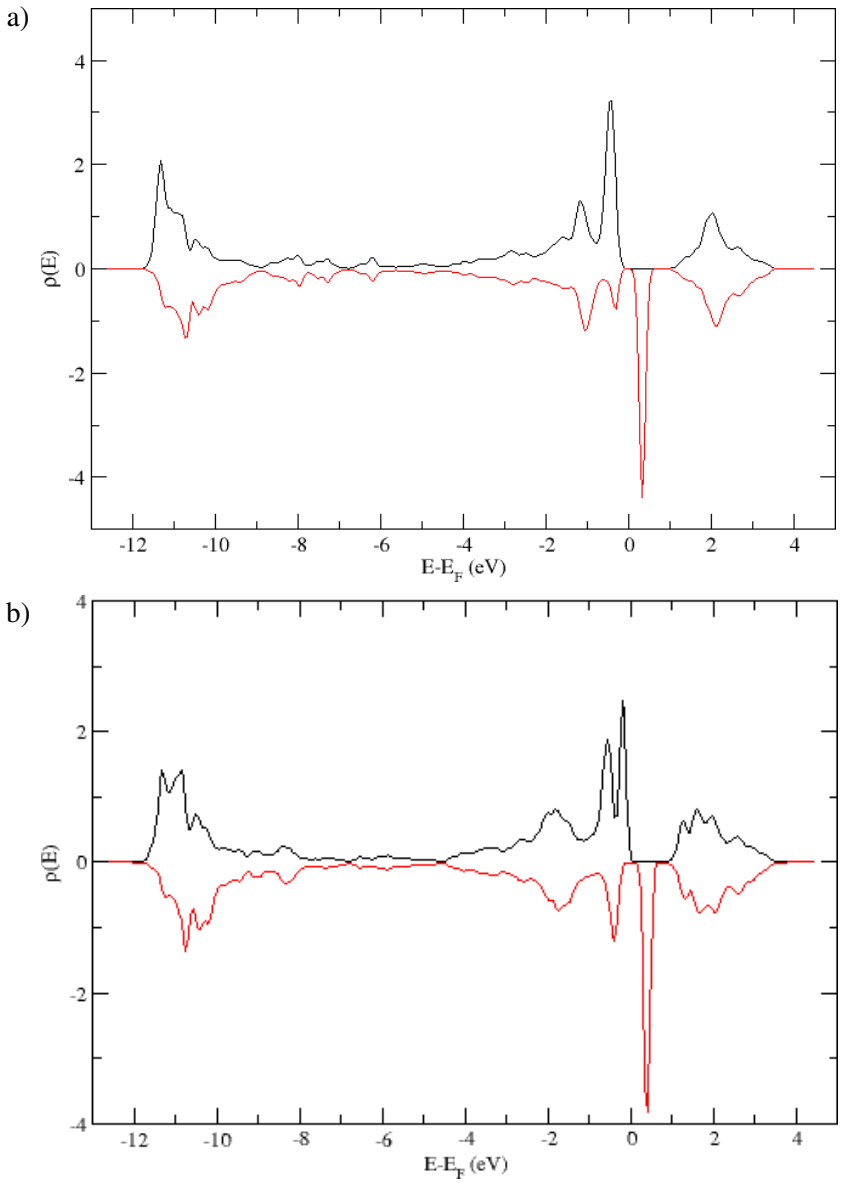

Figure 6.6: LDOS for a Bi adatom at the a) D site and b) U site in the depassivated region of the H:Si(001) surface. The black line represents the majority spin channel and the red line represents the minority spin channel.

atom in the same manner as the Bi adatom with the spin appearing as a p-orbital like shape. At the same isosurface value (0.028 e^{-}/Å^3) the size of the p-orbital varied with atom type, P being the smallest, Bi the largest. For P this is in contrast to the clean surface where the p-orbital shape was not observed. An examination of the spin populations reveals there are still a few partially occupied bands for P, but this is much smaller than on the clean surface. This is not seen at all for As or Bi.

At the U site the structures with spin were marginally more energetically favourable. In both cases the spin is spread across the adatom and the revealed Si atoms, rather than just being on the adatom, as for Bi. The extent of this spreading is greater for P than for As.

Taken together these results suggest that the D site would be suitable for As and possibly P atoms, if spin active atoms other than Bi were required, but that the U site is still not suitable for atoms other than Bi.

6.3 Diffusion into the depassivated region

Having shown that structures with spin active Bi adatoms are possible, the diffusion pathways of these Bi adatoms were investigated. It is no use showing that these structures can form if they are no more likely to stay in place than on the clean surface. In order to achieve this, the Bi was placed at several positions near the depassivated region and allowed to relax. The diffusion between these resulting structures and the D, U or Bi-V structures was then investigated using the CINEB method.

To reach these structures the Bi can come along the trench, along the dimer row, or via an adjacent dimer row, passing through the trench. However, since the Bi has poor mobility on the H:Si(001) surface, except for along the trench, the investigation focused on diffusion along the trench.

Since the revealed Si atoms are buckled, the Bi can approach the depassivated region from either the up or down buckled end. However, this is expected to only have a minor impact, if any, on the energetics of the diffusion process, so was not investigated.

6.3.1 Diffusion into the D site

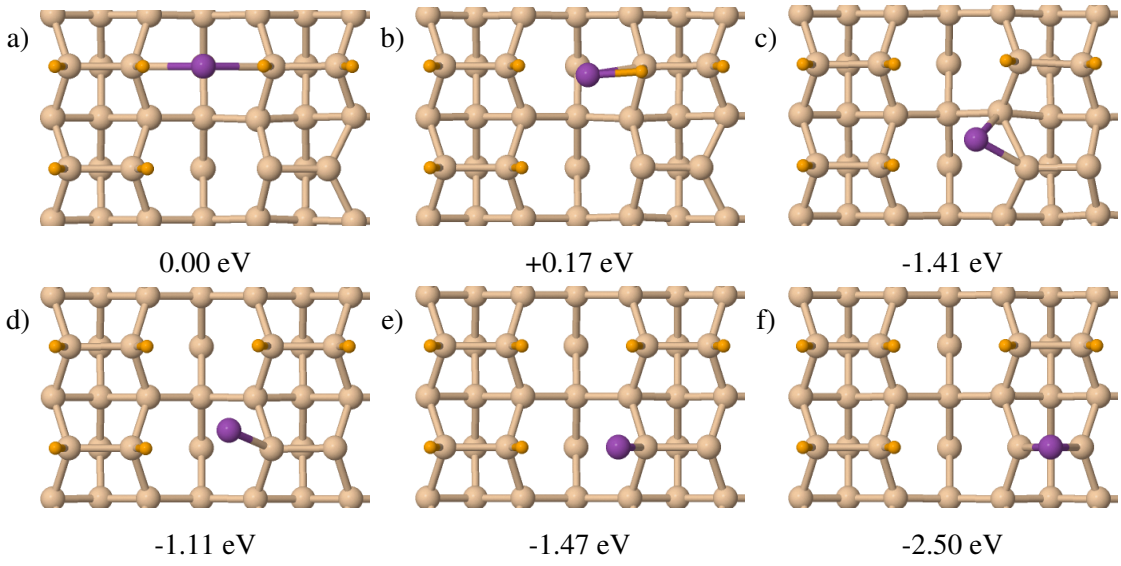

Figure 6.7: Diffusion route for a Bi atom from a) a B site near a depassivated region of the H:Si(001) surface to f) the D site. The route passes through b) an initial maxima, c) an intermediate minima, d) an intermediate maxima, and e) a transition state. All energies given are relative to a).

A route for diffusion into the D site is shown in Figure 6.7. The starting position is a B site near the depassivated region, which has an adsorption energy which only differs from the equivalent site on the H:Si(001) surface by 0.01 eV. Any distances further away from the depassivated region can be treated as exactly the same as the regular H:Si(001) surface. As such only the region between this B site and the D site will be of interest. As a first step the Bi diffuses towards the Si dimer forming a bond with one of the Si dimer atoms, as shown in b) and c). The activation energy for this process is 0.17 eV, whereas the reverse is 1.58 eV. This shows that once the Bi approaches the dimer it is much easier for the Bi to diffuse towards the D site than away from it. As a second step

the Bi rotates so that it is in line with the Si dimer, as shown in d) and then diffuses to the D site, as shown in e) and f). This process has an activation energy of 0.31 eV in the forwards direction and 1.39 eV in the reverse. Similar to the first step, it is much easier for the Bi to diffuse towards the D site, than to diffuse out of it. Even in cases where the Bi could diffuse out to the intermediate minimum shown in c), it is much more likely to return to the D site, than continue to diffuse out to the B site.

It is much easier for the Bi to diffuse into the depassivated region dimer than out, and diffusion out of the D site is much more difficult than on the clean surface. For example, at 300 K diffusion out of the D site would be at a rate of the order of $10^{-11}\ s^{-1}$, for the first step alone, whilst diffusion along the trench into the D site will still be occurring at a rate of the order of $10^{8}\ s^{-1}$. This site will be much more stable than on the clean surface, and control of the temperature can be used to prevent Bi leaving the D site, without preventing diffusion to the D site in the first place. Even at a temperature of 410 K this structure would be as stable as the D site on the clean surface was at 20 K, which is a considerable improvement.

6.3.2 Diffusion into the U site

Diffusion into the U site takes place via a metastable intermediate, as shown in Figure 6.8, which is 1.03 eV higher in energy than the U site. There does not appear to be any energy barrier for a Bi adatom to diffuse to this intermediate from a nearby B site, to the right of this position, nor is there any barrier for diffusion to the U site from this intermediate. So, once a Bi atom gets close enough to this depassivated region, it will immediately diffuse to the U site. After this, the barrier out will be 2.84 eV, meaning that the the U site will be stable enough to use experimentally, even at temperatures above 300 K. In addition the U site will be more stable site than the D site.

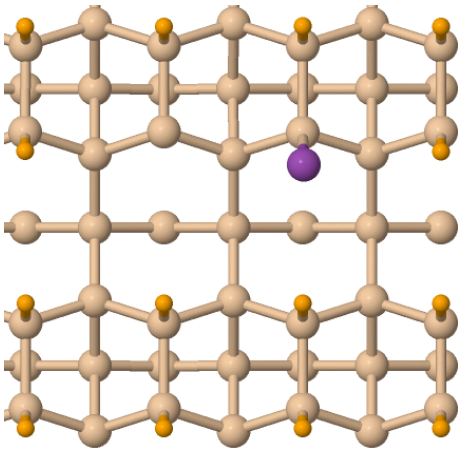

Figure 6.8: Metastable intermediate on the diffusion pathway for a Bi adatom diffusing into the U site.

6.3.3 Diffusion into the Bi-V structure

Diffusion of a Bi atom into a dimer vacancy on the H:Si(001) surface, creating the Bi-V structure, offers an alternative spin active structure which does not require additional patterning of the sur-

face after H passivation. It is important to know the barriers for diffusion of a Bi atom into and out of the dimer vacancy, in order to understand the formation process and assess the stability of the Bi-V structure. It also serves as a useful comparison to diffusion into the depassivated region, since it is likely that dimer vacancies will exist alongside the depassivated regions in a real sample.

The aim was to follow a diffusion pathway of a Bi atom from a nearby C site into the dimer vacancy involving seven intermediate images. However due to time constraints and convergence problems with the calculations, it has not been possible to properly evaluate this route. Diffusion to the B site at the dimers next to the vacancy occurs with no energy barrier, but the details beyond this are not clear. Current results suggest that the Bi will reach an intermediate minimum,which is about 1.7 eV lower in energy than the C site, before needing to overcome a small barrier, of the order of 0.3 eV, to complete the diffusion process. Reversal of this final step requires overcoming a barrier of the order of 1.3 eV. This two step process, and the magnitude of the barriers involved is similar to the process that takes place during diffusion to the D site. Earlier results also indicated that it might be possible to complete the diffusion process without encountering any barriers, but this is also drawn from incomplete calculations. At this time, proper details of the structure and energies of intermediate structures cannot be presented because calculations have not been finalised.

6.4 Multiple Bi Adatoms

Having shown that it is possible to use depassivated regions of the H:Si(001) surface to capture spin active Bi atoms, it is important to know whether it is possible to do the same for multiple adatoms. This could prove useful for spintronics, or for atomic scale devices.

6.4.1 Multiple D sites

Multiple D sites in different arrangements were investigated, as shown in Figure 6.9 the results of which are presented in Table 6.5. For the 4×D structure the Bi atoms were arranged in such a way as to avoid neighbouring Bi atoms forming dimers. The different arrangements made no appreciable change to the adsorption energies per Bi, compared to a single adatom, with E_{ads} of -2.68 eV. In addition there was a single unpaired electron on each Bi atom, meaning the structure could produce an array of qubits. Initial calculations with no restrictions aligned all the spins as either up or down, so as a further test the spins of the Bi atoms were alternated, using the MAGMOM tag in VASP. This allows the user to set the initial magnitude and orientation of the spin on each atom. Both the aligned and alternating spin arrangements are shown in Figure 6.10. This made no noticeable difference to the energies, with changes only of the order of 1 meV, suggesting there is little interaction between the spins of neighbouring Bi adatoms.

This small interaction would prove problematic for quantum computing applications, since there needs to be some degree of communication between the qubits. Further tests on the 2×D structure were performed, including effects such as Hubbard U and LS-coupling. Calculations for the aligned and alternating spin structures were repeated with U values of between 0.5 and 2 eV in intervals of 0.5 eV, with no appreciable effect on the energy differences between the two. These U

Table 6.5: Adsorption energies for arrangements of multiple Bi adsorbed at D sites on the H:Si(001) surface.

Location of Bi atoms	E_{ads}/Bi (eV)	Spin
2×D sites in same row	-2.68	-1
2×D sites in adjacent rows	-2.69	-1
4×D sites in alternating zig-zag pattern	-2.67	-2

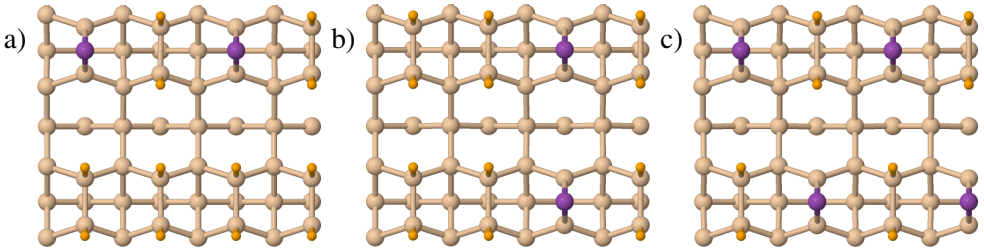

Figure 6.9: Arrangements of multiple D sites. a) 2×D in the same row. b) 2×D in adjacent rows. c) 4×D in zig-zag pattern.

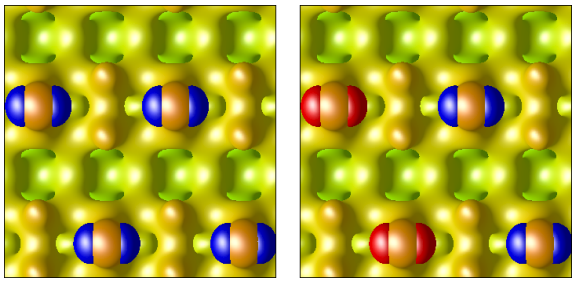

Figure 6.10: The spin difference density and charge density for the structures with 4×D sites, where the spins are all aligned or alternating.

values were chosen arbitrarily, just to test the effect it would have. When LS-coupling is included by turning on the LSORBIT tag, it becomes possible to orient the magnetic moments of each atom relative to a magentic field, using the MAGMOM and SAXIS tags. Several different orientations of the field and the spin were attempted, however, significant energy differences between the spin aligned and anti-aligned structures were not observed. The greatest difference observed was only 1 meV, which occured for spins along the x direction, with the magentic field also along x. It could be that this issue is simply a failing of DFT, but this would not become clear without further tests, such as using hybrid functionals. Unfortunately, the time and computational resources were not available to test this.

Ideally this system would need to be tested experimentally in order to check these results, but based on these simulations it appears that multiple D site adatoms would be a poor choice for quantum computation, due to their lack of interaction. This makes it hard to justify performing these experiments.

6.4.2 Multiple U sites

There are a multitude of different possible arrangements for multiple U sites, and a small selection of these have been investigated for two U sites, as shown in Figure 6.11. The adsorption energies for each are presented in Table 6.6.

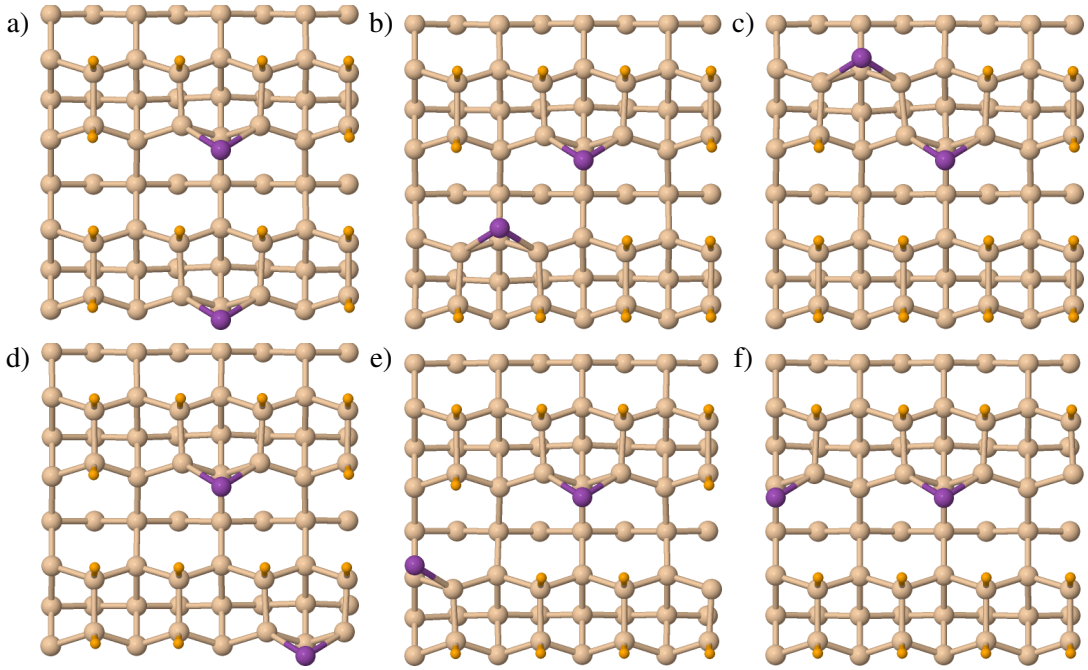

Figure 6.11: Multiple 2×U structures.

Table 6.6: Adsorption energies for different arrangements of 2 Bi in U type sites. Absolute energies for these structures and the depassivated regions without Bi are provided to allow for further comparisons. These energies only having meaning relative to each other. Refer to Figure 6.11 for specific structures.

2×U structure	E_{system} (eV)	$E_{system+Bi}$ (eV)	E_{ads}/Bi (eV)	Spin
a)	-1000.731	-1009.425	-3.02	-1
b)	-1000.709	-1009.421	-3.03	-1
c)	-1000.958	-1009.331	-2.86	-1
d)	-1000.718	-1009.392	-3.01	-1
e)	-1000.732	-1009.396	-3.01	-1
f)	-1000.984	-1009.437	-2.90	-1

In general these structures show little difference in adsorption energy compared to a single U site, with E_{ads} of -3.02 eV. Structure b) even shows an improvement of 0.01 eV over two isolated U sites. Some of the arrangements, namely c) and f) differ significantly from the single atom case. In order to properly assess the energetics of these structures, and the differences between them, it is important to examine the absolute energies of the structures involved, both before and after Bi deposition.

The range of energies observed is greater for the structures prior to Bi deposition than those after, with the lowest energy structure, f), being nearly 0.28 eV lower in energy than the highest

energy structure, b). The differences in energies can be explained by the nature of the exposed Si dangling bonds in each structure. As discussed earlier, it is more energetically favourable for an entire dimer to be revealed, than several half dimers, which explains the low energy of structure c) compared to a), b), d) and e), all of which have very similar energies. Structure f) appears to be an outlier, because it has the lowest energy, despite the fact it has four separate half exposed dimers. This could be because all four are adjacent to each other rather than as two pairs split across the surface, as with the other structures.

The absolute energies of the six final structures by comparison vary over a range of 0.1 eV, with f) once again showing the lowest absolute energy. The main reason for these differences appears to be the relative distances of the Bi atoms from each other. Structures where the Bi atoms are a significant distance from each other, such as d) and e) are higher in energy than those which are closer, such as a), b) and f), suggesting there is an energetically favourable interaction between the Bi atoms as they are brought closer together. Structure c) is an exception to this, and displays the highest absolute energy. This can be attributed to the fact they share the same Si dimer, which has become slightly tilted by their presence.

Since structures a), b), d) and e) all involve Bi adsorbed onto comparatively unstable structures, their adsorption energies are greater than f), which has the lowest absolute energy, but involves adsorption onto a comparatively stable structure. Structure c) has the lowest adsorption energy, because it has a comparitively stable starting structure, but the worst final structure.

All of these structures have an unpaired electron on each Bi atom, which when left unfixed were aligned. Structures without spin on the Bi, equivalent to the M site, could not be obtained for any of these structures either. To check for interactions between Bi, the spins were alternated as shown in Figure 6.12.

In most cases the structures where the spin is anti-aligned are lower in energy, however this is usually below the level of accuracy for energies considered here. Structure c) where the Bi adatoms lie at opposite ends of a Si dimer is the only structure to show an energy difference of above 0.01 eV. The fact that the two Bi atoms share a revealed Si dimer could be a contributing factor in this interaction. This is the largest interaction thus far seen in any of the simulations, making it a potential candidate for future research. The proximity of the Bi atoms is a concern, and will be revisited in Section 6.5. Structures e) and f) on the other hand, show practically no interaction, and suggest a limit on the range of interactions between these Bi atoms. Bi atoms which are separated by more than two Si atoms will only show small interactions, and those separated by more than two Si dimers are likely to show none.

6.5 Formation of ad-dimers

It is also important to consider whether or not additional Bi will bond to the Bi adsorbed in the depassivated region to form dimers. If this happens it could get rid of the desired spin active atoms. In addition to determining whether or not dimers can form, it is also important to consider the energy barriers to their formation. If these barriers are similar or lower than those for the diffusion of single Bi atoms into the depassivated regions, it would cause problems for positioning

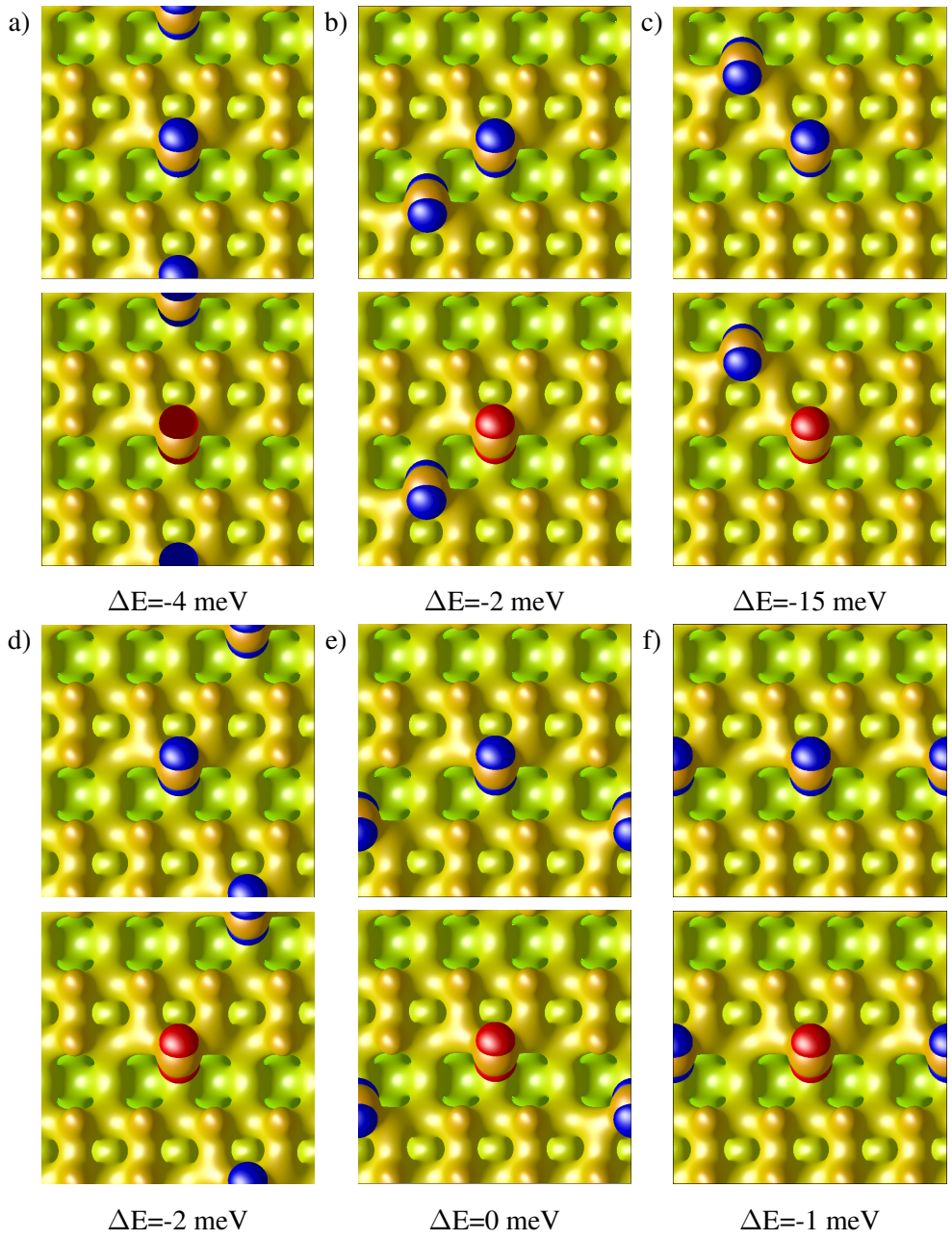

Figure 6.12: Spin density difference and charge density of 2×U structures. Structures are labelled the same as in Figure 6.11. The top row shows the spins aligned, the bottom row anti-aligned. The energy difference, ΔE, is the energy of the anti-aligned structure relative to the aligned structure.

single Bi adatoms on the surface.

Normally, Bi ad-dimers can form between two neighbouring Bi adsorbed on the clean Si(001) surface, covering two of the regular adsorption sites. In the current scheme the surrounding Si dimers are still H terminated, so this is not possible. However, if a second Bi atom enters the same region as first Bi adatom a dimer can form either directly above a Si dimer, or across the ends of two dimers within a row, as shown in Figure 6.13. The Bi dimer above the Si dimer, as shown in a) has an adsorption energy per Bi of -2.76 eV, which is 0.08 eV better than for the individual D site. This dimer could also form if larger areas of the surface were exposed, as demonstrated in c), which could result from the two Bi of Figure 6.11.c) bonding together. This structure has an adsorption energy per Bi of -2.82 eV, which is worse than the separated adatoms, by 0.04 eV per

Bi atom. For the dimer across the Si dimer ends, as shown in b), the adsorption energy per Bi is -3.02 eV, which is the same as for the individual U site. In most cases the formation of ad-dimers is equally or slightly more energetically favourable than the formation of adatoms, and even when adatoms are favoured it is by less than 0.1 eV. In all cases, no spin was observed on the Bi atoms, however in the case of Figure 6.13.c) there were spins on the revealed Si either side of the Bi dimer.

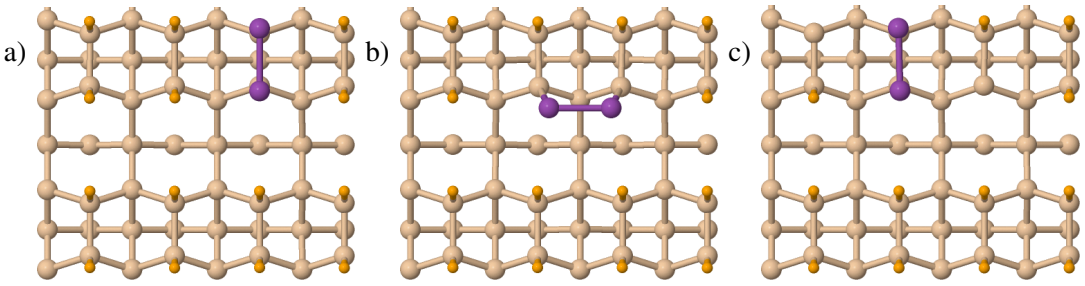

Figure 6.13: Bi dimer structures in depassivated regions of the H:Si(001) surface. a) Bi dimer above a revealed Si dimer. b) Bi dimer above revealed dimer ends, c) Bi dimer above a revealed Si dimer with two additional revealed Si on adjacent dimers at opposite ends of the Bi dimer.

Given this fact it is now important to know what the energy barriers to forming these structures are, which can be found via the CINEB. The end structures were chosen to be the ad-dimer structures from Figure 6.13 and the starting structures were mostly found by placing a second Bi atom in a variety of positions as shown in Figure 6.14 and allowing them to relax. In the case of the structure from Figure 6.13.c), diffusion from the 2×U structure from Figure 6.11.c) was examined.

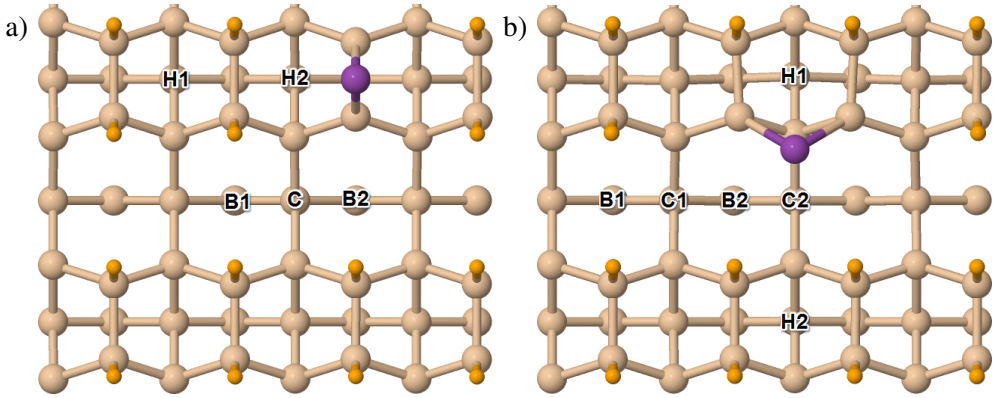

Figure 6.14: a) D and b) U site Bi adatoms with starting positions for a second Bi labelled using the same notation as for the Bi adatoms. Where there is more than one of the same type of site they are also labelled numerically.

6.5.1 D site dimer

When considering the formation of the D site dimer, the resulting structures from placing a second Bi adatom at the positions listed in Figure 6.14.a) can be split into three categories. The first category are those structures where the second Bi behaves as if on the clean surface, such as for the

B1 or H1 positions. These are energetically similar to the same sites on the full H:Si(001) surface, providing good starting points for the diffusion calculations. The second category are those structures where a Bi dimer forms, but both Bi are not adsorbed to the surface, as in Figure 6.15. This occurs for the H2 or C positions, and provides intermediates for the diffusion calculations. The final category are those positions which spontaneously form the dimer structure from Figure 6.13.a), such as the B2 position.

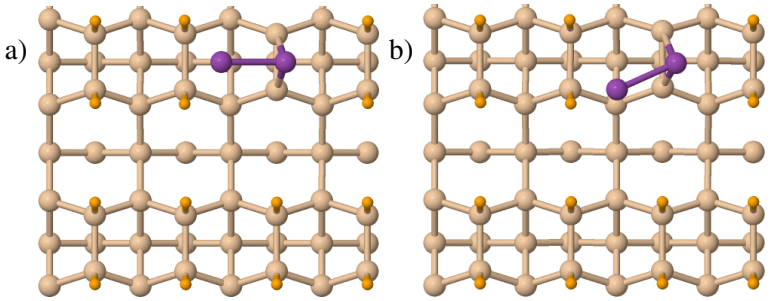

Figure 6.15: Structures where a second Bi has bonded to a Bi adatom at the D site, but has not yet bonded to the Si surface. a) Shows a dimer perpendicular to the direction of the Si dimers, which has an E_{ads} per Bi of -2.14 eV. b) Shows a dimer diagonal to the direction of the Si dimers, which has an E_{ads} per Bi of -1.91 eV .

Diffusion calculations revealed that for the in-trench sites there were no barriers to the formation of the dimer structure. The second Bi adatom proceeds from the B1 position to parallel dimer structure, via the diagonal dimer from Figure 6.15.b) with no intermediate barriers. In principle it is also possible for the dimer to rotate to the perpendicular arrangement, but this is 1.24 eV higher in energy, and thus much less likely to form than the parallel arrangement. There are no barriers to diffusion along the dimer rows from the H1 position to the perpendicular dimer from Figure 6.15.a), however a +0.45 eV energy barrier must be overcome to rotate this to the parallel dimer structure. This route is unlikely because the second Bi will rarely be on the row in the first place, due to the difficulty of diffusing along the rows. Overall these results show that once a second Bi gets within at least a Si dimer of the D site, there will be no barriers to the formation of the Bi dimer.

Figure 6.16 shows an alternative way that a Bi dimer might form above a Si dimer, in this case via diffusion from a 2×U structure. Instead of the movements of the two Bi atoms being mirrored, as might be expected, one of them moved towards a T site first, with the other remaining at roughly its original position as shown in b). This structure is 0.12 eV higher in energy than the 2×U structure, compared with the end dimer structure which is 0.10 eV higher than the 2×U structure. The barrier for the reverse process would therefore only be 0.02 eV. Whilst there is a barrier to the formation of the dimer structure, it is small enough that it would be overcome at all but the lowest temperatures. This means that even though the 2×U structure is more stable than the dimer structure, it is likely that the Bi atoms would continually be switching back and forth between the two.

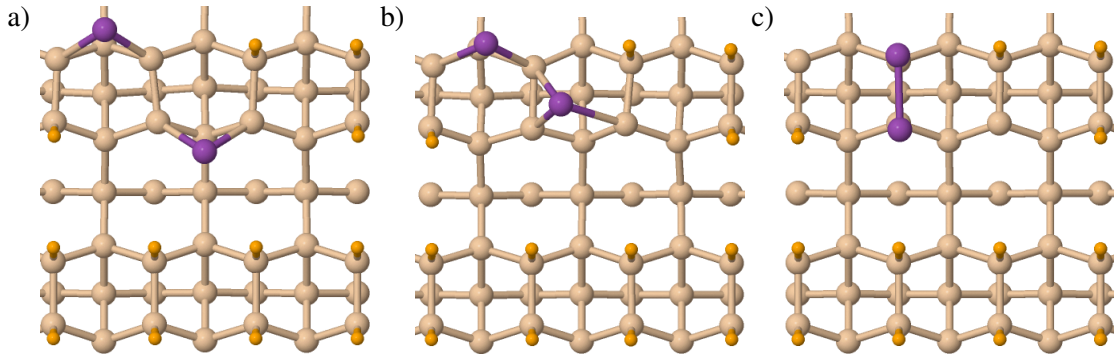

Figure 6.16: Diffusion from a) a 2×U structure, via b) an intermediate structure to c) a dimer structure.

6.5.2 U site dimer

Adding a second Bi adatom at positions near to a U site Bi results in the same three varities of end structures which were noted earlier for the D site dimer. If the second Bi atom is at the B1 site, it is nearly energetically equivalent to the same site on the full H:Si(001) surface, making it a suitable site for starting diffusion calculations. Intermediate structures, where a Bi dimer forms but both Bi are not yet bonded to the Si, as shown in Figure 6.17, form when the second Bi is placed at positions C2 or H1. If the second Bi is placed closer to the first Bi, such as at the C1 or B2 positions it spontaneously relaxes to the dimer structure from Figure 6.13.b).

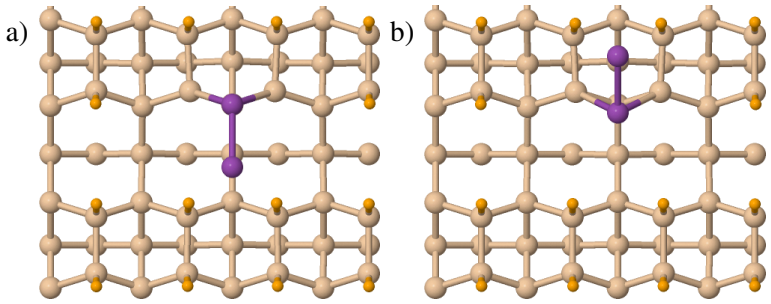

Figure 6.17: Structures where a second Bi has bonded to a Bi adatom at the U site, but has not yet bonded to the Si surface. a) Shows a dimer parallel to the direction of the Si dimers, which lies over the trench between rows. E_{ads} per Bi = -2.10 eV. b) Shows a dimer parallel to the direction of the Si dimers, which lies over the dimer rows. E_{ads} per Bi = -2.11 eV.

There are no, or very small, barriers to the formation of the U site dimer once the second Bi moves within a certain range of the U site. There is a negligible barrier for the second atom at the B1 site to form the parallel dimer which lies over the trench, although further calculations may show there to be no barrier at all. Once either of the parallel dimer structures are formed there are no additional barriers to forming the U site dimer. Just like with the D site dimer, once a second Bi gets within a distance of one Si dimer from the U site, there is nothing stopping the dimer from forming.

6.5.3 Summary

These results show that not only are the addimer structures more or equally energetically favourable compared to the adatom structures, but also the energy barriers to their formation are very low or even zero, once the second Bi gets within a certain distance of the first Bi. This means it would be difficult for single adsorbed Bi atoms to remain as isolated spin active atoms, rather than forming dimers. This does not mean the end of using selectively depassivated regions of the H:Si(001) surface to adsorb Bi atoms in specific positions. Careful control over the Bi coverages can still prevent the formation of dimers, provided there are a sufficient number of depassivated regions on the H:Si(001) surface. There are three possible states for these depassivated regions; empty, occupied by a single Bi atom and occupied by multiple Bi atoms, such as dimers. At low coverages some of the depassivated regions will be filled, with little to no pairs, but also plenty of empty regions. At medium coverages most of the depassivated regions will be filled and small numbers of pairs formed. At high coverages all the depassivated regions will be filled and some pairs will form. If the Bi dose is kept appropriate to the amount of the surface that has been depassivated, then it should be possible to deposit Bi atoms at specific positions without too many ad-dimers. This could allow for the creation of an array of qubits on the surface, or for additional processes which require Bi atoms at specific positions, as will be explored in the next Section.

6.6 Incorporation of Bi into the H:Si(001) surface

Whether or not it is possible to use Bi atoms adsorbed on the Si(001) surface as qubits, the concept of trapping Bi atoms within depassivated regions of the H:Si(001) surface could also be used to incorporate Bi dopants at very specific positions, as is done with P, which would be useful for the Stoneham quantum computing proposal [7]. This method could be used because there is currently no known PH_3 equivalent for Bi, meaning that the methods used to incorporate P at specific locations [6] cannot be used. Instead, the trapped adatoms could incorporate into the surface Si dimers forming a Bi-Si heterodimer, and ejecting an Si out onto the surface.

It is thus important to consider possible routes that could be taken towards Bi incorporation, their related energy barriers, and how this relates to other processes such as diffusion on the surface. At first incorporation into the surface after the removal of two H atoms, as for the D and U sites, was considered (Sec. 6.6.2), however it soon became clear that because of space issues, a larger area involving the removal of at least three H atoms would be needed (Sec. 6.6.3). Before studying the incorporation process, a brief discussion of the Bi-Si heterodimer itself will be presented (Sec. 6.6.1).

6.6.1 The Bi-Si heterodimer

When a Bi atom substitutes into a surface Si dimer it forms a Bi-Si heterodimer where the Bi atom is buckled upwards relative to the Si atom, as shown in Figure 6.18. Unlike on the clean surface, as examined in Section 5.1.4, there is only one possible arrangement for this heterodimer, due to the fact that all the surrounding Si dimers are flat and H passivated. As with the clean surface, the effect of charging the structure was also analysed, the results of which are presented in Table 6.7,

alongside those for the clean surface to allow for a direct comparison. Due to the fact there is an Si atom missing, the energy of this structure cannot be compared directly to the Bi adatoms.

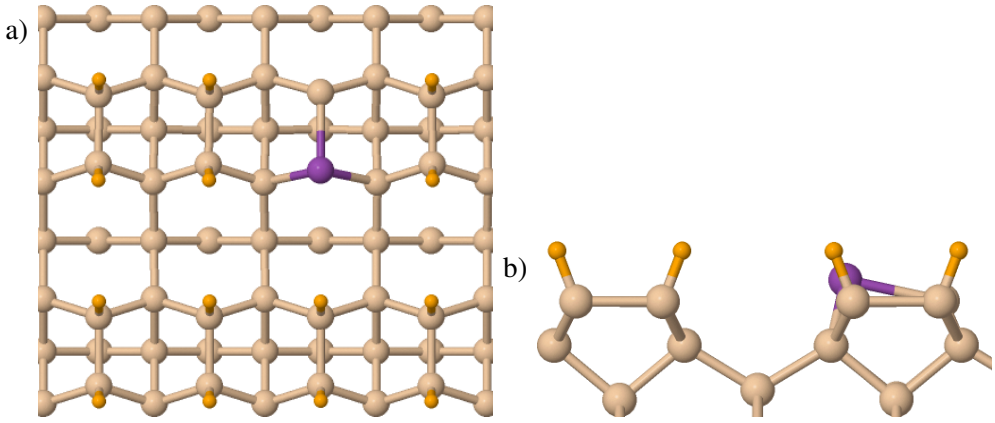

Figure 6.18: Structural model of the Bi-Si heterodimer in a depassivated region of the H:Si(001) surface, showing both a) top and b) side views. In the latter case this shows the buckling of the Bi atom relative to the Si atom, and the rest of the surface Si atoms.

Table 6.7: Bond lengths (L) and buckling angles (θ) for Bi-Si heterodimers in cells with additional electrons. Results are presented for both the clean and H passivated Si(001) surface. N_e indicates the regular cell, whilst N_e+1 and N_e+2 are 1 and 2 additional electrons respectively.

		N_e		N_e+1		N_e+2	
Surface	Structure	L (Å)	θ (°)	L (Å)	θ (°)	L (Å)	θ (°)
Si(001)	HD1	2.76	11.7	2.83	4.3	2.84	4.0
	HD2	2.73	19.4	2.71	20.3	2.70	18.5
H:Si(001)	HD	2.77	12.0	2.84	3.9	2.84	3.7

The heterodimer in the H:Si(001) surface most closely resembles the HD1 structure on the clean surface, with almost identical bond lengths and buckling angles. The response to charging the cell is almost identical as well, with a significant flattening when the first additional electron is introduced, but almost no effect when the second is. The bond lengths and buckling angles also remain approximately the same when clean and H passivated Si(001) is compared. As noted before, the fact that the buckling angle does not completely invert, like with P and As, is probably due to the size of the Bi atom, and the energy cost to pushing it further into the surface.

The fact that in the absence of a surrounding buckling pattern, the Bi-Si heterodimer behaves like the HD1 structure, rather than the HD2, is interesting. It has been unclear why the HD1 structure is observed in experiments for P-Si, even though HD2 is more energetically favourable in its uncharged state [30]. If a Bi-Si heterodimer behaves like the HD1 structure in the absence of a surface buckling pattern, then this would suggest that for a charged system, it is the lower energy structure.

6.6.2 Incorporation of Bi with 2 H atoms removed

The simplest route for incorporation of Bi into the surface is via one of the favourable adsorption sites, such as the D site. This provides a stable starting point for the process, and just requires the Bi atom to substitute with one of the Si atoms it is bonding to, ejecting the Si atom out into the surface. To investigate the energy barriers for this process, it is important to first determine the start and end points for the incorporation. Thus far, only the D site has been considered as a starting point, although the U site could also be investigated, as well as incorporation via diffusion from the trench. Incorporation from the U site was not considered at the time, because the U site lies directly along the diffusion pathway for Bi atoms on the H:Si(001) surface, so it was assumed that dimers or Bi clusters were more likely to form at the U than the D sites. Incorporation directly from the trench would be competing with diffusion to the adsorption sites, and given the low energy barriers to this process, Bi will favour adsorption over incorporation. Given the results for the D site, which suggest the need for the removal of at least three H atoms, it was decided that it would be better to perform these latter investigations in Section 6.6.3.

For the end points, the position of the ejected Si atom relative to the heterodimer is the most important variable. Which side of the dimer the Bi lies is not important, due to the fact that the surrounding Si dimers are all H passivated, so that there is no distinction between HD1 and HD2, like on the clean surface. The ejected Si atom can sit at D, U or B-like sites, examples of which are shown in Figure 6.19, alongside their energies relative to the D site. The U and D-like sites were chosen because on the clean surface both the M and D sites are energetically favourable for an Si atom, the former being very similar in structure to the U site. The B-like site was chosen because it can be achieved with linear movement of the Bi and Si atoms. Adsorption at a U-like site opposite to the position of the Bi atom was not considered due to the amount of rearrangement required. The adsorption sites for the ejected Si atom are described as being D or U-like to give an idea of their location on the surface. Due to the presence of the Bi atom and surface H atoms they cannot be the same as on the clean surface.

In all cases these structures are significantly higher in energy than the D site, ranging from 1 eV to almost 3 eV higher. For incorporation to be considered a reasonable possibility, the process would ideally need to have energy barriers that are lower than that for diffusion out of the D site, or at the very least of the same order. Since the barrier for the first step of the diffusion process is 1.39 eV, this leaves only the D-like ejected Si site as a potential end point for the incorporation process. The U-like and B-like final structures are higher in energy than this barrier, ruling them out before even considering any additional intermediate barriers.

The next matter to consider is the energy barrier for the process of swapping the D site Bi adatom with a Si dimer atom, without first going via any of the other ejected Si positions. To achieve this the Bi and Si atoms would need to rotate within the space of a single Si dimer, since all other nearby Si dimers are still H passivated. Due to the lack of space, and the requirement to break Si-Si and Bi-Si bonds in the process, I considered it unlikely enough not to need to calculate the barrier explicitly.

To address the space problem, additional H atoms could be removed from the surface, to give the Bi adatom and the ejected Si more space to move. Removal of too many H atoms will lead to

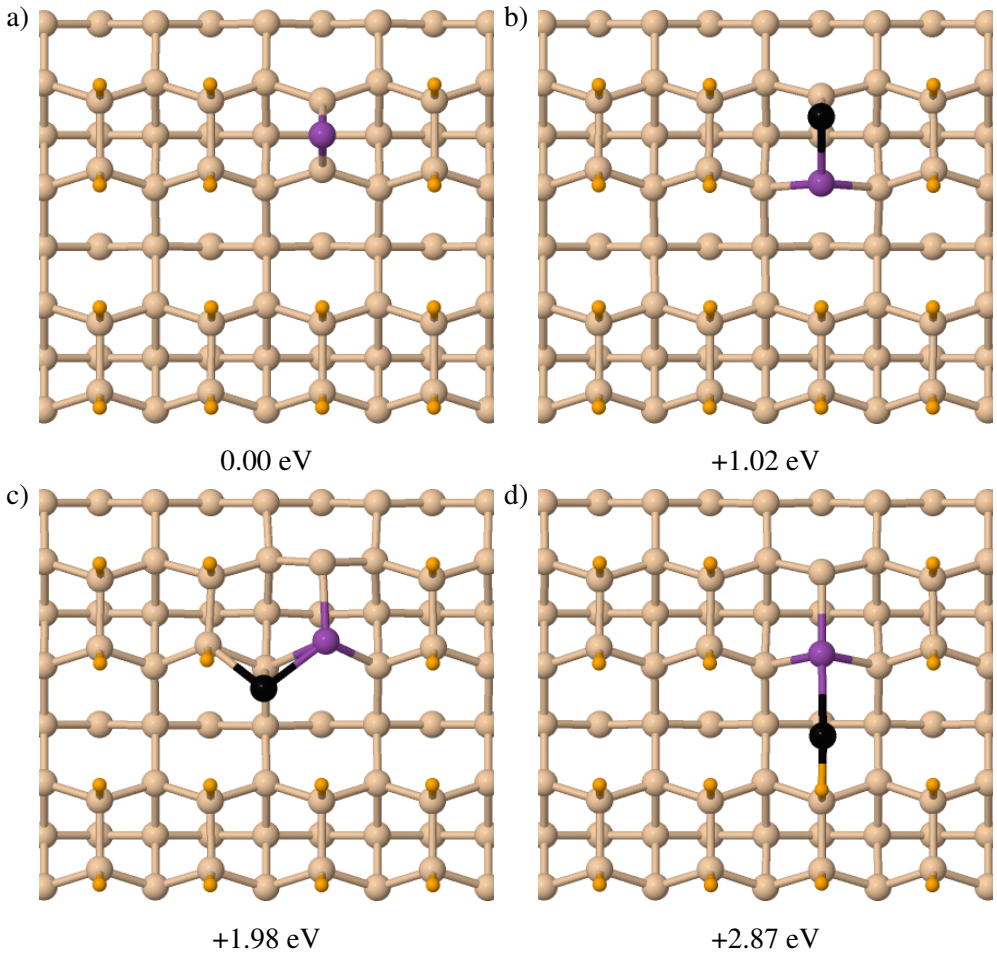

Figure 6.19: Energetic comparison between Bi adsorbed on the H:Si(001) surface and incorporated as a Bi-Si heterodimer in a region with two H atoms removed. Energies are given relative to the D site. a) Bi adsorbed at the D site. b) Bi incorporated with ejected Si at a D-like site. c) Bi incorporated with ejected Si at a U-like site. d) Bi incorporated with ejected Si at a B-like site. The ejected Si atom is indicated in black for clarity. Only structure b) has a lower energy than the barrier for the first step of Bi diffusion out of the D site. However there is not enough space for this exchange to occur.

a return of the diffusion problems associated with the clean surface, so only the removal of one additional H atom has been considered.

6.6.3 Incorporation of Bi with 3 H atoms removed

With the aim of making the incorporation process easier, and thus reducing the associated energy barriers, an additional H atom from dimer neighbouring the original gap was removed. This also allows more starting and end points to be considered for the diffusion process, as demonstrated in Figure 6.20. For example, the Bi can incorporate into both the fully H depassivated Si dimer, and the Si dimer where only one Si atom has been depassivated, as well as opening up more positions for the ejected Si to move to.

This increased space leads to some incorporated structures which are energetically favourable when compared to the adatom structures, moreso than when only two H atoms were removed. For

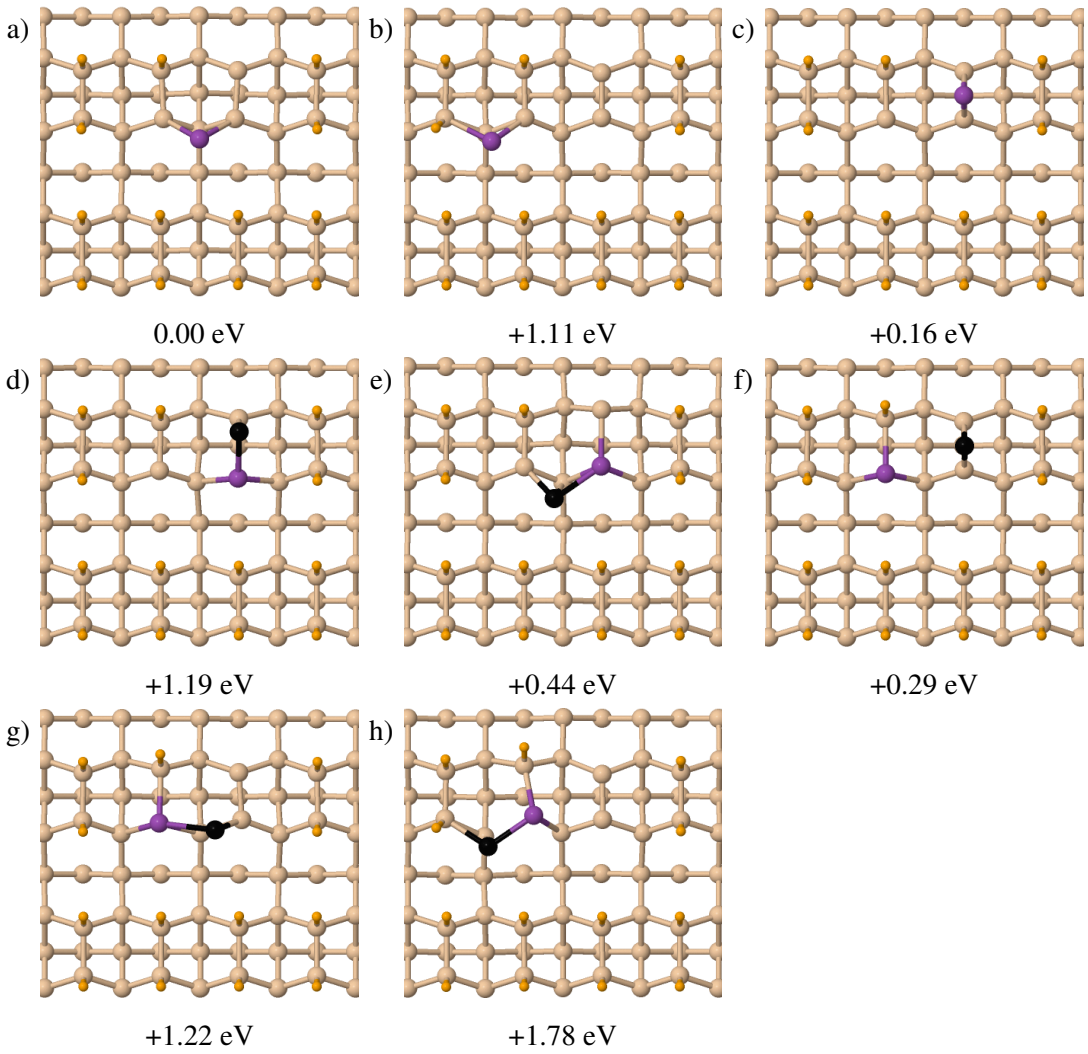

Figure 6.20: Energetic comparison between Bi adsorbed on the H:Si(001) surface and incorporated as a Bi-Si heterodimer in a region with three H atoms removed. Energies are given relative to a), which is the lowest energy structure of the selection. a) Adsorbed Bi at a U site with no H passivated Si. b) a) Adsorbed Bi at a U site with one H passivated Si. c) Adsorbed Bi at a D site. d) Bi incorporated into a Bi-Si dimer without H passivated Si, with ejected Si at a D-like site. e) Bi incorporated into a Bi-Si dimer without H passivated Si, with ejected Si at a U-like site without H passivated Si. f) Bi incorporated into a Bi-Si dimer with H passivated Si, with ejected Si at a D site. g) Bi incorporated into a Bi-Si dimer with H passivated Si, with ejected Si at a U-like site without H passivated Si. h) Bi incorporated into a Bi-Si dimer with H passivated Si, with ejected Si at a U-like site with H passivated Si. Structures such as e) and f) compare favourably to the adatoms sites, suggesting incorporation could be possible before diffusion out of the gap.

example structures e) and f) are less than 0.5 eV higher in energy than the U or D adsorption sites shown in structures a) and c). This can be attributed to the fact that the ejected Si is able to move to more favourable bonding positions, either where it is away from the Bi atom, or where it is not forced to bond to an H passivated Si atom. Compare structures d) and f), where in the latter case the Si atom being able to move to a full Si dimer improves the energy by 0.9 eV. Comparing structure e) to Figure 6.19.c) shows an improvement of 1.7 eV relative to their respecitve D sites, simply due to the fact an H atom has been removed. Structures which are physically unaffected

by the removal of an extra H, such as d), show little difference in energy, with only a 0.01 eV difference compared to Figure 6.19.b) relative to their respective D sites.

These results suggest several promising routes for incorporation, with structures e) and f) being significantly lower in energy than the barriers to diffusion back out into the surface, with d) and g) being of a similar order of magnitude.

In order to assess the viability of incorporation, barriers to several different processes need to be investigated. Firstly diffusion between the adatom sites must be considered, now that there is more space for the Bi atoms to move. Secondly diffusion into and out of the region of H depassivation must be considered. This will be largely the same as for the regular adsorption sites, with slight modifications due to the extra removed H atom. Three routes into the H depassivated region will be directly into a D site and should be the same as when only two H are removed. The final route comes via the U site instead, which should behave in the same way as the regular U site. Finally, incorporation into the surface from the different adsorption sites must be considered.

Many of the possible routes for incorporation have been considered, but by no means all of them. Some routes, such as from structure a) to e), were not considered because the incorporation would require a rotation of the positions of the Bi and Si atoms, which can be difficult to implement in the CINEB method. It is also possible that using more complex routes, rather than a simple linear interpolation, could reveal lower barriers.

Activation energies are presented for a variety of diffusion or incorporation routes in Table 6.8, alongside Figure 6.21 which shows rates of diffusion or incorporation against activation energy for a variety of temperatures.

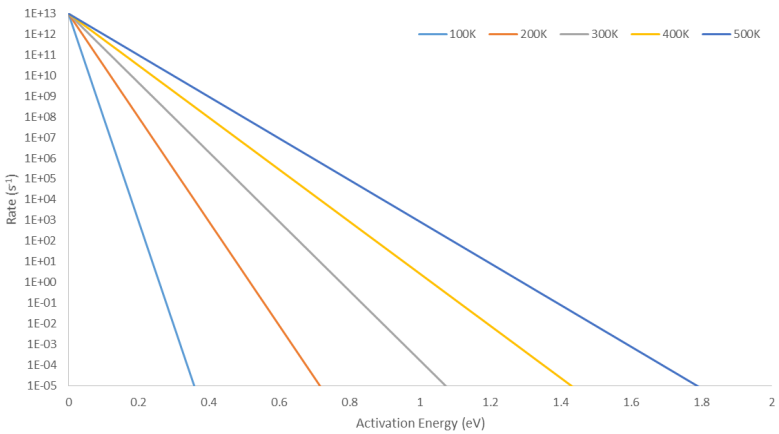

Figure 6.21: Graph showing rates of diffusion or incorporation against activation energy E_A for temperatures ranging between 100 K and 500 K. Rates below 1×10^{-5} are not shown, because these processes would be occuring at a rate of less than one per day.

As on the clean surface, diffusion between the D and U sites is very quick, with a barrier of only 0.16 eV for movement from the U to D site, which is because the D site is 0.16 eV higher in energy and there are no intermediate maxima. This means that within the H depassivated region the Bi will spend most of its time moving back and forth between these two sites.

Diffusion out of this region has significant barriers, regardless of the specific route taken. Leaving via the U site requires overcoming a barrier of 2.73 eV, which for all practical purposes

Table 6.8: Activation energies (E_A) for diffusion or incorporation of a Bi atom on the H:Si(001) surface with a depassivated region of three H atoms. Structures are labelled according to Figure 6.20.

Route	E_A (eV)
C to B on H:Si(001)	0.12
B to C on H:Si(001)	0.20
Into a)	0.00
Out of a)	2.73
Into c) (Step 1)	0.17
Into c) (Step 2)	0.30
Out of c) (Step 1)	1.39
Out of c) (Step 2)	1.58
a) to c)	0.16
c) to a)	0.00
c) to e)	1.56
e) to c)	1.28
a) to d)	1.52
d) to a)	0.33
a) to f)	2.19
f) to a)	1.90
b) to f)	0.64
f) to b)	1.46

will not happen, even at a temperature of 500 K. Leaving via the D site happens in a two step process, requiring barriers of 1.39 and 1.58 eV to be overcome respectively. However, returning back to the D site after step one only has a barrier of 0.30 eV, meaning that the Bi atom is much more likely to return to the D site than travel further into the trench. This effectively traps the Bi atom within the H depassivated region, regardless of how it attempts to leave.

Of all the possible routes, those which lead to structures e) or f) are most desireable, due to their lower energies. However, current results have shown that the barriers to the formation of these structures can be significant. For example it takes over 2 eV to incorporate the Bi from the U site at a) to the final structure in f), despite only a 0.29 eV difference between end points. There may however be other lower energy routes, which have not been found by doing a simple linear interpolation. Incorporation from position b) to f) has the lowest barrier of all, at only 0.64 eV, however it has to be considered that position b) is a metastable intermediate on the route towards the U site at a). This means that it is much more likely that the Bi will diffuse to the U site, rather than incorporate. At best, the incorporation barriers are about 1.5 eV, which is similar to that for the first step of diffusion out of the D site. This raises the possibility that the Bi will occasionally incorporate into the surface, instead of diffusing back into the surface. After this, there is also a chance for the Si to diffuse away from the Bi atom, rather than incorporate back into the surface,

potentially leading to a further improvement in the energy. For example the Si can move from its position in g) to f), improving the energy of the system by almost 1 eV.

The barriers required for the incorporation process raise the competing issue of H diffusion. For the temperatures required to see Bi incorporation on a reasonable timescale, there is also the possibility that the H atoms will start diffusing. The barrier for intradimer hopping is about 1.4 eV, whilst the barrier for intrarow hopping is about 1.7 eV [110], however at higher coverages, such as present here, these barriers are raised slightly [111]. The presence of the Bi adatom or the ejected Si will also likely contribute to a further restriction on H diffusion. The intradimer hopping will be unimportant, because it does not actually change the possible structures, simply their orientation. Intrarow hopping on the other hand could be important, because it will change the position of the depassivated regions, removing some of the specificity of this method, and potentially trapping the Bi in undesirable positions. Thankfully, this has a higher barrier than some of the incorporation barriers.

These results show the potential for incorporating Bi with precision to within ± 1 dimer, however it will require great care in experiment to achieve this. It is possible that other, lower energy, incorporation routes exist, which have not been found here.

6.7 Conclusions

It has been shown that selectively depassivating regions of the H:Si(001) surface prior to Bi deposition can be used to capture spin active Bi adatoms at specific locations, such as the B, D and U sites, without a considerable effect on their stabilities or spin. The barriers to the formation of the D and U sites are slightly larger than on the clean surface, however the barriers for diffusion out of the adatom sites are much larger. The B site was not investigated due to its location in the centre of the trench. Both the D and U adatom sites will remain stable enough to make use of experimentally at up to room temperature, without preventing their formation in the first place.

Similar methods could be used to adsorb smaller Group V atoms, such as P or As, at specific locations, however the choice of spin active sites is reduced. Only the D site displayed a localised spin on the Group V atom. Spin at the U site was delocalised over the adsorbate and the Si atoms it bonded to. In this work the diffusion barriers to their formation have not been investigated, although they are assumed to be similar to Bi.

This method could also be used to build up an array of qubits, but further work would be needed to properly determine the interactions, if any, between neighbouring Bi adatoms. Interactions between the qubits would be required to use these structures for computing purposes.

The formation of ad-dimers is still an issue, because it is more energetically favourable for two Bi atoms to adsorb in the D or U site depassivated regions, than it is for a single adatom. In addition to this, there are no energy barriers to the formation of these structures, once the Bi are within a certain distance of one another. An exception to this result was observed for two Bi atoms adsorbed at U sites on opposite sides of a dimer row, separated by a depassivated Si dimer which they both share. In this case, formation of a Bi dimer above the Si dimer was less energetically favourable, by 0.1 eV, than staying as two U sites. However due to low barriers for

the formation (0.12 eV) or subsequent breaking (0.02 eV) of the dimer, it is expected that the Bi atoms would be constantly moving back and forth between the dimer and two U site structures. Despite these issues with dimer formation, with a low enough coverage of Bi, appropriate to the number of depassivated regions on the H:Si(001) surface, it should be possible to form the adatom structures with relatively few ad-dimers present. Given the right equipment and expertise it should be possible to realise this experimentally.

Further to this, these methods could be adapted to incorporate Bi atoms into the surface at specific positions. Once Bi atoms are adsorbed at D or U sites it is possible for them to substitute for one of the surface Si atoms to create a Bi-Si heterodimer. In order to allow for this incorporation process to take place a third H atom would need to be removed per depassivated region. With only two H removed, there is not enough space for the exchange to occur, or the energetics to do so are worse than for the Bi atom to leave the depassivated region. In a depassivated region of three H atoms, it has been found that some incorporation routes have similar energy barriers to the first step of diffusion out of the depassivated region. Since the Bi atom is more likely to return to the adatom site than complete the second depassivation step, it should be possible to incorporate deposited Bi into the surface before they leave the surface. Achieving this would require great care, because in order to allow incorporation to happen on a reasonable time scale, the temperature of the system would need to be raised. However if it is raised too far, the H atoms will also start to diffuse, getting rid of the specificity that this method offers.

Even without considering depassivation of the surface, other structures which are spin active, such as the Bi-V structure, can form by the deposition of Bi onto the H:Si(001) surface. Whilst lacking the specificity of the depassivated traps, it requires no additional surface patterning, and thus should be easier to realise experimentally. It is likely that defects, such as missing dimers, will be present somewhere on the surface, which would allow for the formation of the Bi-V structure. It has been shown that given such a defect, it is possible for the Bi atom to adsorb in a spin active configuration with only a small barrier to formation.

Chapter 7

Electronic structure of Bi nanoline

Here I present a theoretical investigation into the bias dependent STM appearance of the Bi nanoline on the Si(001) surface. In addition to this, a variety of related structures such as incomplete nanolines, Bi line structures without the Haiku core and other Group V nanolines were investigated to complete the characterisation of this structure. Further investigations, looking at Bi in bulk Si to aid studies into burying Bi nanolines, and an interesting spin structure on the bare Haiku core are presented in Appendices C and D respectively.

Recent experimental results from Christoph Renner's group in Geneva have shown that the appearance of the Bi nanoline in STM images changes with bias voltage, as demonstrated in Figure 7.1. As the positive bias is increased, the nanoline shifts from a zigzag appearance, to bright spots between the dimer rows, to bright spots on the dimer rows. This type of behaviour has not previously been observed in studies of the Bi nanoline. There is relatively little published data for the Bi nanoline at positive biases, and examples provided are at too high a value to see either effect [112]. Specific details such as the between dimer appearance only occur over a small bias range, making their identification difficult. Prior theoretical studies, such as those presented by Miwa *et al.* [47], have examined the Bi nanoline at low negative biases, but consider no details beyond the fact that the Bi nanoline is darker than the surrounding Si. A faint zigzag is visible in their data, but this is not noted.

To investigate the reasons for this behaviour, a detailed study of the electronic structure of the Bi nanoline was performed via simulated STM, using the structural model shown in Figure 7.2. Five distinct regions can be identified across a range of biases, as shown in shown in Figure 7.3. At higher negative biases, there are bright spots at the positions of the Bi atoms. At low negative biases a zigzag pattern is seen along the nanoline. At low positive biases a zigzag is seen in the opposite direction to the low negative bias version. At intermediate positive biases bright spots are seen between the Bi dimers in the trench region. Finally, at high positive biases the bright spots are seen on the Bi dimers. These regions will now be looked at in greater detail to ascertain the origins of these appearances.

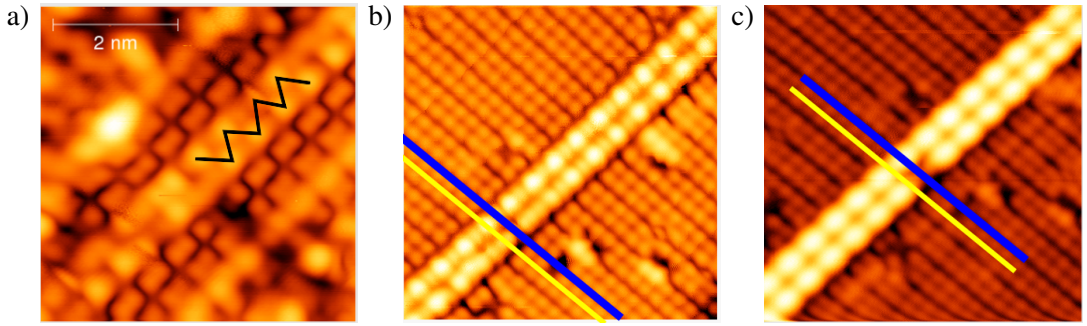

Figure 7.1: STM images of the Bi nanoline at a) +1.2 V, b) +1.5 V and c) +2.0 V. This shows a shift in appearance of the Bi nanoline from a zigzag pattern, to bright spots between the Bi dimer rows, to bright spots on the dimer rows. Images are courtesy of Sigrun Köster from Christoph Renner's group in Geneva. Blue lines in the images indicate the position of the centre of the dimer rows, and yellow lines indicate the position of the trench between rows.

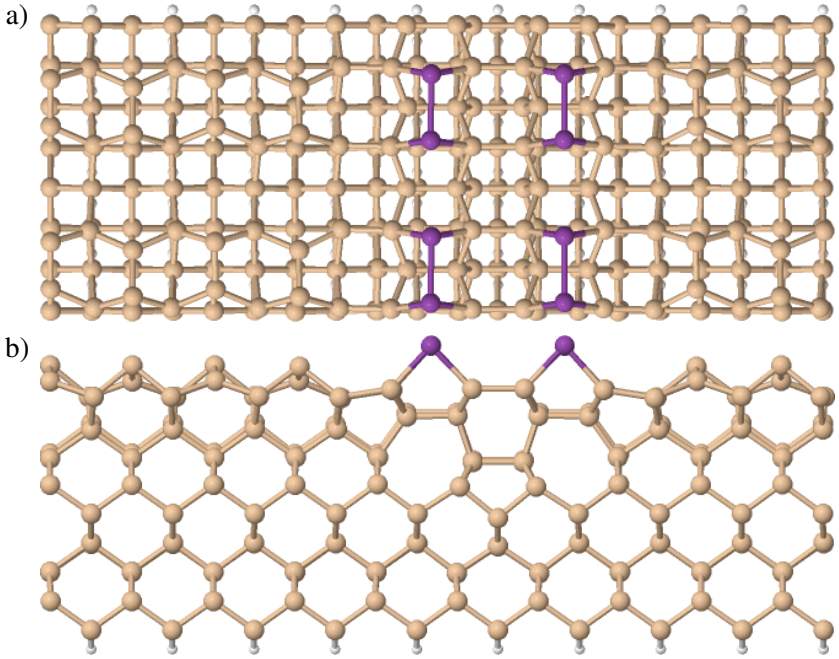

Figure 7.2: Full structural model of the cell used to represent the Bi nanoline in these calculations. a) Top view, rotated to align with the side view. The orientation used to produce simulated STM images is rotated 90° clockwise from this position. b) Side view, showing the Haiku core beneath the Bi nanoline.

7.1 Low positive bias

One of the most striking results is the fact that at lower positive biases, a clear zigzag pattern is visible along the Bi nanoline, as demonstrated in Figure 7.4. This is reminiscent of the buckling pattern seen for the surface Si dimers, despite the fact that the Bi dimers are completely flat. Simulated results provide an excellent match to experimental results, and offer an explanation for these results.

After acccounting for brightness and positional differences, this zigzag can be viewed as a continuation of the pattern of up buckled Si seen on the rest of the surface. The main difference

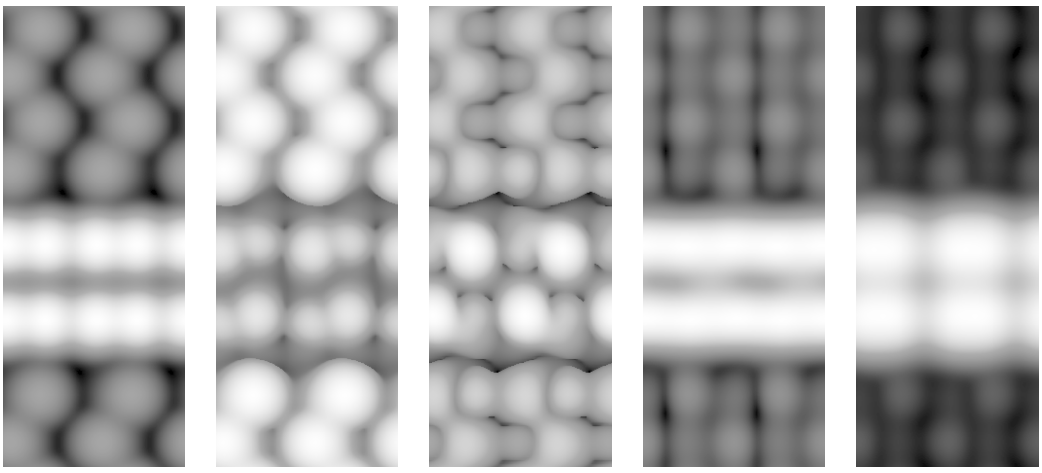

Figure 7.3: Simulated STM images of a 2 Bi dimer long section of the Bi nanoline, showing a shift in appearance with bias voltage. At high negative bias (-2.0 V) bright spots are seen at the Bi atoms. At low negative (-0.5 V) and positive (+0.7 V) biases zigzag patterns are observed along the nanoline with opposite directions. At intermediate positive biases (+1.1 V) the brightest regions are observed between the Bi dimers. Due to the brightness of the Bi nanoline, this is easiest to see by examining the region down the centre of the Bi nanoline. At higher positive biases (+2.0 V) the bright spots are observed on the Bi dimers. All simulated STM images are presented for isosurface values of 0.01 in arbitrary units, unless specified otherwise.

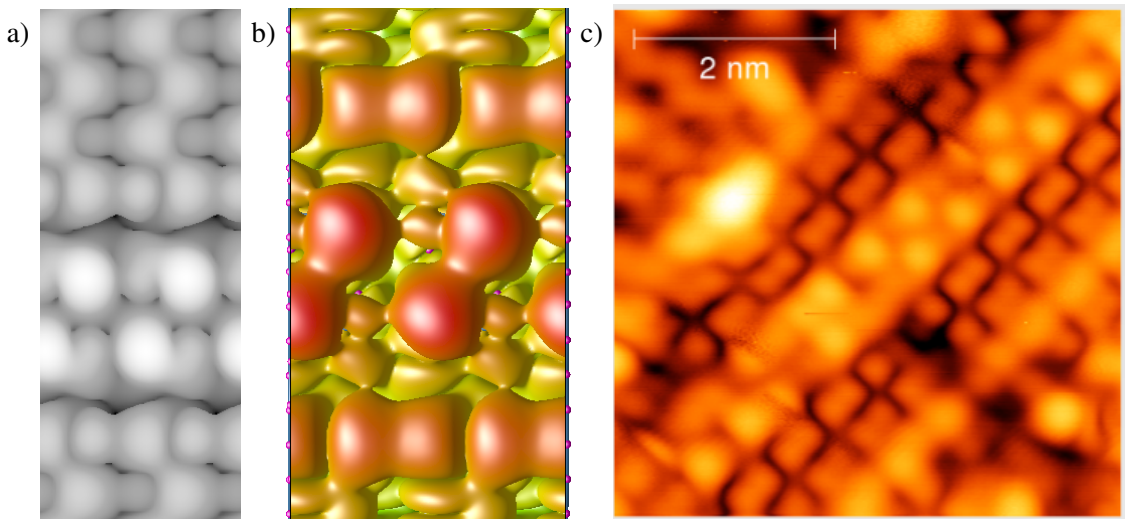

Figure 7.4: Comparison between simulated and experimental results showing the zigzag pattern along the Bi nanoline in addition to a change in appearance of neighbouring Si dimers. a) Simulated STM at +0.7 V. b) Band decomposed charge density of band 851 at 1.14 eV above E_F. This is shown as an example of a band which contributes to the zigzag appearance of the nanoline. c) Experimental STM at +1.2 V. Experimental images are courtesy of Sigrun Köster from Christoph Renner's group in Geneva.

being that the pattern extends across the two Bi dimers, rather than the four Si dimers this region would normally contain. This suggests an electronic coupling between the surface Si and the Bi dimers, because the Bi dimers are physically flat.

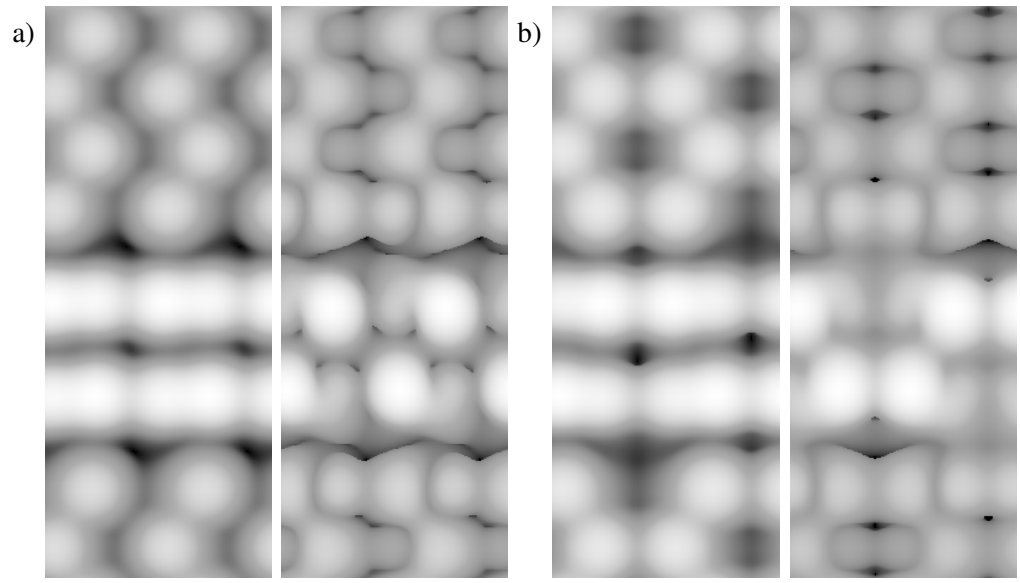

Figure 7.5: Simulated STM images of a 2 Bi dimer long section of the Bi nanoline, with a) p(2×2) or b) c(4×2) surface reconstructions. Both negative and positive bias images are shown. The former is to clarify the positions of the up Si. The latter shows bright spots along the Bi nanoline that coincide with the Si buckling pattern.

To be sure this was not just a coincidence, the buckling of the surrounding Si dimers was altered from a p(2×2) reconstruction to a c(4×2) reconstruction. The c(4×2) reconstruction was found to be 6 meV higher in energy, in contrast to clean Si(001) surface where it is lower in energy. This may explain why the p(2×2) reconstruction is more regularly observed around the Bi nanoline. The resulting simulated STM can be compared to previous results, as in Figure 7.5. It is clear from this that the appearance of the Bi nanoline changes with surface reconstruction. For the c(4×2) reconstruction, the bright spots still match to the positions of the up buckled Si atoms, however because the up Si are arranged differently, the nanoline itself looks different.

This can be extended to other dimer arrangements such as where the Si buckling is mirrored across the length of the nanoline, or the dimers are flat, as shown in Figure 7.6. It is useful to investigate alternatives such as these, because there is no guarantee that in experiment the Si dimers will always be arranged to produce a zigzag pattern.

To test a structure with mirrored buckling, the cell was extended to eleven dimers. This allows the buckling of all the dimers on one side of the nanoline to be flipped, without causing a buckling mismatch at the cell boundary. Results from Figure 7.5 suggest that if the Si buckling is mirrored along the length of the Bi nanoline, then the pattern of bright spots on the Bi dimers should be as well, with the same end of each Bi dimer brightening. The simulations exactly match these predictions, with the bright spots once again matching to the up atom positions.

For flat Si dimers, since there is no difference between dimer ends, the Bi dimer atoms would be expected to all look the same. The simulations once again confirm this result, and provide even more support for the link between surface buckling and Bi dimer appearance. The flat dimer arrangement is significantly worse energetically than either of the p(2×2) or c(4×2), at more than

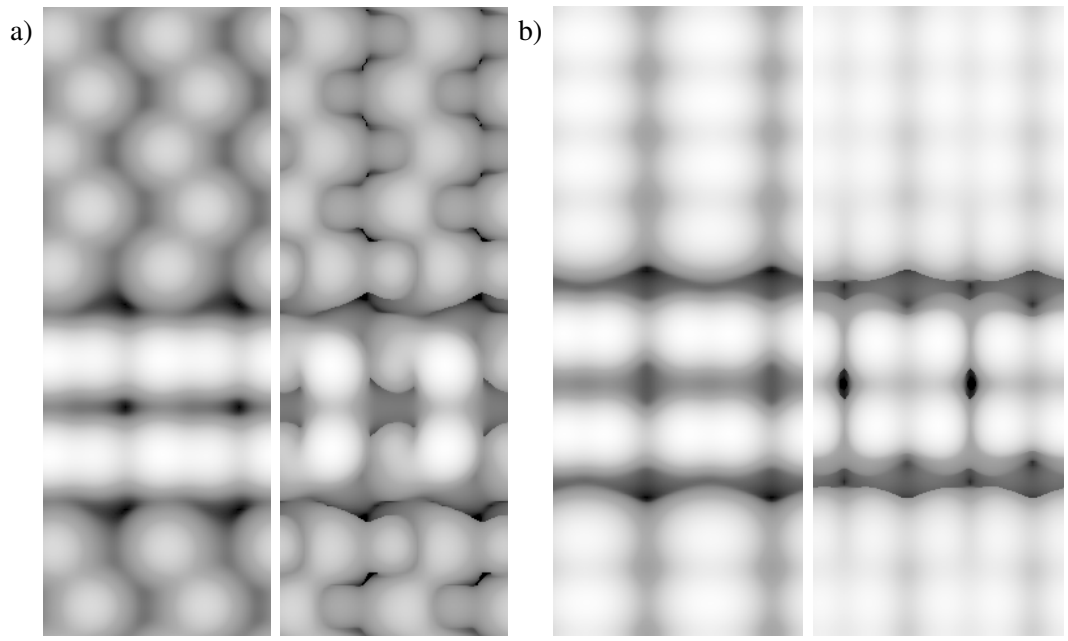

Figure 7.6: Simulated STM images of a 2 Bi dimer long section of the Bi nanoline with different Si arrangements. a) Si dimers in a p(2×2) arrangement with Si buckling mirrored along the length of the Bi nanoline. b) Flat Si dimers. Both negative and positive bias images are shown. The former is to clarify the Si positions. The latter shows that the bright spots still match to the buckling pattern of the neighbouring Si dimers.

2.3 eV higher in energy, which is expected.

These results demonstrate the ability to predict the nanoline appearance based on the Si arrangement. This makes simulations of further variations, including mirrored c(4×2) rows, and mixes of p(2×2) and c(4×2) reconstructions unnecessary.

Currently there is relatively little experimental evidence for these alternative patterns though, since the low positive bias results are fairly scarce, and it can be hard to identify the buckling of the Si in the first place. However this evidence does exist, as shown in Figures 7.7 and 7.8.

Figure 7.7 compares experimental and simulated images for a region of the nanoline on c(4×2) reconstructed Si, but at a slightly higher bias than in previous images. In the simulated image the distinction between the regions corresponding to up and down buckled Si is no longer as clear as before, however a difference in spatial extent is still visible. A similar appearance can be found in the experimental images, confirming these simulations.

Figure 7.8 on the other hand shows experimental results for an extended section of the Bi nanoline with varying surface reconstructions along the length of the line. This results in a variety of patterns on the Bi nanoline itself including zigzags and adjacent spots, which agrees with the results obtained from simulations. The experimental image is complicated by the presence of other structures on the surface such as Mn nanowires and defects, which also influence the appearance of the Bi nanolines.

Another interesting effect seen at lower positive bias is the change in appearance of the Si dimers directly next to the Bi nanoline, compared to those further away, as highlighted in Fig-

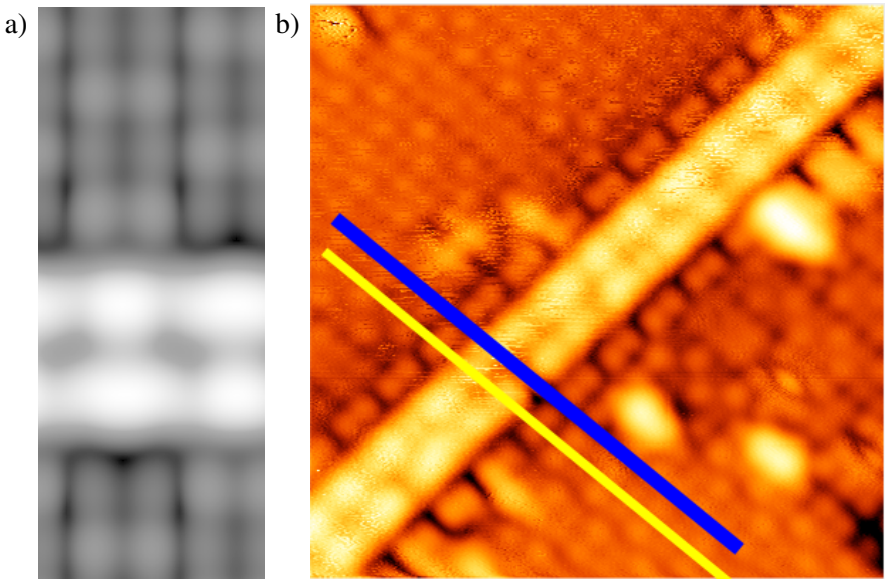

Figure 7.7: Comparison between a) simulated STM at +1.0 V and b) experimental STM at +1.2 V showing the Bi nanoline surrounded by c(4×2) reconstructed Si. Experimental images are courtesy of Sigrun Köster from Christoph Renner's group in Geneva.

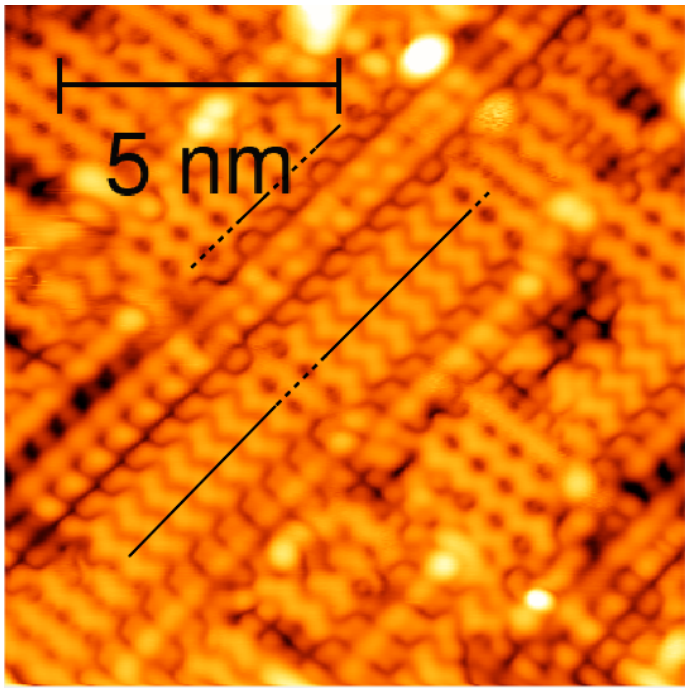

Figure 7.8: Experimental STM image of the Bi nanoline at +1.2 V showing changing arrangements of Si atoms surrounding the Bi nanoline. Regions marked with a filled line are p(2×2), those marked with a dashed line are c(4×2). The bright region of the Si dimer rows corresponds to the down Si atoms. Image courtesy of Sigrun Köster from Christoph Renner's group in Geneva.

ure 7.9. Normally as the bias is increased the periodicity of the entire dimer row shifts, meaning what looks like the trench is actually the middle of the dimer rows. Before this happens, just those Si directly next to the Bi nanoline appear to shift in periodicity, leaving them out of phase with the rest of the row. This is well reproduced by simulations, especially the band decomposed charge

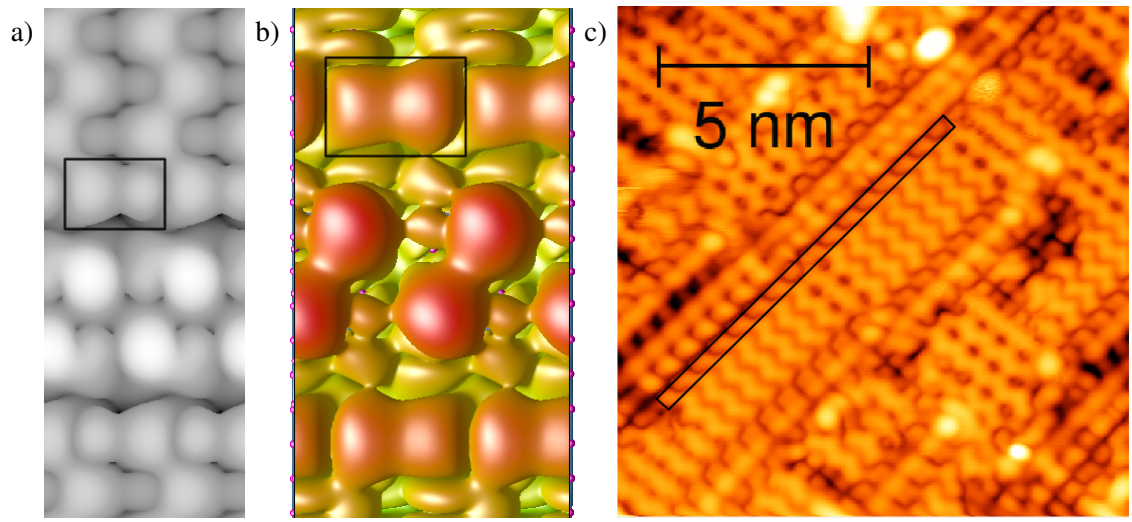

Figure 7.9: Experimental results and simulations which show a phase shift of the Si dimers directly next to the Bi nanoline. Black boxes are used to highlight this effect. a) Simulated STM at +0.7 V. b) Band decomposed charge density of band 851 at 1.14 eV above E_F. c) Experimental STM at +1.2 V. Experimental images are courtesy of Sigrun Köster from Christoph Renner's group in Geneva.

density. It was previously suggested that this is a strain effect related to the Haiku reconstruction [112], however this is also seen for Bi on the Si(001) surface without the Haiku core, as will be examined in more detail in Section 7.9). This suggests it is an electronic effect related to the presence of the Bi dimers on the Si surface.

7.2 Intermediate positive biases

As the bias voltage is increased, both in experiment and simulations, brighter spots are seen between the dimer rows, and darker spots on the rows as shown in Figure 7.10. The between dimer appearance is only seen over a small bias range of about 0.1 to 0.2 V, which in experiment occurs around +1.5 V. When looking at these results it is important to understand that the Si dimer rows undergo an apparent phase shift, making the centre of the rows look like the trench, and vice-versa. This is clearest by comparing the simulated results at isosurface values of 1 and 0.01, where just changing the imaging settings changes the apparent position of the Si dimers. The simulations match the brightness contrast seen in the experimental images, whilst also suggesting an explanation for this appearance. In simulated STM there is a brighter spot between the dimer rows and what looks like two smaller spots on the dimer row. Comparison to the band decomposed charge density shows practically the same picture, but the distinction between the different regions is clearer. This is because both simulated and experimental STM images consider contributions from several different bands, meaning that the picture will never be as clear as from a single band.

This pattern looks strikingly like overlapping atomic p-orbitals, so to confirm this a simple model of overlapping atomic p-orbitals was built. A two dimer long section of the Bi nanoline was represented by eight p-orbitals, arranged as to mimic the positions of eight Bi atoms, an example of which is shown in Figure 7.11. The absolute distances in the model are arbitrary, but the relative

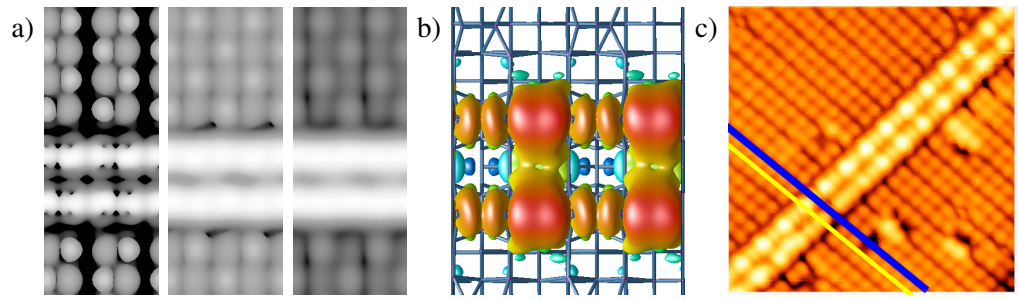

Figure 7.10: Comparison between simulations and experiment, showing the Bi nanoline with the brightest regions between the Bi dimers. a) Simulated STM at +1.1 V and isosurface values of 1, 0.1 and 0.01 in arbitrary units. b) Band decomposed charge density of band 859 at 1.39 eV above E_F. c) Experimental STM at +1.5 V. The blue line indicates the centre of the dimer row, and the yellow the trench between rows. The Si dimers have undergone a phase shift, making it look like the opposite is the case. Experimental images are courtesy of Sigrun Köster from Christoph Renner's group in Geneva.

distances between the centres of the p-orbitals are the same as for the Bi atoms in the real nanoline. The spacing between the dimers is 1.5 times that of the dimer length and the spacing between the dimers rows is twice the dimer length. The extent of the p-orbitals was determined empirically to produce overlaps similar to the previous theoretical results. The relative phase of the p-orbitals, as represented in blue or red, can then be arranged so as to form bonding or anti-bonding regions between neighbouring Bi atoms. When orbitals overlap in phase (blue and blue or red and red) bonding orbitals are formed, whereas if they are out of phase (blue and red) anti-bonding orbitals are formed. The different possible arrangements of these p-orbitals are shown in Figure 7.12.

When the p-orbitals overlap in such a way that there are anti-bonding orbitals on top of the Bi dimers, and bonding orbitals in the trench region between Bi dimers, as shown in b) this closely matches the charge density shown in Figure 7.10, as well as the simulated STM at an isosurface value of 1. This suggests that it is possible to see isolated p-orbitals when imaging the Bi nanoline, and that the change in appearance is due to imaging different bonding or anti-bonding states. However, it does not appear to be possible to access all four of these states.

It is also possible to treat this problem analytically, by considering four overlapping p-orbitals with periodic boundary conditions, which represents a pair of Bi dimers along one side of the Bi nanoline. These results can then be linked back to the graphical representation given in Figure 7.12. As before, the p-orbitals are spaced to match the arrangement of a pair Bi dimers in the Bi nanoline. It is assumed that p-orbitals will only interact with adjacent p-orbitals, with different interaction parameters depending on the distance between orbitals, as shown in Eq. 7.1. Due to periodicity, the 1^{st} and 4^{th} orbitals are treated as adjacent.

$$\begin{aligned} \langle p_n|\hat{H}|p_n\rangle &= \epsilon \\ \langle p_m|\hat{H}|p_n\rangle &= \begin{cases} h_1 & \text{adjacent and near} \\ h_2 & \text{adjacent and far} \\ 0 & \text{else} \end{cases} \end{aligned} \tag{7.1}$$

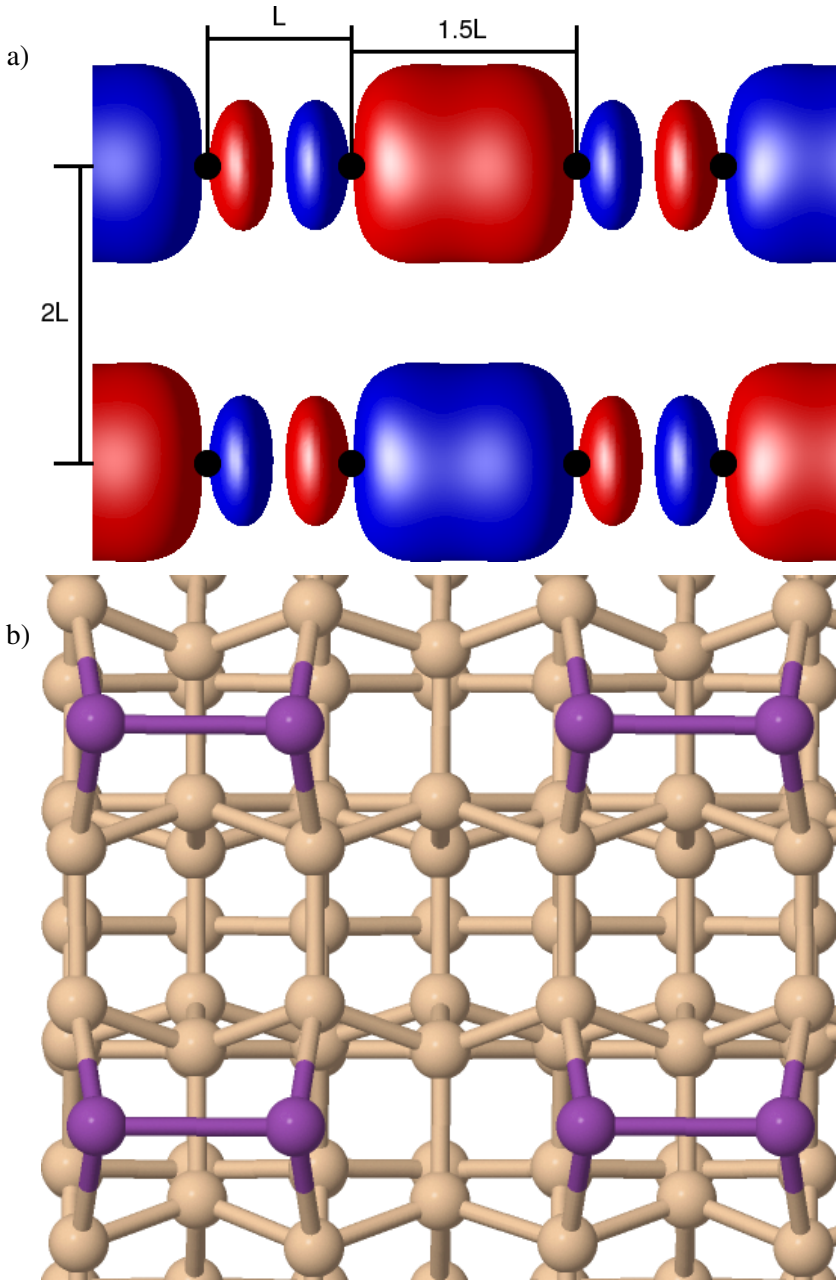

Figure 7.11: a) Schematic for a model of overlapping p-orbitals equivalent to a two dimer long section of the Bi nanoline. The relative phases of the p-orbitals are represented in blue or red. Positions equivalent to those of the Bi atoms are indicated with black circles. The length scale for the model is arbitrary, but the ratios of the dimer length (L), dimer spacing (1.5L) and dimer row spacing (2L) are the same as for the real Bi nanoline. b) Structural model of the section of the Bi nanoline which is being represented by this model.

Here p_n are crystalline p-orbitals with $k = 0$, with n between 1 and 4, h_1 is the overlap function for near p-orbitals, i.e. the Bi-Bi bond, h_2 is the overlap function for far p-orbitals, i.e. the gap over the trench, and ϵ is the energy of a p-orbital. For simplicity this will henceforth be assumed to be zero. The full system can thus be represented as the following matrix:

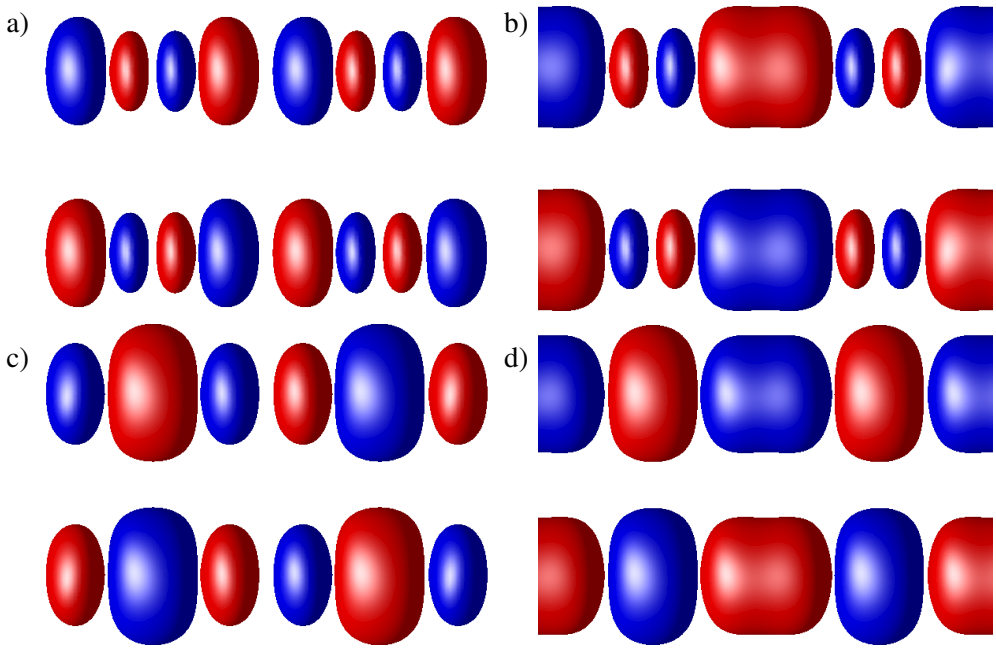

Figure 7.12: Model of overlapping p-orbitals equivalent to a two dimer long section of the Bi nanoline, with the relative phases of the p orbitals represented in blue or red. Those in phase will overlap to form a bonding region, whilst those out of phase will overlap to form an anti-bonding region. a) Anti-bonding in the dimer and trench regions. b) Anti-bonding in the dimer region and bonding in the trench region. c) Bonding in the dimer region and anti-bonding in the trench region. d) Bonding in the dimer and trench regions.

$$\begin{pmatrix} 0 & h_1 & 0 & h_2 \\ h_1 & 0 & h_2 & 0 \\ 0 & h_2 & 0 & h_1 \\ h_2 & 0 & h_1 & 0 \end{pmatrix} \tag{7.2}$$

The eigenvalues, and hence energies for this system can be found by solving

$$\begin{vmatrix} -\lambda & h_1 & 0 & h_2 \\ h_1 & -\lambda & h_2 & 0 \\ 0 & h_2 & -\lambda & h_1 \\ h_2 & 0 & h_1 & -\lambda \end{vmatrix} = 0, \tag{7.3}$$

the full details of which can be found in Appendix B.1. The solutions are as follows

$$\lambda = h_1 + h_2, -h_1 - h_2, h_1 - h_2, -h_1 + h_2. \tag{7.4}$$

These can be related to the visual representations via the eigenvectors, by solving

$$\begin{pmatrix} 0 & h_1 & 0 & h_2 \\ h_1 & 0 & h_2 & 0 \\ 0 & h_2 & 0 & h_1 \\ h_2 & 0 & h_1 & 0 \end{pmatrix} \begin{pmatrix} a \\ b \\ c \\ d \end{pmatrix} = \lambda \begin{pmatrix} a \\ b \\ c \\ d \end{pmatrix}. \tag{7.5}$$

Where a,b,c and d correspond to the eigenvectors of the 1^{st} through 4^{th} p-orbitals respectively. The full details of this are in Appendix B.2, with only the final solutions presented here. There are four possible solutions, each corresponding to one of the scenarios in Figure 7.12. The sign of an individual eigenvector can be related to the relative phases of that p-orbital. So for example negative can mean blue / red, whilst positive means red / blue. This means that if adjacent eigenvectors have the same sign, the p-orbitals will overlap out of phase and thus correspond to an anti-bonding orbital, whereas if their signs are opposite it will corresponds to a bonding orbital.

$$\lambda_1 = -h_1 - h_2, \quad v_1 = \begin{pmatrix} -1 \\ 1 \\ -1 \\ 1 \end{pmatrix} \tag{7.6}$$

If $h_1 and h_2$ are considered to be positive, the lowest energy solution, $-h_1 - h_2$, results in a system where all orbitals are bonding, corresponding to d) from Figure 7.12.

$$\lambda_2 = -h_1 + h_2, \quad v_2 = \begin{pmatrix} 1 \\ -1 \\ -1 \\ 1 \end{pmatrix} \tag{7.7}$$

The next lowest solution is $-h_1 + h_2$. This is because near orbitals will overlap more than far orbitals, hence $h_1 > h_2$, and thus $-h_1 + h_2$ is negative. This solution has bonding orbitals in the dimer region, and anti-bonding orbitals in the trench region, corresponding to c) from Figure 7.12.

$$\lambda_3 = h_1 - h_2, \quad v_3 = \begin{pmatrix} -1 \\ -1 \\ 1 \\ 1 \end{pmatrix} \tag{7.8}$$

The next solution is $h_1 - h_2$, which will be positive. This solution has anti-bonding orbitals in the dimer region, and bonding orbitals in the trench region, corresponding to b) from Figure 7.12 and thus also the experimental results.

$$\lambda_4 = h_1 + h_2, \quad v_4 = \begin{pmatrix} 1 \\ 1 \\ 1 \\ 1 \end{pmatrix} \tag{7.9}$$

The highest energy solution is $h_1 + h_2$, where all orbitals are anti-bonding, corresponding to a) from Figure 7.12.

Taken together these results show that the change in appearance of the Bi nanoline can be attributed to imaging different configurations of atomic p-orbitals. These results are in stark contrast to those seen at bias voltages just a few tenths of a volt lower. The zigzag pattern appears to be as a result of electronic coupling between the Bi dimers in the nanoline and the surface Si

dimers, whereas the ability to image atomic p-orbitals in such a way would suggest near complete decoupling between the surface and the nanoline.

This ability to image a specific configuration of atomic p-orbitals could be interesting from the point of view of studying fundamental physics. The relative ease with which this can be achieved is surprising compared to the significant efforts taken to image, albeit more complicated, molecular orbitals in other systems [113]. However, it would be restricted to just this one very specific system.

A slight improvement in the clarity of the experimental images might be needed, because currently the anti-bonding orbitals cannot be properly distinguished from each other, compared to the separation seen in simulations. However, since STM images integrate over a range of states, and consider contributions from several bands, it is unlikely that experimental images would be as clear as the single band results anyway. The clarity in simulations might also be because the simulations have neglected tip effects, thus making these details clearer.

7.3 High positive biases

As the bias voltage is increased further, the bright spots on the Bi nanoline shift in position again, this time to the dimer rows. This is once again reproduced in simulations as shown in Figure 7.13 and can be explained as imaging the Bi dimers along the nanoline. This result merely confirms previous studies.

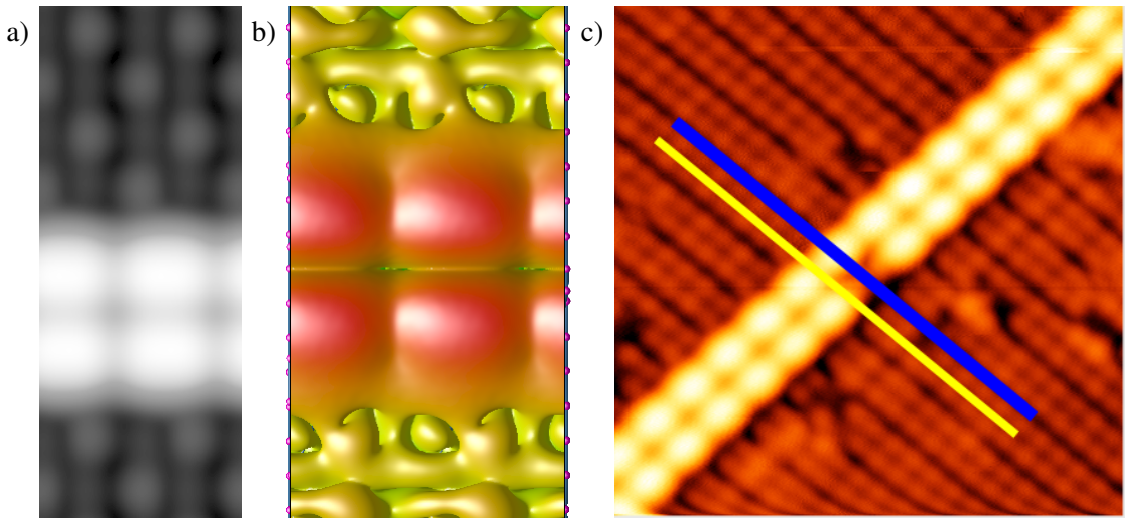

Figure 7.13: Images of the Bi nanoline at high positive biases, showing bright spots on the Bi dimers. a) Simulated STM at +2.0 V. b) Band decomposed charge density of band 861 at 1.48 eV above E_F. c) Experimental STM at +2.0 V. Experimental images are courtesy of Sigrun Köster from Christoph Renner's group in Geneva.

7.4 Low negative biases

The filled states of the Bi nanoline also show a change between lower and higher biases, however the former has not yet been observed experimentally, making comparisons impossible. This is

at least partly due to the fact that Christoph Renner's group reported difficulty producing low negative bias images for this structure experimentally. The switchover occurs at around -0.7 V in simulations, but it is unclear when or if this will be observed experimentally. Successes with matching simulation to experiment at positive biases suggest that these new simulations can be trusted.

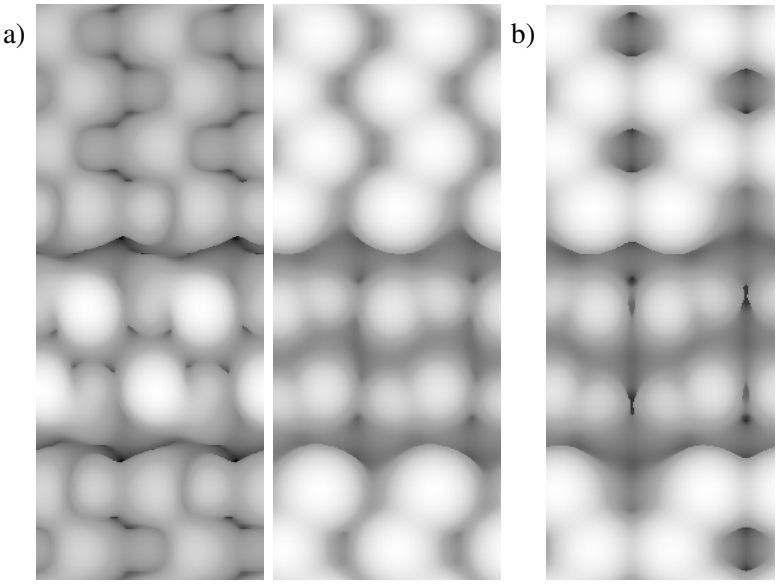

Figure 7.14: Low bias appearance of the Bi nanoline on a) p(2×2) Si and b) c(4×2) Si. The positive bias image is shown for the sake of comparison. The brighter ends of the Bi dimers match to the down Si positions in negative bias images. The distinction between dimer ends is less clear than for positive bias.

As with the low positive bias appearance, a zigzag is observed along the Bi nanoline, as shown in Figure 7.14. However in this case the brighter spots match to the down Si, rather than the up Si. The difference in brightness between the two ends of the Bi dimers is also less distinct than for empty states, making it harder to distinguish this zigzag pattern. In a similar manner to the low positive bias images, comparisons between Bi nanolines on the p(2×2) and c(4×2) reconstructions confirm the link between down buckled Si and the bright spots along the Bi nanoline. These results once again show an electronic coupling between the Si surface dimers and the Bi nanoline.

7.5 High negative biases

The final appearance for the Bi nanoline occurs at higher negative biases as shown in Figure 7.15, where bright spots are observed at each individual Bi atom. There is good agreement between experiment and simulation confirming previous studies.

7.6 Band structure

In addition to the studies of the appearance of the Bi nanoline, I also looked at the band structure in a bit more detail, by examining the single row structure with up to a 10×2×1 k-point mesh,

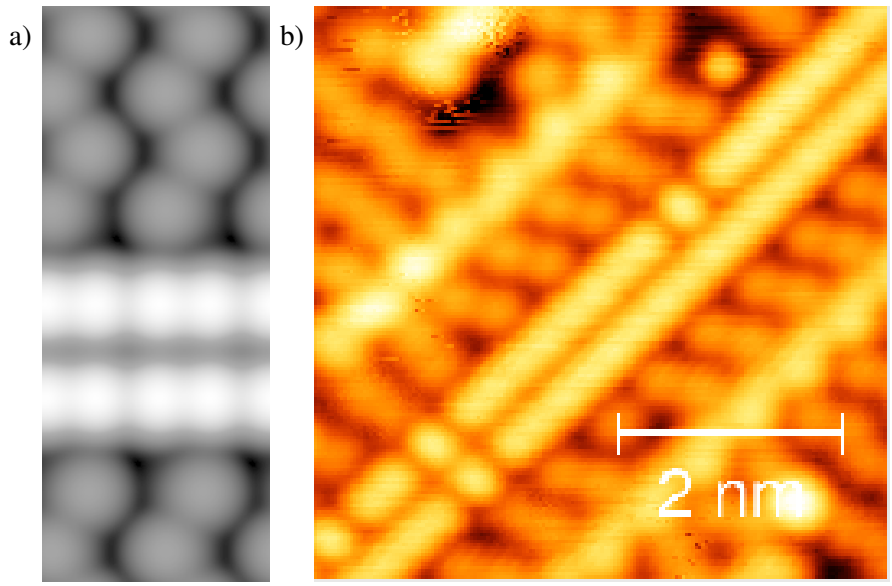

Figure 7.15: High negative bias appearance of the Bi nanoline. a) Simulated STM at -2.0 V. b) Experimental STM at -3.0 V. Bright spots are observed at each individual Bi atom. Experimental images are courtesy of Sigrun Köster from Christoph Renner's group in Geneva.

with the largest number along the direction of the nanoline. The band structure for the ten k-points along the direction of the Bi nanoline are shown in Figure 7.16.

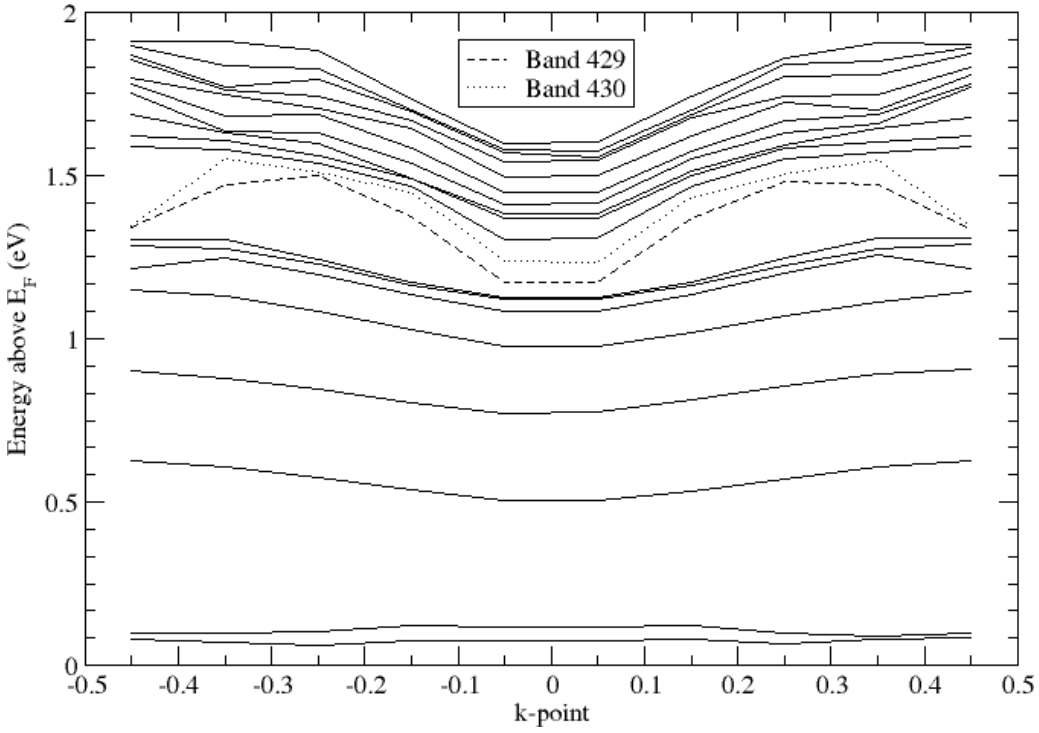

Figure 7.16: Band structure for bands 421 to 440 of a single rowed Bi nanoline, which are from 0.06 to 1.91 eV above the Fermi energy. Individual bands are shown for ten k-points along the direction of the Bi nanoline, in reciprocal space. The energy above E_F of each band is indicated along the y-axis, with the position in reciprocal space of each band along the x-axis.

For some of the bands, most notably bands 429 and 430, there is significant dispersion along

the band. The band decomposed charge density for these specific bands changes from the zigzag to between-dimer appearance as the k-point increases. Dispersion along the band implies delocalisation in real space which suggests interesting electronic properties, such as a 1D metal.

7.7 Bi nanoline variations

Having performed a detailed analysis of the electronic structure of the Bi nanoline, there are still more questions this raises. How reliant is this appearance on the exact positioning of the Bi atoms? How important is the Haiku reconstruction to the appearance of the Bi dimers and the surrounding Si? Is this exclusive to Bi, or does it extend to other Group V atoms and beyond?

To test the importance of Bi positioning, several variations of the Bi nanoline were constructed and their appearance in simulated STM compared. In addition to the regular nanoline, versions including half of the nanoline shifted into the trench between rows, the whole nanoline shifted into the trench or the Bi atoms kept evenly spaced were tested. These structures are shown in Figure 7.17 alongside their relative energies. For the evenly spaced Bi, their x coordinates were kept fixed.

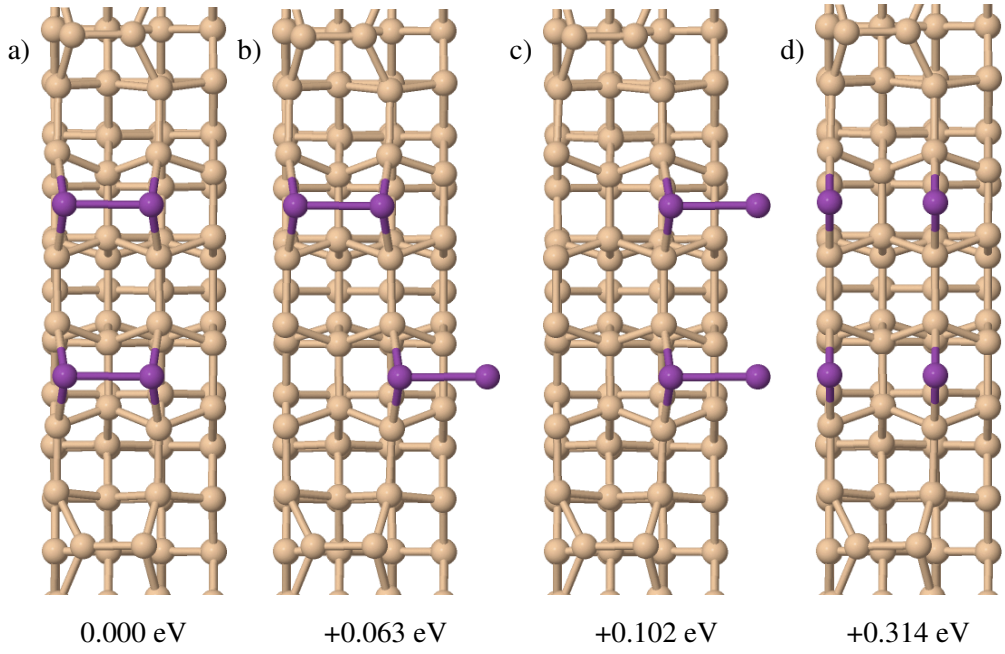

Figure 7.17: Variations of the Bi nanoline. a) Regular Bi nanoline. b) Half of the Bi nanoline shifted into the trench. c) Entire Bi nanoline shifted into the trench. d) Evenly spaced Bi atoms. Energies given are relative to the regular nanoline.

Before considering the simulated STM for these structures it is interesting to note the energy differences between them. The regular version of the Bi nanoline has the lowest energy, as might be expected given that it is the only version observed experimentally. The structures become energetically less favourable as they move further away from this, with the greatest increase coming from breaking the Bi-Bi bonds by evenly spacing the Bi atoms. The slight energy increase from shifting the dimers into the trench is due to the slight increase in Bi-Bi length of less than 0.1 Å. The increase in energy from shifting the first half of the nanoline into the trench is larger than for

shifting the second half into the trench, possibly because the mismatch between the halves leads to an additional increase in energy.

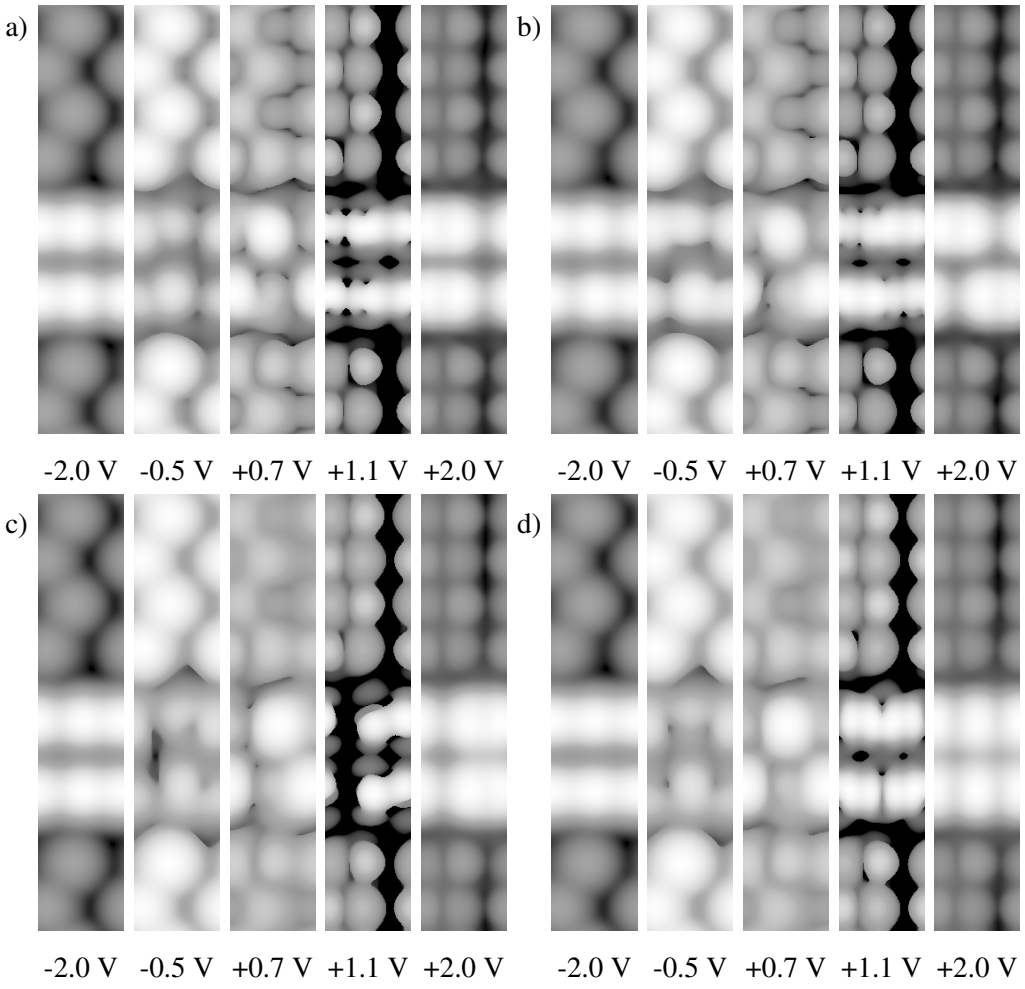

Figure 7.18: Simulated STM images for variations of the Bi nanoline. a) Normal. b) Half shift into trench. c) Full shift into trench. d) Evenly spaced Bi atoms. Results at +1.1 V are presented at an isosurface value of 1 in arbitrary units to clarify the between dimer features.

The simulated STM for these structures, as shown in Figure 7.18, show some interesting results when the different arrangements of Bi are compared at biases within the 5 notable regions. At -2.0 V there is little distinguishable difference between the arrangements, because the brightness of the individual Bi makes it difficult to tell the on dimer and between-dimer regions apart. At -0.5 V the down zigzag pattern is observed with little to differentiate the four variations. There is a slight shift in the positions of the bright and dark spots due to the shift in the physical positions of the Bi atoms. A similar effect is observed at +0.7 V, where the up zigzag pattern is largely unchanged, with differences once again arising from slight physical shifts in atom position.

The most noticeable differences between the structures start to become apparent at +1.1 V, where the location of the Bi dimers has a bearing on the location of features in the simulated STM. For example when half the nanoline is shifted, the appearance of the two halves is out of phase, due to the shift in position of the on-dimer and between-dimer regions. Unexpectedly, the between-dimer appearance is not observed when the entire Bi nanoline is shifted into the trench, despite the fact it is observed for a half shifted nanoline. It is not clear why there is this difference.

The appearance is different again for the evenly spaced Bi, looking the same either side of each Bi atom. This is because the overlap between each Bi will be the same, rather than having separate on-dimer and between-dimer regions. At +2.0 V, since the Bi dimer is being imaged, the physical shifts in location are reflected in the simulated STM images.

These results show that for the zigzag patterns to appear, merely the presence of Bi is necessary, without regard for the exact bonding arrangement of the Bi atoms. As long as the Bi atoms are at roughly the right position they will couple electronically to the surface Si atoms and produce a zigzag pattern. The high negative bias appearance similarly depends more on the physical location of the atoms, which barely changes, rather than the bonding arrangement. The similarities between all the variations at these biases suggests that some of them might have already been observed experimentally, but without realising it.

The between-dimer and on-dimer appearances of the Bi nanoline on the other hand rely on the physical positions of the Bi dimers, meaning their relative phase changes in accordance to the physical positions of the Bi dimers. This makes the distinction between the variations much clearer at higher positive biases, making it harder to believe that these variations have previously been overlooked in experiment.

7.8 Incomplete Bi nanolines

Even though, to the best of my knowledge, incomplete Bi nanolines have not been observed experimentally, modelling these structures might still provide further insight into the details of the Bi nanoline. One question is whether bright spots are still visible in the absence of actual Bi atoms, or whether there is an ehancement of the appearance of Bi atoms, even when the dimer is incomplete. Whether the appearance of individual dimers will change due to the absence of other dimers, or if they all behave in isolation, is also useful information. To test these matters several different structures were constructed as shown in Figure 7.19. The simulated STM are presented in Figures 7.20, 7.21, and 7.22.

For the structures where Bi are only placed at the up and down zigzag positions all that is seen is bright spots at the positions of the Bi atoms, with no interesting additional effects. If there is no Bi at the up zigzag position, no bright spots are observed there. If there is only Bi at the up zigzag position there is no enhanced brightness at this position. Taken together this shows that complete Bi dimers are required to get the zigzag effects.

If half of the Bi nanoline is missing, as in Figure 7.21, most of the interesting effects observed previously disappear. Not only is a zigzag pattern no longer observed at lower biases, but there is practically no distinction between the ends of the remaining Bi dimer. The lack of a zigzag is to be expected, because it has already been shown that the presence of the Bi atoms is vital to this. The lack of distinction between dimer ends for the remaining dimer might be because the exposed Si from the Haiku core are influencing the appearance of this dimer.

Similar effects are observed when only a single Bi dimer is missing from the Bi nanoline, as in Figure 7.22. In this case all Bi dimers adjacent to the gap in the nanoline, whether in the same or adjacent dimer rows, are affected. However any Bi dimers further away behave as normal. At

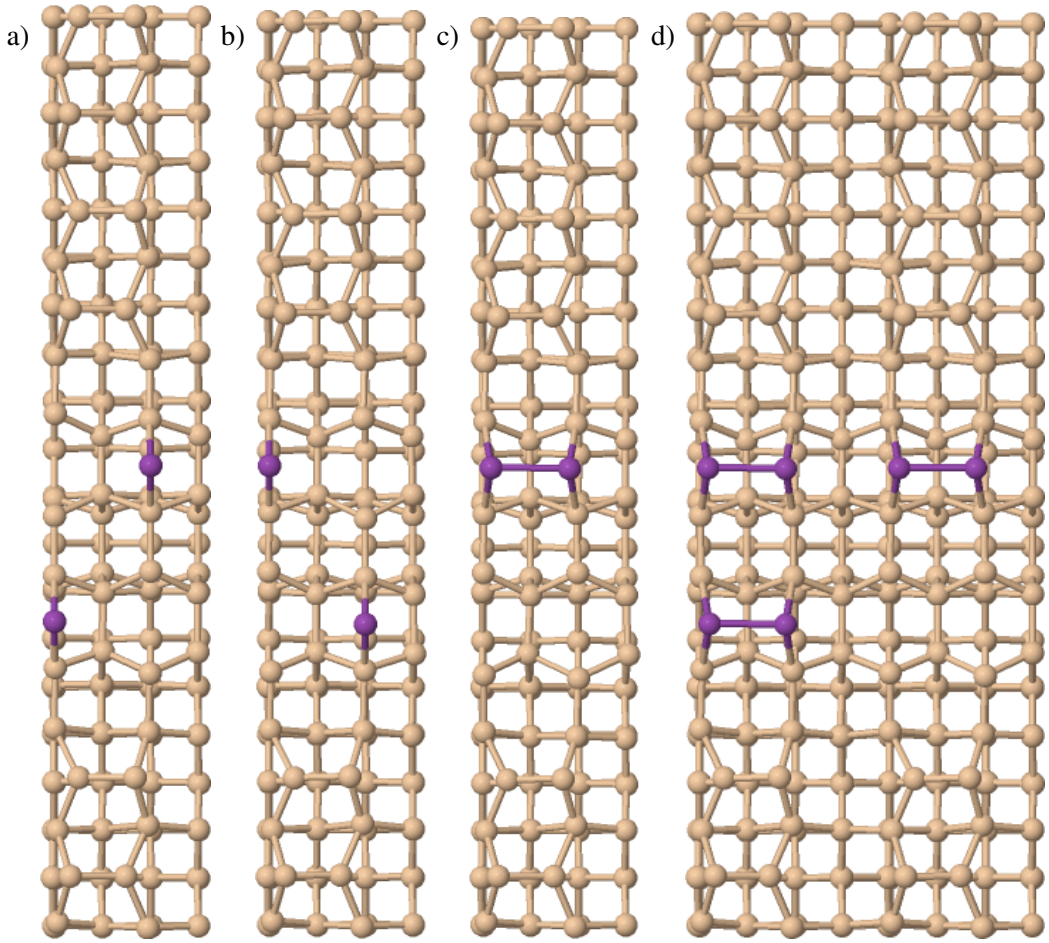

Figure 7.19: Structures for incomplete Bi nanolines. a) Bi only at the up zigzag positions. b) Bi only at the down zigzag positions. c) Half of the nanoline missing. d) A single dimer missing.

low negative biases the down buckled pattern is not observed on the Bi dimers adjacent to the gap. Whereas for low positive bias the up buckled pattern is still observed on the Bi dimer in the adjacent dimer row, but not on the dimer in the same row, although it does display a slight diagonal tilt.

In both cases, this is because of the influence of the Si that have been revealed by the removal of a Bi dimer. Since these Si are unbuckled, it would be expected that the Bi dimer in the same row would not display a brightness contrast between dimer ends. The fact the Bi-Si electronic coupling extends to adjacent rows is a new result, because for all previous nanoline calculations there has never been any revealed Si along the direction of the Bi nanoline. The coupling across rows is smaller than the coupling along rows, as evidenced by the fact that the low positive bias appearance of the dimer in the adjacent row barely changes.

The diagonal tilt observed for the dimer in the same row as the gap is likely due to competing effects from the buckled and unbuckled Si either side of the dimer.

At higher biases the general appearance of the nanoline is unaffected, beyond the fact that there is a dark spot where the dimer is physically missing. This is as expected, because at higher biases the appearance of the nanoline is due to the Bi atoms themselves, rather than a coupling with the surface.

Taken together, these results show that the overall appearance of the Bi nanoline is reliant on

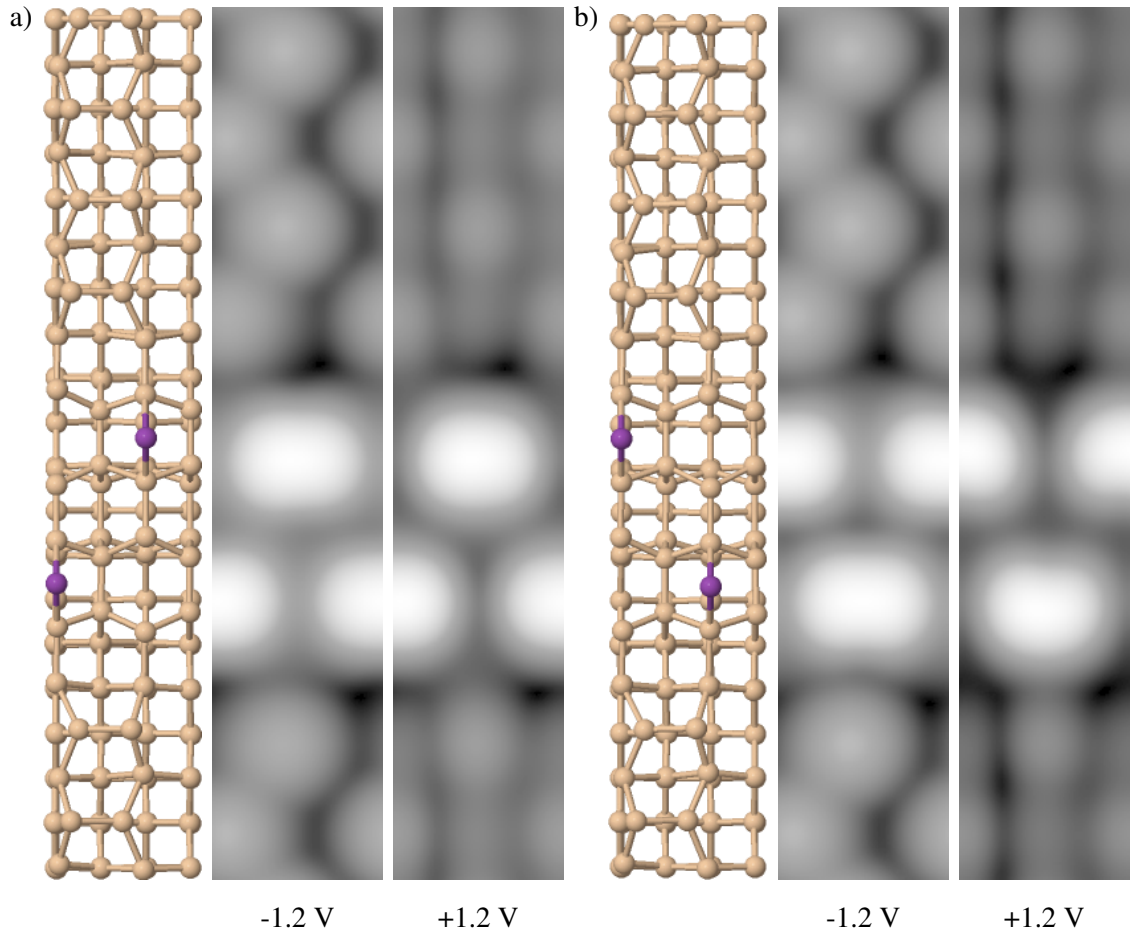

Figure 7.20: Simulated STM for incomplete Bi nanolines, with structural models included for clarity. a) Bi atoms only at the up zigzag positions. b) Bi atoms only at the down zigzag positions. There is practically no difference between the positive and negative bias appearances of these arrangements of Bi atoms.

the nanoline being complete. Removal of Bi atoms not only leaves a gap in the nanoline, but also changes the appearance of nearby Bi atoms, due to the influence of the revealed Si atoms. The Bi nanoline electronically couples to surface Si atoms both along the dimer rows and along the direction of the Bi nanoline, although the latter effect is weaker. This latter effect is more likely to be observable in experiment at the ends of the nanolines, since there is little experimental evidence for nanolines with gaps in them.

7.9 Bi lines on Si without the Haiku core

Until now all of these calculations have looked at Bi lines on the Haiku core, because this is the structure that matches to experimental observations. To gain additional insight into the low bias appearance of the nanoline, the investigation was extended to include Bi lines on the regular p(2×2) surface. Whilst this is not necessarily experimentally verifiable it should give additional details about the interaction between the surface structure and the Bi lines and whether the Haiku core is necessary to see these effects.

Four different arrangements of Bi lines were constructed, as shown in Figure 7.23. Two differ-

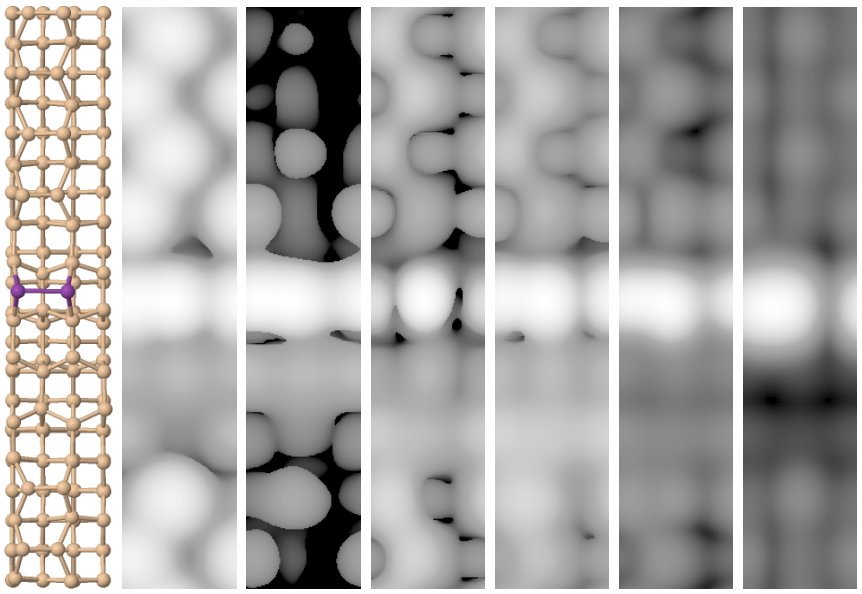

Figure 7.21: Simulated STM for an incomplete Bi nanoline, where half of the nanoline is missing. Structural model is included for clarity.

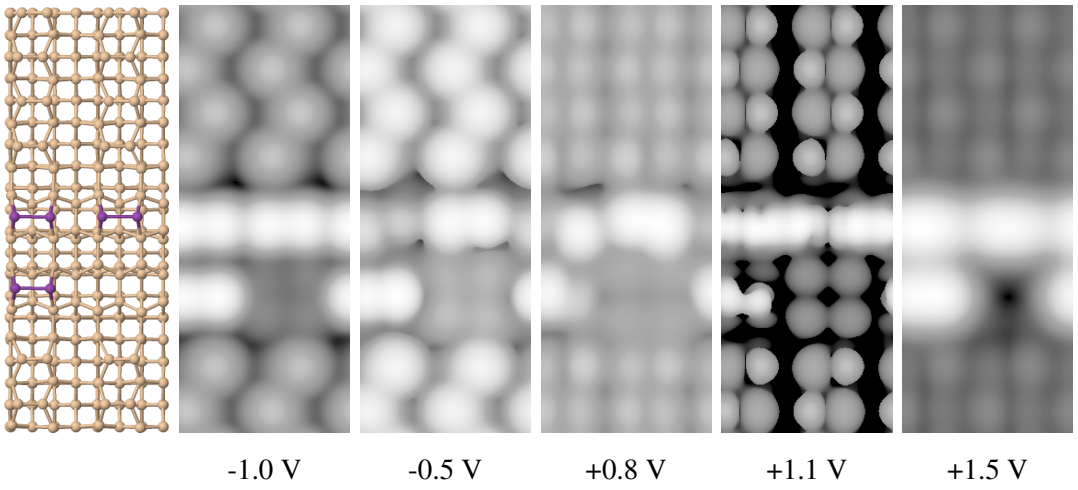

Figure 7.22: Simulated STM for a Bi nanoline with a missing Bi dimer, with the structural model included for clarity. Results at +1.1 V are presented at an isosurface value of 1 in arbitrary units to clarify the between dimer features.

ent versions of the double line, with different spacings were used. For a) the Bi dimers stretched across a space of three Si dimers, the closest possible distance between two neighbouring Bi lines. Whereas for b) a spacing of four Si dimers was used, since this can roughly replicate the spacing of the Bi dimers atop the Haiku core. Examining the different spacings between the dimers might reveal details about the range of interactions between the Bi and Si. The triple line presented in c) also tests this idea and whether the Bi has to be directly next to the buckled Si or not. Finally a single dimer line, as a shown in d), was studied, to see whether the zigzag pattern would disappear under these conditions or not.

The simulated STM images shown in Figure 7.24 detail some of the important features seen for the double line structures. Similarly to the regular nanolines, at low biases there is a brightness

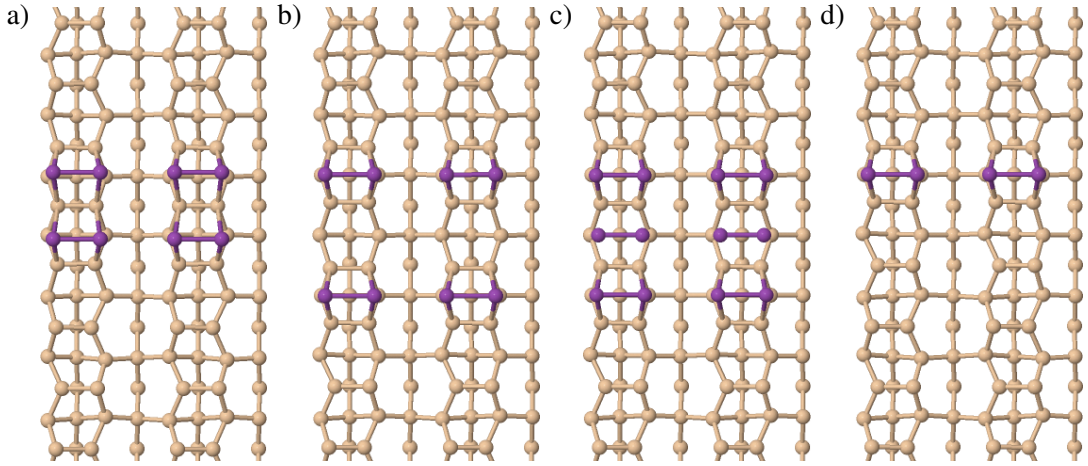

Figure 7.23: Bi dimer lines on the p(2×2) Si surface. a) Two dimer lines covering three Si dimers. b) Two dimer lines covering four Si dimers. c) Three dimer lines. d) Single dimer line.

contrast between individual Bi atoms. The exact pattern observed varies with the spacing of the Bi dimers.

When the Bi dimers occupy a space equivalent to three Si dimers, the left hand atoms of the dimers appear brighter at lower positive biases. This is similar to the pattern seen for the regular Bi nanoline with mirrored p(2×2) buckling, shown earlier in Figure 7.6. Although in this case the bright spots appear to correspond to down Si positions, since they lie next to up buckled Si. Unlike for the regular nanoline there is no observed region where the equivalent up positions are brightest.

As with the regular nanoline, this pattern of bright spots is related to surface buckling, meaning that, with the correct arrangement, a zigzag pattern could be reproduced, as shown in Figure 7.25. In this case the cell was extended to eleven dimers in length, to allow for the flipping of the dimers on one side of the Bi lines, without causing a mismatch at the cell boundaries.

Other interesting features not seen for the regular nanoline are also observed, such as the phase shift at +0.6 V or the bright spot that appears between the dimer lines at +0.8 V. The former coincides with the phase shift for the Si dimers next to the line, suggesting the two might be connected. The bright spots between the dimer lines could be for similar reasons to the between-dimer appearance in the regular nanoline, in this case brought about by the close proximity of the two lines to each other. Further work could investigate these matters in more detail, but the practical applications would be questionable due to the lack of experimental structures to compare with.

When the dimers instead occupy a space equivalent to four Si dimers, a zigzag pattern is observed, in a similar fashion to the regular Bi nanoline. At very low positive biases, such as 0.3 V a zigzag pattern corresponding to down Si atoms is observed, with the zigzag switching to the up Si atoms at 0.5 V. In contrast to the regular Bi nanoline, the down zigzag is more distinctive than the up zigzag, in addition to the fact that the split between these two patterns occurs solely at lower positive biases, rather than at the positive negative divide.

A common feature shared between both structures and the regular nanoline is the strain induced change in appearance of the Si dimers directly next to the Bi lines. This can be seen most

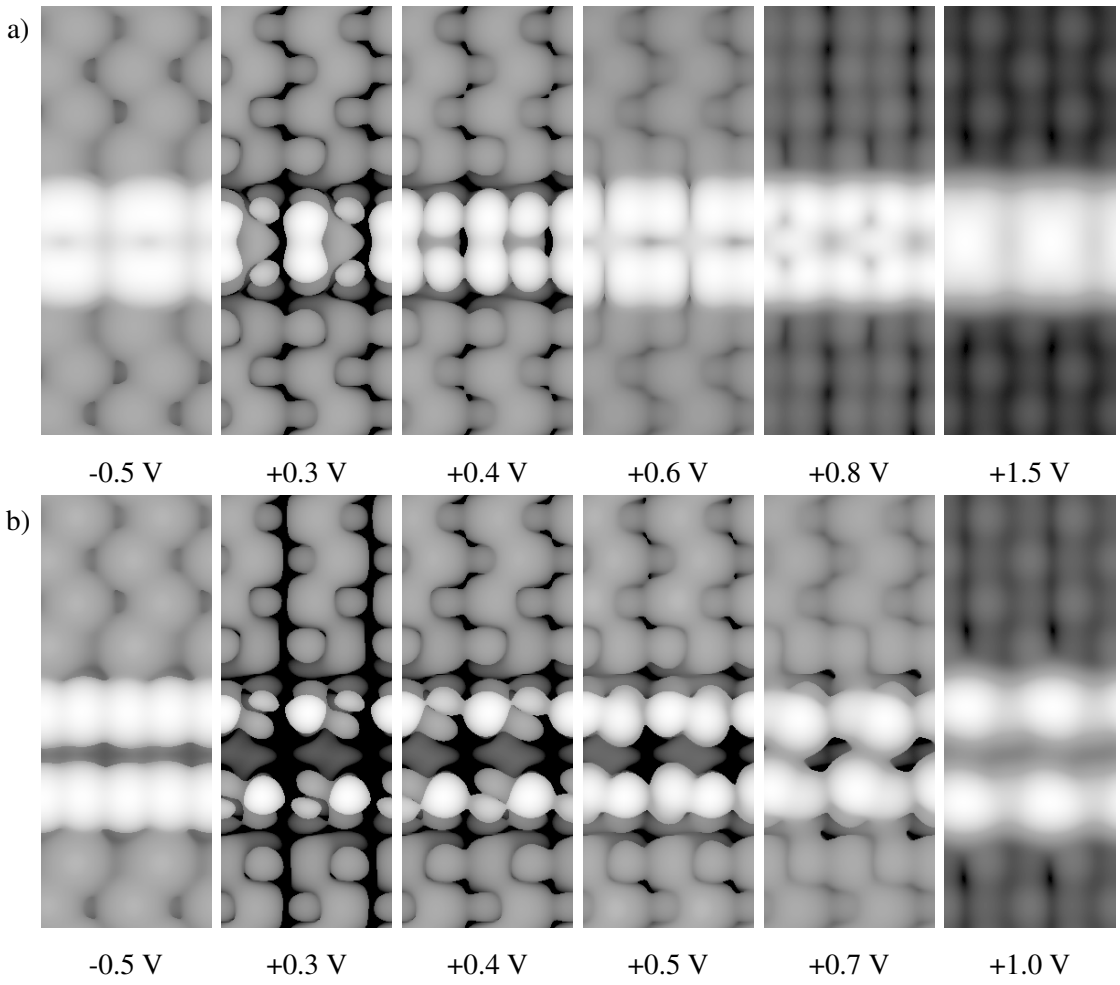

Figure 7.24: Simulated STM images for double Bi dimer lines covering a) 3 Si dimers or b) 4 Si dimers.

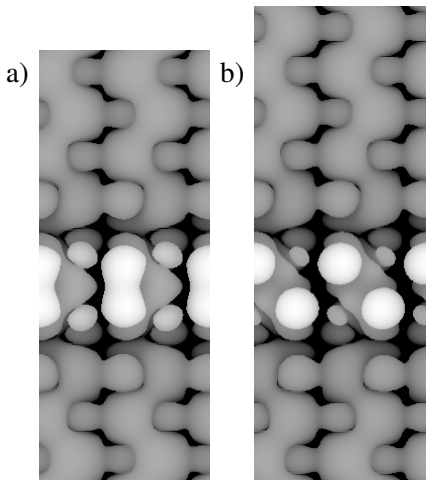

Figure 7.25: Simulated STM images for double Bi dimer lines covering three Si dimers with a) matching dimer buckling or b) mismatched dimer buckling either side of the Bi lines. The simulation cells were ten and eleven dimers long respectively.

clearly at +0.6 V in Figure 7.24.a) and +0.7 V in Figure 7.24.b). Previously this had been assumed to be related to the Haiku core [112], but these results show that this cannot be the case. Instead it is likely due to the presence of the Bi atop the Si surface introducing strain. This result will prove

useful in later research related to the Mn nanowire in Chapter 9.

The triple line structure shows some behaviour unlike any of the other studied structures, as demonstrated in Figure 7.26, however there are still a few familiar features. At low positive biases a zigzag pattern is observable along the line, although in this case the bright spots extend over two Bi atoms instead of the usual one. The outer bright spots match to down Si positions as also observed for the double line at +0.4 V in Figure 7.24.b), with the intermediate Bi line matching to these. This intermediate Bi line is completely isolated from the surface Si dimers, suggesting the electronic coupling between the surface Si atoms and the Bi atoms can extend over multiple Bi atoms. The bright spots only halt when another dimer exposed to surface Si is reached, as demonstrated with the regular nanoline. Further tests of four or more dimer lines could determine the range of this effect, but they have currently not been performed.

At +0.7 V, both the Si dimers next to the lines and the Bi dimers themselves display a phase shift, similar to that seen in Figure 7.24.a) at +0.6 V. The change observed in the Si dimers provides more support for the idea that merely the presence of Bi lines is required, rather requiring the Haiku core. These dimers all return to normal by +0.8 V, barring the central Bi line.

At higher biases, the lines behave as would be expected, simply appearing as bright spots where the Bi dimers are. The inability to make experimental comparisons makes it hard to justify studying this further.

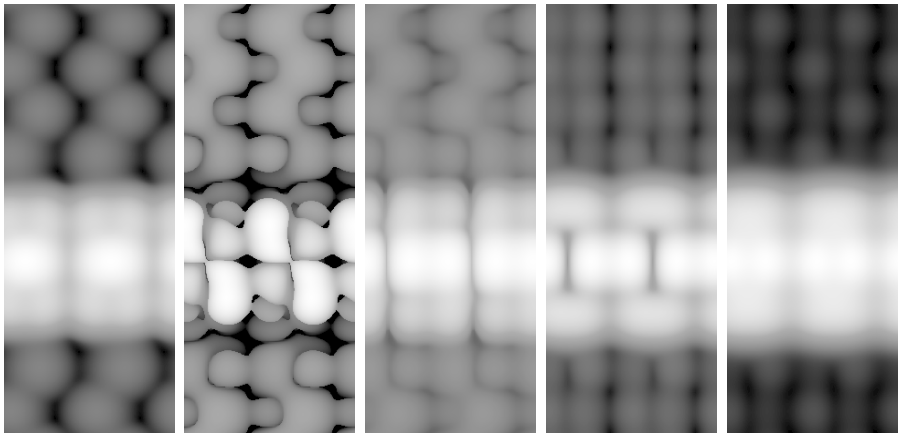

Figure 7.26: Simulated STM images for a triple Bi dimer line on p(2×2) Si.

For the single Bi dimer line it might be expected that there would not be a zigzag pattern, since previous results have relied on the separation between the two halves of the nanoline. However, as Figure 7.27 shows, a zigzag pattern appears along the dimer line, even though it is physically straight. An interesting result is the fact that at very low negative and positive biases, the zigzag pattern matches to the up Si atoms, whilst at slightly higher positive biases, around +0.5 V to +1.1 V, the pattern matches to the down Si atoms. This is the opposite to what is seen for the regular nanoline. Some of these results are similar to those seen for P atoms and dimers on the Si(001) surface [114] which similarly reported structures which look tilted in STM images despite being physically straight.

There are also potential hints of the between-dimer appearance at 1.1 V, however the on dimer part still remains brighter than the between-dimer part, in contrast to the regular nanoline. This is

despite the fact that the inter-dimer separation is the same to within 0.1 Å for both structures. This effect was not observed for any of the other line structures on the regular p(2×2) surface.

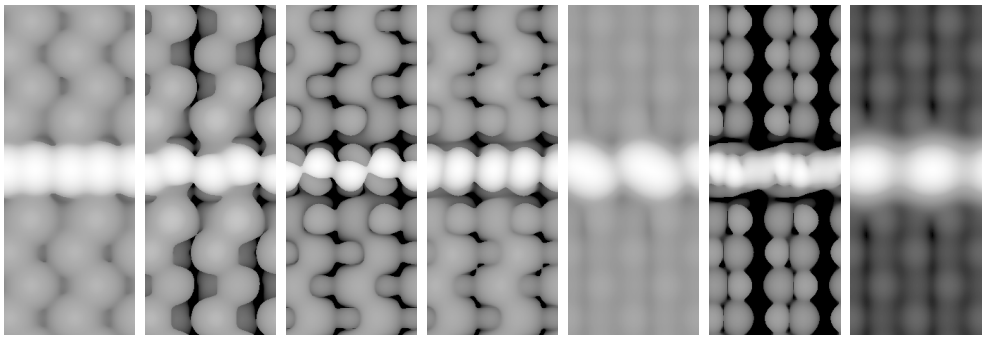

-0.5 V -0.2 V +0.3 V +0.5 V +1.0 V +1.1 V +1.2 V

Figure 7.27: Simulated STM images for a single Bi dimer line on p(2×2) Si. Results at +1.1 V are presented at an isosurface value of 1 in arbitrary units to clarify the between dimer features.

As well as comparing the simulated STM appearances of these structures it can be useful to compare their energetics, based on their adsorption energy per Bi atom, as shown in Table 7.1. Energetically there is little difference between the single dimer line and the double lines spaced over four Si dimers. This might suggest only a limited interaction between the dimer lines of the double lined structure, with them essentially acting as two single lines that are next to one another. It might therefore be expected that the simulated STM for the double line, as shown in Figure 7.24.b), would look like two adjacent copies of the single line, as seen in Figure 7.27, which is not the case. The difference in appearance might be attributed to the fact that for the double lined structure there is only revealed Si on one side of the each dimer line, whereas for the single line both sides have revealed Si. The double lined structure spaced over three Si dimers and the triple lined structure both have worse adsorption energies because of the close proximity of the Bi lines to one another. Multiple Bi dimers share the same Si dimer, which is energetically unfavourable.

Table 7.1: Adsorption energies per Bi atom for different dimer lines on the p(2×2) surface with the Haiku core.

Bi dimer line structure	E_{ads}/Bi (eV)
Single line	-3.267
Double lines (spaced over three Si dimers)	-2.906
Double lines (spaced over four Si dimers)	-3.269
Triple lines	-2.814

When taken together these results show that the Haiku core is not necessary for some of the bias dependent effects, such as the strain feature, or the low bias patterns of the Bi dimers. Electronic coupling between the Si surface and the Bi atoms still exists, resulting in an alternating pattern of bright and dark Bi atoms, and this effect is even visible for a single Bi dimer line.

The regular nanoline with the Haiku core displays the alternating pattern over a wider range of biases, with a clearer distinction between the positive and negative bias appearances. This could

be attributed to the relative separations of the Bi dimers, since the Haiku reconstruction allows for a spacing simply not possible with unreconstructed Si. Compare the 6.3 Å separation for the Haiku core nanoline to the 4.2 Å or 7.7 Å separation respectively for the three and four dimer wide variations on regular p(2×2) Si.

7.10 Alternative nanolines on the Haiku core

Having thoroughly investigated the Bi nanoline, attention now turned to similar nanolines made up of other Group V atoms, to ascertain whether the bias dependent features are exclusive to Bi atoms or not. Previous experimental work might have observed Sb nanolines [115], however there has been practically no follow up work on this matter since, barring a single paper comparing stabilities of Group V atom lines on the clean Si(001) surface and the Haiku core [116]. This work suggested that only Bi and Sb were more stable above the Haiku core, with P and As preferring the regular Si surface arrangement. However recent developments allowing for the removal of the Bi nanoline whilst retaining the Haiku core [44], opens up the possibility for experimental realisation of other Group V nanolines.

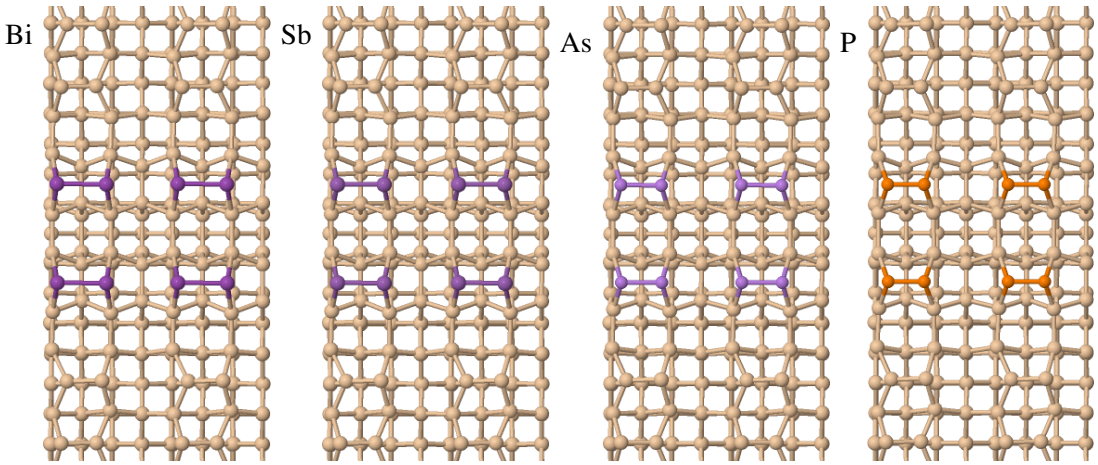

Figure 7.28: Structural models for Group V nanolines on the Haiku core.

Table 7.2: Inter- and intra-dimer distances of Group V nanolines atop the Haiku core.

Gp V atom	Dimer length (Å)	Inter-dimer distance (Å)	Dimer row distance (Å)
Bi	3.12	4.56	6.31
Sb	2.95	4.73	6.29
As	2.57	5.11	6.22
P	2.31	5.37	6.19

To investigate the Group V nanolines, the Bi atoms of the Bi nanoline structure were substituted for either P, As or Sb and allowed to relax, resulting in the structures shown in Figure 7.28. The main difference between all of these structures, apart from the different atom types, is the distances between them, as shown in Table 7.2. As would be expected for the smaller Group V atoms, the dimer lengths are smaller and the distances between dimers are larger. The distance

between dimer rows decreases slightly as the atom size decreases, suggesting a slight repulsive interaction between neighbouring Group V dimers, which is reduced with atom size.

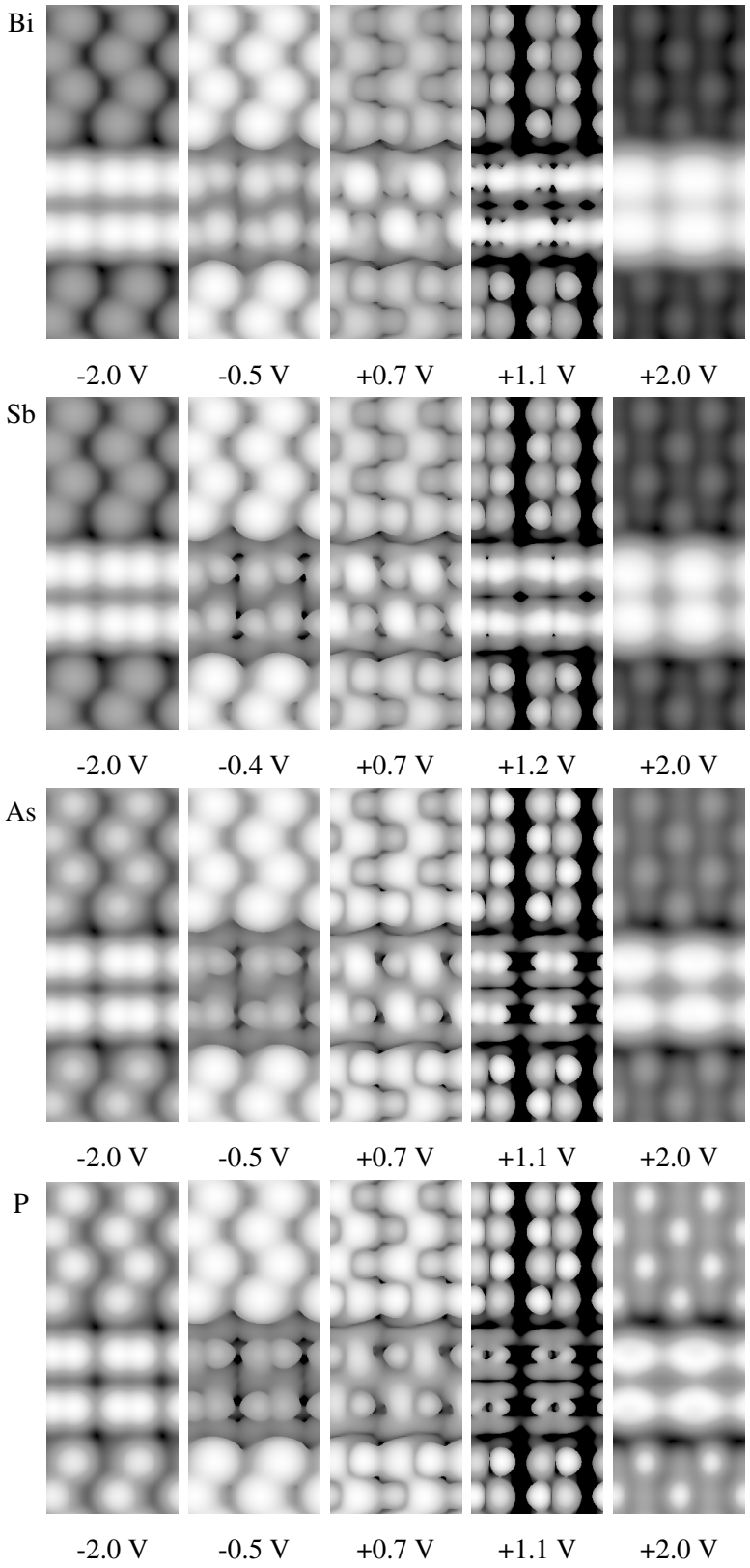

Figure 7.29: Simulated STM images for the Bi, Sb, As and P nanolines, showing the 5 main variations of appearance with bias voltage. Results at +1.1 V are presented at an isosurface value of 1 in arbitrary units to clarify the between dimer features.

The resulting simulated STM images can then be compared as shown in Figure 7.29. The bias dependence of the nanolines is largely the same, with most differences attributed to size differences between the atoms. For example with smaller atoms, the distinction between the individual dimers is more visible at higher negative biases. The zigzag patterns observed at lower positive and negative biases are still visible down to P, however the distinction between the bright and dark ends becomes less clear as atom size decreases. With P and As nanolines the down zigzag pattern is barely visible, and probably would not have been noted without the expectation of seeing it based on the Bi nanoline work. Finally, only Bi shows the between-dimer appearance. This once again is due to size differences, with the p-orbitals of smaller Group V atoms unable to interact across the spacing between dimers.

These results show that most of the distinct features of the Bi nanoline are actually common to all Group V nanolines, although the size of the Bi atoms makes these features easier to observe. The brightness contrast between dimer ends due to a coupling between the Group V dimers and the surface Si dimers occurs regardless of which Group V atoms makes up the nanoline.

The next step is to determine whether this bias dependent appearance is exclusive to Group V atoms, or whether it also extends to other atom types, thus making it a general pattern. It would be too much work to attempt a full survey of the periodic table, especially since none of the structures would be experimentally verifiable at present. Instead the investigation was limited to In and Pb, large Group III and IV atoms respectively, structures for which are shown in Figure 7.30. Simulated STM for these structures are presented in Figure 7.31.

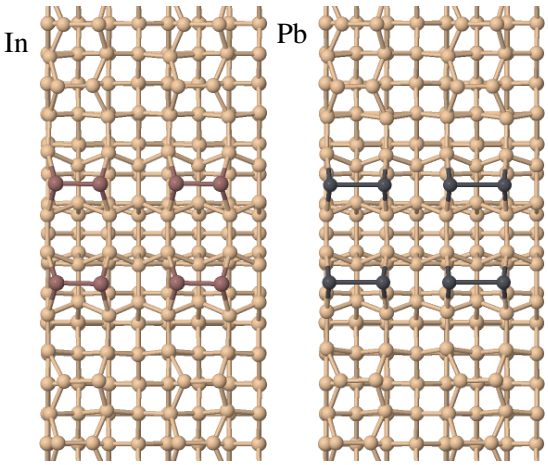

Figure 7.30: Structural models for the In and Pb nanolines on the Haiku core.

It is notable that the simulated STM images for these structures are largely different from those observed for the Group V nanolines. The In nanoline only displays any signs of a zigzag appearance at +0.2 V, which would likely be experimentally inaccessible, even if the nanoline could ever be made. As such this appearance can probably be discounted. The In nanoline also shows interesting features that are not seen for the Group V nanolines. For example at negative biases there is a bright spot in the middle of the In dimers. At lower positive biases, around the +0.3 V to +0.6 V range, the In dimers show a phase shift similar to that observed for Bi lines on Si without the Haiku core, in addition to a phase shift of the neighbouring Si dimers. A further investigation into the differences was not made, because the focus is on the Bi nanolines, and

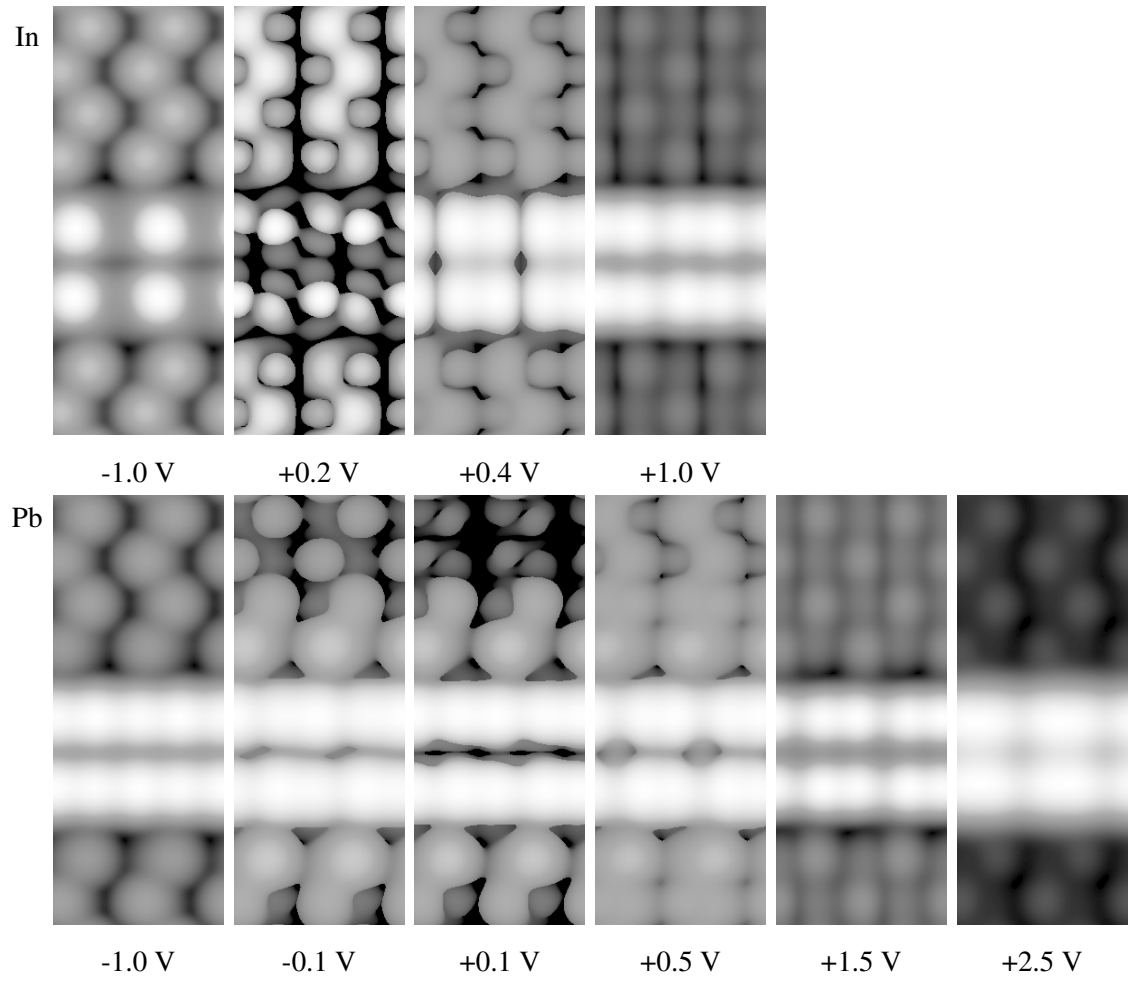

Figure 7.31: Simulated STM images for In and Pb nanolines atop the Haiku core.

simply showing a difference is a useful result.

The Pb nanolines on the other hand show very little variety with bias voltage, the only real distinction being between the positive and negative biases, with no interesting bias dependent features to the nanoline itself. In contrast to previous results, the Si dimers neigbouring the Pb nanoline do not show a phase shift at lower positive biases. Instead of shifting appearance to the trench, they appear as if they were flat dimers, and this effect extends up to two dimers away from the nanoline, as shown at +0.5 V in Figure 7.31. This shows that the Si dimer phase shift does not occur regardless of adsorbed atom type, as could be assumed from all previous results. It is not currently clear whether or not Pb is the only exception, or why it is an exception. A further survey of different atomic species might reveal more exceptions, or general trends.

Based on these results it appears that the specific bias dependent appearance of the Group V nanolines is exclusive to the Group V atoms, and must be related to their electronic structure. Nanolines of other atoms show different bias dependencies, which could be interesting for future research.

7.11 Bi nanoline on Ge

Due to issues keeping the Si surface clean in experiment, it was suggested that using a Ge surface instead might be easier to handle. Leaving aside the issue of whether this could actually be realised experimentally, this raises the question of whether or not the bias dependent appearance of the Bi nanoline will persist or not. To this end the Si in one of the Bi nanoline models was replaced with Ge, the next Group IV atom up, and the lattice constant adjusted accordingly. The simulated STM images for this relaxed structure are presented in Figure 7.32.

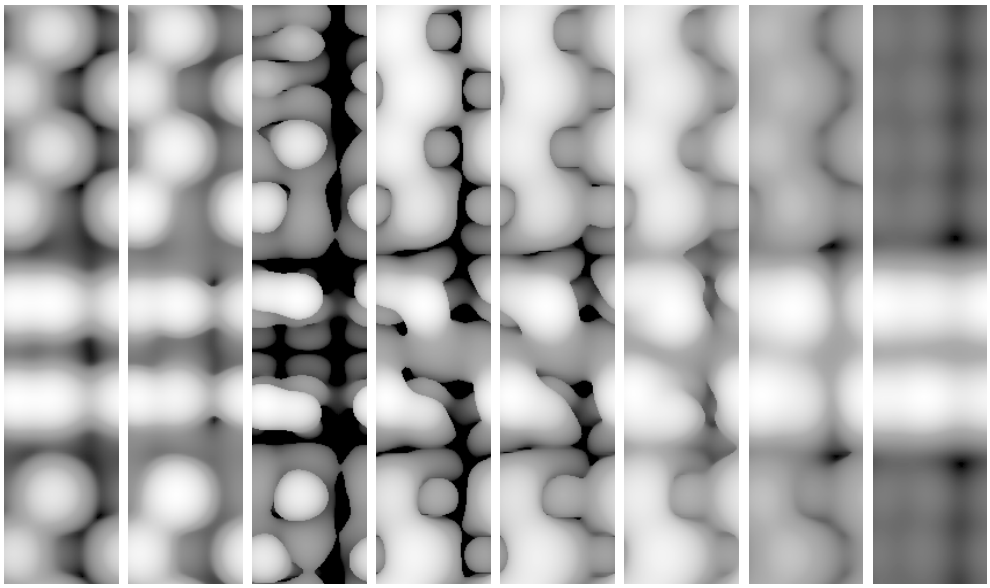

Figure 7.32: Simulated STM images for a Bi nanoline on Ge.

Whilst the appearance of the nanoline is largely unchanged at higher positive and negative biases, the low bias behaviour is different. Bright spots corresponding to down buckled Ge atoms are not observed and the bright spots corresponding to up buckled Ge atoms occur over a smaller range than for the Si structure. In addition the between-dimer appearance is not observed, which can be attributed to the increased inter-dimer distance of about 0.5 Å compared to on Si, due to the larger lattice constant for Ge.

These results show that whilst some of the bias dependent features are reproduced when replacing Si with Ge, the full range can only be seen on Si. At least some of this can be attributed to the changes in inter-Bi distances as a result of the change in lattice constant. There are however issues with using these simulations to predict the appearance of Bi nanolines on the Ge surface, because DFT is known to systematically underestimate the band-gap of semiconductors by 30-40%. This is especially notable for Ge, where a metallic ground state is predicted, which is wrong. If the simulations cannot get this right, it casts doubts on the structures observed in simulated STM, and whether it would truly represent reality.

7.12 Conclusions

Detailed analysis of simulated STM images for the Bi nanoline and related structures, in conjunction with additional models and comparison to experiment has revealed interesting new details about its electronic structure. The appearance of the Bi nanoline shows a strong bias dependence, and is split into five distinct regions. Henceforth, the bias voltages referred to will be taken from simulation, meaning experimental values will vary slightly from these.

At positive biases of +1.3 V or above the nanoline appears as a chain of bright spots which correspond the Bi dimer positions. At negative biases of -0.6 V or above the Bi nanoline appears as a chain of bright spots which correspond to the Bi atom positions. Both of these results have been observed in previous studies. At biases between these ranges the Bi nanoline displays more interesting features, which have previously not been explored. Between -0.5 V and +0.9 V an alternating pattern of bright and dark spots is observed at the positions of the Bi atoms, with the position of the bright spots swapping at 0 V. The pattern often manifests itself as a zigzag running down the length of the nanoline. This can be attributed to an electronic coupling between the buckled Si dimers of the surface and the Bi dimers of the nanoline. This coupling causes bright spots along the nanoline which match to down Si atoms at negative biases and up Si atoms at positive biases, despite the fact the Bi dimers are completely flat. Since the Si(001) surface is often a p(2$\times$2) reconstruction, this lends itself to the observed zigzag pattern, although in principle many different patterns are possible, depending on the arrangement of the Si surface. Since this appearance is strongly dependent on the arrangement of nearby Si, defects in the line, such as missing Bi can remove the alternating pattern by revealing unbuckled Si atoms.

This coupling can be observed for Bi dimer lines on Si, with or without the Haiku reconstruction, and even for a single line. The exact low bias behaviour is strongly influenced by the spacing of the Bi dimers, with the Haiku reconstruction allowing a spacing that would be impossible on unreconstructed Si. A similar effect might be observable if the nanoline was built on Ge, rather than Si, although once again Bi spacing appears to play a role in the specific appearance.

Between +1.1 V and +1.2 V the brightest spots along the nanoline shift to the trench between the Bi dimers. Simulations revealed this was as a result of imaging a specific arrangement of overlapping atomic p-orbitals from the Bi atoms, where the bonding orbitals fall between the dimers and anti-bonding orbitals on the dimers. This could pave the way for studying interesting new physics.

The general bias dependence is mostly reproduced for other Group V atoms, with differences attributed to the size difference between the atoms. As the atoms get smaller, the alternating bright and dark spots become harder to observe. Only Bi displays the between-dimer appearance, because all the other atoms are too small for their p-orbitals to overlap across the trench. Current tests with Group III or IV atoms do not show similar results, suggesting this exact behaviour is exclusive to Group V atoms.

The strain related phase shift of Si at around +0.7 V has also been revealed to be a common feature to many, but not all, line structures on Si, and not an effect that is exclusively due to the Haiku reconstruction as previously thought.

Chapter 8

Feature on the Bi nanoline

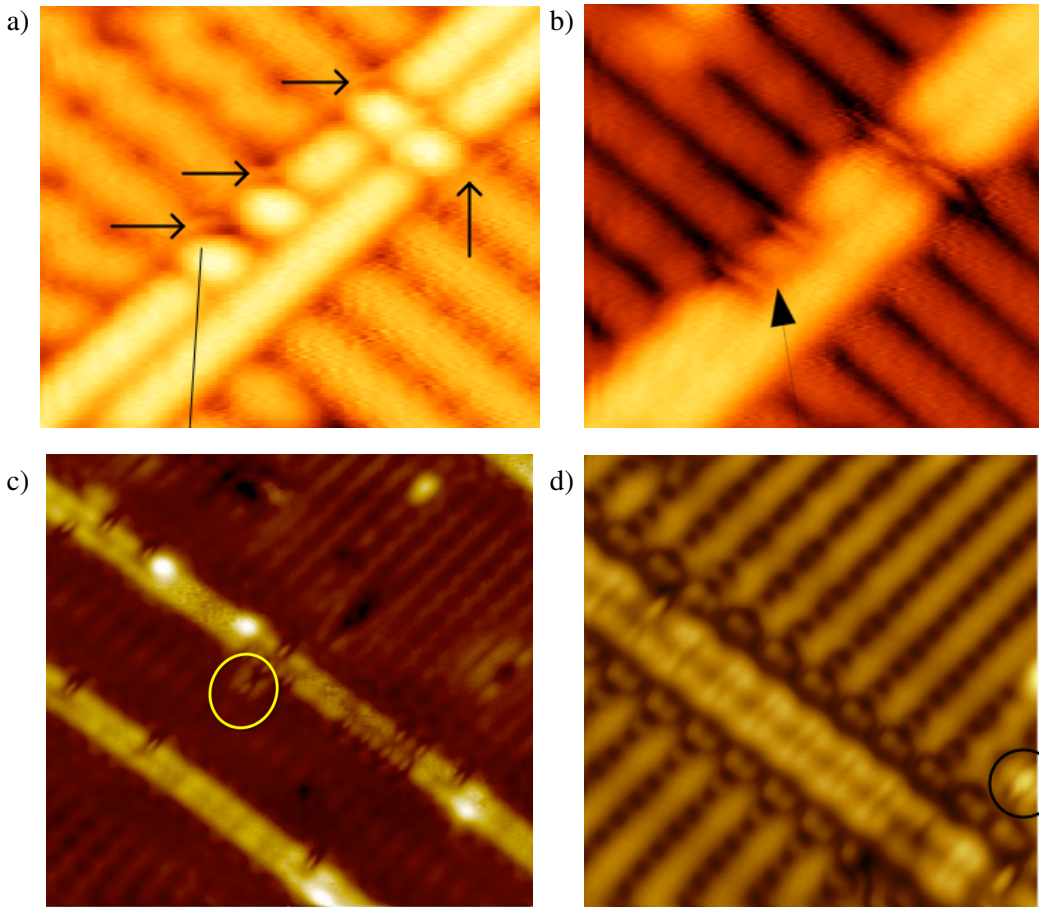

Figure 8.1: Experimental STM images of the Bi nanoline showing features of unknown origin. a) Negative bias appearance. The feature appears as a large round spot with an additional small feature around the spot, indicated by the arrows. On the left side of the nanoline these are slightly curved. On the right they appear straight. b) Positive bias appearance of the same section of nanoline as a). The feature appears as a sharp line. c) Positive bias appearance at +1.30 V, showing a similar sharp feature on the Si surface near to the Bi nanoline, indicated by the yellow ring. The bright white spots along the nanoline could be attributed to water molecules. d) Positive bias appearance at +1.20 V, showing a similar sharp feature on the Si surface near to the Bi nanoline, as indicated by the black ring. Images a), b) and d) are courtesy of Sigrun Sigrun Köster and image c) is courtesy of Maria Longobardi, both from Christoph Renner's group in Geneva.

New experimental results from Christop Renner's group have shown unusual features along the Bi nanoline, examples of which are shown in Figure 8.1, which appear after sample transfer. At negative biases the features appear as round spots, as demonstrated in a), encompassing an entire Bi dimer in length. In addition ring-like features have been observed, which surround the spot on the outer edge of the nanoline, as indicated by the arrows. The rings appear more curved on one side of the nanoline than the other, although it is not clear whether this is a tip effect due to scanning direction or not. At positive biases the feature appears as a sharp line perpendicular to the direction of the Bi nanoline, at the centre of a Bi dimer, as demonstrated in b). Images c) and d) show a similar sharp feature, but on the Si(001) surface near to a Bi nanoline, rather than on the nanoline itself. This raises the possibility that the feature is due to an adsorbate which has replaced a Bi dimer, rather than the nanoline itself.

To aid in characterising this feature I have performed an extensive study of adsorbates on the Bi nanoline, and variations of the nanoline. The primary method for assessing these structures has been to compare the simulated STM images for these structures to the experimental results. This search is guided by details deduced from the experimental results and set up. Even though ultimately the search for its identity is unsuccessful, it still provides a deeper understanding of the Bi nanoline, and a lesson about the limitations of simulations like these.

The results from Figure 8.1 reveal both the minimum possible spacing between adjacent features, and the position of the feature. Features can occupy the space of adjacent Bi dimers, either along or across the nanoline. Whilst the negative bias results only give a general idea of the position of the feature, the positive bias results reveal more details, showing the feature to be at the centre of a dimer row, and that a section of the nanoline still remains between adjacent features along the line.

This suggests that the feature could be due to an adsorbate sitting in the middle of a Bi dimer, pushing the atoms of the Bi dimer further apart. There are three possible sources for this adsorbate, namely the sample, the apparatus, and the atmosphere. Of these the atmosphere seems most likely, because the density of features increases when the transfer speed is increased. There is the possibility that high pressure particles are disrupting the Bi nanoline and inserting themselves into the line.

In addition to this, the feature could be due to modifications or rearrangements of the nanoline, such as a misoriented Bi dimer, or sections of missing nanoline. This latter scenario was inspired by recent work on Si dangling bonds [117] and follow up work [118] which has produced dangling bond arrangements that exhibit a sharp feature exactly like that observed on the Bi nanoline. This opens up the possibility that experiments are observing an interaction between the Si below the Bi nanoline, rather than anything to do with the nanoline itself. As an extension to this, the possibility of an atom adsorbing within gaps in the nanoline was also explored.

8.1 Toy Model

To accompany these simulations of the system, I also built a toy model of the system, to aid in determining the nature of the feature, or to help explain its appearance. The model does not aim

to precisely identify the feature, but merely to provide guidance into potential arrangements of atoms. The model involves finding the solutions to the Schrödinger equation for a particle in a 2D box which is periodic in x. In the models considered here the length of the box along x was considered to be twice the width in y. The Schrödinger equation in the box is solved using the central difference finite difference method, which splits the box into a grid of points, with interval spacing h, which for simplicity is the same in both directions. This results in the following matrix which must be solved

$$E \begin{bmatrix} \psi(1,1) \\ \vdots \\ \psi(m,n) \end{bmatrix} = \hat{H} \begin{bmatrix} \psi(1,1) \\ \vdots \\ \psi(m,n) \end{bmatrix}, \tag{8.1}$$

where $\psi(x,y)$ is the wavefunction at a specific point in the box. At each point in the box the Hamiltonian can be written as

$$E\psi(x,y) = \hat{H}\psi(x,y) = -\frac{1}{2}\nabla^2\psi(x,y) + V(x,y)\psi(x,y) \tag{8.2}$$

in atomic units, where $V(x,y)$ is the potential at a given point in the box. Normally this will be zero everywhere, unless additional potentials are included in the model. It is possible to split $\nabla^2\psi(x,y)$ into x and y components, such that

$$\nabla^2\psi(x,y) = \psi_{xx} + \psi_{yy}, \tag{8.3}$$

where ψ_{xx} and ψ_{yy} denote the second derivatives of ψ with respect to x or y. By using the second order central finite difference, these can be written as

$$\psi_{xx} = \frac{\psi(x+1,y) - 2\psi(x,y) + \psi(x-1,y)}{h^2} \tag{8.4}$$

and

$$\psi_{yy} = \frac{\psi(x,y+1) - 2\psi(x,y) + \psi(x,y-1)}{h^2}, \tag{8.5}$$

where h is the interval spacing mentioned earlier. By inserting both of these expresssions back into Eq. 8.2 and rearranging, it is possible to get an expression for each row of Eq. 8.1,

$$2h^2E\psi(x,y) = (4+2h^2V(x,y))\psi(x,y) - \psi(x+1,y) - \psi(x-1,y) - \psi(x,y+1) - \psi(x,y-1) \tag{8.6}$$

for x and y between 1 and m or n respectively. Since the system is periodic in x, $\psi(m+1) = \psi(1)$ and $\psi(1-1) = \psi(m)$. For the purposes of simulating the Bi nanoline, Gaussian potentials of the form

$$V(x,y) = a\exp(-(b(x-x_0)^2 + 2c(x-x_0)(y-y_0) + d(y-y_o)^2)) \tag{8.7}$$

were introduced into the box. Here a is the magnitude of the Gaussian, b is the extent of the Gaussian in x, c determines the elliptical nature of the Gaussian, d is the extent of the Gaussain in y, and x_0 and y_0 are the coordinates of the centre of the Gaussian. For the potentials used here $b = d$ and $c = 0$.

Initially to simulate the Bi nanoline on its own, four identical potentials were introduced at spacings chosen to mimic the placement of Bi atoms in two Bi dimers, as shown in Figure 8.2. Taking the centre of the box to be at $(0, 0)$, the length of the box to be $2L$, and the width L, the Gaussian potentials were placed at $(\pm 0.3L, 0)$ and $(\pm 0.7L, 0)$. The spacing between these potentials is either $0.4L$, representing the Bi dimer length, or $0.6L$, representing the inter-dimer distance, such that the relative spacing matches to that of the real Bi nanoline. The absolute scale of this model is arbitrary, with the a, b and d parameters determined empirically.

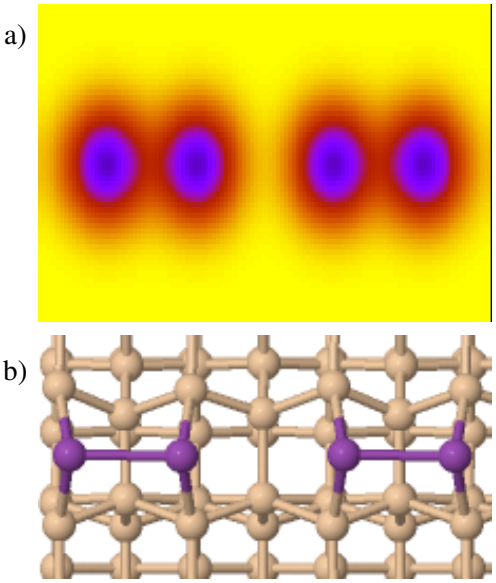

Figure 8.2: a) Toy model of the Bi nanoline, made by considering a 2D particle in box, which is periodic in x. Bi atoms are represented by 4 Gaussian potentials, spaced as to replicate the spacing of Bi atoms in the actual nanoline. Two dimer pairs are shown, with the spacing between the pairs 1.5 times the spacing in the pairs. Colours indicate the depth of the potential wells, starting from yellow with no potential, down to purple. b) Structural model of a two dimer long section of one side of the Bi nanoline, showing the region that the toy model is representing.

To represent the adsorbates, additional Gaussian potentials were included with the same parameters as those which represent the Bi, but at different locations. Either a single potential was added at the centre of one of the 'dimers' at $(0.45L, 0)$, as will be detailed later in Figure 8.3, or two were added offset in y from the centre of the 'dimers' at $(0.45L, \pm\frac{7L}{60})$. The offset in y was chosen as a reasonable guess and was not intended to properly represent actual possible distances in experiment. This arrangement will be covered in Figure 8.4.

The eigenvalues and eigenvectors of $\hat{H}$ can then be computed using the LAPACK routine SYEVD, which calculates those values for a real symmetric matrix using a divide and conquer algorithm [119]. The eigenvalues can then be related to the ground and excited states of that system, and the eigenvectors can be used to generate the associated wavefunctions.

From this model it is possible to produce results that look similar to experiment, with round or sharp features appearing for different excited states. This occurs for elliptical potentials, such as those shown in Figures 8.3 and 8.4. In the former the ellipse is due to an additional potential added at the centre of the dimer, as described earlier. In the latter case the ellipse is due to two

additional potentials, offset in y, as also described earlier.

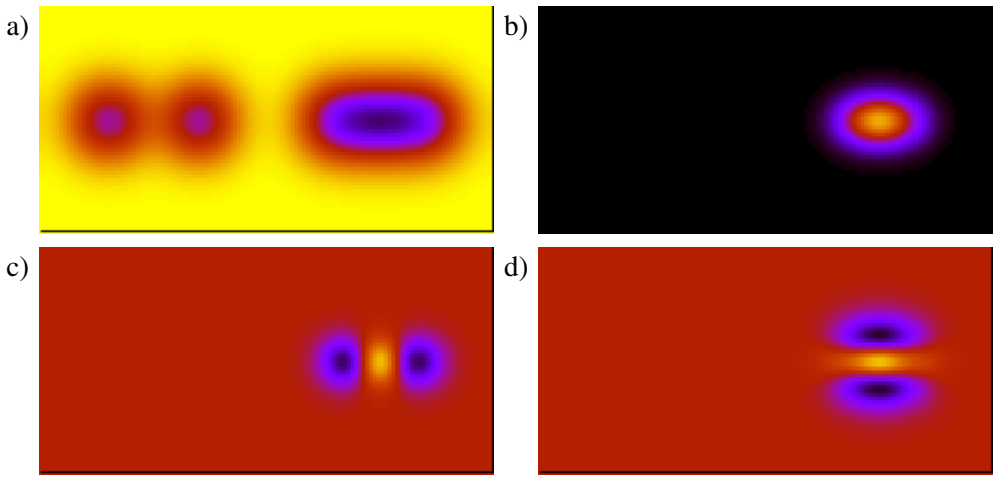

Figure 8.3: Potential and corresponding solutions for a particle in a 2D quantum box periodic in x. a) Top view of a potential representing a section of the Bi nanoline, consisting of a regular Bi dimer on the left, and a Bi dimer with an atom adsorbed at the centre of the dimer on the right. b) Wavefunction for the ground state of the system, showing a round feature centred on the dimer with an adsorbed atom. c) Wavefunction for the 2^{nd} excited state of the system, showing a sharp line running perpendicular to the centre of the dimer with an adsorbed atom. d) Wavefunction for the 10^{th} excited state of the system, showing a sharp line running parallel to the centre of the dimer with an adsorbed atom. The x axis runs horizontal, and the y axis vertical. The colours indicate the heights of the potentials or wavefunctions, from yellow at the highest, to purple at the lowest.

In both cases the ground state appears as a round feature centred on the dimer with adsorbates, which is a good match to the negative bias results seen in experiment. By examining excited state solutions, it is possible to find states where sharp features run perpendicular to the direction of the dimers, such as Figures 8.3.c) and 8.4.d). However, by examining even higher excited states, it is also possible to find states where there is a sharp feature which runs parallel to the dimer direction, such as Figure 8.3.d), which is contrary to any experimental results. As should be expected for such a simple model, it will not reproduce exactly the complex experimental system, since real STM images are due to contributions from many states, rather than the individual states shown here. It is also worth noting that STM results will reveal Ψ^2, rather than Ψ, so care should be taken when trying to make direct comparisons to experiment. Comparing these two perpendicular configurations is still useful, because it shows that the feature is sharper in the direction parallel to the widest part of the ellipse.

This model could still do with some refinements at the moment, because the potential for the dimer with adsorbates is so deep compared to the dimer on its own that the solutions only show the appearance of a single dimer at a time, compared to real results where the entire nanoline is visible. Scaling the size of the adsorbate potentials may help with this. However the model is not aiming to exactly reproduce experiment, but rather show that in principle it is possible to reproduce the sharp experimental feature.

By inspection, it was realised that the sharp feature solutions are equivalent to a solution of the form

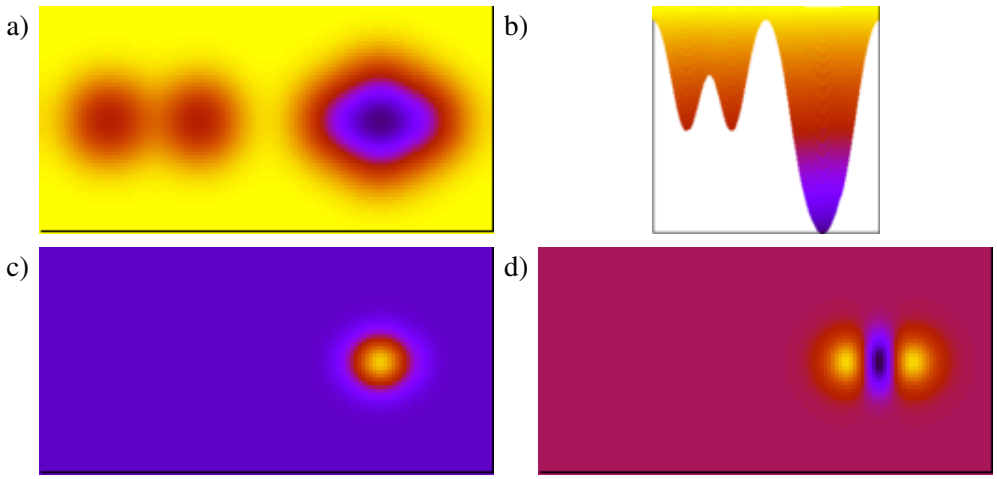

Figure 8.4: Potentials and corresponding solutions for a particle in a 2D quantum box periodic in x. Top view a) and side view b) of a potential representing a section of the Bi nanoline, consisting of a regular Bi dimer on the left, and a Bi dimer with a pair of adsorbed atoms offset in y from the centre of the dimer on the right. c) Wavefunction for the ground state of the system, showing a round feature centred on the dimer with adsorbed atoms. d) Wavefunction for the 3^{rd} excited state of the system, showing a sharp line running perpendicular to the centre of the dimer with adsorbed atoms. When the top view is shown, the x axis runs horizontal, and the y axis vertical. The colours indicate the heights of the potentials or wavefunctions, from yellow at the highest, to purple at the lowest.

Figure 8.5: Potential representations of the sharp feature observed on the Bi nanoline. a) Analytical solution of the form $\Psi(x,y) = (14x^2 + 0.1y^2 - 4)\exp(-x^2 - y^2)$. b) Ψ^2 c) Numerical solution for the potential from Figure 8.4. d) Numerical solution for the potential from Figure 8.3.

$$\Psi(x,y) = (Ax^2 + By^2 - C)\exp(-x^2 - y^2) \tag{8.8}$$

where A, B and C are real numbers. This is demonstrated in Figure 8.5, which shows a good match between an analytical solution of the form $\Psi = (14x^2 + 0.1y^2 - 4)\exp(-x^2 - y^2)$ and the sharp feature solutions from Figures 8.3 and 8.4. Ψ^2 is also provided to give a closer approximation to the STM images.

These models demonstrate the possibility that the ground state of the feature is being imaged at negative biases, and an excited state at positive biases. Whilst the model cannot explicity identify the feature, it does show that in principle a sharp feature is observable without needing a complicated structure. The models provide justification for the feature being either a single atom, or a pair of atoms adsorbed on a Bi dimer.

8.2 Adatoms on the line

A variety of different structures with adatoms or molecules inserted into a Bi dimer of the Bi nanoline have been relaxed, and their simulated STM images compared to the experimental results. Despite these efforts, the exact nature of the feature is still unknown, but there are still some useful details to draw from these results.

8.2.1 Sample

One possibility for the feature is that an atom from elsewhere in the sample has adsorbed atop the Bi nanoline. The most obvious choices for adatoms from the sample would be Si or Bi, since they are the main constituents of the sample. B was also considered, since it is the most common impurity in Si. In most cases the adatom inserts into the Bi dimer and sits 1.8-2.2 Å above the Bi atoms, as shown in Figure 8.6.a) for a B atom. However, it is also possible for a B atom to insert into the dimer in line with the Bi atoms as shown in Figure 8.6.b). The adsorption energies for all these structures are presented in Table 8.1, alongside the results for the adsorbates from the apparatus and the atmosphere, which will be discussed later. The energy difference between the two structure involving B is clear. By moving the B atom closer to the Bi dimer, the adsorption energy almost doubles, and makes the structure much more favourable than both the Bi and Si adsorbates. The smaller size of the B atom compared to Bi or Si probably explains why a similar structure is not observed for the latter species.

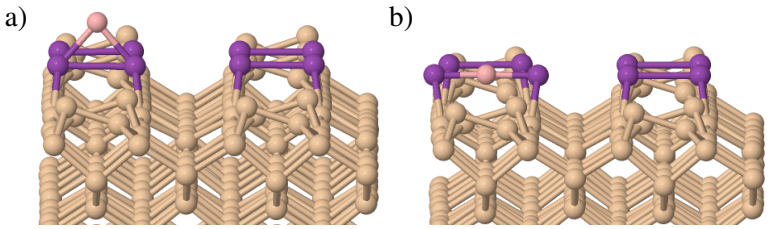

Figure 8.6: Structural model for the Bi nanoline with a) B adsorbed on top of the Bi dimer, 1.9 Å above the Bi and b) B adsorbed on the Bi dimer, at the same height as the Bi atoms. The B atoms are pink.

Simulated STM images were generated for all of these structures, to allow for comparison to the experimental results. The simulated STM in Figures 8.7, 8.9 and 8.10, showing B, Bi and Si above the Bi dimers all look similar, with bright round spots corresponding to the adsorbate atom. These bright spots appear in both positive and negative biases, contrary to experimental results, suggesting none of these are responsible for the feature in experiment. By comparison, when B is at the same height as the Bi dimers, as in Figure 8.8 the B atom is hidden amongst the regular appearance of the Bi nanoline, once again contrary to experimental results.

Whilst these results do not reveal the identity of the feature, it is interesting to note that for positive biases, a very faint ringing pattern is seen around the raised B atom and the Si atom, as indicated by the arrows in Figures 8.7 and 8.10 respectively. This points towards an explanation for the curved feature seen in experiment.

Table 8.1: Adsorption energies for adsorbates on a Bi dimer in the Bi nanoline.

Adatom	E_{ads} (eV)
B (1.9 Å above Bi dimers)	-1.452
B (same height as Bi dimers)	-2.889
Bi	-1.488
Si	-1.302
F (1.7 Å above Bi dimers)	-2.973
F (0.6 Å above Bi dimers)	-3.588
C	-3.016
H	-1.317
N	-2.036
O	-4.055

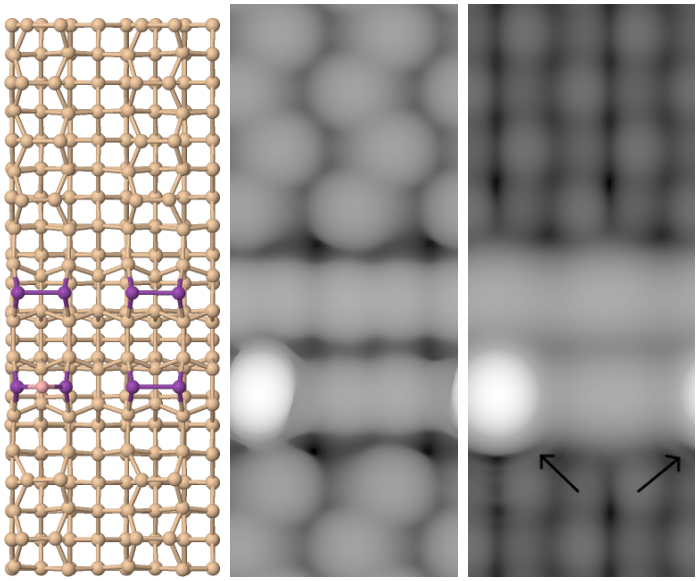

-1.0 V +1.0 V

Figure 8.7: Simulated STM images for the Bi nanoline with a B atom adsorbed at 1.9 Å above the Bi dimer, shown at both positive and negative biases. The structural model is provided for clarity, with the B atom in pink. Arrows on the positive bias image indicate the position of very faint rings around the B atom.

8.2.2 Apparatus

Another possibility is that atoms from the apparatus used to move, or study the sample have managed to find their way onto the Bi nanoline. This could include C, F, CF from the apparatus and W or Pt from the STM tips used. For single atoms the adsorbate was placed in the middle of the Bi dimers and the structure allowed to relax. In the case of CF, the relaxed structure for adsorbed C was taken and F added, pointing out of the plane of the surface, as shown in Figure 8.11. For W and Pt, initial calculations suggested that these atoms would not adsorb onto the Bi nanoline, so calculations were halted.

The adsorption energies for the completed structures are presented in Table 8.1, and show

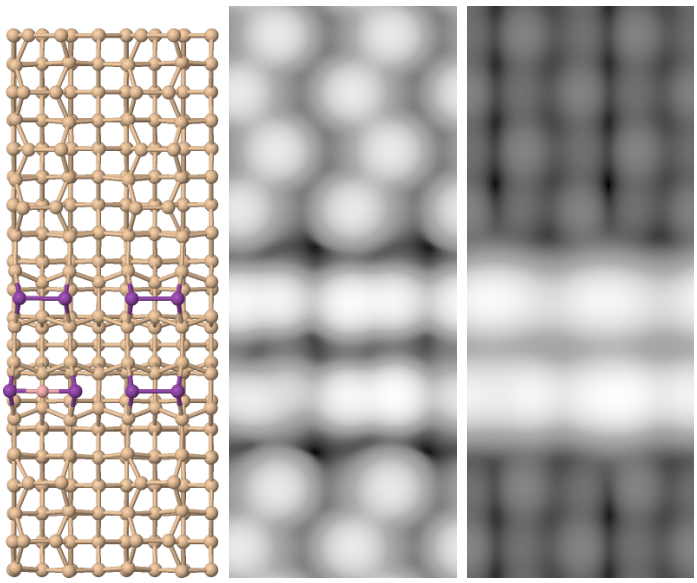

Figure 8.8: Simulated STM images for the Bi nanoline with a B atom adsorbed at the same height as the Bi dimer, shown at both positive and negative biases. The structural model is provided for clarity, with the B atom in pink.

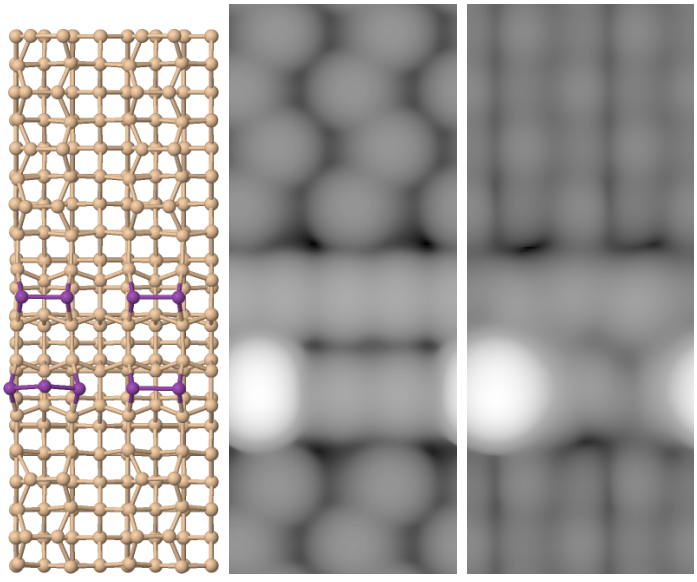

Figure 8.9: Simulated STM images for the Bi nanoline with a Bi atom adsorbed, shown at both positive and negative biases. The structural model is provided for clarity.

similar results to those for the adsorbates from the sample. Similar to B, the F adsorbate is capable of relaxing to different heights, in this case either 1.7 Å or 0.6 Å above the Bi dimers. As before, the lower the height of the adsorbate, the more energetically favourable the structure, although the effect is not as dramatic as for the B atom. Both B and C are more energetically favourable than anything from the sample, which would suggest that they are more likely to adsorb atop the Bi nanoline.

Simulated STM images for these structures show some similarities to the adsorbates from the

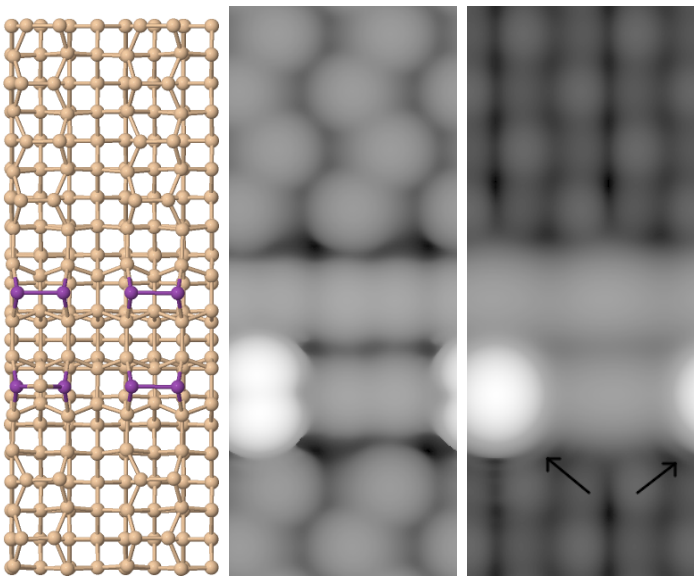

Figure 8.10: Simulated STM images for the Bi nanoline with a Si atom adsorbed, shown at both positive and negative biases. The structural model is provided for clarity. Arrows on the positive bias image indicate the position of very faint rings around the Si atom.

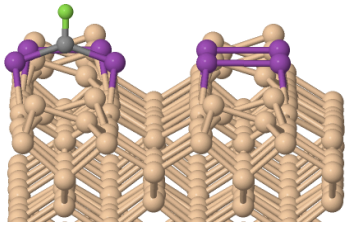

Figure 8.11: Structural model for the Bi nanoline with CF adsorbed out of the plane of the surface. The C atom is in grey and F in green.

sample, with F, C and CF, shown in Figures 8.12, 8.14 and 8.15, all showing bright spots at the positions of the adsorbates for both positive and negative biases. Whereas for the F adatom which is only 0.6 Å above the Bi dimers, in Figure 8.13, it is impossible to distinguish the individual atom from the rest of the nanoline, but it is possible to locate the area in which it has adsorbed. These results suggest that the adatoms tested are unlikely to be the cause for the experimental feature, due to the lack of a sharp feature at positive biases.

As seen earlier, for example in Figure 8.7, there are ringing patterns around most of these adsorbates, most notably in Figure 8.15 for the adsorbed CF, where several clear rings can be seen. This is in contrast to most other adsorbates where the rings are barely visible. The ringing appears for most adsorbates, but the extent and brightness of the rings appears to depend on the atom type. In some cases, including CF, the rings are visible in both positive and negative bias images, whereas experimental results only show a similar feature at negative biases. It is currently not clear whether this is a real effect, or merely an artefact of the simulations. I do not know of any example of a similar effect being observed before, either in experimental or simulated STM, suggesting this is a new phenomenon. For certain values of A, B and C the square of the analytic solution from Eq. 8.8 produces a ring-like structure which compares favourably to the large ring

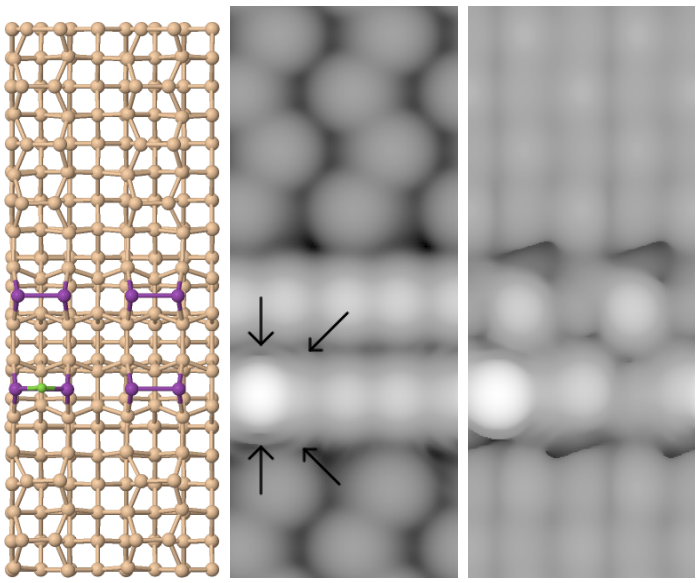

Figure 8.12: Simulated STM images for the Bi nanoline with a F atom adsorbed at 1.7 Å above the Bi dimer, shown at both positive and negative biases. The structural model is provided for clarity, with the F atom in green. Arrows on the STM images indicate the locations of some of the rings observed around the F atom. They are visible both on the outer edge of the nanoline, and at the middle of the nanoline.

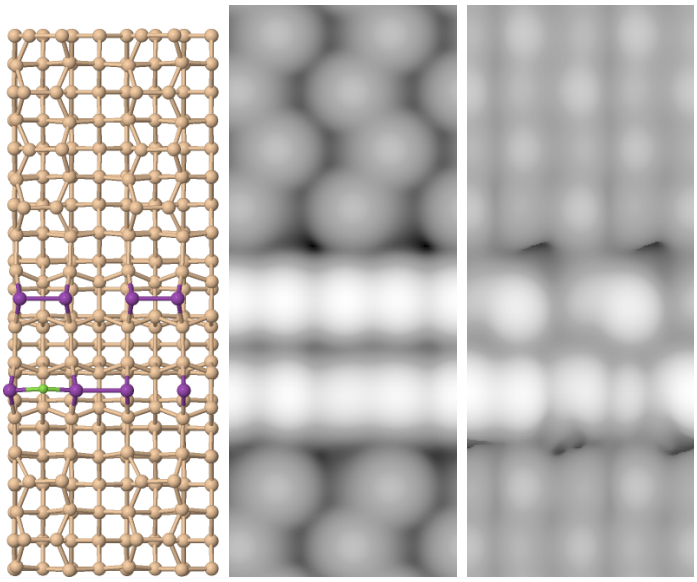

Figure 8.13: Simulated STM images for the Bi nanoline with a F atom adsorbed at 0.6 Å above the Bi dimer, shown at both positive and negative biases. The structural model is provided for clarity, with the F atom in green.

observed around the CF feature, as demonstrated in Figure 8.16. This gives more support to the idea that the ringing is a real effect caused by an adsorbed atom or dimer, rather than just an artefact of the simulations.

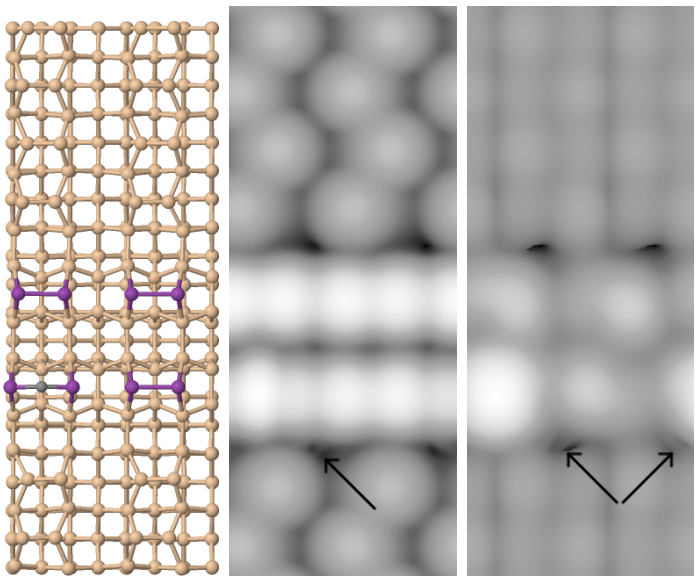

Figure 8.14: Simulated STM images for the Bi nanoline with a C atom adsorbed above the Bi dimer, shown at both positive and negative biases. The structural model is provided for clarity, with the C atom in grey. Arrows on the STM images indicate the locations of some of the very faint rings observed around the C atom.

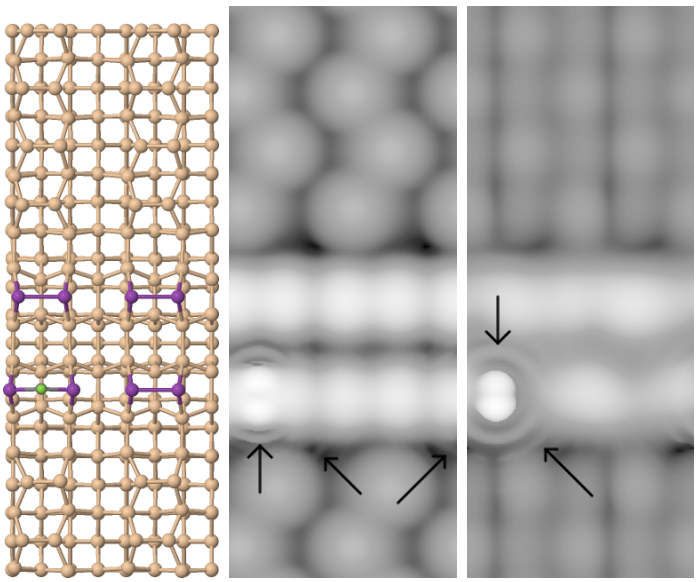

Figure 8.15: Simulated STM images for the Bi nanoline with a CF molecule adsorbed above the Bi dimer, shown at both positive and negative biases. The structural model is provided for clarity, with the C atom in grey and the F atom in green. Arrows on the STM images indicate the locations of some of rings observed around the CF molecule.

8.2.3 Atmosphere

As the sample transfer speed increases, so too does the density of the features, suggesting that a particle from the atmosphere is inserting itself into the nanoline under pressure. This raises many possibilities for the identity of the feature, since there are many different components of the

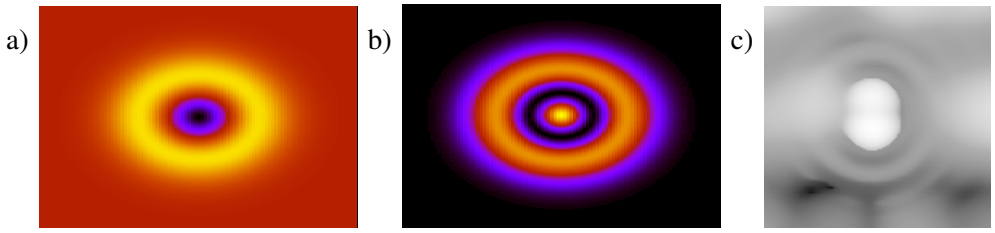

Figure 8.16: Comparison between a) analytic ring structure for $\Psi(x,y) = (x^2 + y^2 - 0.3)\exp(-x^2 - y^2)$, b) Ψ^2 and c) the ring structure seen in simulated STM for the Bi nanoline with adsorbed CF.

atmosphere, encompassing both atomic and molecular adsorbates. Mass spectrometry suggested that CO or N_2, both with molecular weights of 28, were possible identities for the feature, although CO_2 was also strongly suspected to be a candidate.

For atomic adsorbates only N, O and H were considered, due to their relative abundance and reactivity, compared to the noble gases, which were excluded. Adsorption energies for these structures are also presented in Table 8.1. It is interesting to note that of all the atom types currently considered, O has the highest adsorption energy for a single atom, making it the most likely atom to adsorb onto the Bi nanoline, suggesting it as a likely candidate for the feature. Experimentally it should not be too difficult to adsorb O atoms atop the nanoline deliberately, and then compare to the unknown features to check for similarities.

A sample of simulated STM of these structures is presented in Figures 8.17, 8.18 and 8.19. H is too small to see over all the Bi, however it is possible to make out its position by the darker region of the Bi nanoline. O shows a sharp-like feature in negative bias, and a round feature in positive bias, which is unfortunately the opposite bias dependence to the observed experimental results. N shows a similar pattern, but the sharpness is less clear and the round spot is split into two. Once again ringing is seen around the features. None of these results match with experiment, although the reverse bias dependence seen for O is promising.

The situation for molecular species is a little more complicated, because not only are the atom species important, but also their arrangement relative to the Bi dimers. The molecule can be inserted into the Bi dimer parallel or perpendicular to the Bi dimer, or coming out of the plane of the surface, examples of which are shown in Figure 8.20. A variety of molecular species were studied, with varying degrees of success. CH, CO, O_2, N_2 and OH structures were all relaxed, allowing for the creation of simulated STM images, whereas H_2O and CO_2 both encountered problems during relaxations. The calculations showed oscillating behaviour with a residual that could not be reduced, so rough simulated STM images were obtained in order to make a preliminary assessment of suitability. These rough result were obtained through methods such as fixing specific atoms or loosening force tolerances.

Simulated STM images for O_2 and N_2 molecules oriented perpendicular to the Bi bond direction are presented in Figures 8.21 and 8.22, and images for OH, CH and CO molecules coming out of the plane of the nanoline are shown in Figures 8.23, 8.24 and 8.25. Further variations for the CO adsorbate were attempted, such as perpendicular to the Bi dimer, however these relaxed to the out of plane configuration.

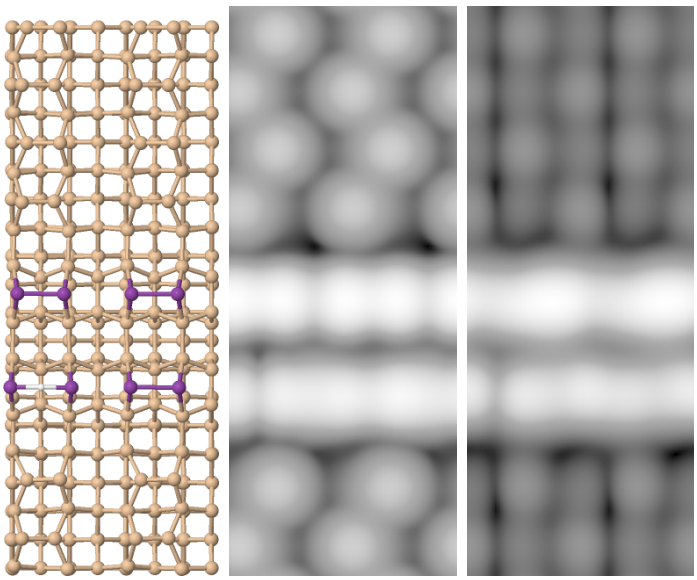

-1.0 V +1.0 V

Figure 8.17: Simulated STM images for the Bi nanoline with an H atom adsorbed above the Bi dimer, shown at both positive and negative biases. The structural model is provided for clarity, with the H atom in white.

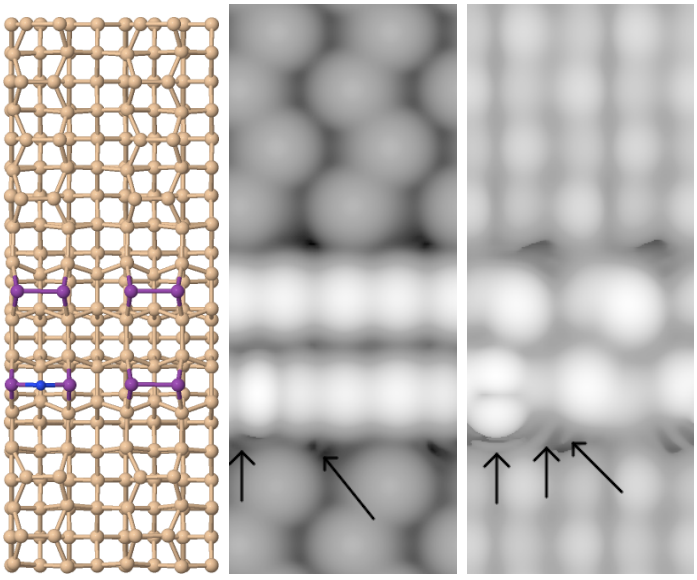

-1.0 V +1.0 V

Figure 8.18: Simulated STM images for the Bi nanoline with a N atom adsorbed above the Bi dimer, shown at both positive and negative biases. The structural model is provided for clarity, with the N atom in blue. Arrows on the STM images indicate the locations of some of rings observed around the adsorbed N atom.

Unfortunately, these structures still fail to match experimental results. In all cases, bar OH, the bright spot in the negative bias images splits into two lobes, rather than being one unbroken spot as in experiment. For CH and N_2 this also happens at positive biases. This can be explained for O_2 and N_2 because the perpendicular arrangement of the adsorbates means that the two atoms are physically separated across the Bi dimer. For CH and CO the split is down the middle of the atom adsorbed atop the C, although the direction is different for these two cases. OH is the only

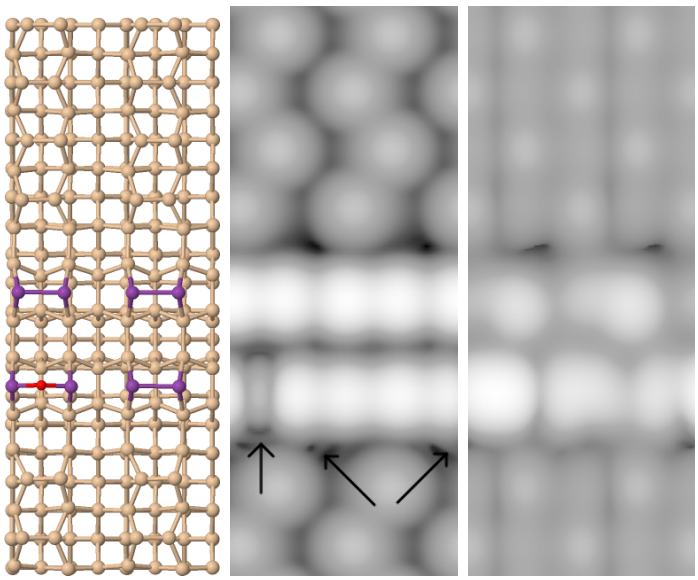

Figure 8.19: Simulated STM images for the Bi nanoline with an O atom adsorbed above the Bi dimer, shown at both positive and negative biases. The structural model is provided for clarity, with the O atom in red. Arrows on the STM images indicate the locations of some of rings observed around the adsorbed O atom.

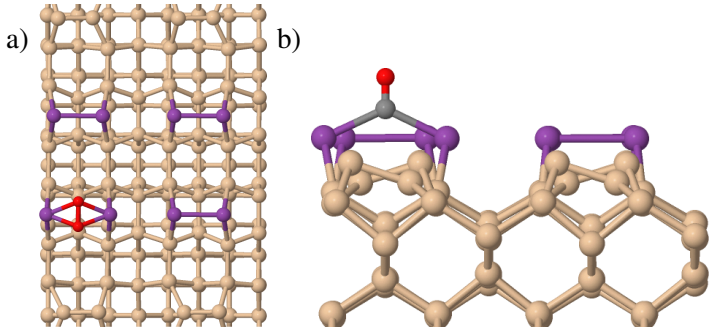

Figure 8.20: Models showing molecules adsorbed atop the Bi nanoline. a) O_2 perpendicular to the Bi dimers. b) CO out of the plane of the surface. C atoms are shown in grey, with O in red.

of these molecular adsorbates that does not show this effect at all, instead showing a bright spot at both biases, with the spot slightly wider at positive bias. This looks somewhat similar to the bright spots observed in Figure 8.1.c), which were attributed to water, or related species, by the experimentalists.

Throughout these simulations the presence of the ring-like structures is still visible, most notably for CO, where the rings are both greater in number and extend for a greater range than any other simulations. This is more supporting evidence for the idea that the rings in experiment are due to a similar effect, rather than a systematic error in all of the simulations. If nothing else it would be interesting to build these adsorbate structures in experiment and test for ring-like structures.

The most heavily studied adsorbate is CO_2, both because of interest expressed experimentally and complications which arose during simulations. The CO_2 molecule can be arranged both parallel and perpendicular to the Bi dimers, meaning both have to be considered. Additionally,

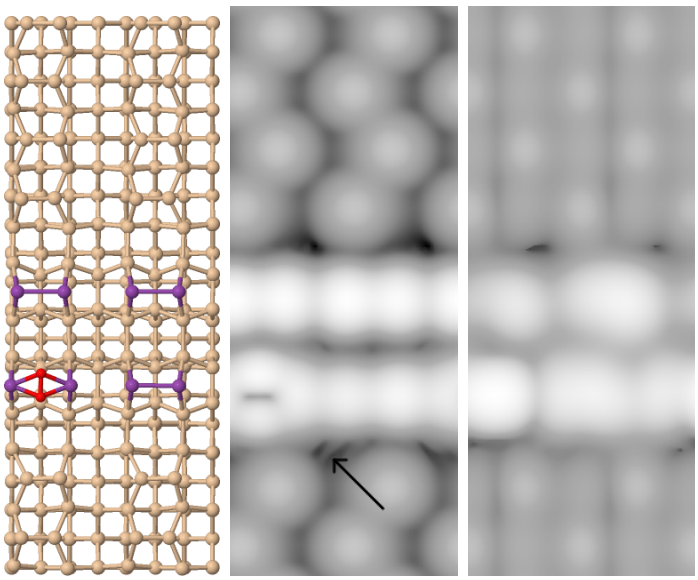

-1.0 V +1.0 V

Figure 8.21: Simulated STM images for the Bi nanoline with an O_2 molecule adsorbed on the Bi dimer in a perpendicular arrangement, shown at both positive and negative biases. The structural model is provided for clarity, with the O atoms in red. The arrow on the STM images indicates the location of a ring observed around the adsorbed O_2.

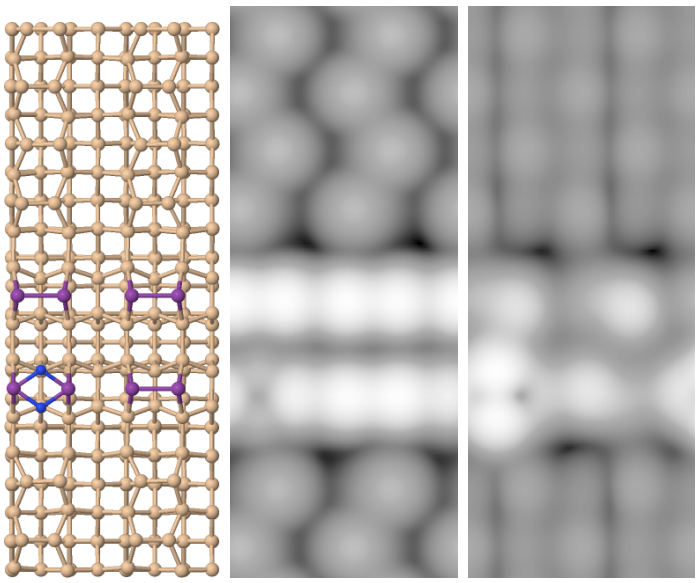

-1.0 V +1.0 V

Figure 8.22: Simulated STM images for the Bi nanoline with a N_2 molecule adsorbed on the Bi dimer in a perpendicular arrangement, shown at both positive and negative biases. The structural model is provided for clarity, with the N atoms in blue.

during relaxations of these structures the forces could not reach the convergence criteria, possibly suggesting a poor choice of initial conditions. To address this the CO_2 was relaxed from a variety of different starting heights, but they all relaxed towards the same end structure. Alternatively the failure to converge can be because the system becomes stuck shifting back and forth between two local minima, rather than finding the global minima. There are some workarounds to this prob-

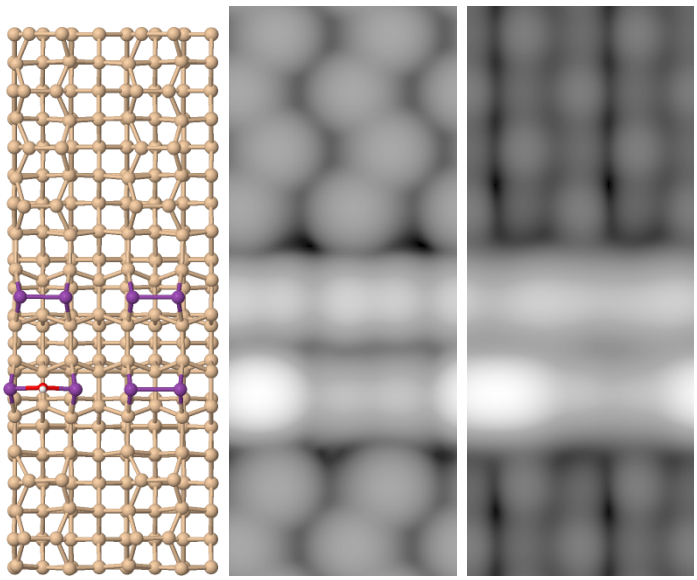

Figure 8.23: Simulated STM images for the Bi nanoline with an OH molecule adsorbed on the Bi dimer, shown at both positive and negative biases. The structural model is provided for clarity, with the H atom in white and the O in red.

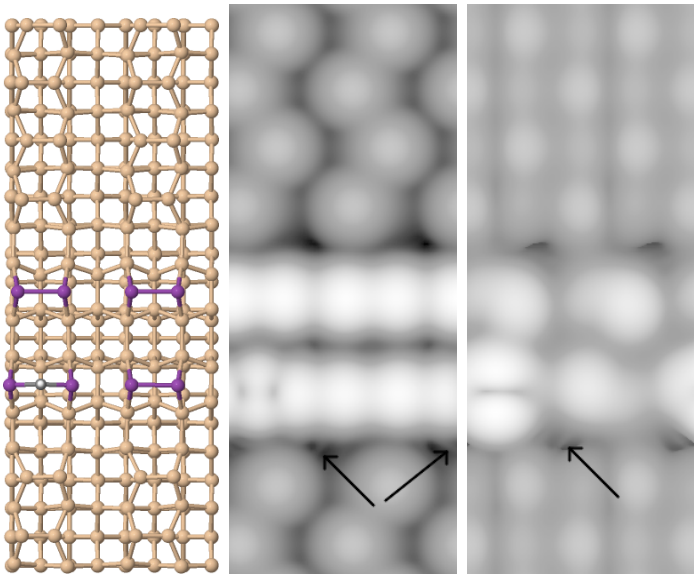

Figure 8.24: Simulated STM images for the Bi nanoline with a CH molecule adsorbed on the Bi dimer in a perpendicular arrangement, shown at both positive and negative biases. The structural model is provided for clarity, with the C atom in grey and the H atom in white. Arrows on the STM images indicate the locations of some of rings observed around the adsorbed CH molecule.

lem, the simplest of which involves weakening the force convergence criteria to higher values than 0.02 eV/Å. In practice, this often meant stopping the calculations and taking static calculations of that particular arrangement, regardless of the forces on the system. This allowed a preliminary assessment of suitability to be made, based on the rough simulated STM, rather than spending large amounts of time on a potentially wrong structure. Examples of these rough structures are

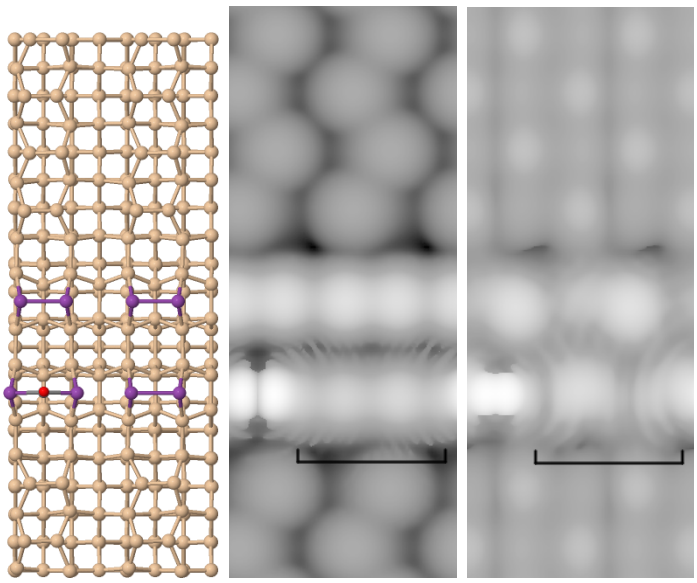

Figure 8.25: Simulated STM images for the Bi nanoline with a CO molecule adsorbed on the Bi dimer in a perpendicular arrangement, shown at both positive and negative biases. The structural model is provided for clarity, with the C atom in grey and the O atom in red. The regions containing ring-like features are indicated by the brackets.

shown in Figure 8.26.

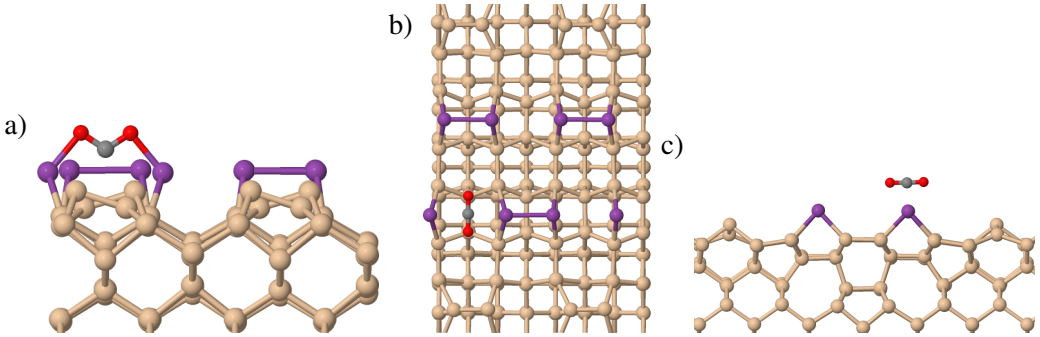

Figure 8.26: Models showing CO_2 molecules adsorbed atop the Bi nanoline, either a) parallel or b), c) perpendicular to the Bi dimers. Both b) top and c) side views are shown of the perpendicular CO_2 to give an idea of the height it sits above the Bi nanoline. Structure a) has forces relaxed to $<$0.09 eV/Å, whilst for b) it is $<$0.2 eV/Å.

For the parallel CO_2 an unusual M shape is formed, with forces relaxed to $<$0.09 eV/Å. On the other hand, for perpendicular CO_2 the forces could only be relaxed to $<$0.2 eV/Å, with the CO_2 itself only loosely physisorbed to the surface, despite disrupting the Bi bonding beneath it.

The simulated STM for these structures are presented in Figure 8.27 and show that they are not worth relaxing further. There is little to suggest a sharp feature at positive biases in either case, with the CO_2 staying relatively bright and round for both positive and negative biases. At higher isosurface values, such as shown in c), it is easier to make out the O atoms of the CO_2, making it appear sharper than for lower isosurface values, however, in doing so this eliminates the round feature at negative biases. On top of this, the ringing features are still visible for both of these

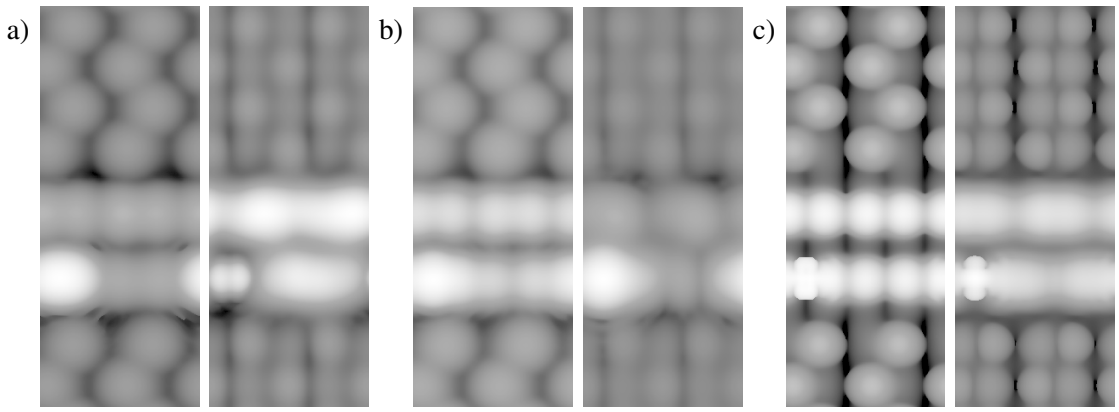

Figure 8.27: Simulated STM images for the Bi nanoline with CO_2 adsorbed. a) Parallel arrangement using the structure shown in Figure 8.26.a). b) and c) Perpendicular arrangement using the structure shown in Figure 8.26.b). The latter is shown at an isosurface value of 0.5 to make the O atom clearer. Each pair gives a sample view of the adatom at positive and negative biases.

structures, although much less so for the perpendicular structure than the parallel one.

Given that in all other cases the adsorbed species bonded directly to the Bi atoms, it would make sense to try structures where the C atom of the CO_2 was bonded directly to the Bi atoms. To achieve this, the C was fixed in place at a variety of heights, and the O atoms allowed to relax, examples of which are shown in Figure 8.28. To speed up calculations they were performed with a one dimer wide cell, which represents the smallest possible spacing between features. Unlike when the CO_2 was fully free to move, many of these structures were able to relax fully, with their energies presented in Table 8.2. There is a trend of decreasing energy with increased height of the C atom above the Bi nanoline, which fits with the results seen for a free to move CO_2, where the CO_2 would relax towards a position 2 Å above the surface.

Table 8.2: Energies for CO_2 adsorption on the Bi nanoline with the C atoms at fixed heights. Energies are given relative to the structure with the C atom at the lowest height compared to the Bi dimers.

Height relative to Bi dimers (Å)	ΔE (eV)
+0.5	0
+0.7	-0.26
+1.0	-0.49
+1.3	-0.76

The simulated STM for these structures, as shown in Figure 8.29, display differences in appearance due to the height of the CO_2 relative to the surrounding Bi dimers. Moving from a) to c) the height of the C atom increases, and this is reflected in the increasing brightness of the CO_2 molecule. For a), the CO_2 molecule is darker than the surrounding Bi, regardless of bias voltage, in contrast to experimental results. As the height is increased, the CO_2 appears as a bright feature at negative biases, similar to in experiment, most notably for c). However, in all cases the simulated STM fails to reproduce the positive bias behaviour. For a) and b), no sharp feature is observed,

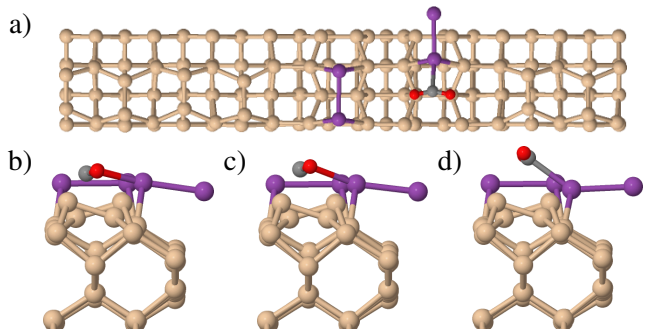

Figure 8.28: Structural models for the Bi nanoline with CO_2 adsorbed atop and thee C atom held fixed. a) Top down view with C fixed at 1.3 Å above the Bi nanoline. C fixed at b) 0.5 Å, c) 0.7 Å and d) 1.3 Å above the Bi nanoline.

with the region immediately around the CO_2 actually darker than the Bi atoms. For c) on the other hand, the brightness of the CO_2 feature increases with bias voltage, in contrast to the experimental results, where the sharp feature becomes dimmer. All of these results taken together suggest that, regardless of orientation or relative height, it is unlikely that the feature is due to adsorbed CO_2.

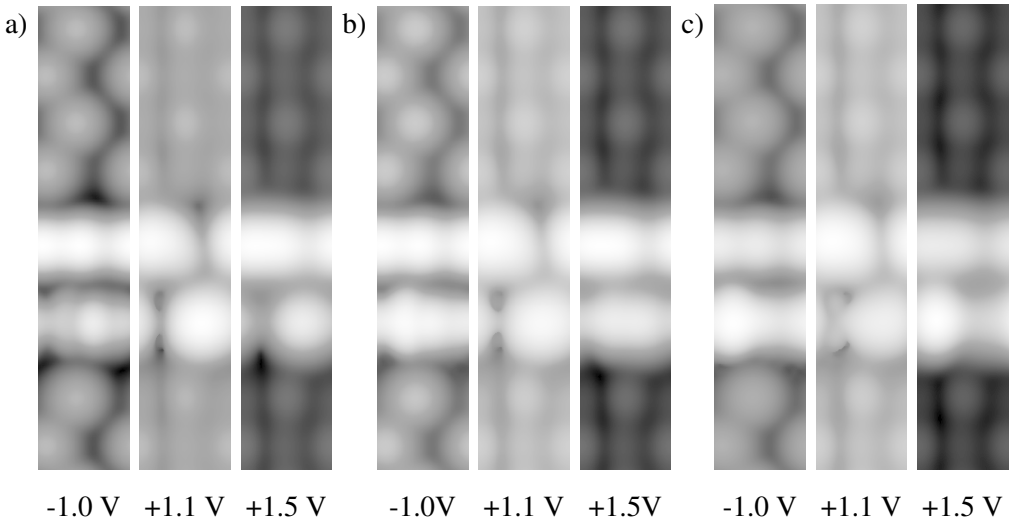

Figure 8.29: Simulated STM images for the Bi nanoline with CO_2 adsorbed with the C atom fixed at heights of a) 0.7 Å, b) 1.0 Å and c) 1.3 Å above the Bi nanoline.

The final adsorbate considered was water, due to its relative abundance, and the suspicion that the other bright features in Figure 8.1.c) are due to water. Confirmation of this might not help directly with determining the sharp feature, but it would at least help narrow the search criteria. Water was considered in both parallel and perpendicular configurations as shown in Figure 8.30. Similar to CO_2, only rough versions of the simulated STM could be obtained, which are presented in Figure 8.31.

Surprisingly, there is little difference in the appearance between the two configurations. Regardless of orientation, the water appears as an extended bright spot in both positive and negative biases. The main difference between the two is the extent of the bright spot perpendicular to the nanoline direction, which as you would expect is greater for the perpendicular arrangement. The overall appearance is comparable to an adsorbed OH, as shown earlier in Figure 8.23, with the

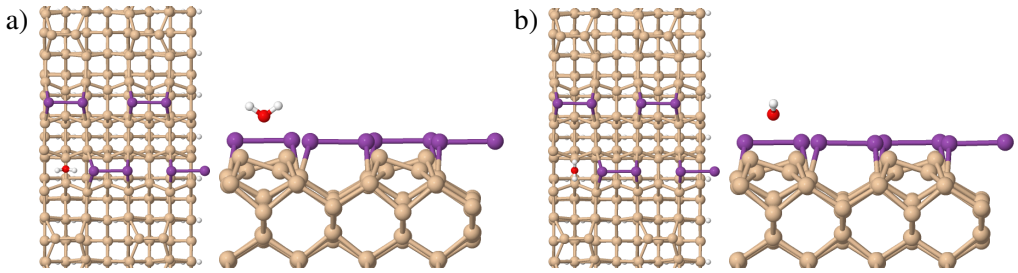

Figure 8.30: Structural models for the Bi nanoline with water adsorbed atop, showing both top down and side views of the a) parallel and b) perpendicular configurations.

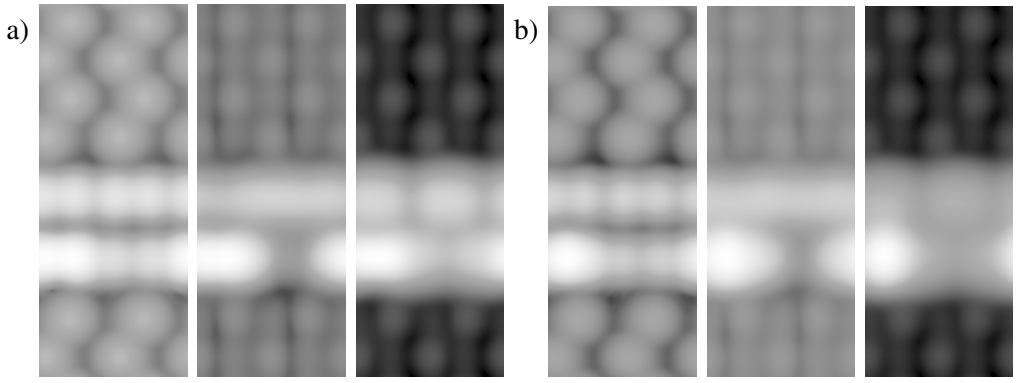

Figure 8.31: Simulated STM images for the Bi nanoline with H_2O adsorbed in a) parallel and b) perpendicular configurations, the same as shown in Figure 8.30.

main difference being the increased extent of the bright spots for water. This is not surprising, given that the difference between the two is only down to a single H atom. This is completely unlike the feature being searched for, however it does match well to the additional bright spots from Figure 8.1.c). Despite the fact these water arrangements are not fully relaxed, these results support the idea that the additional features are in fact water, as suspected by the experimentalists.

Given the current lack of success with adsorbates on the Bi nanoline, it is worth considering what could be going wrong with these calculations, or what alternatives still exist. The most straightforward answer is that the correct adsorbate has not yet been identified. Further calculations, for example considering less abundant particles in the atmosphere, may yet identify the feature, but there is no guarantee that this is the correct method to follow. It is possibile that current simulations will never correctly identify the feature, because the simulations themselves are lacking. Some of the appearance of the feature could be due to tip effects, which have thus far been neglected. If this is the case it could mean that one of the adsorbates already studied is correct, it was just missed because of simplifications in the model.

Another possibility is that studying adsorbates has been the wrong line of enquiry as far as identifying the feature is concerned. There exist other possibilities related to modifying the Bi nanoline, for example missing or misoriented dimers, which is where the focus will now shift.

8.3 Modifications of Bi nanolines

Modifications to the structure of the Bi nanoline itself not only offer new possibilities for identifying the experimental feature, but also the chance to study more details about the bias dependent appearance of the Bi nanoline, and how it changes with these modifications. The two primary modifications studied involve misoriented dimers or missing Bi atoms. In the former case, a misoriented dimer sits at the correct location for the feature, and is oriented in the correct direction. In the latter case the work was inspired by the striking similarities between the feature on the Bi nanoline and the sharp features seen on Si dangling bond networks [117]. This opens up the possibility that the feature could be due to Si dangling bonds, rather than the Bi nanoline itself.

A misoriented dimer is considerd to be one which has rotated 90° out of phase with the rest of the dimers, as shown in Figure 8.32. This structure has previously been studied [120], but not with simulated STM in mind. In agreement with previous results the rotated dimer structure was found to be higher in energy than the regular nanoline, although the magnitude of the change differed slightly. In the current study an increase of 0.89 eV was found, whereas previously an increase of only 0.8 eV was reported [120]. For current purposes all that matters is that the misoriented structure is significantly less energetically favourable than the regular nanoline and thus less likely to occur.

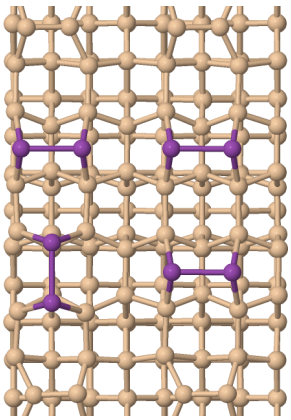

Figure 8.32: Bi nanoline with a misoriented Bi dimer.

Figure 8.33 shows simulated STM images for this structure, which once again fail to match experimental results. The misoriented dimer appears neither as a sharp feature, nor a round feature, instead simply looking like the other Bi dimers, but rotated by 90°. This is not particularly surprising, given that this reflects the actual physical situation, and that there is no particular reason to believe that rotating the dimer would have a dramatic effect on its appearance. There is a notable result at lower positive biases, such as +0.7 V, where the dimer appears to have a tilt to it, despite being physically straight. This is similar to results noted for P on the regular Si(001) surface [114], suggesting that this behaviour is common to Group V dimers oriented perpendicular to the direction of the Si dimers. Finally, the presence of the misoriented dimer has little effect on the appearance of the other dimers. The only noticeable change occurs at +1.1 V, where the between dimer appearance is not observed on the side with the misoriented dimer. This is because the misorientation means that the neighbouring p-orbitals can no longer overlap. The lack of change

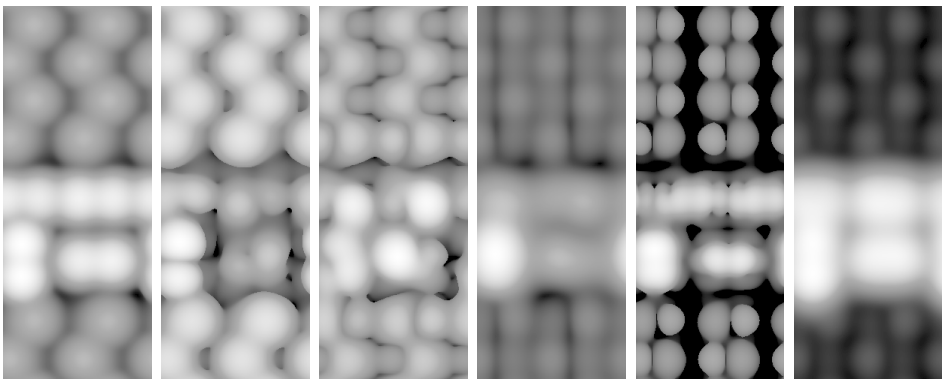

Figure 8.33: Simulated STM images for the Bi nanoline with a misoriented Bi dimer, using the structure shown in Figure 8.32. Results at +1.1 V are presented at an isosurface value of 1 in arbitrary units to clarify the between dimer features.

at other biases can be attributed to the fact that even though the dimer has been rotated by 90°, it is still bonding to the same Si atoms, and thus no additional Si has been revealed.

Given the failure of the misoriented dimer in explaining the experimental results, attention now turns to modifications which reveal the Si beneath the Bi nanoline. So far, both a missing dimer and a misplaced dimer have been considered, as shown in Figure 8.34, with the cell extended to three dimer rows in order to accomodate the misplaced dimer.

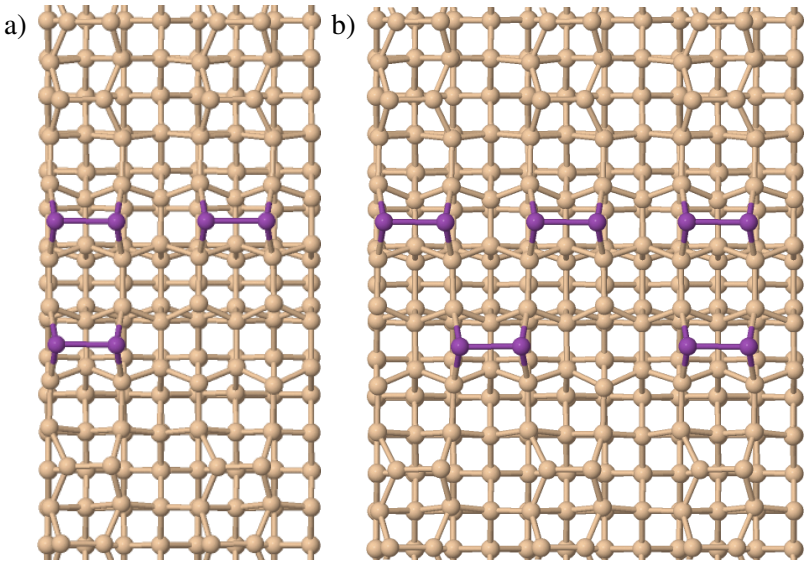

Figure 8.34: Models showing the Bi nanoline with a) a missing dimer and b) a misplaced dimer.

In both cases two Bi atoms are missing, revealing four underlying Si atoms, but in different positions. In the missing dimer case all the Si are next to each other, whereas for the misplaced dimer, the pairs of revealed Si atoms are separated by the misplaced Bi dimer. This means that both structures have four Si dangling bonds, which is confirmed by the spin difference densities shown in Figure 8.35. Without placing restrictions on the systems, they relaxed to structures where the spins alternate between up on the inner side of the nanoline, and down on the outer side. Further checks for energy variation with spin arrangement were not performed, because it was assumed to

have little effect on the simulated STM for these structures, although it could be worth considering in the future.

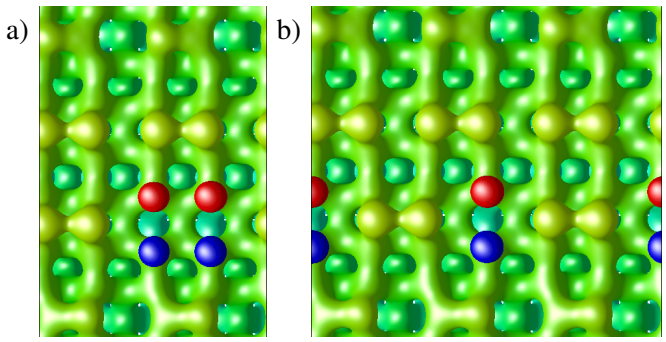

Figure 8.35: Charge and spin difference density plots for the a) missing dimer and b) misplaced dimer structures. Four Si dangling bonds are visible in both structures, with alternating spins.

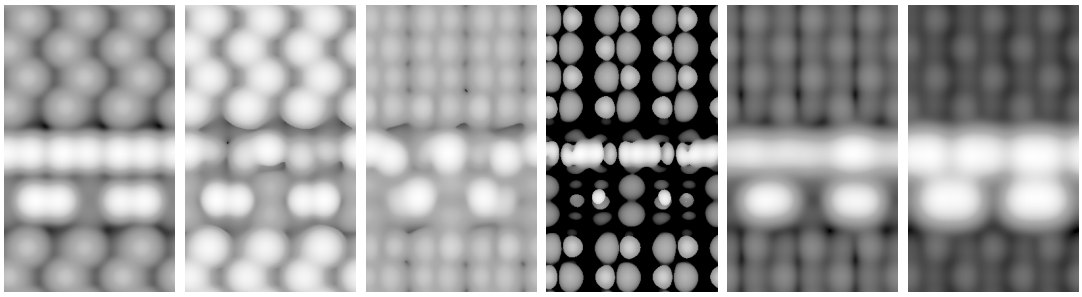

Figure 8.36: Simulated STM images for a triple row section of the Bi nanoline where one Bi dimer is shifted out of phase with the rest and two Bi atoms are missing. Results at +1.0 V are presented at an isosurface value of 1 in arbitrary units to clarify the between dimer features. The structural model for this structure cam be found in Figure 8.34.

Simulated STM for the missing dimer was shown earlier in section 7.8, specifically Figure 7.22, so will not be recounted here. Simulated STM for the misplaced dimer on the other hand is a new result, and is shown in Figure 8.36. For the misplaced dimer, there is a visible gap between the dimers, due to the missing Bi, however there is no sign of any feature. As with the missing dimer, the removal of Bi atoms not only changes the appearance of the nanoline at the location of the missing atoms, but also the appearance of those Bi atoms neighbouring the missing atoms, most notably at lower biases. For example, at -0.5 V in Figure 8.36, the Bi atoms next to the two gaps appear as bright spots. For the left dimer this is at a down Si position, agreeing with results for the regular nanoline, however it is brighter than would be expected. This is demonstrated by direct comparison to the right dimer, which is the same as for the regular nanoline. By contrast, the brighter spot on the central dimer now sits at an up Si position, contrary to the regular behaviour of the nanoline. In both cases the enhancement to the brightness of the Bi atom is due to the newly revealed Si atoms. The dimer on the right, next to the misplaced dimer, also changes in appearance compared to the regular nanoline, despite the fact that it has not moved from the regular position. This is due to the revealed Si either side of the dimer.

Similarly at low positive biases, such as +0.8 V, the Bi atoms which lie next to the gaps are

bright, regardless of the Si arrangment in the rest of the surface. This is most noticeable for the left dimer, where both ends are bright, resulting in a visible tilt to the dimer, despite physical straightness.

The lack of a feature of any kind suggests that it might not be worth pursuing the idea that the experimental results are due to interactions between Si dangling bonds. However, this behaviour is difficult to model with DFT, due to the fact that the excited states of the dangling bonds become tangled in the conduction band [117]. This means that the lack of positive results could be due to a failing of the method, rather than the choice of structure. Another matter to consider is that the spacing between the Si dangling bonds here is different from that of the dangling bond wires. When a sharp feature appears for the Si dangling bond wires there is an intermediate H passivated Si, whereas here the Si dangling bonds are directly adjacent. Reproducing this spacing would be difficult without completely changing the structure of surrounding Bi dimers as well.

These results are not without merit, because they provide useful information on the nature of the feature. If it involves missing Bi in some way, this would be reflected in a change to the brightness pattern along the other side of the nanoline at low biases. Current experimental results suggest that the feature does not have an effect on the dimer behind it, however there are too few results to state this conclusively. Figures 7.1.a) and 7.8 contain examples useful for this analysis, however the presence of disorder and defects makes this analysis hard.

Another possibility is that the feature is due to the replacement of a Bi dimer with either a Bi atom or one of the previously studied adatom species. Figures 8.1.c) and d) show examples of similar sharp features on regions of the Si(001) surface rather than the Bi nanoline, suggesting that the feature might not be due to insertion into a Bi dimer, but rather adsorption on Si. I could find no evidence in the literature of a sharp feature like this for other adsorbates or defects on Si(001).

To test this idea out, one of the dimers in the Bi nanoline was replaced with other species of atoms, positioned at the centre of the revealed Si. Several different species were attempted, including single Bi, W, Pt and O atoms and an O_2 molecule. Of these only Bi and W were sucessfully relaxed, although a rough structure was also produced for O. These 3 structures are all shown in Figure 8.37.

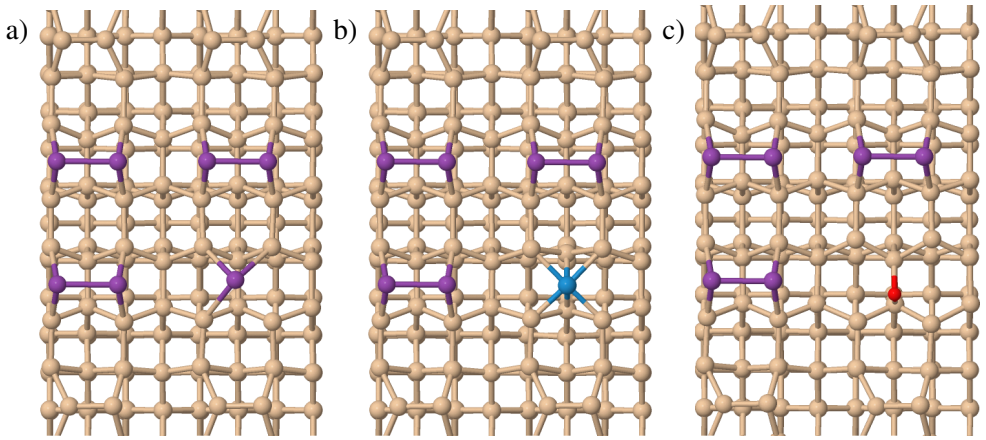

Figure 8.37: Structural models for the Bi nanoline with one dimer replaced by a a) Bi atom, b) W atom or c) an O atom. The Bi atom is 3 coordinate, whilst the W atom is at least 4 coordinate and the O atom 2 coordinate. The W atom is shown in light blue.

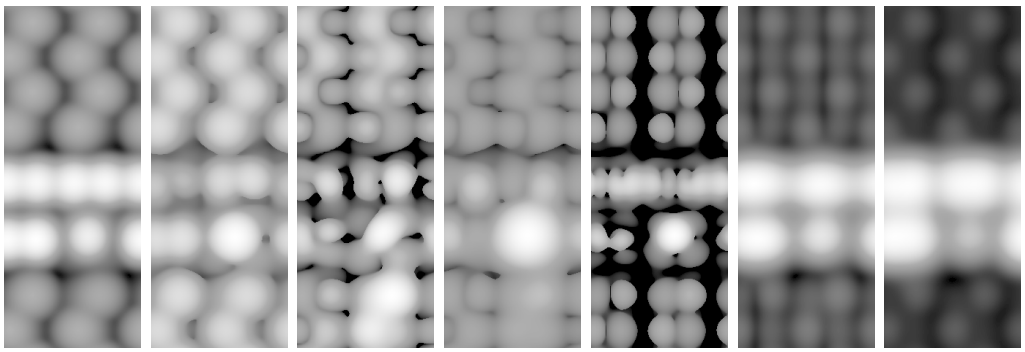

-1.0 V -0.4 V +0.5 V +0.8 V +1.2 V +1.5 V +2.5 V

Figure 8.38: Simulated STM images for the Bi nanoline with a dimer replaced by a single Bi atom. Results at +1.2 V are presented at an isosurface value of 1 in arbitrary units to clarify the between dimer features. The structural model is shown in Figure 8.37.a).

When a Bi dimer is replaced with a single Bi atom the resulting structure always relaxed to a 3 coordinate Bi atom with no spin, where each of the Bi-Si lengths varied. The simulated STM for this structure has some promising features as shown in Figure 8.38, however it once again fails to completely match experiment. At negative biases there is a good agreement with experiment, because the Bi appears as a bright spot at the centre of the dimer row with a visible gap between the feature and the rest of the nanoline. There is however no sign of any ring-like features. At positive biases the Bi atom still appears as a round spot, which darkens with increasing bias voltage. This lack of a sharp feature is in contrast to experimental results, but the darkening does match to behaviour seen in experiment.

As noted for the modified Bi nanolines, the appearance of the rest of the nanoline, especially at lower biases, is also a useful comparative tool. In this case the regular zigzag patterns is largely maintained, and there is much less of a change compared to when the entire Bi dimer is missing. This effect is most noticeable at low negative biases, such as -0.4 V.

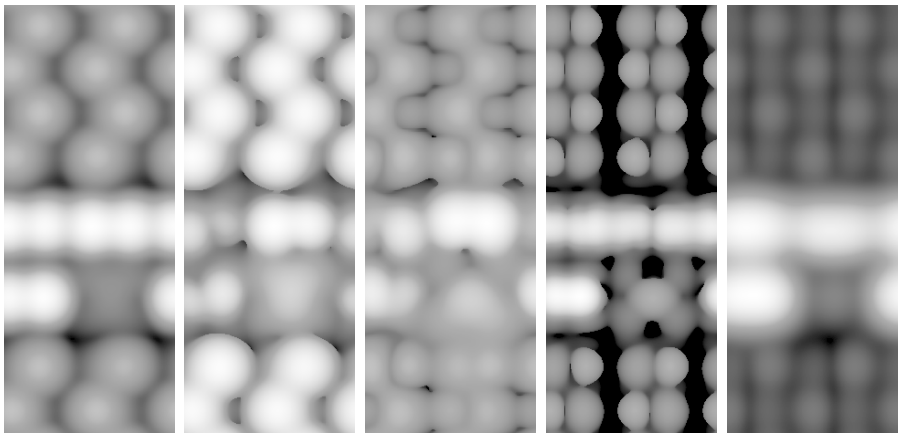

-1.0 V -0.4 V +0.7 V +1.2 V +1.5 V

Figure 8.39: Simulated STM images for the Bi nanoline with a dimer replaced by a single W atom. Results at +1.2 V are presented at an isosurface value of 1 in arbitrary units to clarify the between dimer features. The structural model is shown in Figure 8.37.b).

Results for the single W and O atoms, shown in Figures 8.39, and 8.40 are less promising,

because the W and O atoms themselves are barely visible, with the O atom actually darker than the surrounding Si at higher positive biases. This immediately rules them out as being responsible for the feature. In both cases the appearance of the remaining Bi dimers is the same as when a Bi dimer is missing, providing even more evidence against these structures.

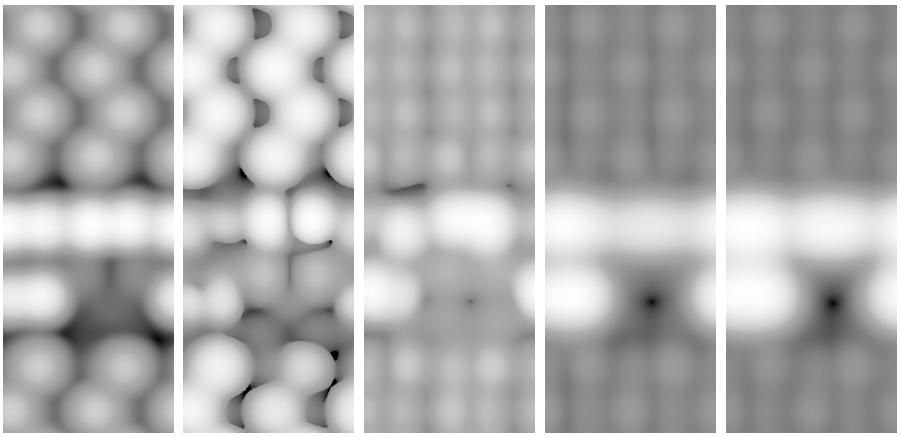

Figure 8.40: Simulated STM images for the Bi nanoline with a dimer replaced by a single O atom.The structural model is shown in Figure 8.37.c).

Of the currently tested structures only the replacement of a Bi dimer by a Bi atom comes close to matching the experimental results, and even then only at negative biases. It is also the only case observed so far, where the effect on the other Bi dimers is relatively small. Why this is the case is not entirely clear, given the small sample size. It might be due to the size difference between Bi and W or O, or simply because it is a Bi atom, like the rest of the nanoline.

8.4 Conclusions

The true nature of the experimental feature is still not clear. In principle it could be either an atom or a perpendicular dimer pair adsorbed on a Bi dimer, however none of the tested structures which fit this description were successful. One of the closest was a single adsorbed O atom, which despite favourable adsorption energies displayed the reverse bias dependence to experiment.

Even if these results cannot help identify the feature, they are still useful in other ways. Firstly they have shown that it is possible for other atom types to insert into the Bi nanoline, in some cases with a significant gain in adsorption energy. This supports the idea of using the Bi nanoline to template other nanolines, or to make mixed nanolines.

The simulations also revealed ring-like structures around adsorbates on the Bi nanoline, which has not been previously observed. Determining their true nature could prove to be an interesting future project. Important questions such as what causes them, and can they be put to practical use, still need addressing. Without experimental studies of these structures it is hard to tell whether the rings are merely an artefact of the simulation or an undiscovered new effect. If real this would be an exciting result, because it would demonstrate the capability to image subatomic features.

Studying direct modifications to the nanoline might not have identified the feature, but it did help determine what it cannot be. Modifications which remove Bi atoms result in a change to the

low bias appearance of the remaining Bi atoms which is not replicated in experimental images with the feature. This helps to narrow the possible search criteria down significantly, and provides interesting information about the appearance of the Bi nanoline in general. However, it should be noted that when a Bi dimer is replaced by a single Bi, the negative bias appearance at least is a very good match for experiment.

Since all current structures have failed to reproduce the experimental results, it is important to consider why this has occured. One possibility is that DFT simply cannot correctly reproduce this structure. This would mean that no matter what further variations were attempted none of them could ever match experiment completely. One of the structures already studied might be correct, but poorly represented by these simulations. If this is the case then future work would need to address extensions which could properly represent this problem, for example including tip effects in the simulated STM. Another possibility is that the correct adsorbate or structural reconstruction simply has not been considered yet. For example, this work has not considered the possibility of an adsorbate and a Bi atom switching places. Further progress with simulations may require a brute force approach such as Ab Initio Random Structure Searching (AIRSS) [121] in the future. One of the most useful routes for future study would be to deliberately create some of these defective nanolines, such as the lines with adsorbed O, to check not only how it compares to simulations, but also the features previously seen in experiment.

Chapter 9

Mn Nanowire

A successful model of the Mn nanowire on the Si(001) surface must reproduce all of the features observed in experimental STM images. One of the most interesting results is that at negative biases the nanowire exhibits a noticeable asymmetry, which manifests itself as a sawtooth appearance. This type of behaviour can be seen in Figures 9.1.a) and b), from which a few additional pieces of information can be gathered. The individual units of the nanowire have a diagonal, almost triangular appearance, suggesting the presence of additional Mn which cannot be imaged directly. The sawtooth appears to be due to the internal structure of the nanowire, because if Si is missing from directly next to the nanowire it has no effect on the sawtooth appearance. At positive biases the nanowire appears as a series of bright spots centred in the trench between rows, as demonstrated in Figure 9.1.c). This suggests the presence of Mn atoms in the trench between rows. In addition, at lower positive biases, the Si dimers directly next to the Mn nanowire show a phase shift, as shown in Figure 9.2, which is the same behaviour as observed for the Bi nanolines. There have already been several attempts to characterise the Mn nanowire, such as the C chain [57] or the Wang trimer [58], however I do not believe a definitive structure has yet been found.

Trying to determine the physical structure of the Mn nanowire has involved an extensive search of the possible arrangements for Mn on the Si(001) surface, encompassing old models (Sec. 9.1), variations and extensions to them (Sec. 9.2), and new ideas incorporating known adsorption sites for Mn or derived from random structure searching (Sec. 9.3). Over forty different structures were tested, with some providing new insights into the structure of the Mn nanowire, but many others simply providing details of which structures to rule out. In some cases this was because the choice of structure was made based on a misinterpretation of experimental results, meaning they could never represent reality. In most cases the structures simply failed to reproduce the experimental features better than older models, or even failed to reproduce any of them. In a few cases the structures could not be relaxed sufficiently to produce useful STM images. Even though the negative results might not contribute to determining the structure of the Mn nanowire, they might be useful for identifying other Mn structures. Many of these negative results are collected in Appendix E.

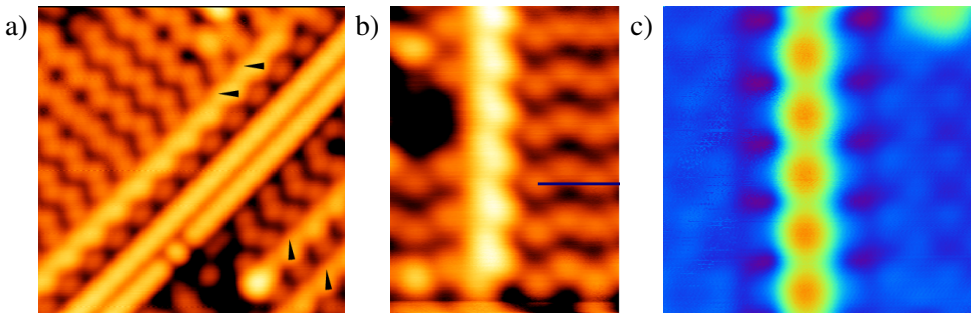

Figure 9.1: Experimental STM images of the Mn nanowire at a variety of bias voltages. a) Mn nanowire at - 2.0 V. Arrows indicate a diagonal tilt to individual units of the Mn nanowire. b) Mn nanowire at -2.5 V, showing the Mn nanowire with a sawtooth appearance, regardless of the surrounding Si. c) Mn nanowire at +1.8 V. The Mn nanowire appears as a series of bright spots centred in the trench between dimer rows. Images are courtesy of Sigrun Sigrun Köster from Christoph Renner's group in Geneva.

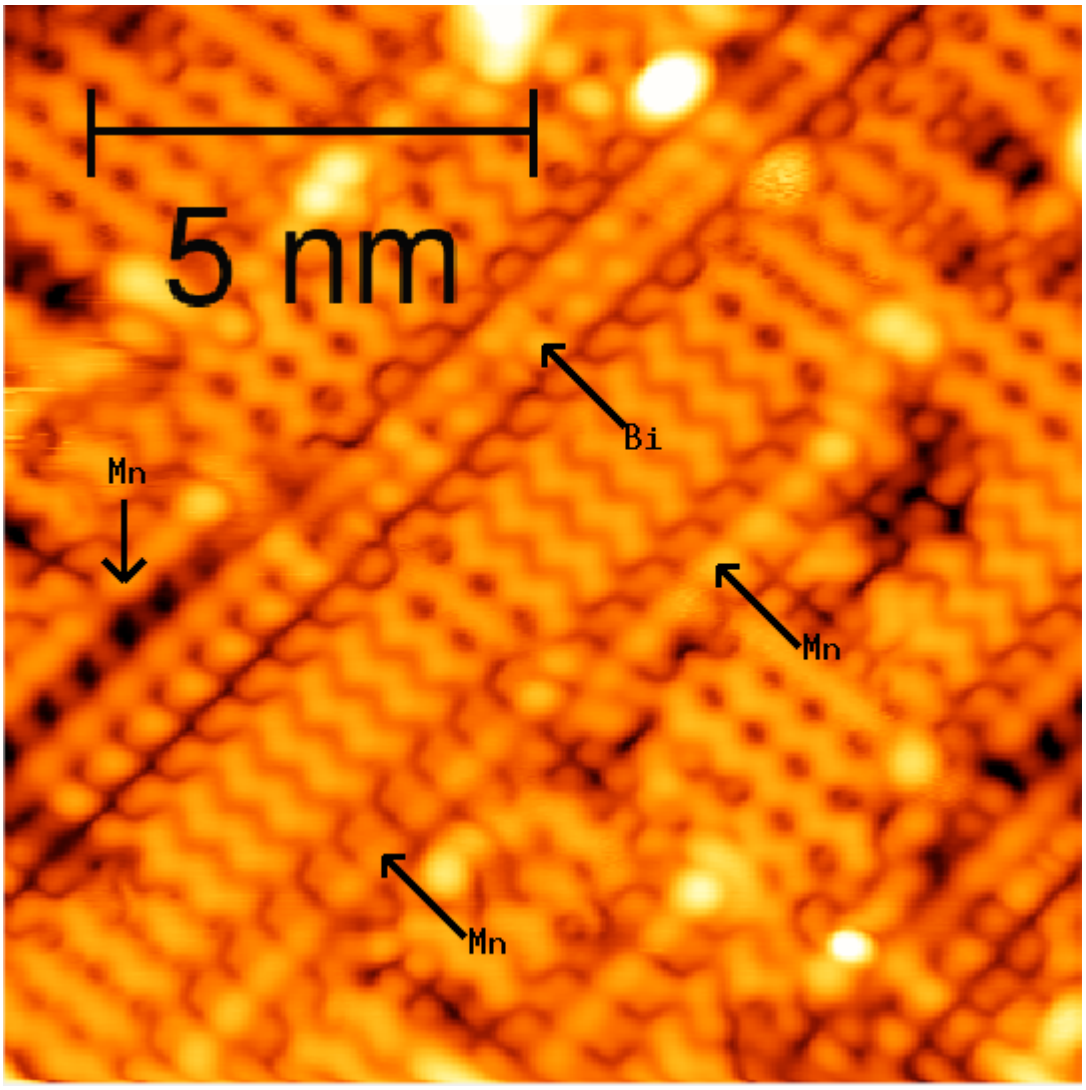

Figure 9.2: Experimental STM image at +1.2 V containing both the Mn nanowire and the Bi nanoline. The Si directly next to both types of nanostructure show a phase shift relative to the Si dimer rows. Image courtesy of Sigrun Sigrun Köster from Christoph Renner's group in Geneva.

9.1 Revisiting Old Models

A good place to start for examining the Mn nanowire is to re-check older models and test where they succeed and fail when compared to experiment. This can be used to guide future investigations, and provide structures to improve upon. Two of the most prominent structures were re-examined, namely the C chain and the Wang trimer.

9.1.1 C chain

The C chain consists of a chain of Mn atoms adsorbed at the C site in the middle of the trench, as shown in Figure 9.3. Calculations revealed that the lowest energy spin arrangement for the system found so far, with E_{ads} per Mn of -1.75 eV, has Mn atoms with an up spin of 5/2 and all the down Si atoms in the C chain with a down spin of 1/2, as shown in Figure 9.4. Initial tests showed that forcing this spin on the system via the NUPDOWN and MAGMOM tags in VASP would help the system relax faster, but that calculations run without these tags would also eventually relax to the same structure. In addition to studying the C chain under regular conditions, it was also studied using the DFT+U method, with the same spin arrangement. This has little effect on the physical structure of the C chain, beyond raising the height of the Mn atoms by 0.23 Å. There is however a noticeable effect on the E_{ads} per Mn, which is reduced to -1.11 eV.

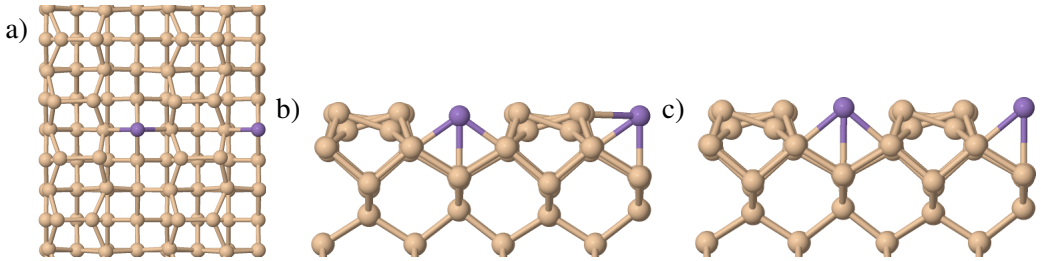

Figure 9.3: Structural models of the C chain relaxed using regular DFT and DFT+U. a) Top view of the regular C chain. b) Side view of the regular C chain. c) Side view of C chain relaxed using DFT+U. The Mn atoms are raised in height by 0.26 Å compared to the structure from regular DFT. Mn atoms are represented in purple.

Examining these structures in simulated STM, as shown in Figure 9.5, reveals some interesting features which can be related back to the experimental results. At negative biases a diagonal is visible across each unit of the C chain, matching the direction and location observed in experiment. This diagonal is across the trench between two up Si atoms, with the Mn filling in the gap in the middle. When DFT+U is used the appearance of the diagonal is more consistent along its whole length, due to the raised height of the Mn atoms. However, there is no sign of a sawtooth appearance, and no possibility of any asymmetry to this structure, which contradicts experimental results. On its own the C chain cannot fully reproduce the negative bias appearance of the Mn nanowire, but it could make a good base for other models.

The information gained from the negative bias images is still useful, because it reveals the origin of some of the experimental features, even if the complete structure is not clear. The C chain shows that the appearance of the Mn nanowire does not necessarily have to be due to Mn

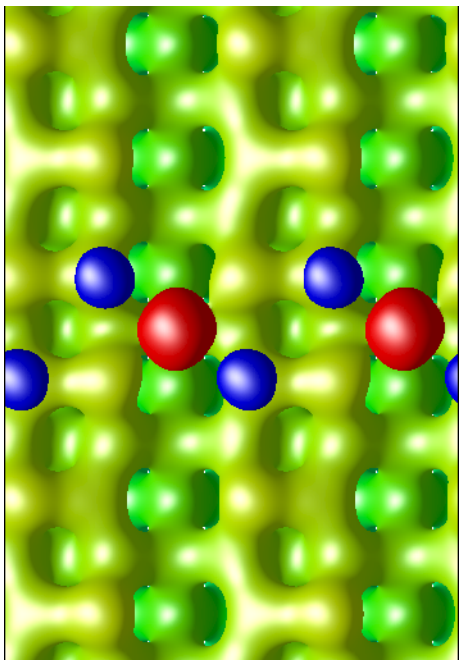

Figure 9.4: Spin arrangement along the C chain with up spin of 5/2 on the Mn and down spin of 1/2 on the down Si. Up spin is represented in red, with down spin in blue. Charge density is presented in green yellow and colour coded by height.

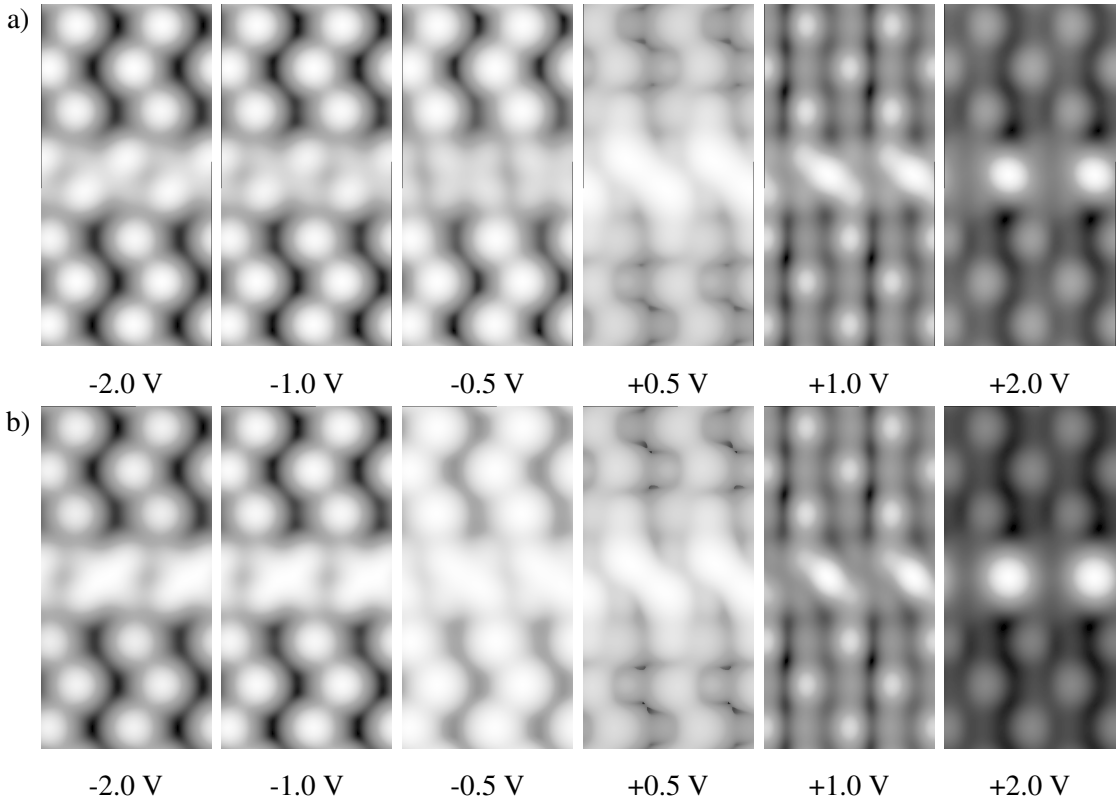

Figure 9.5: Simulated STM images for the C chain at a variety of bias voltages. a) Regular C chain. b) C chain from the DFT+U method. Unless stated otherwise all simulated STM images are presented for an isosurface value of 0.01 in arbitrary units.

atoms, but could also be due to the enhancement of nearby Si atoms. The diagonals in experiment coincide with the positions of up Si, which is supported by the C chain model. This suggests that

the correct model should involve atoms at this position in some form, whether that means as Si atoms, or as substituted Mn atoms. This detail cannot be deduced from the C chain alone.

The C chain performs less well at positive biases, with a diagonal appearing in the opposite direction at lower positive biases. This diagonal extends across the neighbouring down Si atoms, and is not observed in experiment. There is also a visible difference between the Si dimers directly next to the C chain, and those further away, in a similar manner to experiment, although some of the details of this is obscured by the brightness of the C chain itself.

At higher positive biases the simulated STM performs better, with a bright round feature observed at the centre of the trench, corresponding to the Mn atom. This provides quite a good match to the experimental results, but is perhaps not wide enough. Experimental results show little to no gap between each unit of the nanowire, whereas these simulations are localised in the centre of the trench. This suggests that the positive bias appearance of the nanowire is due to one or multiple Mn atoms in the trench region.

The C chain model works surprisingly well for such a simple model, and reveals important details to consider for future models. The biggest problem with this model is the lack of a sawtooth at negative biases. Introducing extra Mn into the model might cause an asymmetry to the model, without getting rid of the features which already match to experiment. Its relatively low adsorption energy is also a concern, but this could be remedied by introducing more Mn.

9.1.2 Wang trimer

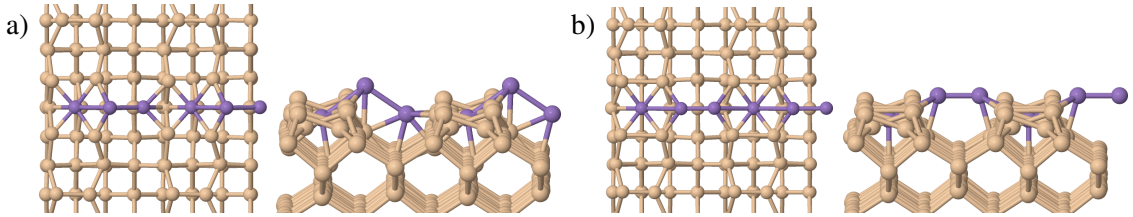

Figure 9.6: Structural models for the Wang trimer with different buckling angles. a) Top and side view of the Wang trimer with a 34° Mn dimer buckling angle. b) Wang trimer with a flat Mn dimer.

The current favoured structure in the literature is the Wang trimer [58], which consists of 3 Mn atoms per nanowire unit. One Mn atom sits at the H site on the dimer row, whilst the remaining two form a buckled dimer in the trench between rows, as demonstrated in Figure 9.6.a). The original study suggested that the structure buckles spontaneously during relaxation or at least makes no mention of them manually introducing the buckling [58]. This would suggest that the buckled structure is lower in energy than the flat structure, however the lowest energy structure I found was for a flat variation of the structure. In addition, the buckled structures I did find all had buckling angles ranging between 28° and 34°, which are greater than the 20° originally reported. The energy of the Wang trimer is very sensitive to both buckling angle and spin arrangements as detailed in Table 9.1. The different spin and buckling arrangements were obtained either by allowing the structure to relax with no constraints placed on the calculations, or by forcing certain arrangements using NUPDOWN and MAGMOM tags in VASP. Without performing a full study

on this matter it might be difficult to separate out the individual influences, or guarantee that the lowest energy structure has been found. Since it was uncertain whether this was the correct structure or not, only the simplest variations were attempted. Calculations were also extended to include DFT+U, however this resulted in an increase of buckling angle to almost 45°, and a shift of the up buckled Mn onto the dimer rows, with the resulting STM images failing to match experiment.

Table 9.1: Adsorption energies per Mn atom for the Wang trimer with different buckling angles and spin arrangements. Arrows indicate spin up or spin down. Unless indicated otherwise labelling starts at the H site Mn at the left of the simulation cells shown in Figure 9.6.

Mn buckling angle (°)	Spin arrangement	E_{ads}/Mn (eV)
0	None	-2.90
0	↑↓↓↑↓↓	-2.97
0	↑↓↑↓↑↓	-3.11
28	None	-2.84
32	↓↑↓↑↓↑	-3.03
34	↑ on up Mn ↓ on down Mn with ↑ > ↓	-3.06

The most noticeable changes with spin arrangement occur for the flat Wang trimer, where the effects of buckling can be ignored. This arrangement has both the lowest and one of the highest energy structures, depending on how the spins are arranged. If the anti-ferromagnetic (AFM) structure is indeed a global minimum for the Wang trimers this raises the question of why the previous study suggested spontaneous buckling, given that this would raise the overall energy of the structure rather than reduce it. However, the small energy differences between the buckled and flat arrangements suggests that it would be relatively easy to switch back and forth between the two.

For the buckled structures a change in buckling angle of a few degrees can reduce the adsorption energy by about 0.2 eV per Mn, although the change in spin arrangement might also contribute to this. It is possible that other buckling arrangement exist with lower energies, but I was not able to find them. Further investigation of this matter would only be necessary if the Wang trimer was undoubtedly the correct structure for the nanowire, or if a small change in buckling angle dramatically changed the STM images. It is also worth noting that regardless of arrangement, the E_{ads} per Mn for all of these structures shows an improvement of over 1 eV compared to the C chain, which only has an E_{ads} per Mn of -1.75 eV. This improvement in energy makes it more likely that a Wang trimer related structure is responsible for the experimental results.

Simulated STM images for two of the most significant variations of the Wang trimer are shown in Figure 9.7. At first glance the negative bias STM images for the buckled Wang trimer appear to be a good match for the experimental results. One side of the line looks flat, whilst the other looks bumpy, reproducing the sawtooth appearance noted in experiment. The reason for this appearance can be explained by considering the buckling of the Wang trimer relative to the surrounding Si dimers [59]. The bright, almost triangular region of the Wang trimer is due to a combination of the up buckled Mn atom, and the two Si atoms it bonds to. Since the Mn atom is raised, it also pulls

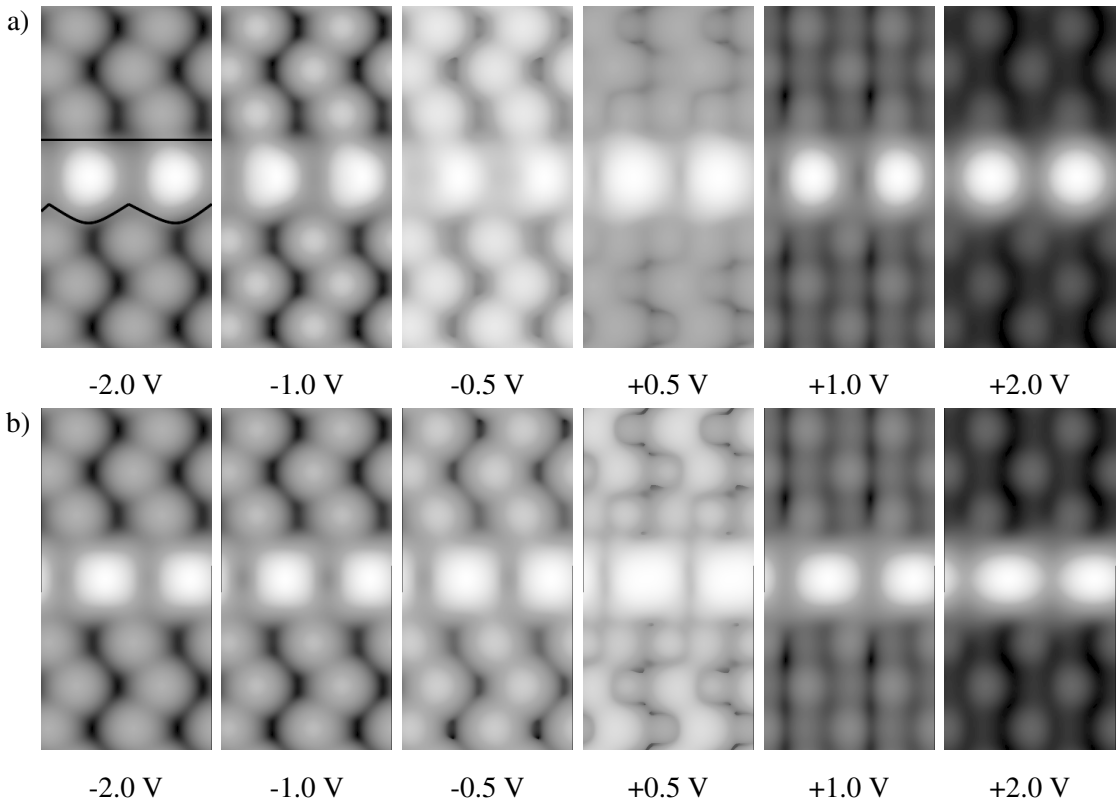

Figure 9.7: Simulated STM images for the Wang trimer at a variety of bias voltages. a) Wang trimer with a 34° dimer buckling. b) Wang trimer with a flat Mn dimer. The results at -2.0 V for a) have been annotated to indicate the regions claimed to reproduce the sawtooth appearance.

up these Si atoms relative to the others, making them more visible in the simulated STM. This has not been noticed in previous studies, and is contrary to the experimental results, which shows a diagonal feature extending across the trench, rather than stopping in the middle. The buckling of the Si dimers next to this feature can then influence the overall appearance of the nanowire. If the bright spot coincides with a down Si, a bumpy edge is seen, if it coincides with an up Si a flat edge is seen.

Based on this information alone it provides a convincing explanation for the sawtooth appearance of the nanowire, however there are additional experimental results which suggest this structure is not valid, as shown in Figure 9.8. The experimental STM shows a region of the Mn nanowire next to a region of missing Si, however the appearance of the Mn nanowire in this region is exactly the same as it is for the regular Si(001) surface. From the arguments put forward by Fuhrer *et al.* [59], there should be a round appearance to both sides of the nanowire, but this is clearly not the case. Simulations for the buckled Wang trimer in similar scenarios, with either a missing dimer or two missing up Si next to what is considered the flat side of the nanowire, do however show a round appearance on both sides of the nanowire. This is contrary to experimental results and provides definitive evidence against the Wang trimer.

The results at positive biases are mixed, with the Wang trimer working better at higher positive biases than lower. At lower positive biases the rounded triangular shape of the trimer is still visible, which is not seen in experiment, but as the bias is increased this becomes a round feature, centred on the raised Mn atom. This latter result is closer to experiment. In addition, at lower positive

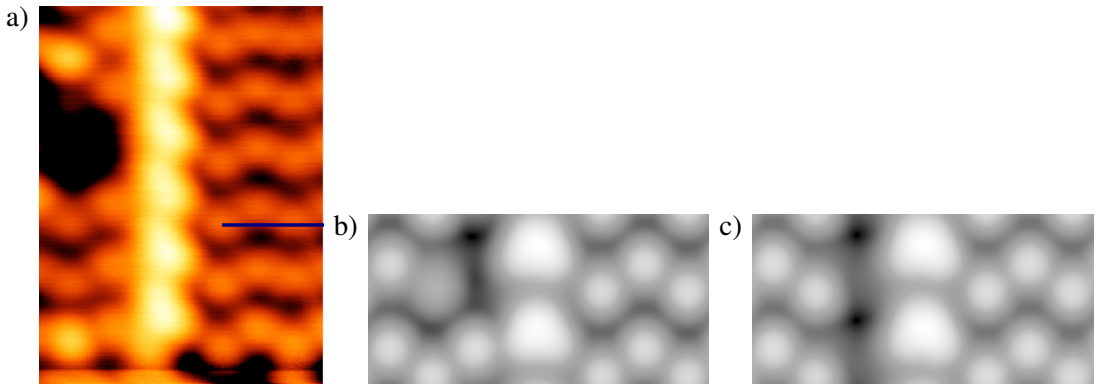

Figure 9.8: STM images showing a gap in the Si surface directly next to the Mn nanowire. a) Experimental STM image at -2.5 V showing that the flat side of the sawtooth is still maintained despite the absence of Si. b) Simulated STM at -2.0 V of the buckled Wang trimer with a neighbouring Si dimer missing. c) Simulated STM at -2.0 V of the buckled Wang trimer with neighbouring up Si atoms missing. Experimental images are courtesy of Sigrun Sigrun Köster from Christoph Renner's group in Geneva.

biases the Si dimers next to the Mn nanowire change in appearance relative to the other Si dimers.

By comparison, the flat Wang trimer reproduces the positive bias appearance much better, but gets the negative bias appearance completely wrong. Since the central dimer is flat and completely straight, there is no sign of a sawtooth or a diagonal at negative biases. It is unlikely that intermediate buckling angles would solve these issues, since previous work at presumably 20° [59] has the same general appearance and issues as those detailed here.

At first it appears that the Wang trimer reproduces the negative bias results well, but upon closer examination and with the aid of new experimental results it does not hold up well. The sawtooth appearance of the nanowire must be due to nanowire itself, or atoms contained within the two dimer wide nanowire region, and cannot be influenced by the arrangement of the nearby Si. The positive bias results are useful, because they suggest that the Mn nanowire contains an Mn dimer in the trench region, and that a flatter dimer will produce a larger feature, which is a better match to experiment. On its own the Wang trimer cannot be the correct model for the Mn nanowire, but it could make a good base for future models.

9.2 Extensions to Old Models

The C chain and Wang trimer individually reproduce some features of the experimental results, but cannot satisfy all of them at once. One possible method to rectify this is to extend these models, either by adding more Mn, or by rearranging the Mn and Si positions slightly. This might introduce the missing features, without getting rid of the ones that are already there.

9.2.1 C chain

The main problems with the C chain model are that it does not reproduce the sawtooth appearance, and that the Mn atom is not particularly visible at negative biases, unless calculations are

performed using DFT+U. Several different ideas were explored for modifying the C chain, with limited amounts of success. Many of the less sucessful models are presented in Appendex E.1, because they do not directly contribute to identifying the Mn nanowire.

One way to change the C chain is to alter the structure without adding any Mn. By placing the Mn higher above the surface before relaxation it was hoped that this might find a structure where the Mn was more visible, but all this did was relax back to the original C chain structure. Modifying the positions of the Si atoms directly around the Mn was equally unsuccessful. For example, using a c(4×2) reconstruction, means that the repeated unit of the nanowire is two dimer rows, rather than one, which does not match experiment. A more detailed account of this structure is provided in Appendix E.1.1.

Another possibility is that the asymmetry observed in experiment is due to charge transfer effects, rather than a physical change of structure. This is difficult to model properly in VASP and most attempts to charge the surface experienced convergence problems. In the one successful case it had no effect at all on the simulated STM of the structure.

A final option is to introduce more Mn atoms into the structure to enhance certain features, such as the brightness of the diagonal, or to introduce a sawtooth appearance into the model. Adsorbing more Mn atoms around the C site could create a sawtooth appearance at negative biases, but would also likely be visible at positive biases as well. This is not desired, because at positive biases only a round feature centred on the trench should be visible. To get around this problem, substitutional and subsurface Mn were considered.

Substituting the Si which directly surround the C site for Mn atoms, as shown in Figure 9.9, was intended to enhance the brightness of those positions without requiring much physical change to the buckling structure of the surrounding dimers. Rather than enhance these positions, the substitution of Si for Mn actually made these positions darker in simulated STM. Failures of these models and a lack of Si aggregation near the Mn nanowire, rule out substituted structures such as these. Full details of this research can be found in Appendix E.1.2.

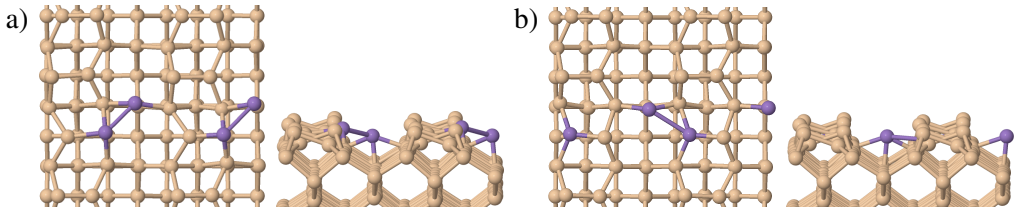

Figure 9.9: Structural models for Mn chains including substitutional Mn and adsorbed Mn. a) Top and side views of the C+S chain. b) Top and side views of the C+dS chain.

Subsurface Mn, such as that shown in Figure 9.10, was hoped to enhance the visibility of the Si directly above them, without the Mn atoms themselves actually being visible in the STM images. In most cases the subsurface Mn successfully enhanced the brightness of the Si atoms directly above them, but at the cost of no longer being able to see the C site Mn. Since these extensions were largely unsuccessful full details can be found in Appendix E.1.3.

Currently no extensions to the C chain have managed to improve the match between experiment and theory. Trying to bolt on other structure to the C chain in the hope of introducing specific

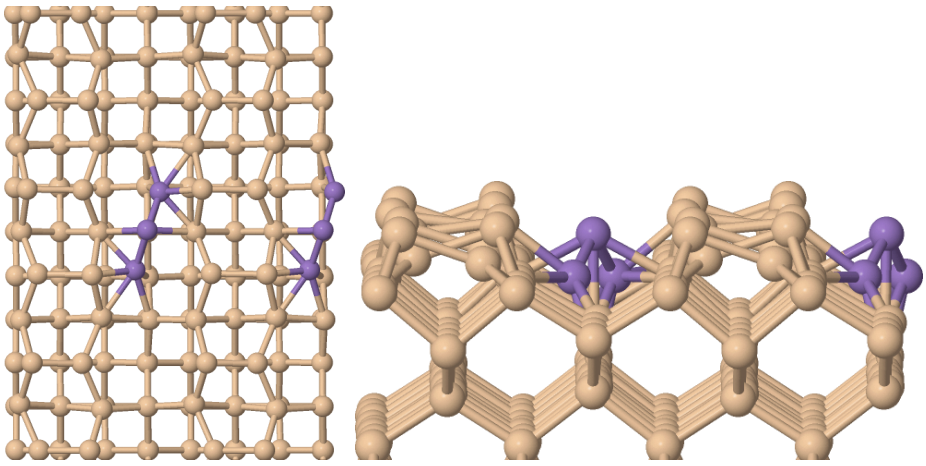

Figure 9.10: Structural model of the C+2B' chain showing top and side views of the structure.

features, whilst not affecting others, does not work.

9.2.2 Wang trimer

Despite its failings, the Wang trimer provides a structure which can be easily modified and then compared with the original and experiment. Variations on the Wang trimer can be made by swapping positions of the Mn and Si atoms around and relaxing the structure again. Alternatively the effect of removing the Mn at the H site can be tested, because whilst it is not actually visible in the simulated STM images, it may contribute to the stability of these structures. Full details of the Wang trimer variants can be found in Appendix E.2.

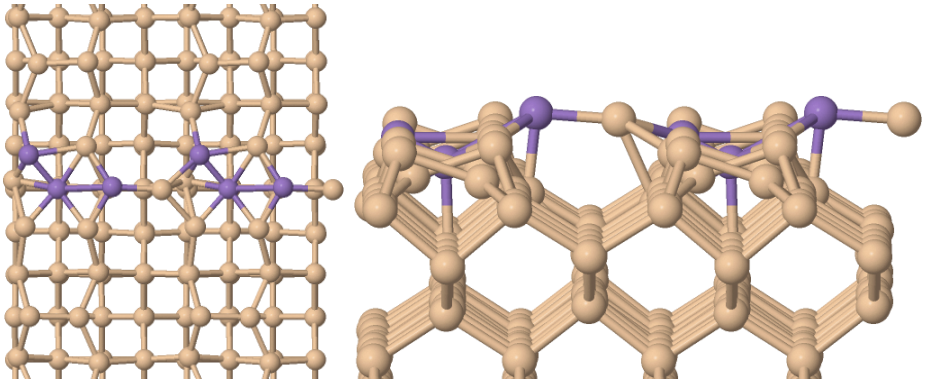

Figure 9.11: Structural model for a variant of the Wang trimer where the down buckled Mn of the Wang trimer has been exchanged with one of the up Si atoms.

The most successful variant so far involves exchanging the positions of the down buckled Mn, and the up buckled Si next to it, as shown in Figure 9.11, resulting in a structure which contains two Mn-Si heterodimers, one in the trench, the other in the dimer row. When relaxed the resulting trench heterodimer has a much smaller buckling angle of 5.1°, compared to the regular Wang trimer. The E_{ads} per Mn for this structure is worse than the regular Wang trimer at -2.74 eV. The simulated STM, in Figure 9.12, for this structure shows some promising features that align with experimental results.

At negative biases a sawtooth appearance is visible along the nanoline, which is not reliant

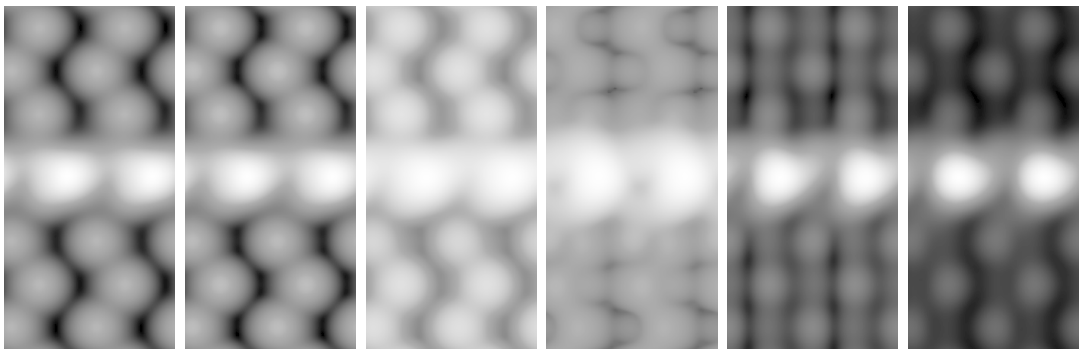

-2.0 V -1.0 V -0.5 V +0.5 V +1.0 V +2.0 V

Figure 9.12: Simulated STM for a Wang variant where the down buckled Mn of the Wang trimer has been exchanged with one of the up Si atoms.

on the arrangement of neighbouring Si dimers. The flat side has contributions from the Mn-Si heterodimers in the trench and the dimer row, as well as the Si bonded to the up buckled Mn. The sawtooth appearance on the other side is due to the different environments of the dimer Si atoms which bond to the trench heterodimer. On one side the dimer Si is bonded to an Mn atom, on the other it is bonded to an Si atom, with the former contributing to the bumps of the sawtooth. At first inspection this sawtooth does not appear to show a particularly clear diagonal, which is a key feature of the experimental results. If the isosurface value is increased, as in Figure 9.13, then the diagonal or triangular nature of the trimer becomes clearer. In addition to the central bright spot from the Mn-Si dimer, three of the four surrounding Si contribute, leading to a triangular shape. The only Si which does not contribute to this is the one which bonds to the Si of the trench Mn-Si heterodimer.

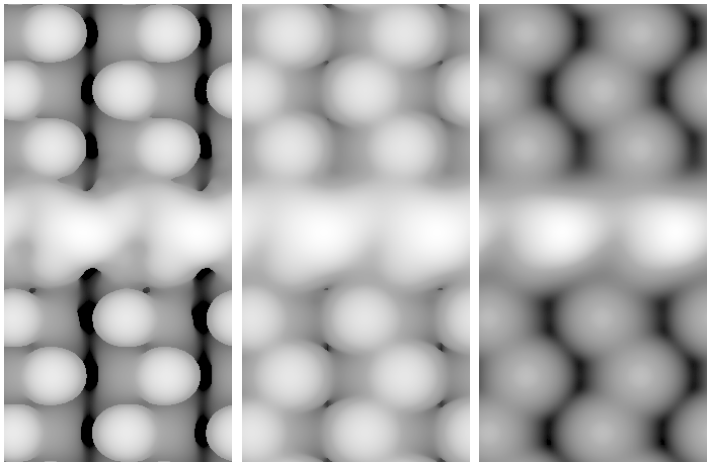

1 0.1 0.01

Figure 9.13: Simulated STM for a Wang variant at -1.0 V, where the down buckled Mn of Wang trimer has been exchanged with one of the up Si atoms. The images shown are at different isosurface values, in arbitrary units.

At positive biases the simulated results look similar to experiment, but there are still a couple of issues. At low positive biases, instead of being round, the central feature looks triangular, in a similar fashion to earlier results for the regular Wang trimer. On the positive side, at +0.5 V

the Si dimers directly next to the Mn nanowire appear different from the rest of the surface, in a similar manner to experiment. Above about +1.0 V the nanowire takes on an oval shape similar to experiment, but with a tail that extends to the position of the substituted Mn atom, a result not seen in experiment. The match to experiment is better at higher values, such as +2.0 V.

This model provides a very good match to experiment, and I think is the best so far considered, however I am not yet convinced it is the correct structure. The model performs badly at very low positive biases, when compared with the currently available experimental results, only displaying a rounder feature above about 1.0 V. There is however a lack of experimental results below 1.0 V, making proper comparisons difficult. The biases at which features occur in simulation will not exactly match those from experiment, often shifting by tenths of a volt, but without the experimental data it is hard to make definitive conclusions.

Aside from this there are also issues of the energy of the structure, and the formation process. With a higher energy than the regular Wang trimer there are doubts that this variation would form instead of the normal Wang trimer. This Wang variant is also a fairly complicated structure, involving Mn and Si exchange. It seems unlikely that this could occur in the same way over the distances required to create regular nanowires. The energy barriers to formation would also need to be considered given that nanowires can form at room temperature.

9.3 Other Models

In addition to exploring older models and their extensions, other structures for the Mn nanowire were also considered. This included Mn in dimer vacancies, subsurface Mn, H site Mn and reconstructions of the Si surface. Many of these offered no new insights into the structure of the Mn nanowire, but might instead be useful for identifying other Mn structures on Si(001). Results for most of these structures are collected in Appendix E.3.

One of the models with more interesting results involved a subsurface reconstruction below the Mn nanowire, similar to the Haiku core of the Bi nanoline. This was considered because at the time a reconstruction was still believed to be the cause of the phase shift of the neighbouring Si dimers at lower positive biases. The Haiku core would not be a suitable base though, because it is four Si dimers wide, rather than the two dimers required for the Mn nanowire. Instead a reconstruction known as A type was used, which is essentially a half size Haiku reconstruction, as shown in Figure 9.14. In the A type region the subsurface Si is rearranged into two outer five membered rings and one inner seven membered ring, just like the Haiku core, but extending for a smaller distance. The Si dimers across the top of the seven membered rings run perpendicular to the rest of the surface, whilst the surface Si of the five membered rings buckle as if they were surface dimers.

Wire structures can then be built atop these and compared with experiment. One idea explored was placing Mn at the C site, as shown in Figure 9.15. In this new Si arrangement the Mn bonds atop of one of the perpendicular Si dimers, whilst flattening the remaining Si within the A type region. As a result, the Mn is in the middle of the trench with the same immediate environment in all directions, unlike the regular surface where it was surrounded by both up and down Si. Due to

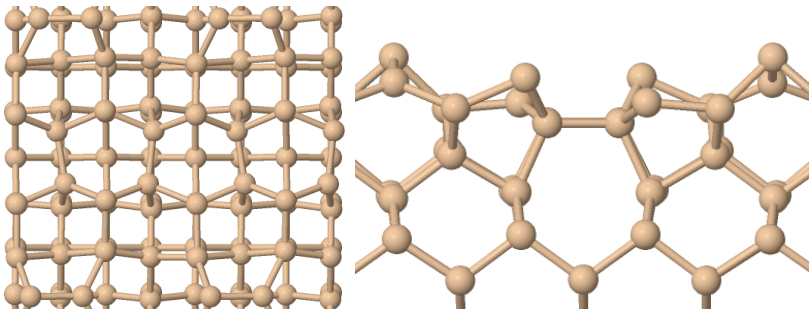

Figure 9.14: Structural model for the A type reconstruction of the Si surface, showing both the top and side views. The Si surface reconstructs into five and seven membered rings, rather than the normal six, with the surface dimers in this region running perpendicular to the Si dimer rows. Surface Si in the five membered rings still buckle like the dimer rows. For the top view the regular dimer rows run from top to bottom, with the dimer row of the A type region running left to right across the centre of the image.

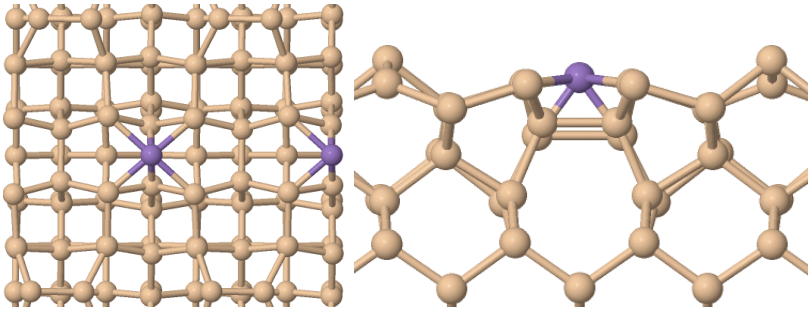

Figure 9.15: Structural model for the A type reconstruction of the Si surface with Mn adsorbed at the C site position, showing both the top and side views. The Mn atom bonds atop one of the Si dimers which now runs perpendicular to the direction of the dimer rows.

the fact that A type region is physically lower than the rest of the surface, the adsorbed Mn is lower in height than the surface up Si. If DFT+U is used the Mn is raised up by 0.7 Å but otherwise the structure is mostly the same.

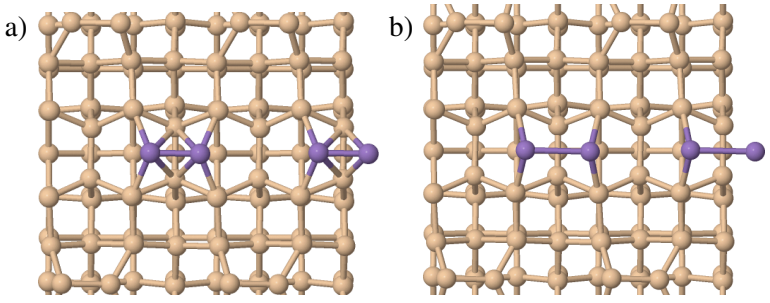

Figure 9.16: Structural model for the A type reconstruction of the Si surface with Mn dimers adsorbed in the trench region. a) Regular dimer structure. b) Dimer structure using DFT+U.

Another wire structure examined was made of Mn dimers in the A type region, placed in line with the surface trench, as shown in Figure 9.16. Under normal conditions the Mn dimers are 2.29 Å long with a very slight tilt of 1.5°. When DFT+U is used the dimers extend to 3.03 Å with a tilt of 1.3°.

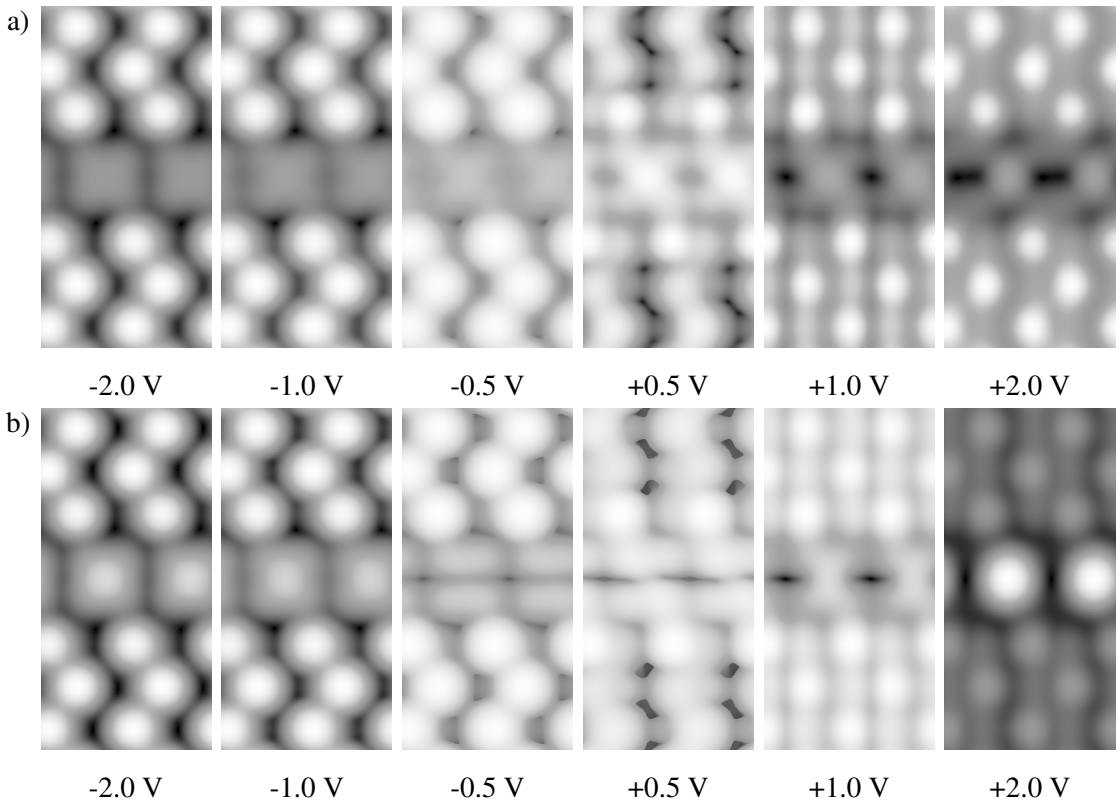

Figure 9.17: Simulated STM for C chain on A type Si. a) Regular DFT. b) DFT+U.

Both of these structures have been considered with regular DFT and DFT+U and the resulting structures examined in simulated STM. The C site Mn, shown in Figure 9.17, suffers from the fact that it is physically lower than the surrounding Si. As a result the C site Mn looks darker than the rest of the surface at nearly all bias voltages, and fails to match experimental results at all. When using DFT+U, since the Mn are 0.7 Å higher, they are more visible at higher biases, such as +2.0 V. For negative biases and lower positive biases the Mn still remain dimmer than the rest of the surface. Due to the symmetric nature of the Si around the Mn atoms there is also no sign of a diagonal or sawtooth appearance at negative biases.

The Mn dimers fare better, as shown in Figure 9.18, with the positive bias results a good match for the experimental results. The Mn dimers appear as extended round spots in the trench regions, with little gap between each unit. The results at +2.0 V match well to the experimental results from Figure 2.6.c) and the feature remains roughly the same for all positive biases. In addition, at +0.5 V the Si next to the nanowire experience a phase shift similar to the experimental results. Using DFT+U makes the Mn atoms move further apart, and makes the positive bias appearance of this structure worse, with its wire region looking like one unbroken line by +2.0 V. The negative bias appearance barely changes between regular DFT and DFT+U, and in both cases fails to match experiment. Whilst there is a slight diagonal tilt to the bright spots, due to the tilt of the dimers, it is in the wrong direction, and there is no possibility of a sawtooth.

Extending this model to bring in a sawtooth appearance is problematic because of the height of the Si within the A type region. There are no Si of comparable heights to the Mn that could contribute to the appearance of the wires. This means that the presence of extra Mn would need to be responsible for these changes, which would likely then be visible at positive biases which is

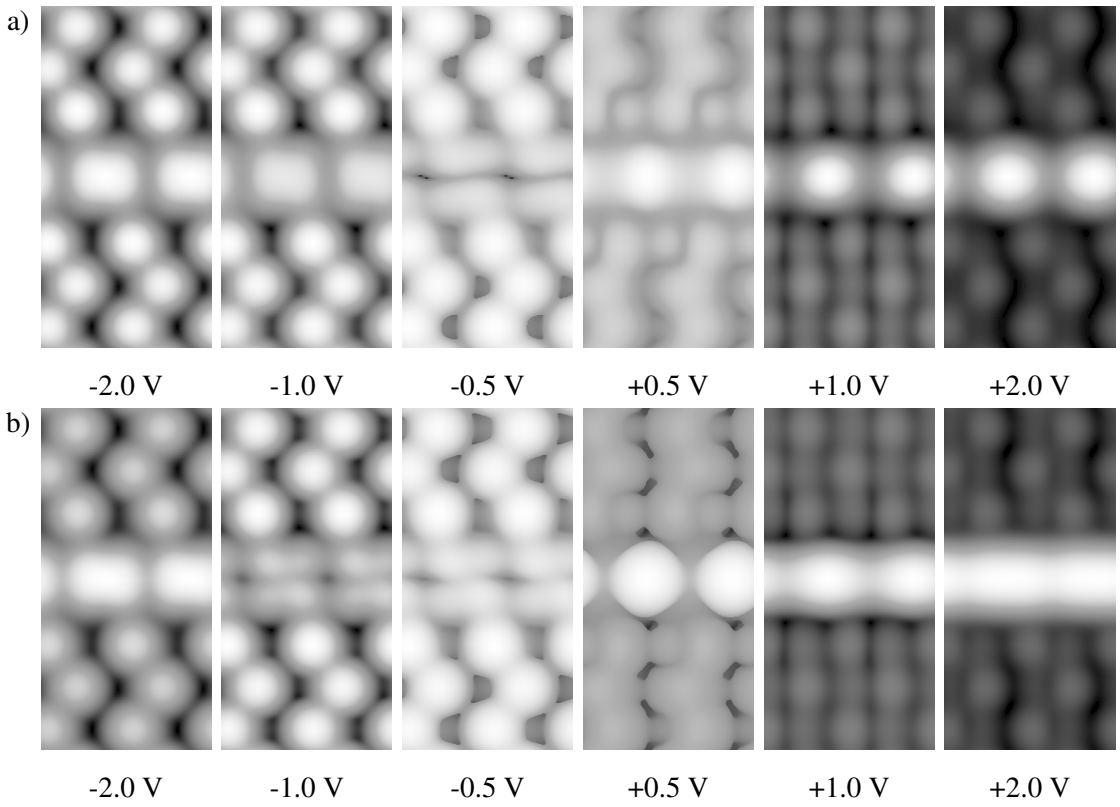

Figure 9.18: Simulated STM for Mn dimers on A type Si. a) Regular DFT. b) DFT+U.

undesirable.

Whilst these A type models do not provide a structure for the Mn nanowire they do provide some useful results. It is possible to reproduce some of the experimental features with Mn on this reconstructed surface, but the fact that the reconstructed Si is physically lower than the normal Si surface means that all of the features of the Mn nanowire must be due to the Mn alone. This makes it difficult to reconcile the differences between positive and negative biases, where the nanowire switches from a series of round features to a sawtooth appearance. It therefore seems unlikely that a reconstruction such as this occurs for the Mn nanowire. Results for the Mn dimer reinforce the idea that the positive bias appearance of the nanowire is due to a dimer in the trench region.

To aid in creating other new structures Ab Initio Random Structure Searching (AIRSS) methods [121] were employed by Andrew Morris, but unfortunately did not produce any presentable results. This can be attributed to several different factors. Firstly, the AIRSS method is guided by a search for the lowest energy structure. Whilst it is likely that the Mn nanowire structure will have a low energy, it might not be the global minimum. Often this would result in low energy structures which could not possibly represent the Mn nanowire.

Another big problem is the input parameters for the search. The amount of Mn per wire unit is currently unknown, and convincing structures can range between one and three Mn atoms. AIRSS methods can only do one of these searches at a time, and it vastly increases the computational time required if several different searches need to be made, especially since only one of them will actually be relevant to the real structure. It is also unclear which other atoms to allow to move, or whether an extensive surface reconstruction is required, like for the Bi nanoline.The less atoms that are fixed in the model, the more expensive it becomes to perform a search, and the harder it

becomes to extract meaningful results. Due to factors such as these, the search was restricted to three Mn atoms or less, and only the surface Si dimers were allowed to move.

Finally, even in cases where a reasonable looking structure was produced by the AIRSS methods it would then encounter convergence problems when I tried to replicate the structure using VASP, meaning simulated STM images could not be produced. Reassuringly a few of the results did look close to variations of the Wang trimer. This method is potentially useful, especially when lacking inspiration for new structures, but needs better defined input parameters, which would require further experimental work.

9.4 Conclusions

Despite the best efforts, the structure of the Mn nanowire still remains elusive. Older models have been found to be lacking, and the current favoured structure in the literature, the Wang trimer, shown to be wrong. Close study of these structures and comparison to experiment has however revealed important details of the Mn nanowire. The diagonal noted in the experimental results coincides with the positions of up Si atoms, and is visible in models such as the C chain. So the arrangement of the Si atoms around the Mn is an important factor to consider, alongside the position of the Mn atoms themselves. These atoms could even be substituted Mn, as long as they are in the correct positions.

From studies into the Wang trimer it had been believed that the sawtooth appearance was due to an interplay between the buckling of the Wang trimer, and the surrounding Si atoms. New experimental results showing that missing Si does not change the appearance of the nanowire, coupled with simulations which show that the Wang trimer behaves contrary to this, have provided evidence against this model. The sawtooth must be due to the internal structure of the nanowire region.

Several results have supported the idea that the round feature observed at positive biases is due to a dimer in the trench region. The precise details of this dimer is unclear, because it could either be an Mn dimer or an Mn-Si heterodimer, either of which could be flat or buckled.

A new best model has been developed, based on a variation of the Wang trimer, made by swapping a down buckled Mn with an up buckled Si. This results in a sawtooth appearance at negative biases, and a round appearance at higher positive biases. There are lingering doubts over the tail that the round feature has at lower positive bias, which means I am not confident in calling the structure solved yet. It is also a fairly complicated structure, which raises further doubts about it forming in a systematic way. This is compounded by the fact that energetically the system is worse than both the flat and buckled versions of the regular Wang trimer. The flat AFM version of the Wang trimer is still one of the most energetically favourable structures found, despite the fact it mostly fails to reproduce the experimental results.

At this point many possible options have been exhausted and there does not seem to be a clear way forward in the search for the structure of the Mn nanowire. Theoretical models can only go so far with incomplete experimental results. The most useful work that could be done right now would be further experimental work. A question that still hangs over the Mn nanowire is

exactly how many Mn atoms there are in each individual unit. If this was known then it would become much easier to work out the structure, because future searches, such as those using AIRSS methods, could be more focused. It would also be useful to have more experimental STM images at very low positive biases, but this might not be possible.

The search for the Mn nanowire has also taught important lessons about interpreting results, whether experimental or theoretical. If experimental results are misinterpreted it is very easy to spend time pursuing models which have no relation to reality. It is also necessary to make sure that theoretical results actually match to reality, rather just looking like they do under specific circumstances, as was the case with the Wang trimer.

Chapter 10

Conclusions and future work

This work has demonstrated both the successes and limitations of using DFT to study nanostructures on the Si(001) surface, and of using the Tersoff-Hamman approximation to calculate simulated STM images. Whilst there have been fantastic successes, for example in explaining the electronic structure of the Bi nanoline, there have also been much less fruitful areas of research, such as the Mn nanowires. It has also taught me the necessity of collaboration between experiment and theory. Theoretical studies must be grounded in an understanding of what is physically possible, or guided by experimental results that lack an explanation on their own. When performing a simulation to explain experimental results, a proper understanding of these results is needed, otherwise it is very easy to pursue ideas which have no bearing on reality. For example with the Mn nanowire, structures with a width of over two dimers were tested, despite the later realisation that the Mn nanowire cannot extend beyond this range.

Another result which lead to constant confusion and misinterpretation was the Si dimer row phase shift observed at higher positive biases. Both experimental and simulated STM images make it appear as if the centre of the dimer row is the trench between rows, and vice versa. This makes examining the Bi nanoline and Mn nanowire difficult, because it makes features appear to occur in line with the trench between rows, when in reality they are in the centre of the Si dimer rows. It is very easy to draw incorrect conclusions from the results in the bias ranges where this occurs, and a careful examination of the full set of results is needed to avoid this. Pitfalls such as these are easier to avoid in collaborative work, because everyone involved can act as a check on the interpretation of results.

Since much of this work has focused on using theoretical simulations to try and explain known experimental results, it has proven useful to be able to draw on a wide range of expertise. Experimentalists provided a better understanding of what is physically possible, as well as a knowledge of the experimental conditions, which helped to constrain the search criteria in cases such as the feature on the Bi nanoline. Drawing on the knowledge of theorists with experience in determining the physical structures of nanostructures, such as the Bi nanoline, also proved invaluable during the search for the structure of the Mn nanowire.

The theoretical studies performed here can be split into roughly three different categories, speculative studies, studies of known structures and studies of currently unknown structures.

DFT has proven to be most successful when applied to known structures and can offer results

which are not easily accessible to experiment. This is exemplified by the investigation into the electronic structure of the Bi nanoline. The structure of the Bi nanolines is known, and it had been thought that all details of their electronic structure was known. However new experimental results showed that there is a strong bias dependence to the STM appearance of the nanoline, which is reproduced exactly by simulations. At lower positive biases there is an electronic coupling between the Bi dimers and the surface Si dimers, which usually manifests itself as a zigzag pattern of bright spots along the length of the Bi nanoline. The bright spots correspond to the positions of what would be up atoms, despite the fact the Bi dimers are completely flat. Simulations have allowed the exploration of less commonly seen surface arrangements, showing other possibilities for arrangements of bright spots, which were found in experimental results upon closer inspection. A similar electronic coupling is also seen at negative biases, except with down Si atoms. There are currently no experimental results to compare to, but considering the great successes of the model at other biases it is expected that simulations at these biases will also be shown to be correct. At intermediate positive biases the bright spots switch to the trench between dimer rows, and can be attributed to imaging individual p-orbitals. At higher positive biases the Bi dimers are imaged, whilst at higher negative biases the individual Bi atoms are imaged.

DFT has thus far proven to be less successful when attempting to determine new structures, or identify unknown features. This is less to do with failings of DFT itself, but rather a reflection of the difficulty of the task at hand. DFT is just a tool used to get results and cannot succeed without user input. No matter how good the tools are, if the inputs are wrong, the correct answer will not be found. In cases such as the Mn nanowire, simulations are the only way to solve the structure, because there is only so much information that can be extracted from experiment alone. Even with a careful consideration of all available experimental data and prior attempts, a degree of inspiration, perseverence, and sometimes just luck is required to make progress in searches like these. Developments in techniques like Ab-Initio Random Structure Searching (AIRSS) may take some of the guesswork out of this in the future, but the final results will still need to be assessed by the user.

The search for the identity of the Bi nanoline feature and the structure of the Mn nanowire have not been unfruitful, despite failing to reach their respective goals. It has not yet been possible to find an adsorbate on the Bi nanoline which appears as a sharp feature at positive biases and a round feature at negative biases, but other interesting effects have been observed. The closest structure found so far is an adsorbed O atom, which displays the opposite bias dependence. The most interesting result to come out of this search is the fact that many of the STM images show rings around the adsorbates, an effect that has never been observed before, to the best of my knowledge. This opens up the possibility of future work to find these rings in experiment, or else show they are an artefact of simulations. If real, it would demonstrate the capability of imaging subatomic features for this set of modifications to the Bi nanoline. During the course of the search, it was also shown that missing Bi will affect the appearance of the Bi nanoline, beyond simply the fact that sections of it will be missing. A weaker electronic coupling is observed along the direction of the nanolines, which cannot be seen for complete nanolines.

As it currently stands the correct structure of the Mn nanowire is still unknown, but important

steps have been made towards finding it. The previous best model, the Wang trimer, has been shown conclusively to be wrong, and superceded by a new variant which exchanges the positions of Mn and Si atoms within the trimer. Despite improvements I do not believe that an exact match to experiment has been achieved. However the cause of several important features is now clearer. The bright feature at positive biases is likely due to a dimer sitting at the centre of the trench, whilst the diagonal observed at negative biases is due to atoms sitting at the up buckled Si positions. In addition, the sawtooth appearance of the nanowire must be due to the internal structure of the nanowire region, and cannot be due to the relative arrangements of the nanowire and the surrounding Si, as has been suggested in the past. The large amount of simulated STM data collected throughout this search could prove useful in the future for identifying other features. New experiments will be vital for progress with simulations at this point, because new ideas are currently exhausted. The most important piece of information that would help future theoretical studies would be exactly how many Mn there are per nanowire unit. With this information future searches can be much more focused.

The final area to which DFT has been applied is speculative research, which could guide future experiments. Simulations can give an idea of whether a structure or procedure is viable without having to do experiments. If it is shown to be unfeasible then it means time and resources will not be wasted trying to achieve it experimentally. The main area this has been applied to is the capture of spin active Bi atoms on the Si(001) surface. Having shown that it is possible to get spin active Bi on the clean Si(001) surface, it became clear that they are too mobile to be of practical use. It was shown that careful depassivation of the H:Si(001) surface can be used to make traps for spin active Bi atoms, but that great care must be taken to achieve this experimentally. In addition this might work as a viable scheme for incorporating Bi atoms at specific positions. The next step is to actually try and implement this scheme experimentally.

Further speculative work has been performed in other areas, such as examining alternative nanolines on the Haiku core, or looking at Bi dimer lines without the Haiku core. These have both revealed interesting effects, even if there is currently no experimental counterpart. The general pattern of behaviour of the Bi nanoline is not just restricted to Bi atoms, but can extend to other Group V atoms. Work with the Bi dimer lines without the Haiku core revealed that the phase shift of neighbouring Si dimers at lower positive biases is not due to a subsurface reconstruction, as previously suspected, but simply due to the presence of a chain of adsorbates. This proved a useful result for the study of the Mn nanowire.

In all of these areas there is still more work to be done, either via experiments or simulations. The Bi/H:Si(001) system is the closest to completion at the moment and would be best served by trying to implement the scheme detailed here experimentally. The details of the electronic structure of the Bi nanoline is pretty much solved, barring the fact that it would be good to have low negative bias results to directly compare to simulations. However, the indentity of the feature still needs to be found, and experiments will need to lead the way. The most useful experiments to try would be adsorbing specific atoms or molecules to the Bi nanoline. This could assess the reliability of current simulations and investigate whether or not the ringing effect is real. It also might succeed where simulations failed, and produce results which match to earlier experiments. In regards to

the Mn nanowire, the most important detail to know is how much Mn there is per nanowire unit. If it is possible to deduce this from further experiments, then it means future theoretical searches can be more focused, and that AIRSS methods might be more useful.

Investigating the termination of the Bi nanolines could provide an interesting new area of research. The reasons for doing this would be twofold. Firstly, to find out what the ends of the Bi nanoline look like in low bias STM images. Based on the simulations provided here it would be expected that both Bi at the end would be bright, regardless of the Si arrangements, due to the exposed Si in the path of the nanoline. Secondly, the structure of the Si at the nanoline ends is unclear. It is unknown whether there is a sharp divide between the Haiku and regular Si at the point where the Bi stops, or if the Si changes back gradually via intermediate structures. Simulations could be used to address both problems, but the size of simulation cells required might make this prohibitively expensive with VASP.

Appendix A

Building an atomic scale switch

On the clean Si(001) surface both the M and U Bi adatom structures are observed, the former being more energetically favourable. One of the most striking differences between these is the fact that the M site does not have spin on the Bi adatom, whilst the U site does. Another noticeable difference is the distance between the Bi atom and the subsurface Si below it. For the M site this distance is 2.77 Å, whilst for the U site this is 3.26 Å. If it was possible to control this turning on and off of spin, then an atomic scale switch could be built. Unfortunately, on the clean Si(001) surface this switching would be too fast to be useable, and also runs into the problem of the Bi diffusing onto other parts of the surface. However on the H:Si(001) surface only the U site with spin on the Bi was observed, with a distance of 3.35 Å from the subsurface Si. The M site has not thus far been observed, which could be due to the presence of nearby H. If this is the reason for the lack of the M site, it should be possible to remove nearby H atoms and allow the formation of the M site again. This would allow for the turning on and off of spin, by removing or adding H atoms at specific positions, thus making an atomic switch. To address this idea, the removal of one or two H atoms from the positions labelled in Figure A.1 has been investigated. Removal of larger amounts of H could lead to the diffusion of Bi through the larger depassivated region, which is undesirable. Even the removal of two H from the positions labelled 5 could introduce this problem.

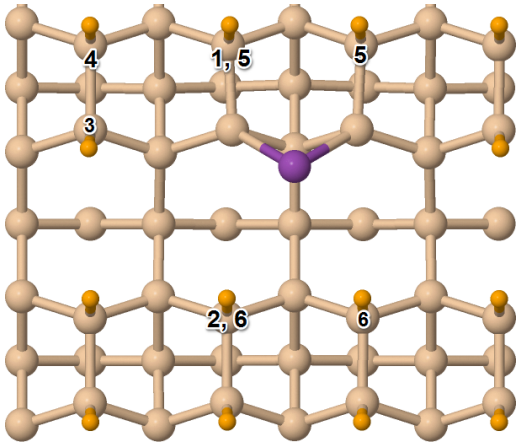

Figure A.1: Locations of the removed H from nearby a U site Bi adatom on the H:Si(001) surface. Where the same number is used in two locations this indicates the removal of two H at once.

A.1 Removal of a single H atom

To determine why the M site was no longer observed, single H atoms from around the Bi adatom were removed from positions 1 to 4 as labelled in Figure A.1. This was to determine whether the presence of nearby H, prevented the formation of the M site. In addition to simply removing the H atom and relaxing the structure the effect of different spin configurations was investigated, the results of which are presented in Table A.1.

Table A.1: Energy and structural differences between different spin configurations for structures on the H:Si(001) surface where a single H has been removed from near the U site. Locations of removed H are labelled as in Figure A.1. ΔE is the energy of the structure, relative to highest energy configuration studied, in this case, an H atom removed from position 1, and no spins on either the Bi or the revealed Si. Bi-Si$_{sub}$ is the distance between the Bi atom and the Si atom directly beneath it. Arrows indicate spin direction.

Location of removed H	Spin arrangement	ΔE (eV)	Bi-Si$_{sub}$ (Å)
1	Si - Bi -	0	3.35
1	Si ↑ Bi ↓	-0.215	2.96
1	Si ↑ Bi ↓	-0.250	3.30
1	Si ↑ Bi ↑	-0.251	3.31
1	Si ↓ Bi -	-0.152	3.11
2	Si ↑ Bi ↓	-0.265	3.29
2	Si ↑ Bi ↑	-0.258	3.28
2	Si ↓ Bi -	-0.156	3.16
3	Si ↑ Bi ↓	-0.269	3.28
3	Si ↑ Bi ↑	-0.260	3.30
3	Si ↓ Bi -	-0.160	3.17
4	Si ↑ Bi ↓	-0.257	3.35

Removing an H from position 4 has no effect on the Bi adatoms. This shows that only those H atoms which directly neighbour the depassivated region have an influence on the Bi adatom. The removal of an H from position 1, on the other hand, allows the Bi to move to different heights, whilst still retaining its spin. Unlike on the clean surface the lower the Bi is, the higher the energy of the structure. Since only position 1 has structures with these height differences it suggests that the H atoms on the ends of the dimers opposite the Bi adatom contribute to the lack of an M site.

Another difference to note with structure 1 is that it is the only structure where a full Si dimer has been depassivated, meaning it is possible for the Si dimer to buckle. How this buckling angle varies with spin arrangement is shown in Table A.2, also included is the effect of charging the structure by introducing an additional electron. The relative orientation of the spins on the Bi and Si has no effect on the buckling angle of the Si dimer, which remains practically flat. If there is no spin on either the Bi or the Si, then the dimer buckles upwards by nearly 9 $^\circ$ in the direction of the Bi atom. However, this might not be a physical system, because there should be an unpaired electron on both the Bi and the Si, unless electron transfer has happened. If the structure is charged,

the buckling angle is reversed, with the Si that is not bonded to the Bi buckling upwards by about 8 °, due to the Si dangling bond.

Table A.2: Buckling angles for the revealed Si dimer for structure 1 from Figure A.1. A positive buckling angle indicates that the Si bonded the the Bi was buckled up. A negative buckling indicates that the Si not bonded to the Bi atom was buckled up. Arrows indicate spin direction. For the charged structure an extra electron was added to the system.

Spin arrangement	Buckling angle (°)
Si - Bi -	8.6
Si ↑ Bi ↓	1.4
Si ↑ Bi ↑	1.5
Charged	-8.4

Since both the Bi and newly revealed Si atom will have unpaired electrons, it is no surprise that configurations with spin on both are more energetically favourable than those without. Whether these spins are aligned or anti-aligned can also influence both the energetics of the system, and the physical height of the Bi adatom. For position 1 aligned spins is more energetically favourable than anti-aligned, but only by 1 meV. By comparison, for both position 2 and 3 the anti-aligned configuration is more energetically favourable, but even here the differences only just approach 0.01 eV. With such small energy differences it is difficult to make firm statements about the interaction between the Bi and Si spins.

A.2 Removal of two H atoms

The removal of additional H atoms reveals more dangling bonds on the Si atoms not directly bonded to the Bi atom, potentially allowing it to switch from the U configuration to the M. Removal of H atoms from positions 5 and 6 in Figure A.1 is one way to achieve this. The former results in a small clean region, whilst the latter tests whether the H across the trench from the Bi are preventing the formation of the M site. As before the spin configurations were varied, the results of which are presented in Table A.3.

As expected structures with spins on both of the Si and the Bi are the most energetically favourable, since the structure has three unpaired electrons. The only situation where this is not the case is when the revealed Si are buckled, because this causes charge transfer between the Si, resulting in only a single unpaired electron, that of the Bi.

Alternating the spin on the Bi compared to the Si only results in a minor change in the energy, of about 0.01 eV, whereas alternating the spins on the Si causes larger changes of up to 0.08 eV. This energy change for the different Si spin arrangements is the same whether or not the Bi has spin. This shows that there is little interaction between the spins on the Bi and the Si atoms, in comparison to the interaction between the spins on just the neighbouring Si.

The Bi adatom was expected to move closer to the Si surface once H had been removed from position 5, however this was not the case. The flatness of the Si dimers compared to the clean surface, as shown in Table A.4, is one possible cause. On the clean surface the Si dimers are still

Table A.3: Energy and structural differences between different spin configurations for structures on the H:Si(001) surface where two H have been removed from near the U site. Locations of removed H are labelled as in Figure A.1. ΔE is the energy of the structure, relative to highest energy configuration studied, in this case, an two H atoms removed from position 6, and no spins on either the Bi or the revealed Si. Bi-Si_{sub} is the distance between the Bi atom and the Si atom directly beneath it. Arrows indicate spin direction.

Location of removed H	Spin arrangement	ΔE (eV)	Bi-Si_{sub} (Å)
6	Si - Si - Bi -	0	3.11
5	Si ↑ Si ↑ Bi -	-0.006	3.11
5	Si ↑ Si ↑ Bi ↓	-0.102	3.15
5	Si ↑ Si ↓ Bi ↓	-0.136	3.22
5	Si ↑ Si ↑ Bi ↑	-0.098	3.33
6	Si ↑ Si ↑ Bi -	-0.004	3.18
6	Si ↑ Si ↑ Bi ↓	-0.116	3.29
6	Si ↑ Si ↓ Bi -	-0.087	3.15
6	Si ↑ Si ↓ Bi ↑	-0.185	3.25
6	Si - Si - Bi ↓	-0.084	3.22
6	Si ↑ Si ↑ Bi ↑	-0.102	3.27
6 buckled	Si - Si - Bi ↓	-0.126	3.26

buckled like the rest of the dimer row, whereas in the depassivated region all of the Si dimers are still approximately flat. It might be possible to introduce buckling into the latter model, but at this time it has not been attempted.

Table A.4: Buckling angles for the revealed Si dimers for structure 5 from Figure A.1, compared to the U structure on the clean Si(001) surface. Left and Right indicates the position of the Si dimer relative to the Bi atom as shown in the same Figure. A positive buckling angle indicates that the Si bonded the the Bi was buckled up. A negative buckling indicates that the Si not bonded to the Bi was buckled up.

Surface	Dimer position	Buckling angle (°)
Clean Si(001)	Left	11.4
	Right	-8.5
Depassivated region of H:Si(001)	Left	1.2
	Right	1.2

Another possibility is that the H at position 6 are also restricting the movement of the Bi. However the removal of the H from position 6 on their own also does not allow for the formation of the M site. Removal of four H atoms, from both the 5 and 6 positions, could allow for the M site. This is a large amount of H to be removing and adding back each time the switch is turned on or off, making it impractical in reality. This is without even addressing the concerns over Bi diffusion raised by extending the depassivated region.

A.3 Conclusions

These results show that this method cannot be used to turn the spin on the Bi atom on and off, at least not without reintroducing the problem of rapid Bi diffusion. Removal of large numbers of H atoms would not only allow the Bi to adsorb at the M site, but also all the other adatom sites within the depassivated region. This undoes all the effort taken to make the adatom stable and immobile in the first place. The interactions between Bi and Si spins within the system could be an interesting area for future research.

Appendix B

Overlapping p-orbitals

B.1 Calculating eigenvalues

The determinant from eq. 7.3 is solved in the following way.

$$
\begin{aligned}
\begin{vmatrix} -\lambda & h_1 & 0 & h_2 \\ h_1 & -\lambda & h_2 & 0 \\ 0 & h_2 & -\lambda & h_1 \\ h_2 & 0 & h_1 & -\lambda \end{vmatrix} &= -\lambda \begin{vmatrix} -\lambda & h_2 & 0 \\ h_2 & -\lambda & h_1 \\ 0 & h_1 & -\lambda \end{vmatrix} - h_1 \begin{vmatrix} h_1 & h_2 & 0 \\ 0 & -\lambda & h_1 \\ h_2 & h_1 & -\lambda \end{vmatrix} + 0 - h_2 \begin{vmatrix} h_1 & -\lambda & h_2 \\ 0 & h_2 & -\lambda \\ h_2 & 0 & h_1 \end{vmatrix} \\
&= +\lambda^2 \begin{vmatrix} -\lambda & h_1 \\ h_1 & -\lambda \end{vmatrix} + \lambda h_2 \begin{vmatrix} h_2 & h_1 \\ 0 & -\lambda \end{vmatrix} + 0 \\
&\quad - h_1^2 \begin{vmatrix} -\lambda & h_1 \\ h_1 & -\lambda \end{vmatrix} + h_1 h_2 \begin{vmatrix} 0 & h_1 \\ h_2 & -\lambda \end{vmatrix} + 0 \\
&\quad - h_2 h_1 \begin{vmatrix} h_2 & -\lambda \\ 0 & h_1 \end{vmatrix} - h_2 \lambda \begin{vmatrix} 0 & -\lambda \\ h_2 & h_1 \end{vmatrix} - h_2^2 \begin{vmatrix} 0 & h_2 \\ h_2 & 0 \end{vmatrix} \\
&= \lambda^2(\lambda^2 - h_1^2) + \lambda h_2(-\lambda h_2) - h_1^2(\lambda^2 - h_1^2) + h_1 h_2(-h_1 h_2) \\
&\quad - h_1 h_2(h_2 h_1) - h_2 \lambda(\lambda h_2) - h_2^2(-h_2^2) \\
&= \lambda^4 - 2(h_1^2 + h_2^2)\lambda^2 + h_1^4 + h_2^4 - 2h_1^2 h_2^2 = 0
\end{aligned}
\tag{B.1}
$$

In order to simplify the final result, let $x = \lambda^2, y = h_1^2$ and $z = h_2^2$ such that

$$x^2 - 2x(y + z) + y^2 + z^2 - 2yz = 0. \tag{B.2}$$

This quadratic equation can then be solved for x to find

$$x = y + z \pm \sqrt{yz}. \tag{B.3}$$

This can then be converted back to an equation in terms of λ

$$\lambda = \pm\sqrt{h_1^2 + h_2^2 \pm 2h_1 h_2}, \tag{B.4}$$

which has 4 possible solutions as specified in eq. 7.4.

B.2 Calculating eigenvectors

The eigenvectors of eq. 7.5 are found in the following way.

First eq. 7.5 can be rewritten as four separate equations

$$\begin{aligned} h_1 b + h_2 d &= \lambda a \\ h_1 a + h_2 c &= \lambda b \\ h_2 b + h_1 d &= \lambda c \\ h_2 a + h_1 c &= \lambda d \end{aligned} \tag{B.5}$$

These can be rewritten to give a and c in terms of b and d

$$\begin{aligned} a &= \frac{h_1 b + h_2 d}{\lambda} \\ c &= \frac{h_2 b + h_1 d}{\lambda}. \end{aligned} \tag{B.6}$$

This can then be inserted into the second part of eq. B.5 to give b in terms of d

$$b = \frac{2 h_1 h_2 d}{\lambda^2 - h_1^2 - h_2^2}. \tag{B.7}$$

By assuming $d = 1$, and inserting the four values for λ from eq. 7.4 into eq. B.7, it is possible to calculate b. These results can then be inserted back into eq. B.6 to obtain a and c and thus the full eigenvector. The full solutions are shown in equations 7.6, 7.7, 7.8 and 7.9.

Appendix C

Burying the Bi nanoline

Burying the Bi nanolines in a layer of epitaxial Si would allow them to be used for nanoelectronic applications, however the structure of the lines post-burying is unclear. Unlike on the surface, it is not possible to observe the buried lines directly, and their structure must be deduced from other measurements, such as X-ray scattering [51]. Based on prior results it has been suggested that the 1D character and Bi dimerisation of the nanoline is maintained upon burying, with the Bi bonding to the Si overlayer, leaving a vacancy in which the Haiku core can reconstruct to regular bulk Si.

New experimental results from Koichi Murata suggest that the coordination number for the Bi in an embedded nanoline could be either two or three, but it is not clear whether this number includes Bi-Bi bonds or just the Bi-Si bonds. Results also suggest that the Bi dimers of the nanoline are maintained. The embedded structure has two Bi-Si bonds in the crystal plane that are 2.67 Å in length, in addition to another vertical to the crystal plane of 2.61 Å.

To aid in characterising the structure of buried Bi nanolines I have investigated Bi defects in bulk Si. This work covers single and double Bi defects in addition to Si vacancy defects. The former two can be related directly to the buried Bi nanolines, whilst the latter allows energy comparisons to be made between the different Bi defect structures. Details from these simulations, such as Bi-Si bond lengths and Bi coordination, can then be compared to the new experimental results.

C.1 Results and Discussion

Four different single Bi defect structures were studied, as shown in Figure C.1, with the coordination numbers and bond lengths for each structure presented in Table C.1.

Table C.1: Coordination number and bond lengths for a variety of single Bi defects in bulk Si. Structures are labelled as in Figure C.1.

Structure	Bi coordination number	Bi-Si bond lengths (Å)
a)	4	2.65
b)	3	2.78
c)	6	2.97
d)	4	2.93, 3.18

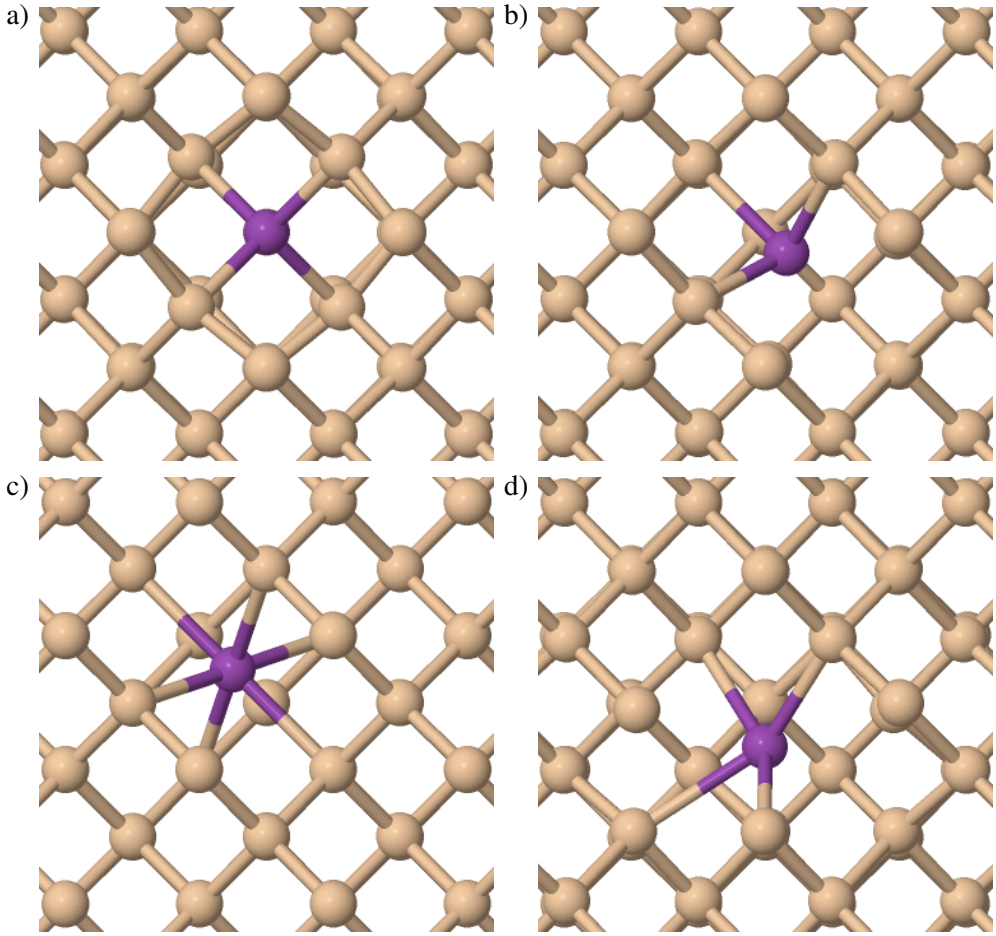

Figure C.1: Structural models for a Bi atom in bulk Si with different numbers of Si vacancies. a) Bi defect at a lattice site. b) Bi defect at a lattice site and one Si vacancy. c) Bi defect between two lattice sites and one additional Si vacancy. d) Bi defect at a lattice site and two Si vacancies.

These results show that as the number of vacancies around the Bi increases, so too does the Bi-Si bond length. This is because there is more free space for the Bi atom to move into, reducing the strain on the system. The coordination numbers for these structures are mostly as would be expected. At a regular lattice site the Bi will be four coordinate, so the removal of Si from around it should reduce this accordingly. The reason why the two vacancy structure is four, rather than two, coordinate is because the Bi can move into the extra space created by the vacancies, and form weak bonds to Si which would normally be inaccessible. For the Bi which sits between two lattice sites, which are both empty, the Bi is six coordinate because it bonds to all six of the remaining Si from around those lattice sites.

It can also be instructive to compare the relative stabilities of these structures, since this could help determine which are more likely to form. A direct comparison of the energies of these structures is not possible, because the simulation cells contain different numbers of atoms. Instead the following quantity can be calculated:

$$\Delta E = E_{Si+V} + E_{Bi} - E_{Si+Bi} \tag{C.1}$$

where E_{Si+V} is the energy of bulk Si with the appropriate number of vacancies, E_{Bi} is the energy of a single Bi atom and E_{Si+Bi} is the energy of one of the Bi defect structures. These

results are presented in Table C.2.

Table C.2: Energies of Bi defect structures relative to Bulk Si with vacancies and atomic Bi. Structures are labelled as in Figure C.1.

Structure	ΔE(eV)
a)	-4.611
b)	-4.630
c)	-4.600
d)	-4.169

Comparing the energies of the different single Bi defect structures shows only a small difference in stability. The structures with one or fewer additional Si vacancies only vary over a range 0.03 eV, meaning that there is practically no difference in their relative stabilities. The only case where there is a significant difference is for the structure with a double Si vacancy, which is almost 0.5 eV worse in energy than any of the other structures. This might be because even though the Bi atom has more space to move into, thus relieving strain, the Bi bonds to fewer Si atoms counterbalancing this effect.

Structures containing two Bi defects, such as those shown in Figure C.2, were also studied, with the distances between neighbouring Bi varied from nearest to next next nearest neighbour sites. Due to the size of the cells, this is approaching the limit of how far the Bi atoms can be moved away from one another.

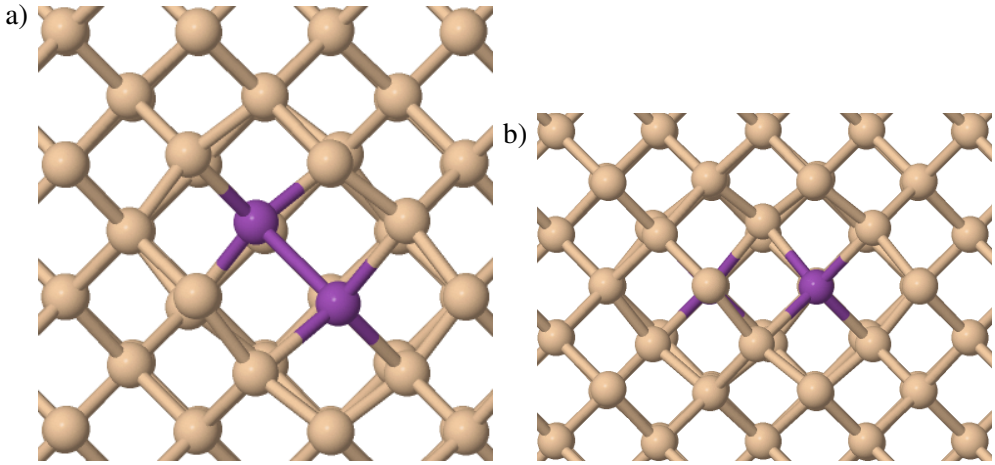

Figure C.2: Structural models for two Bi atoms in bulk Si at different distances from each other. a) Two Bi at nearest neighbour sites (N). b) Two Bi at next nearest neighbour sites (NN). Two Bi at next next nearest neighbour sites (NNN) are not shown because both Bi cannot be viewed clearly at the same time.

The coordination number and bond lengths for these structures are presented in Table C.3. There is little difference between the Bi-Si bond lengths observed here compared to that for a single Bi defect with no additional Si vacancies. Regardless of the distances between the Bi atoms the Bi-Si bond lengths only vary by 0.02 Å at most. This would be expected given that there is no additional space for the Bi atoms to move into.

Table C.3: Coordination number and bond lengths for a variety of double Bi defects in bulk Si. N, NN and NNN refer to the relative positions of the Bi atoms, specifically Nearest, Next Nearest and Next Next Nearest neighbour atoms.

Structure	Bi coordination number	Bi-Bi bond length (Å)	Bi-Si bond lengths (Å)
N	4	2.94	2.65
NN	4	NA	2.65, 2.67
NNN	4	NA	2.66

The energies of these structures can be compared directly because they contain the same number of atoms, just rearranged slightly, and are presented in Table C.4.

Table C.4: Relative energies of the double Bi defect structures compared to the lowest energy structure, where the Bi are at next next nearest neighbour positions.

Structure	ΔE(eV)
N	+0.044
NN	+0.107
NNN	0

There is relatively little energetic difference between the 3 studied structures, with only a 0.1 eV difference at most. With these three data points it is not possible to tell if there are any general trends in stability, since there does not appear to be a simple relationship between Bi distance and energy. The increase in energy going from N to NN might have something to do with the fact a Bi-Bi bond is no longer present. Increasing the separation further to properly test the energy dependence would need larger cells, and would fall outside of the realms of this work. This is because for an embedded Bi nanoline the Bi atoms should still be close to each other.

These simulated results can now be compared to the latest experimental results. The Bi-Si bond lengths in the crystal plane of 2.67 Å closely match those for a single Bi defect at a lattice site without any nearby vacancies, and the double defect structures, with at most a 0.02 Å difference. This suggests that the Bi atom is likely to be sitting at a lattice site after embedding. The shorter 2.61 Å length is unexpected, because this is shorter than all the Bi-Si lengths from simulation, suggesting part of the structure is more close packed than just neighbouring lattice sites. The previously suggested model for embedded nanolines involved the Bi bonding to the Si overlay, leaving vacancies between the Bi and what used to be the Si surface. If this structure were true, longer Bi-Si lengths would be expected than those recorded in experiment, due to the propensity of Bi to move into vacancies. The coordination number of two or three suggested by experiment is unusual given the bond lengths. A higher number would be expected given the bond lengths, otherwise the Bi and Si would not be so closely packed. If this number is only considering Bi-Si bonds, the the presence of Bi-Bi bonds could restore the expected coordination number of four.

C.2 Conclusions

The structure of the embedded Bi nanoline is likely related to lattice site Bi defects, although it is unclear what specific modification takes place. It is unlikely that there are any surrounding vacancies, otherwise longer bond lengths would be recorded. The shortest experimental bond length suggests the Bi might even be more tightly packed than in regular bulk Si. Previously it was suggested that the Haiku core would not survive the embedding process, because this reconstruction is energetically unfavourable in bulk Si. However, some of the Si-Si bond lengths in the Haiku are slightly shorter than in bulk Si, so I believe there is a possibility that some of it might survive the embedding process.

Simple defect models cannot reproduce the experimental results for the embedded Bi nanoline, meaning a more complex structure must be present. To determine what the true structure is would require further modelling, which could become quite complex, especially considering the potential presence of the Haiku core. I do not believe that the previously suggested model could be correct in light of these results.

Appendix D

Haiku Stripe

By use of a dedicated H cracker [44, 52, 53] it is possible to remove the Bi nanoline from the Si(001) surface without disrupting the underlying Haiku reconstruction, resulting in what is known as a Haiku stripe. As well as providing direct evidence for the Haiku reconstruction and a template for future nanolines, it also allows for the study of surface Si arrangements which are not possible on the regular Si (001) surface. The Haiku stripe consists of Si dimers which are oriented perpendicular to the rest of the surface Si dimers, and can display several different surface arrangements. As well as buckling like the regular surface dimers they are also stable as flat dimers, and may even display entire dimers which alternate in height [53]. Neither of these are observed for the regular Si(001) surface. This work aims to address under what conditions the alternating height Si dimers, as shown in Figure D.1, can occur.

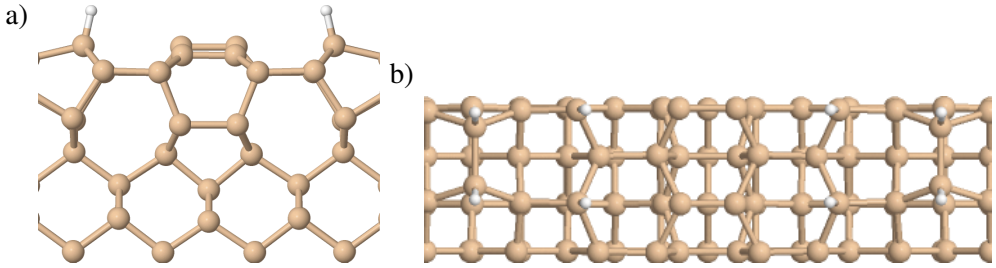

Figure D.1: Structural model of the Haiku stripe. a) Side view showing the slight height differences between flat Si dimers. b) Top view showing the H passivation of other surface Si, and the orientation of the Haiku stripe dimers relative to the Si dimer row. The Haiku stripe runs from the top to bottom of b).

D.1 Results and Discussion

The energies and height differences between the central dimers for several different spin arrangements of the Haiku stripe are presented in Table D.1. Any attempts to fix the individual spins of the four dimer Si to specific values all relaxed to the no overall spin structure.

There are two noticeable results to take away from this. Firstly the fact that the energy of the structure increases with each step up in overall spin. Given that the structure could have 4 Si dangling bonds, it might be expected that the structure with +2 overall spin would be lower in

Table D.1: Relative energies for different spin arrangements of the Haiku stripe and accompanying dimer arrangement

Overall spin	Relative energies (eV)	Dimer height difference (Å)
0	0.00	0.01
+1/2	+0.22	0.03
+1	+0.38	0.35
+3/2	+0.92	0.05
+2	+1.30	0.00

energy, rather than being the overall highest. Instead the lowest energy structure has no overall spin, and displays no actual spin on any of the four Si atoms. Instead of having the dangling bonds that would normally be expected for flat Si dimers, there appears to be a charge transfer between the dimer ends, getting rid of the dangling bonds.

Secondly, the only structure where there is a significant height difference between the two dimers is observed when the overall spin of the system is +1. The spin distribution on this structure is also slightly unusual. Instead of, for example, the spin being split across the two higher Si dangling bonds, it is instead distributed amongst all four Si, with a greater amount on the higher Si, as shown in Figure D.2.

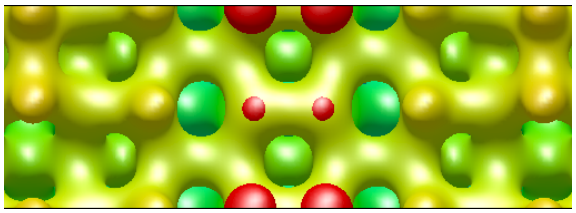

Figure D.2: Spin density difference and charge density for the Haiku stripe with an overall spin of +1. Red indicates spin up, and other colours charge density coloured by height.

Further tests to determine the effect of k-point choice on the final structure were also performed, this time restricted to the no spin and +1 spin structures as shown in Table D.2.

Table D.2: Energy difference between Haiku stripe with no overall spin and +1 spin (Δ E) for a variety of k-point meshes.

K-point sampling	Δ E (eV)
2×1×1	+0.376
4×1×1	+0.439
6×1×1	+0.442
8×1×1	+0.443
10×1×1	+0.443

This shows that the earlier choice of a 2×1×1 k-points is not enough to converge energy differences to within 0.01 eV. However beyond a 4×1×1 mesh only meV energy differences are observed, with a 10×1×1 mesh offering no real advantages over a 8×1×1 mesh, for the level

of accuracy used here. Increasing the density of k-points makes the no spin structure even more energetically favourable than the +1 structure.

For the structure with alternating Si dimer heights, despite the energy differences between the $2\times1\times1$ and $10\times1\times1$ results, there is little physical difference in structure, with the height difference between Si dimers staying at 0.35 Å throughout. This suggests a $2\times1\times1$ mesh might be sufficient for reasonable simulated STM images, such as those presented in Figure D.3.

The height difference between Si dimers is evident by the brightness contrast, with the higher Si dimer appearing brighter than the lower Si dimer. This contrast is evident over a range of bias voltages, although it is harder to discern at large negative bias voltages.

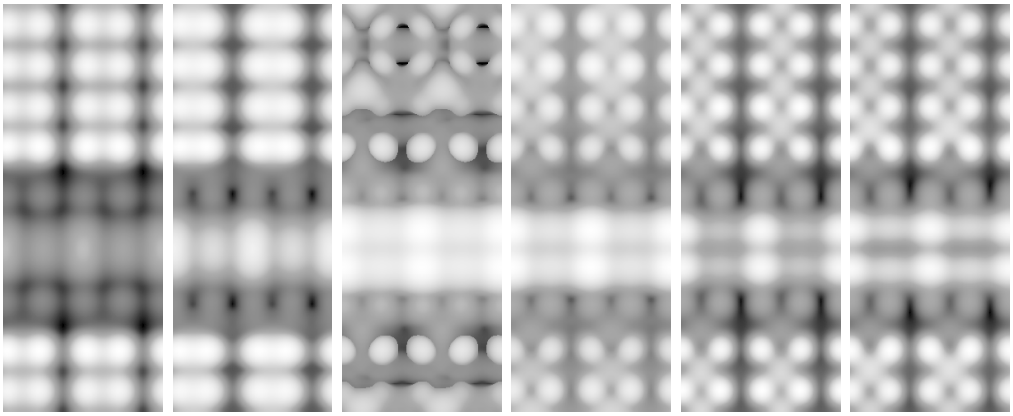

Figure D.3: Simulated STM for the Haiku stripe with Si dimers at alternating heights. Images have been doubled up to make features easier to see. Height differences can be deduced from changes in the extent and brightness of the features on the Haiku stripe. All images are presented at an isosurface value of 0.01 in arbitrary units.

At this point it is instructive to compare these results with experimental results, such as those shown in Figure D.4. The area labelled B is the most relevant, because it is believed to be due to flat Si dimers which alternate in height. There is a good match between theory and experiment, with alternating bright and darker spots.

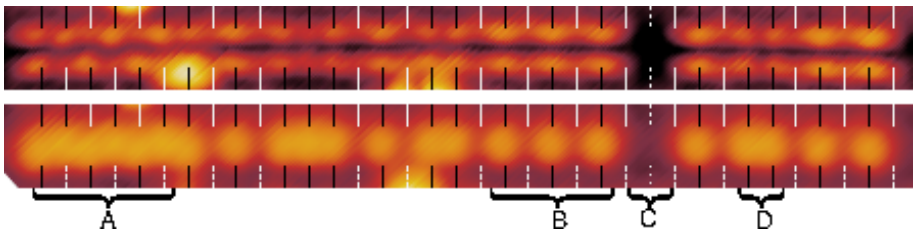

Figure D.4: Experimental STM images of a Haiku stripe where different arrangements of Si dimers are visible. The upper image is at +2.5 V, and the bottom at -2.5 V. The different areas have been labelled as follows: A. Buckled Si dimers. B. Flat dimers alternating in height. C. H passivated dimers. D. Flat dimers. Image reproduced with permission of David Bowler.

D.2 Conclusions

An extensive study of the structure of the Haiku stripe for different spin arrangements has found that in the vast majority of cases flat Si dimers at the same height are preferable compared to dimers of alternating heights. The only case in which a two dimer section can retain an alternating height pattern is when the system has an overall spin of +1. This structure produces a good match to experimental results when STM images are compared.

The global minimum for flat dimers is a structure with no overall spin, which raises the question of why the alternating height structure would ever be observed instead. In addition I do not have an explanation for why the alternating height structure is only seen for one very specific spin configuration. The spin variations investigated here was not exhaustive, meaning that there might still be further ways to produce dimers which alternate in height. Future investigations could try and resolve some of these issues, in addition to finding out whether or not there are any practical applications for this arrangement.

Appendix E

Further Mn structures

This appendix contains details of all remaining Mn structures not covered in detail in Chapter 9. These structures do not necessarily contribute directly to determining the structure of the Mn nanowire, but could prove useful for identifying other Mn structures on the Si(001) surface.

E.1 C chain related structures

Here I present the many extra variations of the C chain model which failed to replicate the experimental results any better than those detailed in Chapter 9. Extensions to the C chain model were explored because of the fact that the basic model reproduced some of the experimental features well, such as the diagonal tilt, or the round feature in the middle of trench. It was hoped that extensions could introduce the sawtooth feature without removing these other features, but these extensions were rarely successful.

E.1.1 C chain and c(4×2) Si

The study of the Mn nanowire has focused on the p(2×2) surface reconstruction, because this is observed in experiment. This does not guarantee that the Si within the nanowire region still maintains this reconstruction, because it is possible for it to rearrange in the presence of Mn atoms. This idea was explored for the C chain model with either the whole of the surface, or just the two dimers directly in the nanowire region changed to the c(4×2) reconstruction. This showed that the arrangement of the Si dimers which are outside of the nanowire region have very little effect on the energy, physical structure or appearance in simulated STM of these structures. For the c(4×2) reconstruction the Si atoms exist in either up or down pairs across the trench, and as a result the Mn atom adsorbs closer to the up pair, as demonstrated in Figure E.1. This means that the position of the Mn atom alternates with each unit of the chain. The resulting structure is the same, regardless of how the other Si dimers are arranged, and the energetics of the system is largely unchanged. E_{ads} per Mn is -1.27 eV for the C chain on the full c(4×2) surface, whilst it is -1.35 eV when only the dimers in the nanowire region are changed. The small difference could be attributed to the mismatch of dimer buckling along the rows which results from only changing those in the nanowire region.

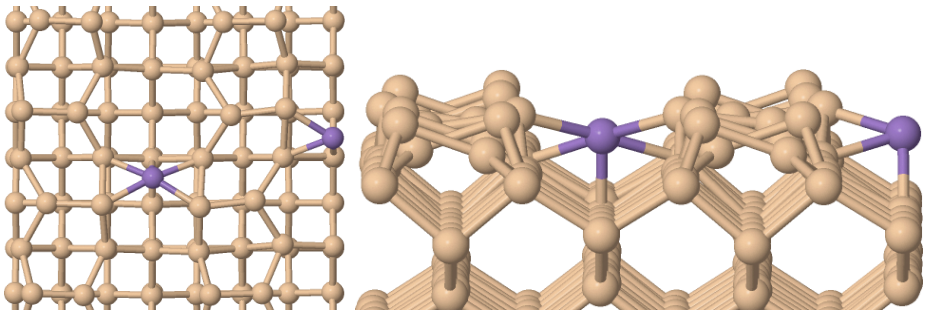

Figure E.1: Structural model for the C chain where the Si dimers either side of the Mn are in the c(4×2) reconstruction. Both the top and side views of the model are shown.

Aside from the changes related to the arrangement of the outer Si dimers, there is little difference between the simulated STM images for the two structures, as shown in Figure E.2. Regardless of bias voltage the Mn atoms themselves are not visible, and can only be found by their influence on the nearby Si atoms. At negative biases these Si appear darker than the rest of the surface. At low positive biases, such as +0.5 V, all of the Si within nanowire region appear brighter than the rest of the surface. As the bias is increased the brightness of the surrounding up and down Si atoms decreases, but the down atoms still remain brighter than those in the rest of the surface. These structures are nothing like the experimental Mn nanowire, due to the fact that the Mn atoms are not visible and that the appearance of the line is not constant from unit to unit.

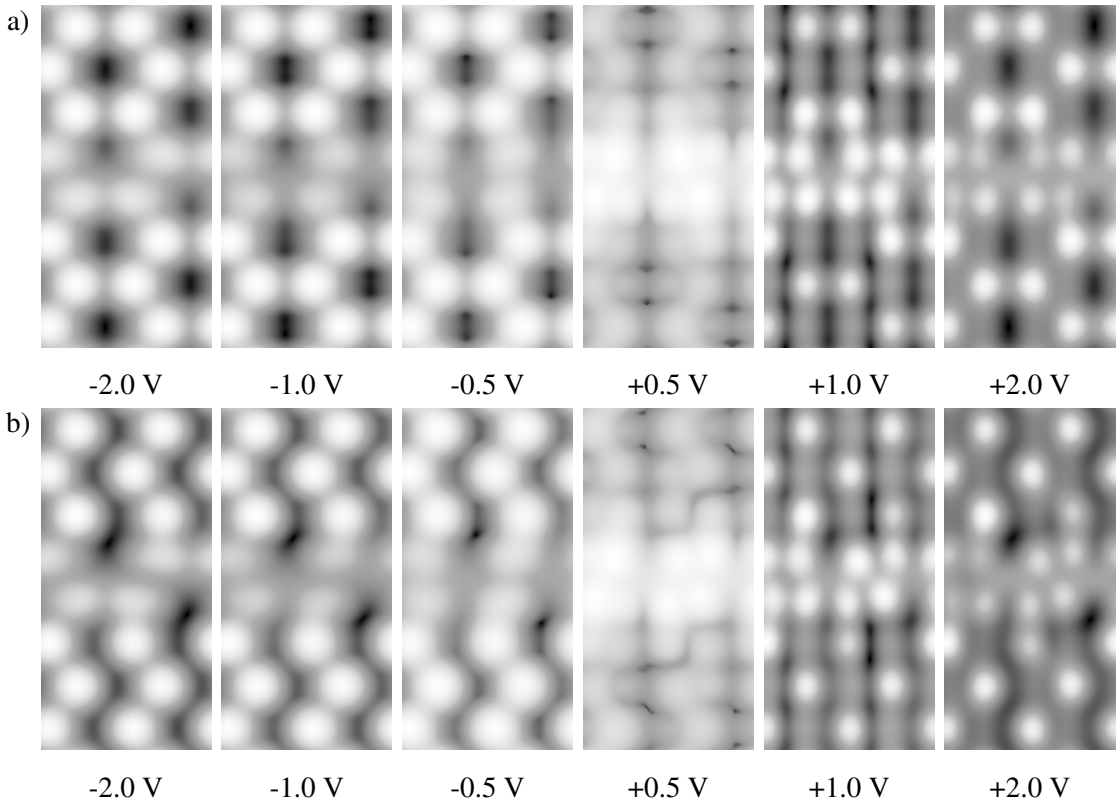

Figure E.2: Simulated STM for the C chain structure where some of the Si has been arranged in the c(4×2) reconstruction. a) Entire surface arranged in the c(4×2) reconstruction. b) Only the dimers directly around the Mn arranged in the c(4×2) reconstruction. All images are presented at an isosurface value of 0.01 in arbitrary units.

E.1.2 C chain and substituted Mn

The idea of substituted Mn atoms was explored due to the realisation that the diagonal appearance of individual units in the Mn nanowire was due to atoms at the up buckled Si positions. They do not necessarily have to be Si atoms and could just as easily be Mn atoms. It had been hoped that substitution on one side of the C chain might cause enough of an asymmetry to create the sawtooth appearance without disrupting the other features. This work covers both substitution on its own and in combination with C site Mn. Studying substitution on its own will provide some idea of the effect it could have on the appearance of the C chains.

To start with, Mn can substitute for either the up or down Si within a Si dimer, which will be referred to as S and dS respectively. Chains of these structures can then be built, either running along a single line of dimers or along two, as shown in Figure E.3. Since these structures were built assuming the complete removal of the substituted Si, their energies cannot be directly compared to the other Mn wire structures. It is possible to compare the S and dS chains directly, which shows the former to be 0.81 eV lower in energy, meaning it is more energetically favourable for the Mn atom to be in the up position. There must be a barrier to the flipping of the buckling of the Mn-Si dimers, because for the dS chains the Mn atoms still remain in the down position. This is probably related to maintaining the buckling pattern along the dimer rows.

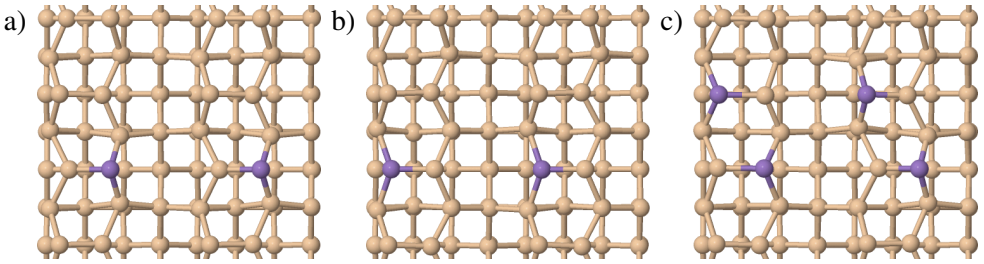

Figure E.3: Structural models for several different substituted Mn chains. a) Mn substituted for up Si along one line of Si dimers, also known as an S chain. b) Mn substituted for down Si along one line of Si dimers, also known as a dS chain. c) Mn substituted for up Si along two lines of Si dimers, also known as a 2S chain.

It is useful to examine the simulated STM for these structures, as shown in Figure E.4, before combining them with the C chain. The S chains on their own cannot replicate the experimental appearance of the Mn nanowire, due to the physical placements of the atoms being wrong. These images can still be used to assess the suitability of combining S and C chains, or for identifying other structures in the future.

At all negative biases the Mn atoms appear darker than the rest of the surface, and for the dS chain this extends to the nearby Si atoms. For the dS chain the Mn atom itself cannot be distinguished, but the effect on nearby Si atoms is clear. The up buckled Si that it bonds to appears much dimmer than the rest of the surface, and the up Si directly adjacent to the Mn atom also appear dimmer, an effect that is most visible at lower biases, such as -0.5 V.

At positive biases the substituted Mn leads to a bright feature in the region of the Mn atom. For the single S chain, the Mn appears as a bright round spot, which is larger and brighter than the surrounding Si atoms. This looks very similar to the experimental Mn nanowire, but in the wrong

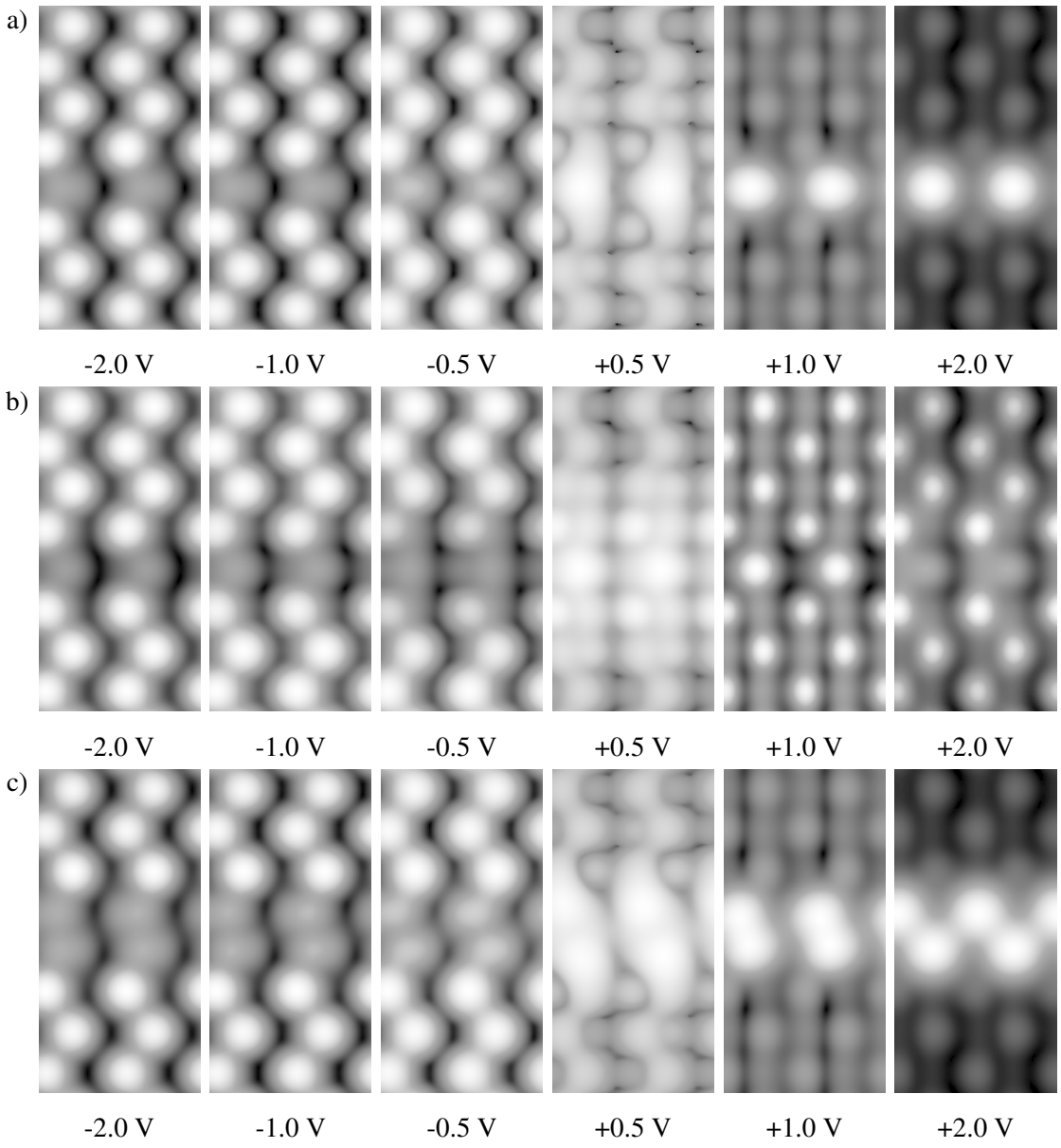

Figure E.4: Simulated STM for Mn substituted into surface Si dimers. a) S chain along one line of Si dimers. b) dS chain along one line of Si dimers. c) 2S chains along two lines of Mn dimers.

position. For the experimental nanowire the bright spots sit in the middle of the trench between the dimer rows, and not on the dimer rows themselves. The same effect is seen for the 2S chain, where the alternating position of the Mn atoms results in a bright zigzag pattern. The dS chain behaves a little differently because the Mn atom itself is not visible, but it does influence the appearance of the Si in the Mn-Si dimer. At lower positive biases it appears brighter than the other Si, but as the bias is increased, for example to +2.0 V, it becomes darker.

These are not promising results as far as combination with the C chain is concerned. To introduce a sawtooth appearance there needs to be a brightness increase at the up atom positions at negative biases, contrary to the results for the S chains on their own. In addition to this the Mn then needs to appear darker than the surrounding Si at positive biases, so as to not influence the appearance of the C site Mn too much. Once again this does not appear to be the case.

Despite these problems, combinations of C and S chains were still attempted, because the

simulated STM images for the combined structures could differ from simply an overlay of their individual appearances. In order to introduce an element of asymmetry and hopefully the saw-tooth appearance, the C+S and C+dS chains were studied, as shown in Figure E.5. Of these two models only the C+S chain could be relaxed fully, so the C+dS chain results are presented for a structure which still has forces of over 1 eV/Å. Given this, it would not be wise to draw too many conclusions from the structural model and the simulated STM for the C+dS chain. It also means that direct comparison of the energies of the two structures cannot be made. For both models the C and S site Mn bond to each other, although this has little effect on their positions. The C site Mn still remains roughly in the middle of the trench, whilst the S site Mn remain in either the up or down position respectively. Other models, such as the C+2S chain, were not studied due to being too symmetric.

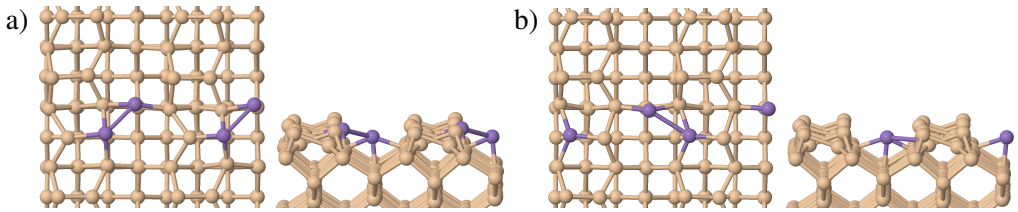

Figure E.5: Structural models for Mn chains including substitutional Mn and adsorbed Mn. a) Top and side views of the C+S chain. b) Top and side views of the C+dS chain.

Simulated STM for these structures, as presented in Figure E.6, show that the effect of the S site Mn is roughly the same in the presence of the C site Mn as on its own. At negative biases the side of the structure with the Mn-Si dimer appears darker than the side without, regardless of whether the Mn atom is in the up or down position. This is reversed at lower positive biases where the Mn-Si dimers appears brighter than the rest of the surface. For the C+S chain there is little to indicate the presence of the C site Mn, with the bright spot centered on the S site Mn, and with a tail like feature at +1.0 V which extends along the Mn-Si heterodimer. At higher biases it is more or less indistinguishable from the S chain on its own. The C+dS chain on the other hand starts off with a bright spot on the up Si of the Mn-Si heterodimer, but shifts to the C site position and extends across to the neighbouring up Si. This is unexpected, since those Si are no different from the rest of the surface Si, and this was not observed for the C chain on its own. Overall, these changes mean that the C+S chains are worse matches to experiment than the C chain alone.

Closer examination of the simulated images for the C+S chain, especially at negative biases, raises concerns about the calculations, because the two halves of the images look different. If the calculations have been performed correctly and the simulation cell set up correctly, then both halves should be the same, since it is meant to be repeated units of a nanowire. Combined with the lack of force convergence on the C+dS model, this suggests that both simulations might not be completely accurate representations of real structures. Given that these models actually made the match to experiment worse, it is not a major concern to try and address these problems.

On top of all the problems related to these specific structures, there is also a general problem with the type of substitution studied here. Since the ejected Si has not been included in the model, this would suggest that it has moved to another part of the surface. The experimental results show

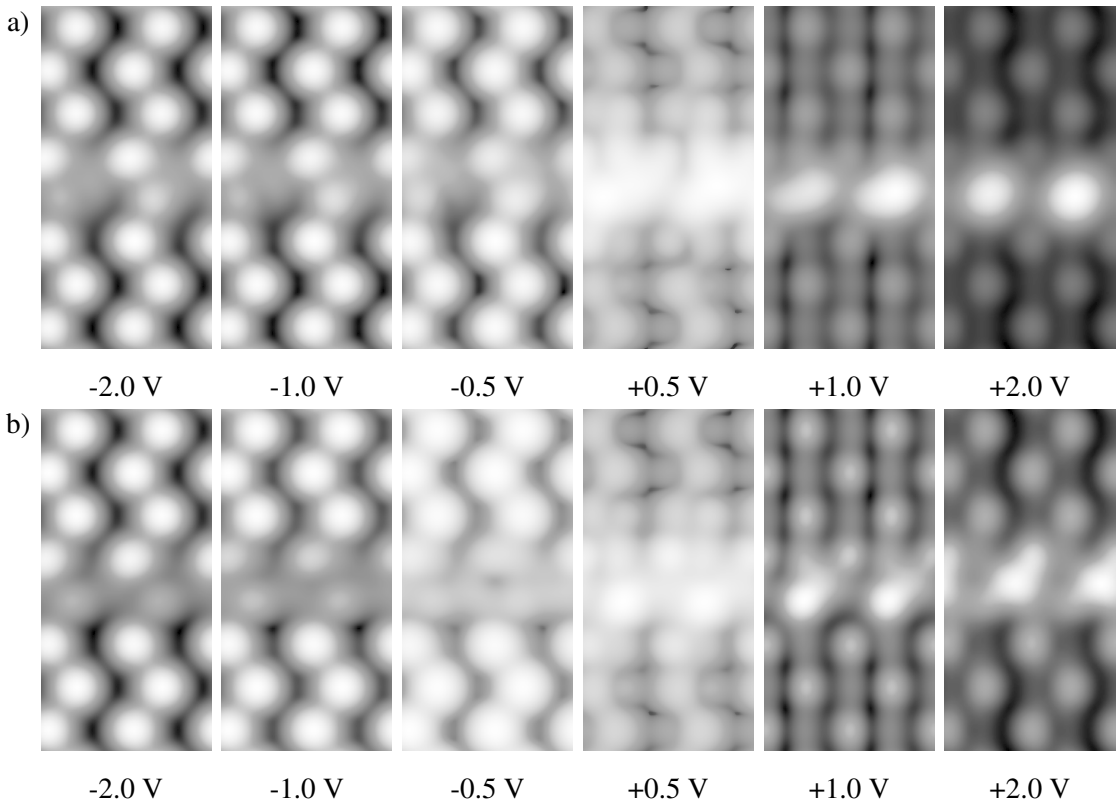

Figure E.6: Simulated STM for Mn chains including substitutional Mn and adsorbed Mn. a) C+S chain. b) C+dS chain.

no sign of an aggregation of ejected Si around the wires, or anywhere else in the surface, meaning this cannot be happening. In order to properly model Mn substitution and relate it to the nanowire structure, simulations would need to consider structures where the Si still remains in the nanowire region. This can lead to complicated structures which have not been considered.

E.1.3 C chain and subsurface Mn

Another extension to the C chain which was explored involved subsurface Mn below the surrounding Si dimers. Even though this would mean that the Mn atoms themselves would not be visible, this is likely to lead to a change in structure of the Si directly above, which would be reflected in the simulated STM. Interstitial subsurface Mn in the third Si layer were considered, in positions known as I_2 and I_3 [122]. I_2 lies below the up atom of a surface Si dimer, whilst I_3 lies below a down atom. Both single and double line structures were considered in conjunction with the C chain, however they all encountered convergence problems, only allowing for preliminary assessments of suitability. None of these structures gave results worth noting.

Another subsurface position considered was the B' site, which lies lower down than the regular B site and instead of being in the middle of the trench lies partway between the middle and one of the surface Si dimers. This results in slightly different structures if the Mn sits closer to a down or up Si atom. These B' sites can then be combined with the C chain as either single or double chains.

The simplest way is to combine either the B' or down B' with the C chain, the former of which is shown in Figure E.7, the latter failed to relax fully. Both of these structures could introduce

asymmetry into the chain, and hopefully a sawtooth appearance. The C+B' chain has an E_{ads} per Mn atom of -1.77 eV, which is barely different from the C chain on its own. The simulated STM for this structure, as presented in Figure E.8, looks nothing like the experimental results. At negative biases there is little difference between the region with or without Mn and the Mn atoms themselves are not visible. The Mn atoms are still not visible at positive biases, with the up Si near the B' Mn appearing brighter than the rest of the surface instead.

Table E.1: Adsorption energies for different combined C and B' chains.

Chain structure	E_{ads}/Mn (eV)
C+B'	-1.77
C+B' down	NA
C+2B'	-2.08
C+2B' down	-2.20
C+B'+B' down	-2.40

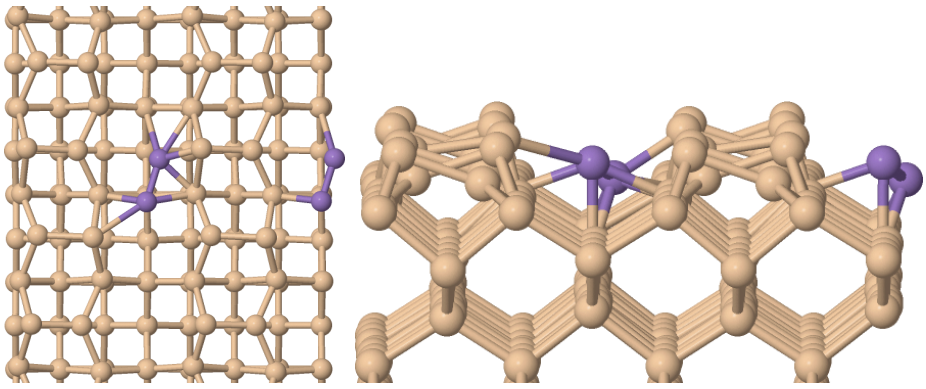

Figure E.7: Structural model of the C+B' chain showing both top and side views.

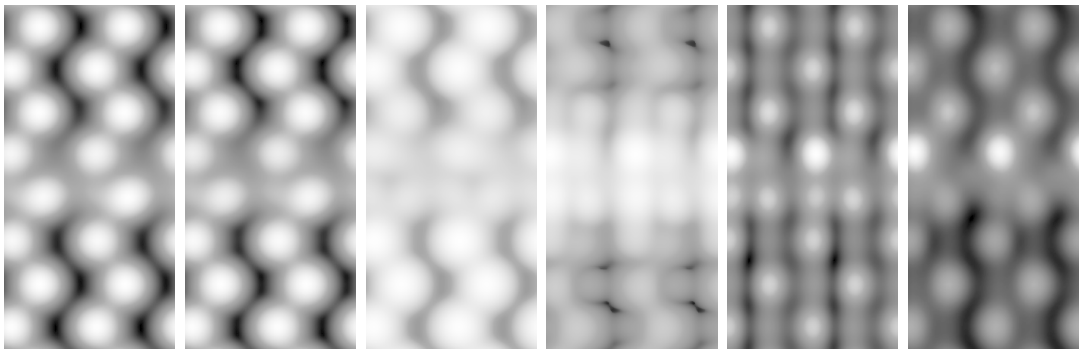

-2.0 V -1.0 V -0.5 V +0.5 V +1.0 V +2.0 V

Figure E.8: Simulated STM for the C+B' chain structure at a variety of bias voltages.

A similar effect is seen for all other structures which include Mn at the B' positions. The C+2B' chain structure, detailed in Figures E.9 and E.10, shows a slight enhancement of the down Si at both positive and negative biases. Apart from this it is hard to tell that there is any Mn present, because the Mn atoms themselves are not visible. The C+2B' down chain, detailed in Figures E.11 and E.12, looks mostly the same as the C chain at negative biases. However at positive biases it

makes the undesirable features of the C chain worse, such as the diagonal in the wrong direction, and causes an on-row diagonal between down Si. Finally, the C+B'+B' down chain, detailed in Figures E.13 and E.14, once again brightened Si atoms as the most noticeable features. At negative biases the Si opposite the Mn appear brighter, whilst at positive biases those next to the Mn do. As before the Mn itself is barely visible. The energies for all of these structures are presented in Table E.1.

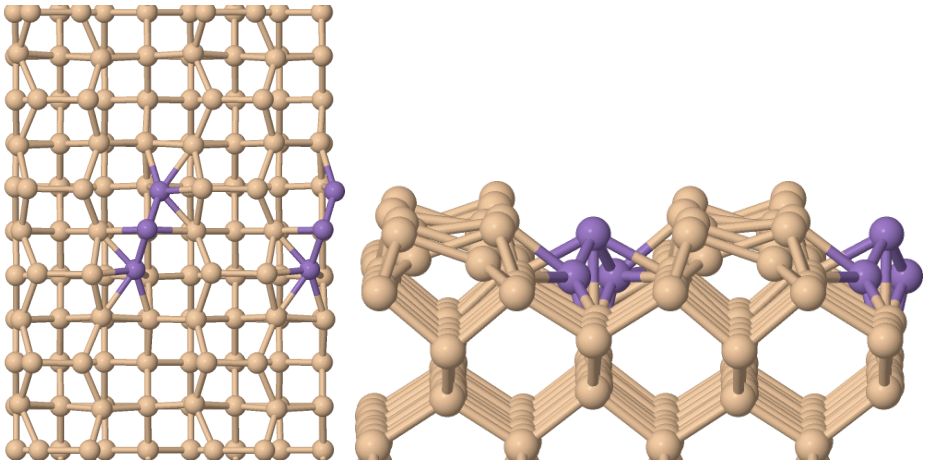

Figure E.9: Structural model of the C+2B' chain showing both top and side views.

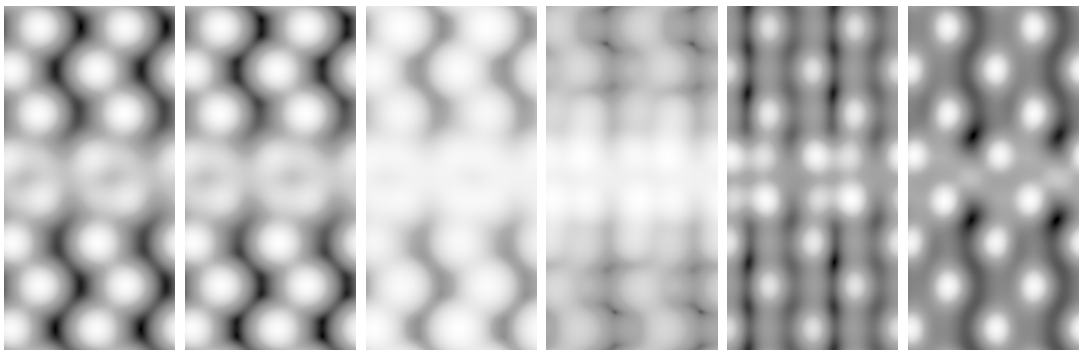

Figure E.10: Simulated STM for the C+2B' chain structure at a variety of bias voltages.

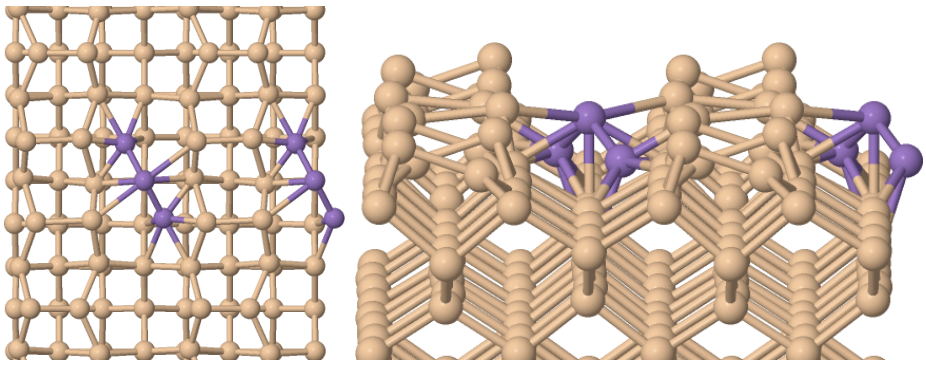

Figure E.11: Structural model of the C+2B' down chain showing both top and side views.

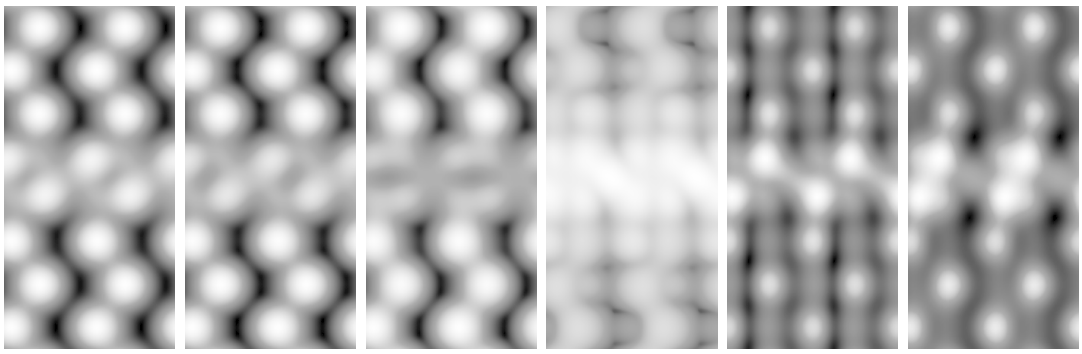

-2.0 V -1.0 V -0.5 V +0.5 V +1.0 V +2.0 V

Figure E.12: Simulated STM for the C+2B' down chain structure at a variety of bias voltages.

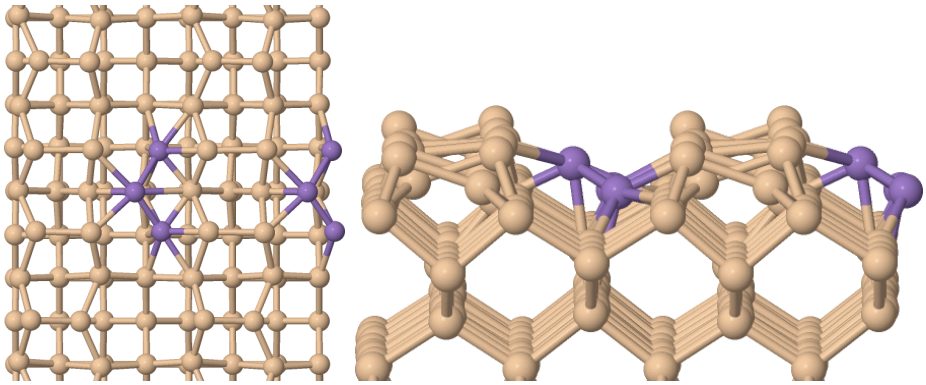

Figure E.13: Structural model of the C+B'+B' down chain showing both top and side views.

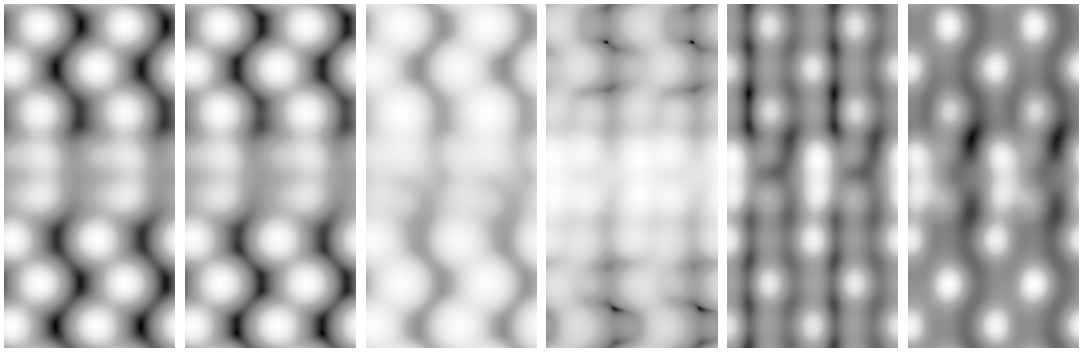

-2.0 V -1.0 V -0.5 V +0.5 V +1.0 V +2.0 V

Figure E.14: Simulated STM for the C+B'+B' down chain structure at a variety of bias voltages.

E.2 Wang variations

In addition to the Wang trimer variant detailed in Chapter 9, several other models were attempted involving the exchange of Si and Mn atoms. Both the up and down buckled Mn can exchange for any of the four surrounding Si atoms, however investigating every single variant of the Wang trimer would be very time consuming, and only those deemed likely to produce positive results were attempted.

Exchanging the down Mn with the up Si on the opposite side of the trench, as shown in Figure E.15, was considered because it is a very similar structure to the one presented in Chapter 9. This could enhance the sawtooth appearance because the new Mn position coincides with the

position of the bumpy features. The resulting simulated STM, as shown in Figure E.16, fails to reproduce the experimental results better than prior models. At negative biases the central feature appears too straight, with no sign of a sawtooth, except possibly at lower values such as -0.5 V. This does not match up to experiment where the sawtooth is still clear at values above -2.0 V. The positive bias images are a fairly good match for experiment, barring the usual problems seen below +1.0 V where the central feature takes on a triangular rather than round shape. This model reinforces the need for a central dimer, but still cannot get the sawtooth right.

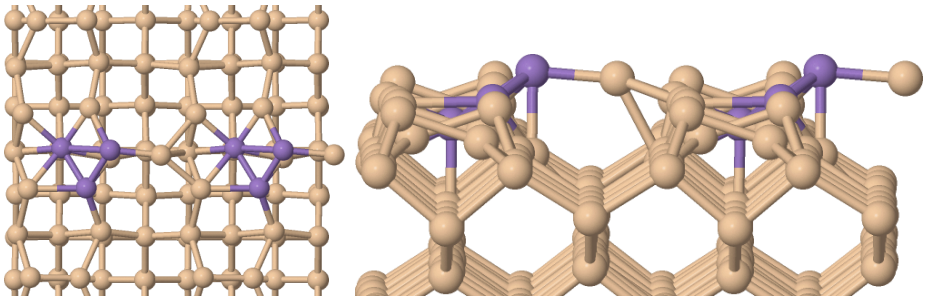

Figure E.15: Structural model of a Wang trimer variant where the down Mn have been exchanged with the up Si from the opposite side of the trench. Both top and side views are shown.

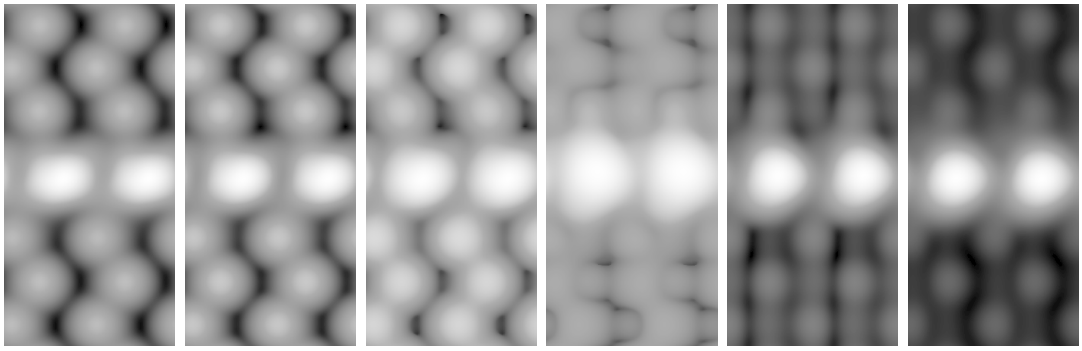

-2.0 V -1.0 V -0.5 V +0.5 V +1.0 V +2.0 V

Figure E.16: Simulated STM for a Wang trimer variant where the down Mn have been exchanged with the up Si from the opposite side of the trench.

Several structures involving the exchange of the up buckled Mn for nearby Si were also considered, as shown in Figures E.17, E.19, and E.21. These structures exchanged the Mn with the up Si on the opposite side of the trench, the adjacent down Si, and the adjacent up Si respectively. Simulated STM for all three structures are presented in Figures E.18, E.20, and E.22, however since only the first of these three structures was fully relaxed, so the latter two are rough results. For all three structures the up buckled Si of the trench Mn-Si heterodimer is the most noticeable feature, appearing as a bright round spot regardless of bias voltage. This appearance is modified slightly based on the location of the exchanged Mn within the dimer row. If the Mn lies on the opposite side of the trench to the up buckled Si then there is no discernable effect, as shown in Figure E.17. If instead the Mn is on the same side of the trench as the up buckled Mn, it will result in the bright spot extending in the direction of that Mn atom, as shown in Figures E.19 and E.21. This results in diagonals that either run in the wrong direction, or are positioned wrong compared to experimental results.

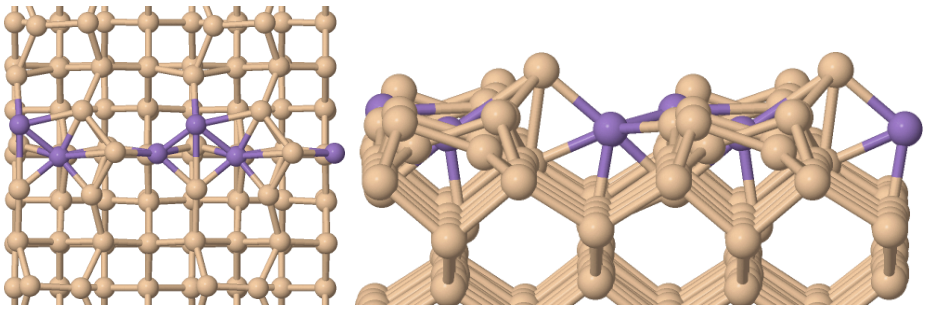

Figure E.17: Structural model of a Wang trimer variant where the up Mn have been exchanged with the up Si from the opposite side of the trench. Both top and side views are shown.

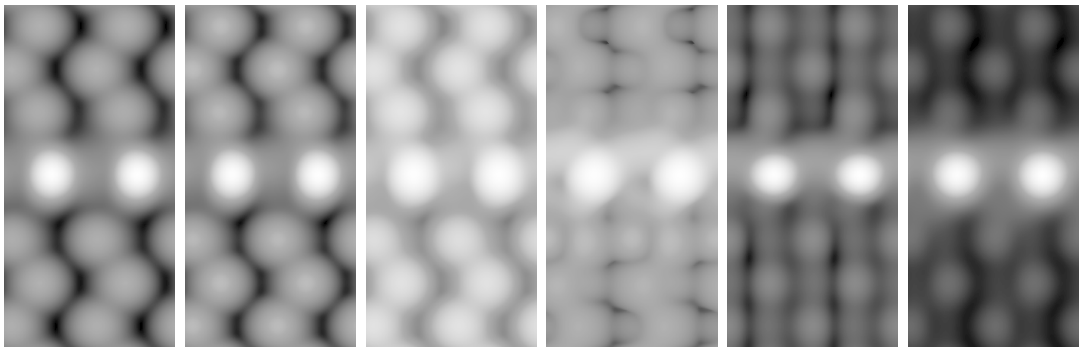

Figure E.18: Simulated STM for a Wang trimer variant where the up Mn have been exchanged with the up Si from the opposite side of the trench.

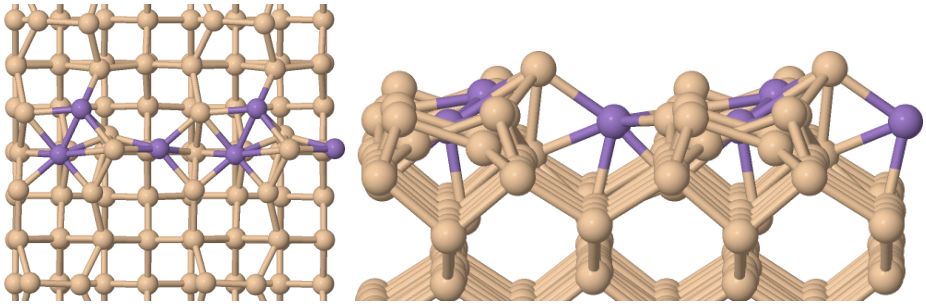

Figure E.19: Structural model of a Wang trimer variant where the up Mn have been exchanged with the adjacent down Si. Both top and side views are shown.

A final structure considered involved exchanging both of the buckled Mn for the up buckled Si, as shown in Figure E.23, which results in a flat Si dimer across the trench. The simulated STM shows a bright feature in the middle of the trench with a slight diagonal tilt, as demonstrated in Figure E.24. At higher negative or positive biases the feature looks straighter, whilst at lower biases the diagonal is more pronounced. The feature can be attributed to both the Si dimer and the up buckled Mn either side of it. The former is responsible for the main body of the feature, whilst the latter is responsible for the diagonal tilt. I do not think that the diagonal observed is as pronounced as in experiment, and that it is not possible to make out a sawtooth appearance at negative biases, thus ruling out this structure.

It is interesting to compare the energies for all of Wang trimer variants since they all contain

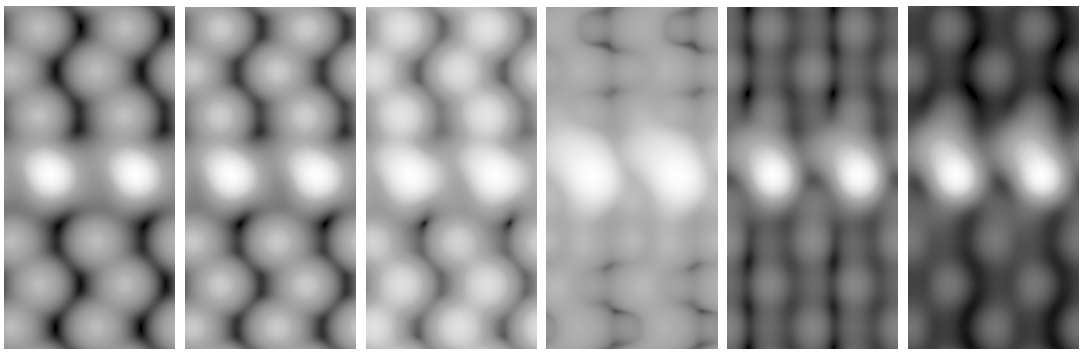

-2.0 V -1.0 V -0.5 V +0.5 V +1.0 V +2.0 V

Figure E.20: Simulated STM for a Wang trimer variant where the up Mn have been exchanged with the adjacent down Si.

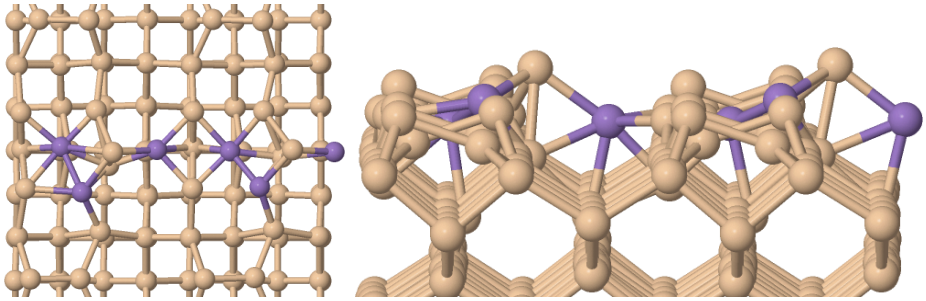

Figure E.21: Structural model of a Wang trimer variant where the up Mn have been exchanged with the adjacent up Si. Both top and side views are shown.

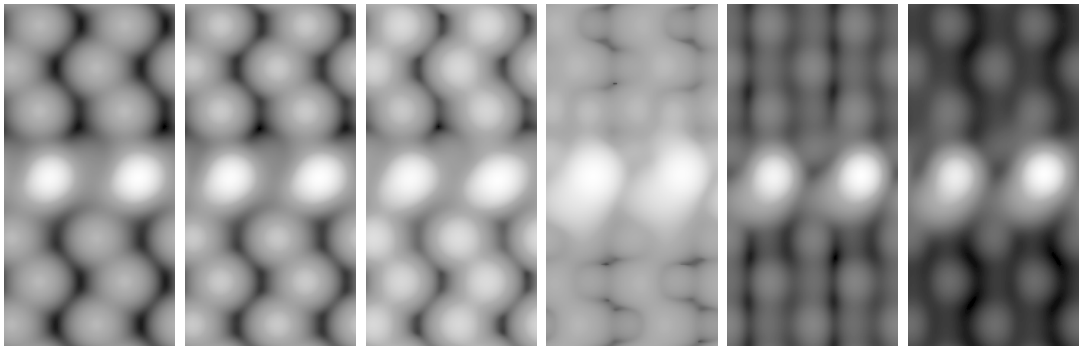

-2.0 V -1.0 V -0.5 V +0.5 V +1.0 V +2.0 V

Figure E.22: Simulated STM for a Wang trimer variant where the up Mn have been exchanged with the adjacent up Si.

the same number of Mn atoms, just rearranged slightly. The data presented in Table E.2, which excludes those two structures which failed to fully relax, shows that there is relatively little energetic difference between each structure, with only a difference of 0.37 eV per Mn between the highest and lowest energy configurations. The Wang trimer variant where the down Mn is exchanged for the adjacent up Si most closely reproduces the experimental STM results, but is actually the highest energy configuration out of all of these structures. This suggests that blindly searching for the lowest energy structure might not in all cases replicate the experimental results, and might help explain why the AIRSS results were not as useful as hoped. Care should be taken with some of these results, because the Wang trimer variants were not investigated for spin effects, so it is

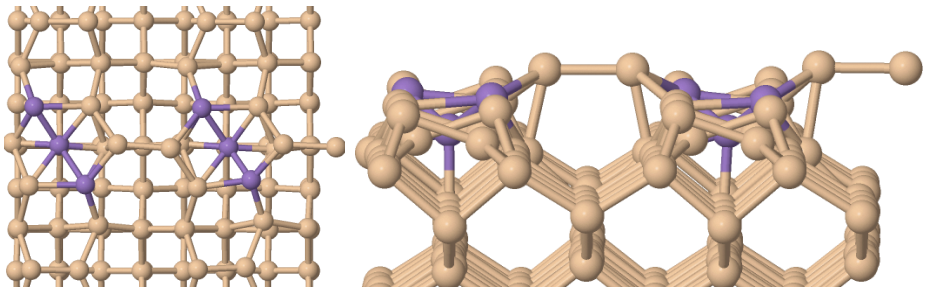

Figure E.23: Structural model of a Wang trimer variant where the both buckled Mn have been exchanged with nearby up Si. Both top and side views are shown

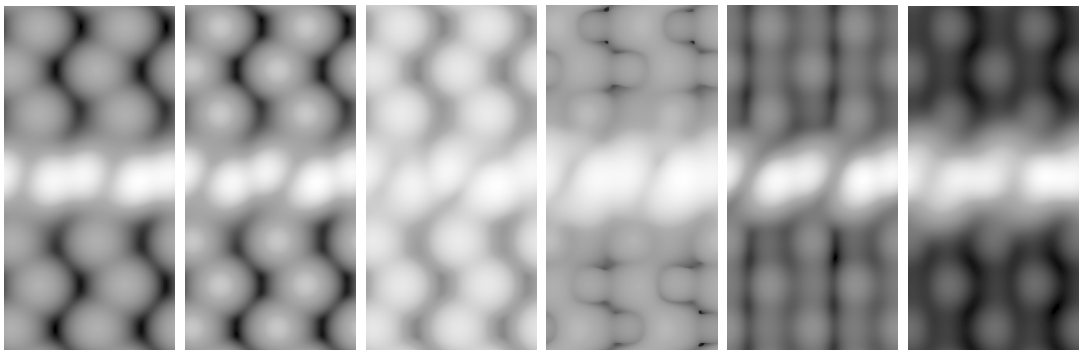

-2.0 V -1.0 V -0.5 V +0.5 V +1.0 V +2.0 V

Figure E.24: Simulated STM for a Wang trimer variant where both buckled Mn have been exchanged with nearby up Si.

possible that lower energy versions of the variants could be found, like was done with the regular trimer.

Table E.2: Adsorption energies for different combined C and B' chains.

Wang trimer variant	E_{ads}/Mn (eV)
Regular	-3.06
Flat	-3.11
Down Mn exchanged with adjacent up Si	-2.74
Down Mn exchanged with opposite up Si	-2.76
Up Mn exchanged with opposite up Si	-2.80
Mn dimer exchanged with up	-2.94

Overall, these new variants do not perform better than the one detailed in Chapter 9, but they do give a fuller picture of the effect of exchanging Mn and Si atoms. There are no current plans to examine all the remaining Wang trimer variants.

E.3 Other Mn structures

At the early stages of the search for the structure of the Mn nanowire the extent of the nanowire along the dimer rows was not clear. At low positive biases a phase shift of the Si dimers next to the nanowire occurs, in a similar fashion to what is observed for the Bi nanoline. At the start of the

search the work detailed in Section 7.9 had not yet been completed, which showed that the phase shift was just caused by adatoms adsorbed on the Si(001) surface. Without this knowledge it was believed that the phase shift might be due to hidden Mn atoms, or a subsurface reconstruction of Si similar to the Haiku core. This lead to the study of several structures which, in hindsight, are unrelated to the Mn nanowire. Some of these structures will be detailed here, in addition to any other Mn structures studied during the course of the search. Whilst these results are not helpful for identifying the Mn nanowire, they can be used to identify other features.

E.3.1 Sub-D chains

Previously it had been found that the most favourable position for a Mn atom on the regular Si(001) surface was the interstitial position directly below a Si dimer [122]. Here it will be referred to as Sub-D site, because it is a subsurface position directly below the D site. Mn atoms are most likely to be in positions with the lowest energy, so it would make sense if the Mn nanowire included a Sub-D site.

When a Mn atom is at a Sub-D site it affects not only the Si dimer which is directly above, but also those which lie either side of the Mn atom, as demonstrated in Figure E.25. The E_{ads} per Mn for this structure is -4.06 eV, which is much greater than any of the other structures studied. The dimer directly above the Mn atom is flattened and raised in height relative to the other surface Si dimers in order to accomodate the Mn atom. The Si dimers adjacent to the Mn atom are also affected, flattening and lowering in height relative to the other surface Si dimers. This is presumably due to the effect of the Mn atom on subsurface Si, which is compensated for by lowering these dimers.

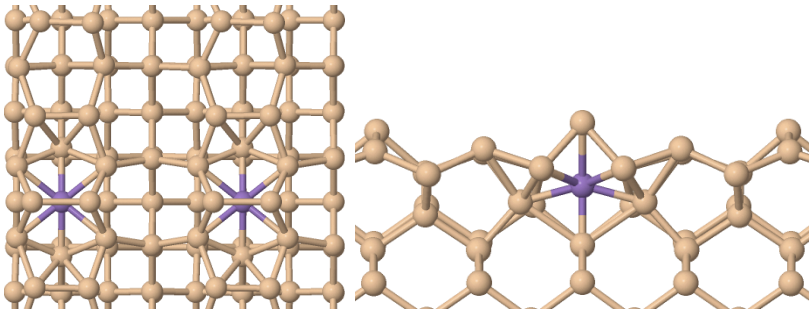

Figure E.25: Structural model for a chain of Mn atoms at the Sub-D site, showing both the top and side views. The Si dimers directly above the Mn atoms are flattened and raised in height relative to the other surface Si dimers, whereas the dimers either side of the Mn are flattened and lowered in height.

Given that the influence of a single Mn atom can spread over 3 Si dimers it is worth knowing how this is reflected in the simulated STM images of the structure, as shown in Figure E.26. At higher negative biases the location of the Sub-chain is clear, with the raised Si dimer appearing as a bright round spot which is larger and slightly brighter than the other surface dimers. This is to be expected because it is flat and physically higher than the other surface dimers, which are buckled. The dimers either side appear dark compared to the other Si dimers, because they are physically lower down in the surface, at about the down atom positions. As the negative bias is decreased, so

too is the brightness of the central dimer. The appearance of the Sub-D chain is largely the same at positive biases, with the neighbouring dimers appearing darker than the surrounding Si, and the raised dimers appearing brighter. The main difference being that the raised dimers are visible as two spots, one for each Si atom, rather than the unbroken spot seen at negative biases.

-2.0 V -1.0 V -0.5 V +0.5 V +1.0 V +2.0 V

Figure E.26: Simulated STM for a Sub-D chain of Mn atoms.

Since the influence of a single Sub-D chain extends over a width of three Si dimers, the influence of two adjacent chains should extend over four Si dimers, consisting of two raised Si dimers and two lowered Si dimers. This matches to the idea of an Mn nanowire whose influence can be seen over a range of four Si dimers. To confirm this a model was built with 2 rows of adjacent Sub-D chains, as shown in Figure E.27, and the simulated STM, as shown in Figure E.28 was examined.

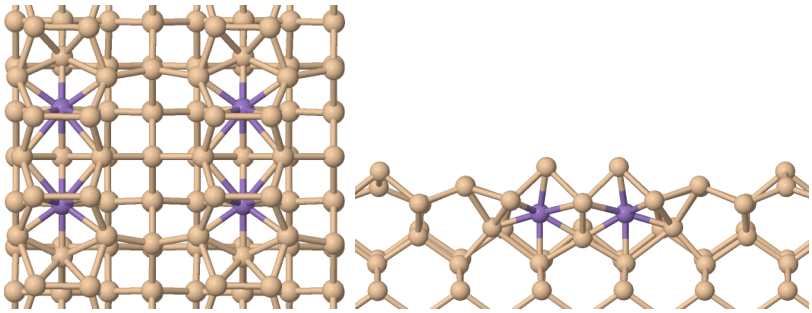

Figure E.27: Structural model for two chains of Mn atoms at Sub-D sites, showing both the top and side views. The Si dimers directly above the Mn atoms are flattened and raised in height, whereas the dimers either side of the chains are flattened and lowered in height.

As expected the two dimers above the Mn atoms were raised, whilst those either side were lowered in height compared to the other surface Si dimers, meaning that the width of the structure now extends over 4 dimers. In addition, the raised Si dimers no longer lie directly above the Mn atoms, but have slightly moved towards the centre of the structure. The E_{ads} per Mn for this structure is even greater than for a single line, at -4.16 eV.

This at first might seem surprising, because two isolated chains would extend over six dimers, rather than the four here, so it might be expected that the double chain structure would have a smaller effect, rather than a larger one on the overall energy of the system. This might be compensated for by other effects, such as the proximity of the Mn atoms to one another.

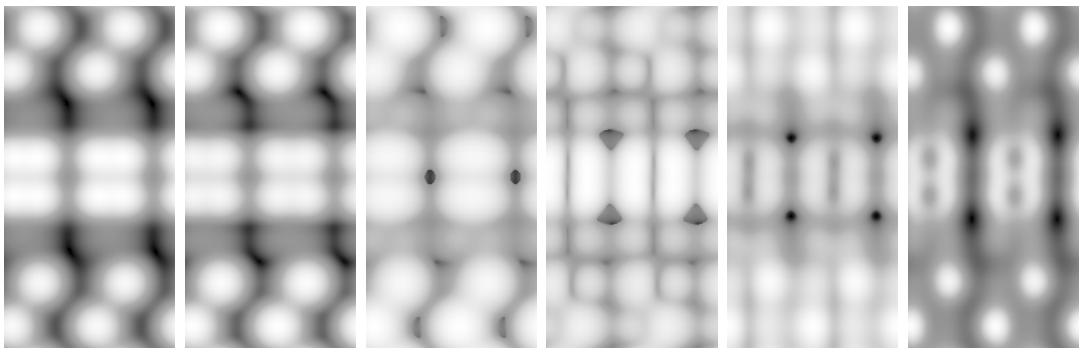

-2.0 V -1.0 V -0.5 V +0.5 V +1.0 V +2.0 V

Figure E.28: Simulated STM for two adjacent Sub-D chains of Mn atoms.

The simulated STM for the structure at negative biases is as would be expected based on the results for a single chain. Two two raised dimers appear as bright spots, whereas the two lowered dimers appear darker than the surrounding surface. The results for positive biases are a bit more unusual. At lower positive biases it looks as if the raised Si dimers run perpendicular to the other surface dimers, even though they have exactly the same orientation. As the bias is increased the dimers begin to look more and more like a figure of eight, as is clear at +2.0 V, with a dark spot in the middle of each Si dimer, and a brighter region between the two dimers. This is a very noticeable effect, so Sub-D chains be easily identified in experiment if they were ever observed in the future.

The problem with this model is that regardless of bias voltage the influence of the Mn always persists over four Si dimers, because the outer two Si dimers are always physically lower in height. This is contrary to experimental results where an effect over four Si dimers is only observed at lower positive biases. Thus these models would never be able reproduce the experimental results, unless the structure of the outer dimers could be changed without also introduced other features.

Extensions to this model, including features such as C site Mn, or a Mn dimer across the trench in either buckled or flat configurations were also attempted, but the full results are not worth presenting. In all cases E_{ads} per Mn was worse than the 2 Sub-D chains on their own, at -3.16 eV, -3.17 eV and -3.19 eV when combined with the C chain, flat Mn dimers and buckled Mn dimers respectively. This combined with the relative complexity of each structure makes it seem unlikely they will ever be observed experimentally. The results from Section 7.9 means that the appearance of the Si dimers next to the Mn nanowire is a result of adsorbed Mn, rather than having to be as a result of surface reconstructions. As such, the extensions to the Sub-D chains will not help identify the Mn nanowire.

E.3.2 H site Mn

Whilst the idea of hidden Mn near the main nanowire was still being considered, the H site was examined. The idea was that Mn either side of the main nanowire might cause the phase shift in the Si dimers at lower positive bias without the Mn atoms themselves appearing in STM images. In hindsight this cannot work, because the nanowire has to be contained within a two dimer wide region, but at the time this had not been certain. Knowing what H sites or combinations of H sites

look like could still be useful for identifying other adsorbed Mn.

To start it is useful to know what an H site Mn, as shown in Figure E.29, looks like in isolation. This Mn atom itself is not visible in the simulated STM images shown in Figure E.30, but there is a notable effect on the surrounding Si atoms. At negative biases the surrounding Si appear darker than the rest of the surface, making the location of the Mn atom clear, even though the Mn itself cannot be seen. At lower positive biases all of the atoms which surround the Mn look brighter than the rest of the surface, although the up Si are still brighter than the down Si. At higher positive biases the surrounding Si darken just like at negative biases. Thus H site Mn can be identified by looking for regions where a pair of adjacent Si dimers appear dark relative to the rest of the surface.

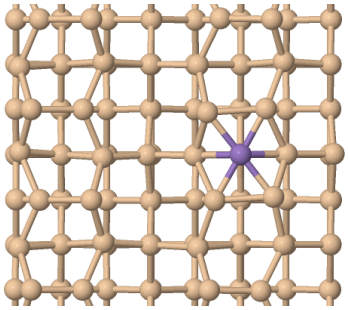

Figure E.29: Structural model showing the top view of an H site Mn.

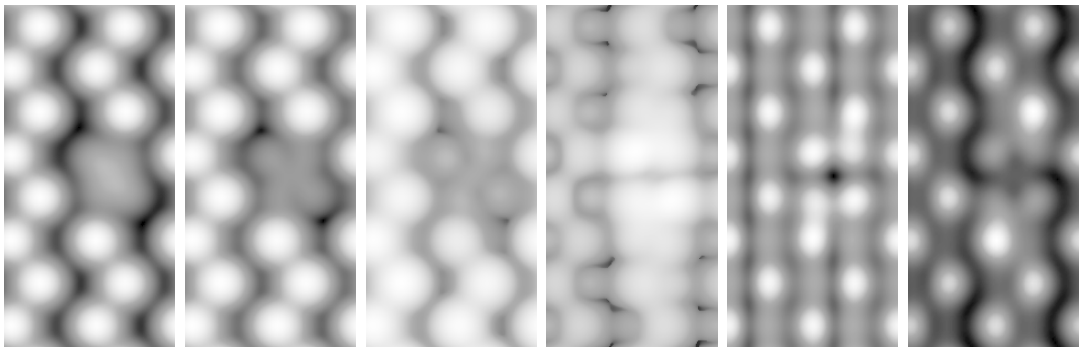

Figure E.30: Simulated STM for Mn at an H site.

Multiple H sites can be combined in a variety of ways, as shown in Figures E.31 and E.33. This includes H sites adjacent to each other in the same row, diagonal to each other across rows, and as single or double chains. Simulated STM for all of these structures show similarities to the single H site, but their proximity causes some differences in the intermediate regions. In all cases the Mn atoms themselves are still not visible.

The Si surrounding the adjacent H sites are still darker than the rest of the surface, as shown in Figure E.32.a). However something has gone wrong with the simulations, because the lower H site is visibly different from the upper H site, when they should be the same, given the identical environments. This does not change the overall trends for the adjacent H sites, but it does suggest the calculations should have been repeated. At positive biases the central Si between both H sites appears brighter than the rest of the surface, and this is maintained to higher biases than was seen

for individual H sites. If the positions of the Mn atoms were not already known it would be easy to mistake this bright region as an Mn structure, rather than being between two Mn atoms.

The individual H sites in the diagonal arrangement look practically the same as a completely isolated H site, as shown in Figure E.32.b). The surrounding Si are darker than the rest of the surface at higher biases and brighter at lower biases. The same is true for a single H chain, as shown in Figure E.34.a). It appears that when separated by the trench the individual H sites will not influence the appearance of each other.

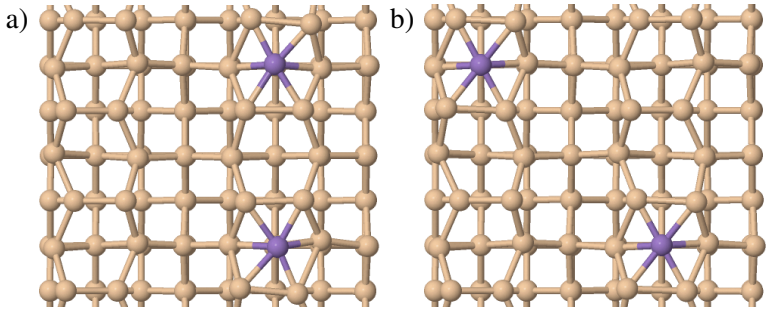

Figure E.31: Structural models for combinations of H site Mn atoms. a) Adjacent H sites. b) Diagonal H sites.

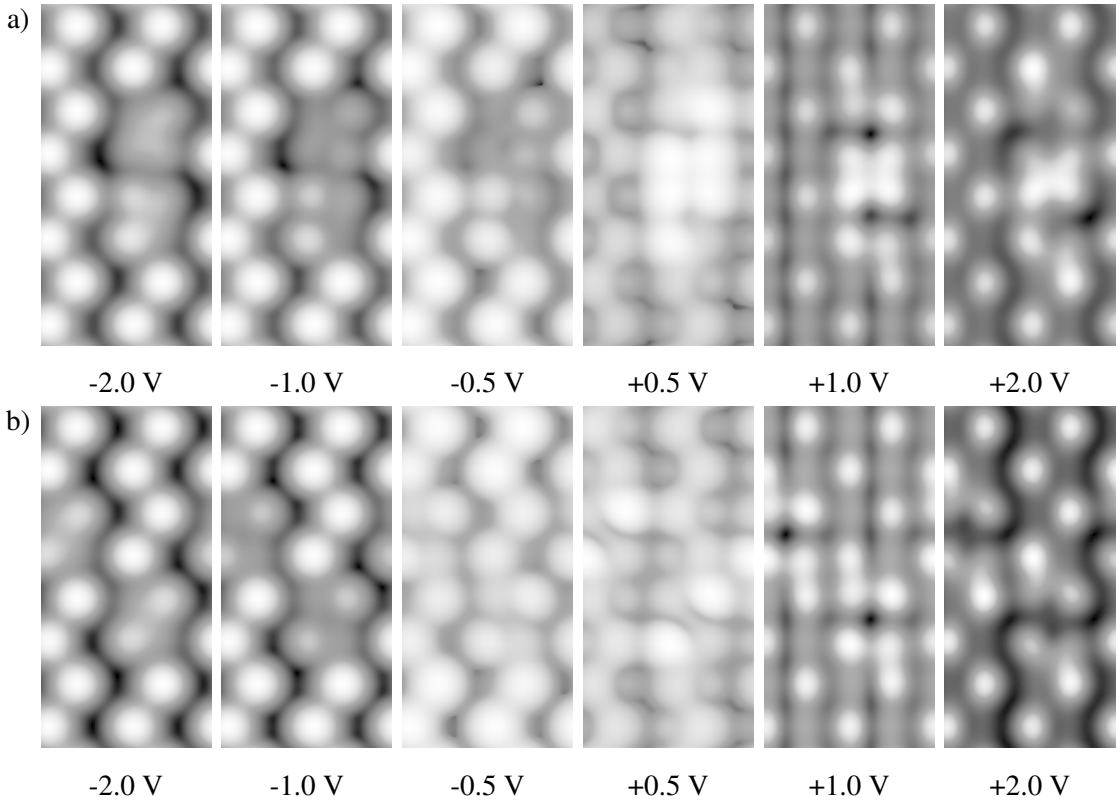

Figure E.32: Simulated STM for Mn atoms at H sites. a) Adjacent H sites. b) Diagonal H sites.

The double H chain structure, as shown in Figure E.34.b), looks like an extended version of the adjacent H chain. There is a greater effect on the Si dimers which appear between the Mn atoms than those which are on the edges of the structure. At negative biases the up atoms of the outer dimers are only slightly darker than the rest of the surface, whilst the central dimers are much darker. At positive biases the up atoms of the outer dimers are slightly brighter than the rest of the

surface, whilst the entirety of the central dimers are brighter than the rest of the surface. It looks as if there is a structure running down the middle of the two lines of Mn atoms, even though there is nothing other than Si in that region.

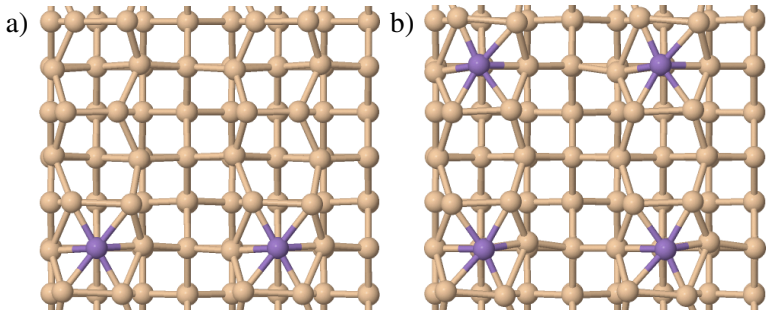

Figure E.33: Structural models for chains of H site Mn atoms. a) Single H chain. b) Double H chain.

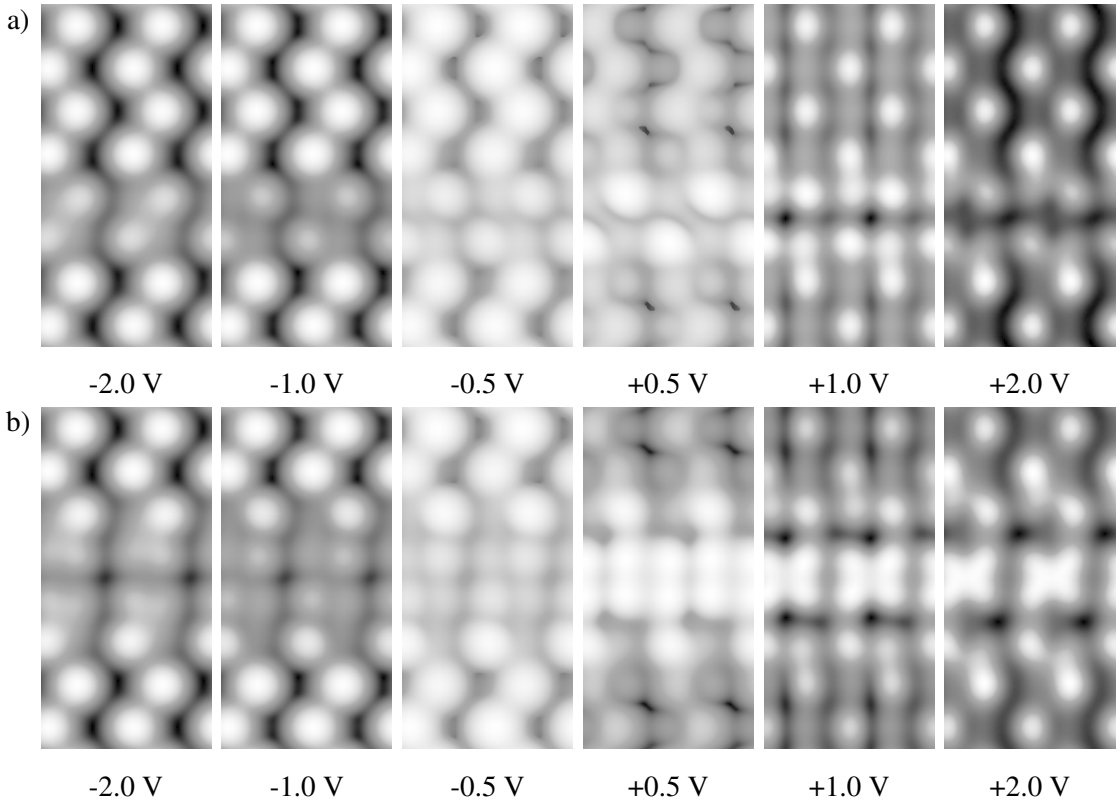

Figure E.34: Simulated STM for chains of Mn atoms at H sites. a) Single H chain. b) Double H chain.

The energies for all of these structures are presented in Table E.3, and shows that H site Mn in close proximity to each other are less energetically favourable than those which are separated. This suggests that the chain structures are less likely to form than the Mn to simply remain separated.

E.4 Mn and dimer vacancies

A structure studied which does not have a direct relation to the Mn nanowire, but which could form on the Si(001) surface is an Mn atom in a Si dimer vacancy. In real experiments there will

Table E.3: Adsorption energies for different arrangements of H site Mn atoms.

H structure	E_{ads}/Mn (eV)
Single H	-2.84
H adjacent	-2.78
H diagonal	-2.73
H chain	-2.68
2 H chains	-2.69

be missing dimer defects on the Si(001) surface and it could be possible for deposited Mn to adsorb in these defects. Figure E.35 shows an example of such a structure, where an Mn atom has adsorbed in the middle of such a defect. The Si dimers either side of the defect are flattened and lowered, and new Si dimers which run perpendicular the other surface dimers have formed across the missing dimer defects. Some of these changes are reflected in the simulated STM images shown in Figure E.36. Since the Si dimers either side of the missing dimer defect are physically lower they appear darker than the rest of the surface, except at lower positive biases such as +0.5 V. This is because at those biases the down Si appear brighter than the up Si, and thus so too would the lowered Si either side of the defect. The Mn atom itself is not visible at any biases, and in fact at higher positive biases, such as +2.0 V, it is significantly darker at the Mn position compared to the rest of the surface. These results mean that it would be quite hard to tell apart missing dimer defects with and without Mn atoms.

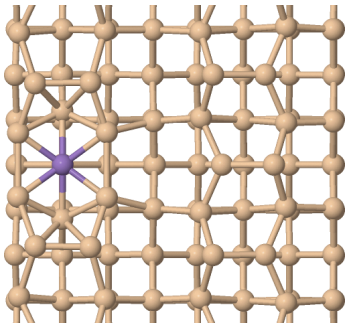

Figure E.35: Structural model for an Mn atom in a Si dimer vacancy.

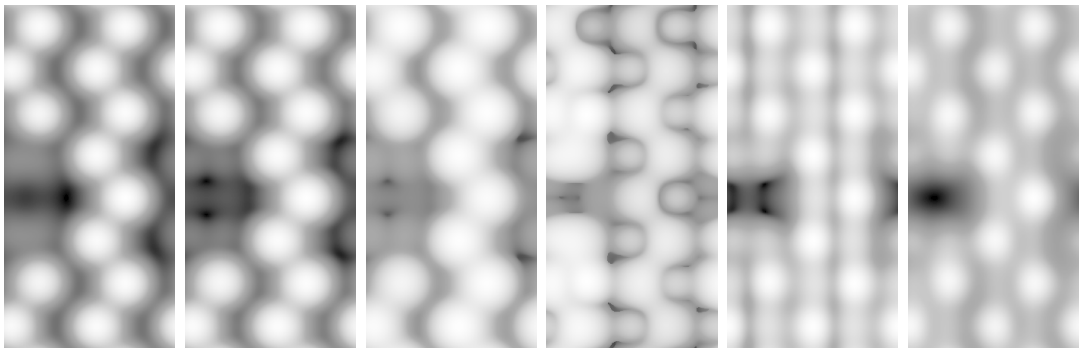

-2.0 V -1.0 V -0.5 V +0.5 V +1.0 V +2.0 V

Figure E.36: Simulated STM for an Mn atom in a Si dimer vacancy.

Bibliography

[1] C. J. Kirkham, V. Brázdová, and D. R. Bowler, "Bi on the si(001) surface," *Phys. Rev. B*, vol. 86, p. 035328, Jul 2012.

[2] G. W. Morley, M. Warner, A. M. Stoneham, P. T. Greenland, J. van Tol, C. W. M. Kay, and G. Aeppli, "The initialization and manipulation of quantum information stored in silicon by bismuth dopants," *Nature Mater.*, vol. 9, pp. 725–729, SEP 2010.

[3] M. H. Mohammady, G. W. Morley, and T. S. Monteiro, "Bismuth Qubits in Silicon: The Role of EPR Cancellation Resonances," *Phys. Rev. Lett.*, vol. 105, p. 067602, Aug 2010.

[4] J. J. Pla, K. Y. Tan, J. P. Dehollain, W. H. Lim, J. J. L. Morton, D. N. Jamieson, A. S. Dzurak, and A. Morello, "A single-atom electron spin qubit in silicon," *NATURE*, vol. 489, pp. 541–545, SEP 27 2012.

[5] K. Saeedi, S. Simmons, J. Z. Salvail, P. Dluhy, H. Riemann, N. V. Abrosimov, P. Becker, H.-J. Pohl, J. J. L. Morton, and M. L. W. Thewalt, "Room-temperature quantum bit storage exceeding 39 minutes using ionized donors in silicon-28," *Science*, vol. 342, no. 6160, pp. 830–833, 2013.

[6] M. Fuechsle, J. A. Miwa, S. Mahapatra, H. Ryu, S. Lee, O. Warschkow, L. C. L. Hollenberg, G. Klimeck, and M. Y. Simmons, "A single-atom transistor," *NATURE NANOTECHNOLOGY*, vol. 7, pp. 242–246, APR 2012.

[7] A. Stoneham, A. Fisher, and P. Greenland, "Optically driven silicon-based quantum gates with potential for high-temperature operation," *JOURNAL OF PHYSICS-CONDENSED MATTER*, vol. 15, pp. L447–L451, JUL 16 2003.

[8] D. R. Bowler, "Atomic-scale nanowires: physical and electronic structure," *Journal of Physics: Condensed Matter*, vol. 16, no. 24, p. R721, 2004.

[9] K. Miki, J. H. G. Owen, D. R. Bowler, G. A. D. Briggs, and K. Sakamoto, "Bismuth-induced structures on Si(001) surfaces," *Surf. Sci*, vol. 421, no. 3, pp. 397 – 418, 1999.

[10] A. Macdonald, P. Schiffer, and N. Samarth, "Ferromagnetic semiconductors: moving beyond (Ga, Mn)As," *NATURE MATERIALS*, vol. 4, pp. 195–202, MAR 2005.

[11] R. J. Hamers, R. M. Tromp, and J. E. Demuth, "Scanning tunneling microscopy of si(001)," *Phys. Rev. B*, vol. 34, pp. 5343–5357, Oct 1986.

[12] A. Ramstad, G. Brocks, and P. J. Kelly, "Theoretical study of the si(100) surface reconstruction," *Phys. Rev. B*, vol. 51, pp. 14504–14523, May 1995.

[13] Y. Wang, X. Chen, and R. J. Hamers, "Atomic-resolution study of overlayer formation and interfacial mixing in the interaction of phosphorus with Si(001)," *Phys. Rev. B*, vol. 50, pp. 4534–4547, Aug 1994.

[14] R. D. Bringans, D. K. Biegelsen, and L.-E. Swartz, "Atomic-step rearrangement on Si(100) by interaction with arsenic and the implication for GaAs-on-Si epitaxy," *Phys. Rev. B*, vol. 44, pp. 3054–3063, Aug 1991.

[15] M. Richter, J. C. Woicik, J. Nogami, P. Pianetta, K. E. Miyano, A. A. Baski, T. Kendelewicz, C. E. Bouldin, W. E. Spicer, C. F. Quate, and I. Lindau, "Surface extended-x-ray-absorption fine structure and scanning tunneling microscopy of Si(001)2×1-Sb," *Phys. Rev. Lett.*, vol. 65, pp. 3417–3420, Dec 1990.

[16] S. Bulavenko, I. Koval, P. Melnik, N. Nakhodkin, and H. Zandvliet, "STM investigation of the initial adsorption stage of Bi on Si(100)-(21) and Ge(100)-(21) surfaces," *Surf. Sci*, vol. 482-485, no. Part 1, pp. 370 – 375, 2001.

[17] H. Noh, C. Park, D. Jeon, K. Cho, T. Hashizume, Y. Kuk, and T. Sakurai, "Adsorption of Bi on Si(001) surface - An atomic view," *J. Vac. Sci. Technol. B*, vol. 12, pp. 2097–2099, MAY-JUN 1994.

[18] N. Takeuchi, "Adsorption of group III and group V metals on Si(001): One-dimensional versus two-dimensional growth," *Phys. Rev. B*, vol. 63, p. 035311, Dec 2000.

[19] N. Takeuchi, "First principles calculations of the adsorption of single group III and group V atoms on Si(001)," *Surf. Sci*, vol. 482, pp. 44–48, JUN 20 2001.

[20] J. M. Bennett, O. Warschkow, N. A. Marks, and D. R. McKenzie, "Diffusion pathways of phosphorus atoms on silicon (001)," *Phys. Rev. B*, vol. 79, APR 2009.

[21] P. Sen, B. Gupta, and I. Batra, "Structural studies of phosphorus induced dimers on Si(001)," *Phys. Rev. B*, vol. 73, FEB 2006.

[22] S. Tang and A. J. Freeman, "Importance of adsorbate-adsorbate interactions for As and Sb chemisorption on Si(100)," *Phys. Rev. B*, vol. 48, pp. 8068–8075, Sep 1993.

[23] S. Tang and A. Freeman, "Bi-induced reconstructions on Si(100)," *Phys. Rev. B*, vol. 50, pp. 1701–1704, JUL 15 1994.

[24] D. R. Bowler, "Structure of atomically perfect lines of bismuth in the Si(001) surface," *Phys. Rev. B*, vol. 62, pp. 7237–7242, Sep 2000.

[25] G. E. Franklin, S. Tang, J. C. Woicik, M. J. Bedzyk, A. J. Freeman, and J. A. Golovchenko, "High-resolution structural study of Bi on Si(001)," *Phys. Rev. B*, vol. 52, pp. R5515–R5518, Aug 1995.

[26] K. Chuasiripattana and G. P. Srivastava, "Rotation of ad-dimers in the initial stages of Bi and Si deposition on the Si(001) surface," *Phys. Rev. B*, vol. 71, p. 153312, Apr 2005.

[27] J. Shan, Y. Wang, and R. Hamers, "Adsorption and dissociation of phosphine on Si(001)," *JOURNAL OF PHYSICAL CHEMISTRY*, vol. 100, pp. 4961–4969, MAR 21 1996.

[28] S. R. Schofield, N. J. Curson, M. Y. Simmons, F. J. Rueß, T. Hallam, L. Oberbeck, and R. G. Clark, "Atomically Precise Placement of Single Dopants in Si," *Phys. Rev. Lett.*, vol. 91, p. 136104, Sep 2003.

[29] N. J. Curson, S. R. Schofield, M. Y. Simmons, L. Oberbeck, J. L. O'Brien, and R. G. Clark, "Stm characterization of the si-p heterodimer," *Phys. Rev. B*, vol. 69, p. 195303, May 2004.

[30] M. W. Radny, P. V. Smith, T. C. G. Reusch, O. Warschkow, N. A. Marks, H. Q. Shi, D. R. McKenzie, S. R. Schofield, N. J. Curson, and M. Y. Simmons, "Single P and As dopants in the Si(001) surface," *JOURNAL OF CHEMICAL PHYSICS*, vol. 127, NOV 14 2007.

[31] J. LYDING, T. SHEN, J. HUBACEK, J. TUCKER, and G. ABELN, "Nanoscale patterning and oxidation of H-passivated Si(001)-2x1 surfaces with an ultrahigh-vacuum scanning tunneling microscope," *APPLIED PHYSICS LETTERS*, vol. 64, pp. 2010–2012, APR 11 1994.

[32] E. T. Foley, A. F. Kam, J. W. Lyding, and P. Avouris, "Cryogenic UHV-STM Study of Hydrogen and Deuterium Desorption from Si(100)," *Phys. Rev. Lett.*, vol. 80, pp. 1336–1339, Feb 1998.

[33] T. SHEN, C. WANG, G. ABELN, J. TUCKER, J. LYDING, P. AVOURIS, and R. WALKUP, "Atomic-scale desorption through electronic and vibrational-excitation mechanisms," *SCIENCE*, vol. 268, pp. 1590–1592, JUN 16 1995.

[34] L. Soukiassian, A. J. Mayne, M. Carbone, and G. Dujardin, "Atomic-scale desorption of h atoms from the $\mathrm{Si}(100) - 2 \times 1 : \mathrm{H}$ surface: inelastic electron interactions," *Phys. Rev. B*, vol. 68, p. 035303, Jul 2003.

[35] M. Hersam, N. Guisinger, and J. Lyding, "Silicon-based molecular nanotechnology," *NANOTECHNOLOGY*, vol. 11, pp. 70–76, JUN 2000.

[36] L. Soukiassian, A. J. Mayne, M. Carbone, and G. Dujardin, "Atomic wire fabrication by {STM} induced hydrogen desorption," *Surface Science*, vol. 528, no. 13, pp. 121 – 126, 2003. Proceedings of the Ninth International Workshop on Desorption Induced by Electronic Transitions.

[37] J. N. Randall, J. W. Lyding, S. Schmucker, J. R. Von Ehr, J. Ballard, R. Saini, H. Xu, and Y. Ding, "Atomic precision lithography on Si," *JOURNAL OF VACUUM SCIENCE & TECHNOLOGY B*, vol. 27, pp. 2764–2768, NOV 2009.

[38] J. N. Randall, J. R. Von Ehr, J. B. Ballard, J. H. G. Owen, and E. Fuchs, "Automated Scanning Tunneling Microscope image analysis of Si (100):H 2 x 1 surfaces," *MICROELECTRONIC ENGINEERING*, vol. 98, pp. 214–217, OCT 2012.

[39] M. Naitoh, H. Shimaya, S. Nishigaki, N. Oishi, and F. Shoji, "Scanning tunneling microscopy observation of bismuth growth on Si(100) surfaces," *Surf. Sci*, vol. 377-379, pp. 899 – 903, 1997.

[40] J. H. G. Owen, K. Miki, and D. R. Bowler, "Self-assembled nanowires on semiconductor surfaces," *Journal of Materials Science*, vol. 41, no. 14, p. 32, 2006.

[41] H. ZANDVLIET, H. WORMEESTER, D. WENTINK, A. VANSILFHOUT, and H. ELSWIJK, "Why monatomic steps on Si(001) are always rough," *PHYSICAL REVIEW LETTERS*, vol. 70, pp. 2122–2125, APR 5 1993.

[42] M. Naitoh, M. Takei, S. Nishigaki, N. Oishi, and F. Shoji, "Structure of Bi-Dimer Linear Chains on a Si(100) Surface: A Scanning Tunneling Microscopy Study," *Jpn. J. Appl. Phys.*, vol. 39, no. Part 1, No. 5A, pp. 2793–2794, 2000.

[43] J. H. G. Owen, K. Miki, H. Koh, H. W. Yeom, and D. R. Bowler, "Stress Relief as the Driving Force for Self-Assembled Bi Nanolines," *Phys. Rev. Lett.*, vol. 88, p. 226104, May 2002.

[44] J. H. G. Owen, F. Bianco, S. A. Koester, D. Mazur, D. R. Bowler, and C. Renner, "One-dimensional Si-in-Si(001) template for single-atom wire growth," *APPLIED PHYSICS LETTERS*, vol. 97, AUG 30 2010.

[45] G. Srivastava and R. Miwa, "Nanostructure formation aided by self-organised Bi nanolines on Si(001)," *Applied Surface Science*, vol. 254, no. 24, pp. 8075 – 8082, 2008.

[46] J. MacLeod, R. Miwa, G. Srivastava, and A. McLean, "The electronic origin of contrast reversal in bias-dependent {STM} images of nanolines," *Surface Science*, vol. 576, no. 13, pp. 116 – 122, 2005.

[47] R. H. Miwa, J. M. MacLeod, A. B. McLean, and G. P. Srivastava, "The equilibrium geometry and electronic structure of Bi nanolines on clean and hydrogenated Si(001) surfaces," *Nanotechnology*, vol. 16, no. 10, p. 2427, 2005.

[48] J. Javorsky, J. H. G. Owen, M. Setvin, and K. Miki, "Electronic structure of Bi lines on clean and H-passivated Si(100)," *JOURNAL OF PHYSICS-CONDENSED MATTER*, vol. 22, MAY 5 2010.

[49] S. Yagi, W. Yashiro, K. Sakamoto, and K. Miki, "Surface bismuth removal after Bi nanoline encapsulation in silicon," *Surface Science*, vol. 595, no. 13, pp. L311 – L317, 2005.

[50] K. Miki, H. Matsuhata, K. Sakamoto, G. Briggs, J. Owen, and D. Bowler, "Bismuth and antimony nanolines in a Si epitaxial layer," in *MICROSCOPY OF SEMICONDUCTING*

MATERIALS 1999, PROCEEDINGS (Cullis, AG and Beanland, R, ed.), no. 164 in INSTITUTE OF PHYSICS CONFERENCE SERIES, pp. 167–170, Inst Phys, Electron Microscopy & Analy Grp; Royal Microscop Soc; Mat Res Soc; Hitachi Sci Instruments Ltd; JEOL (UK) Ltd; FEI Ltd, 1999. Conference on Microscopy of Semiconducting Materials, UNIV OXFORD, OXFORD, ENGLAND, MAR 22-25, 1999.

[51] O. Sakata, W. Yashiro, D. R. Bowler, A. Kitano, K. Sakamoto, and K. Miki, "Encapsulation of atomic-scale Bi wires in epitaxial silicon without loss of structure," *Phys. Rev. B*, vol. 72, p. 121407, Sep 2005.

[52] F. Bianco, J. H. G. Owen, S. A. Koester, D. Mazur, C. Renner, and D. R. Bowler, "Endotaxial Si nanolines in Si(001):H," *PHYSICAL REVIEW B*, vol. 84, JUL 29 2011.

[53] F. Bianco, D. R. Bowler, J. H. G. Owen, S. A. Koester, M. Longobardi, and C. Renner, "Scalable Patterning of One-Dimensional Dangling Bond Rows on Hydrogenated Si(001)," *ACS NANO*, vol. 7, pp. 4422–4428, MAY 2013.

[54] H. Liu and P. Reinke, "Formation of manganese nanostructures on the Si(100)-(2 $\times$ 1) surface," *Surf. Sci.*, vol. 602, no. 4, pp. 986 – 992, 2008.

[55] C. Nolph, H. Liu, and P. Reinke, "Bonding geometry of Mn-wires on the Si(100)(2 $\times$ 1) surface," *Surface Science*, vol. 605, no. 1314, pp. L29 – L32, 2011.

[56] X. Luo, S. B. Zhang, and S.-H. Wei, "Theory of Mn supersaturation in Si and Ge," *Phys. Rev. B*, vol. 70, p. 033308, Jul 2004.

[57] A. M. P. Sena and D. R. Bowler, "A density functional theory study of Mn nanowires on the Si(001) surface," *J. Phys.: Condens. Matter*, vol. 23, no. 30, p. 305003, 2011.

[58] J.-T. Wang, C. Chen, E. Wang, and Y. Kawazoe, "Magic Monatomic Linear Chains for Mn Nanowire Self-Assembly on Si(001)," *Phys. Rev. Lett.*, vol. 105, p. 116102, Sep 2010.

[59] A. Fuhrer, F. J. Rueß, N. Moll, A. Curioni, and D. Widmer, "Atomic Structure of Mn Wires on Si(001) Resolved by Scanning Tunneling Microscopy," *Phys. Rev. Lett.*, vol. 109, p. 146102, Oct 2012.

[60] P. Hohenberg and W. Kohn, "Inhomogeneous electron gas," *Phys. Rev.*, vol. 136, pp. B864–B871, Nov 1964.

[61] W. Kohn and L. J. Sham, "Self-Consistent Equations Including Exchange and Correlation Effects," *Phys. Rev.*, vol. 140, pp. A1133–A1138, Nov 1965.

[62] G. Kresse and J. Hafner, "*Ab initio* molecular dynamics for open-shell transition metals," *Phys. Rev. B*, vol. 48, pp. 13115–13118, Nov 1993.

[63] G. Kresse and J. Furthmüller, "Efficient iterative schemes for *ab initio* total-energy calculations using a plane-wave basis set," *Phys. Rev. B*, vol. 54, pp. 11169–11186, Oct 1996.

[64] R. Martin, *Electronic Structure: Basic Theory and Practical Methods*. Cambridge University Press, 2004.

[65] J. Perdew, K. Burke, and M. Ernzerhof, "Generalized gradient approximation made simple," *Phys. Rev. Lett.*, vol. 77, pp. 3865–3868, OCT 28 1996.

[66] J. P. Perdew, J. A. Chevary, S. H. Vosko, K. A. Jackson, M. R. Pederson, D. J. Singh, and C. Fiolhais, "Atoms, molecules, solids, and surfaces: Applications of the generalized gradient approximation for exchange and correlation," *Phys. Rev. B*, vol. 46, pp. 6671–6687, Sep 1992.

[67] D. R. Hamann, M. Schlüter, and C. Chiang, "Norm-conserving pseudopotentials," *Phys. Rev. Lett.*, vol. 43, pp. 1494–1497, Nov 1979.

[68] D. VANDERBILT, "SOFT SELF-CONSISTENT PSEUDOPOTENTIALS IN A GENERALIZED EIGENVALUE FORMALISM," *PHYSICAL REVIEW B*, vol. 41, pp. 7892–7895, APR 15 1990.

[69] P. E. Blöchl, "Projector augmented-wave method," *Phys. Rev. B*, vol. 50, pp. 17953–17979, Dec 1994.

[70] G. Kresse and D. Joubert, "From ultrasoft pseudopotentials to the projector augmented-wave method," *Phys. Rev. B*, vol. 59, pp. 1758–1775, Jan 1999.

[71] A. J. Cohen, P. Mori-Snchez, and W. Yang, "Insights into Current Limitations of Density Functional Theory," *Science*, vol. 321, no. 5890, pp. 792–794, 2008.

[72] J. P. Perdew and A. Zunger, "Self-interaction correction to density-functional approximations for many-electron systems," *Phys. Rev. B*, vol. 23, pp. 5048–5079, May 1981.

[73] S. Kümmel and J. P. Perdew, "Optimized effective potential made simple: Orbital functionals, orbital shifts, and the exact Kohn-Sham exchange potential," *Phys. Rev. B*, vol. 68, p. 035103, Jul 2003.

[74] V. I. Anisimov, J. Zaanen, and O. K. Andersen, "Band theory and Mott insulators: Hubbard U instead of Stoner I," *Phys. Rev. B*, vol. 44, pp. 943–954, Jul 1991.

[75] V. I. Anisimov, I. V. Solovyev, M. A. Korotin, M. T. Czyżyk, and G. A. Sawatzky, "Density-functional theory and NiO photoemission spectra," *Phys. Rev. B*, vol. 48, pp. 16929–16934, Dec 1993.

[76] H. Eyring, "The activated complex in chemical reactions," *JOURNAL OF CHEMICAL PHYSICS*, vol. 3, pp. 107–115, FEB 1935.

[77] E. Wigner, "The transition state method.," *TRANSACTIONS OF THE FARADAY SOCIETY*, vol. 34, no. 1, pp. 0029–0040, 1938.

[78] M. J. S. Dewar, E. F. Healy, and J. J. P. Stewart, "Location of transition states in reaction mechanisms," *J. Chem. Soc., Faraday Trans. 2*, vol. 80, pp. 227–233, 1984.

[79] J. Klimes, D. R. Bowler, and A. Michaelides, "A critical assessment of theoretical methods for finding reaction pathways and transition states of surface processes," *JOURNAL OF PHYSICS-CONDENSED MATTER*, vol. 22, p. 074203, FEB 24 2010.

[80] G. Henkelman and H. Jonsson, "A dimer method for finding saddle points on high dimensional potential surfaces using only first derivatives," *JOURNAL OF CHEMICAL PHYSICS*, vol. 111, pp. 7010–7022, OCT 15 1999.

[81] M. J. Rothman and L. L. L. Jr., "Analysis of an energy minimization method for locating transition states on potential energy hypersurfaces," *Chemical Physics Letters*, vol. 70, no. 2, pp. 405 – 409, 1980.

[82] G. Barkema and N. Mousseau, "The activation-relaxation technique: an efficient algorithm for sampling energy landscapes," *COMPUTATIONAL MATERIALS SCIENCE*, vol. 20, pp. 285–292, MAR 2001.

[83] H. Jónsson, G. Mills, and K. W. Jacobsen, "Nudged Elastic Band Method for Finding Minimum Energy Paths of Transitions," in *Classical and quantum dynamics in condensed phase simulations* (B. J. Berne, ed.), pp. 385–404, World Scientific, 1998.

[84] G. Henkelman, B. Uberuaga, and H. Jonsson, "A climbing image nudged elastic band method for finding saddle points and minimum energy paths," *J. Chem. Phys.*, vol. 113, pp. 9901–9904, DEC 8 2000.

[85] L. PRATT, "A statistical-method for identifying transistion-states in high dimensional problems," *J. Chem. Phys.*, vol. 85, pp. 5045–5048, NOV 1 1986.

[86] R. Elber and M. Karplus, "A method for determining reaction paths in large molecules: Application to myoglobin," *Chem. Phys. Lett.*, vol. 139, no. 5, pp. 375 – 380, 1987.

[87] G. BINNIG, H. ROHRER, C. GERBER, and E. WEIBEL, "TUNNELING THROUGH A CONTROLLABLE VACUUM GAP," *APPLIED PHYSICS LETTERS*, vol. 40, no. 2, pp. 178–180, 1982.

[88] G. Binnig, H. Rohrer, C. Gerber, and E. Weibel, "Surface studies by scanning tunneling microscopy," *Phys. Rev. Lett.*, vol. 49, pp. 57–61, Jul 1982.

[89] W. A. Hofer, A. S. Foster, and A. L. Shluger, "Theories of scanning probe microscopes at the atomic scale," *Rev. Mod. Phys.*, vol. 75, pp. 1287–1331, Oct 2003.

[90] W. Hofer, A. Fisher, R. Wolkow, and P. Grutter, "Surface relaxations, current enhancements, and absolute distances in high resolution scanning tunneling microscopy," *PHYSICAL REVIEW LETTERS*, vol. 87, DEC 3 2001.

[91] J. TERSOFF and D. HAMANN, "THEORY AND APPLICATION FOR THE SCANNING TUNNELING MICROSCOPE," *PHYSICAL REVIEW LETTERS*, vol. 50, no. 25, pp. 1998–2001, 1983.

[92] J. TERSOFF and D. HAMANN, "THEORY OF THE SCANNING TUNNELING MICROSCOPE," *PHYSICAL REVIEW B*, vol. 31, no. 2, pp. 805–813, 1985.

[93] W. Hofer and J. Redinger, "Scanning tunneling microscopy of binary alloys: first principles calculation of the current for PtX (100) surfaces," *SURFACE SCIENCE*, vol. 447, pp. 51–61, FEB 20 2000.

[94] W. Hofer and A. Fisher, "Determining surface magnetization and local magnetic moments with atomic scale resolution," *SURFACE SCIENCE*, vol. 515, pp. L487–L492, SEP 1 2002.

[95] W. Hofer, "Challenges and errors: interpreting high resolution images in scanning tunneling microscopy," *PROGRESS IN SURFACE SCIENCE*, vol. 71, pp. 147–183, JUN 2003.

[96] C. CHEN, "TUNNELING MATRIX-ELEMENTS IN 3-DIMENSIONAL SPACE - THE DERIVATIVE RULE AND THE SUM-RULE," *PHYSICAL REVIEW B*, vol. 42, pp. 8841–8857, NOV 15 1990.

[97] C. CHEN, "ORIGIN OF ATOMIC RESOLUTION ON METAL-SURFACES IN SCANNING TUNNELING MICROSCOPY," *PHYSICAL REVIEW LETTERS*, vol. 65, pp. 448–451, JUL 23 1990.

[98] W. Hofer, J. Redinger, and R. Podloucky, "Modeling STM tips by single absorbed atoms on W(100) films: 3d and 4d transition-metal atoms," *PHYSICAL REVIEW B*, vol. 64, SEP 15 2001.

[99] J. BARDEEN, "TUNNELLING FROM A MANY-PARTICLE POINT OF VIEW," *PHYSICAL REVIEW LETTERS*, vol. 6, no. 2, pp. 57–&, 1961.

[100] R. BALLINGER and N. MARCH, "BOND-LENGTHS AND FORCE CONSTANTS FOR METHANE, SILANE AND GERMANE," *NATURE*, vol. 174, no. 4421, p. 179, 1954.

[101] W. Gale and T. Totemeier, *Smithells Metals Reference Book*. Elsevier Science, 2003.

[102] R. R. Wixom and A. F. Wright, "Formation energies, binding energies, structure, and electronic transitions of Si divacancies studied by density functional calculations," *PHYSICAL REVIEW B*, vol. 74, NOV 2006.

[103] H. Seong and L. Lewis, "First-principles study of the structure and energetics of neutral divacancies in silicon," *PHYSICAL REVIEW B*, vol. 53, pp. 9791–9796, APR 15 1996.

[104] D. Makhov and L. Lewis, "Stable fourfold configurations for small vacancy clusters in silicon from ab initio calculations," *PHYSICAL REVIEW LETTERS*, vol. 92, JUN 25 2004.

[105] V. P. Markevich, A. R. Peaker, S. B. Lastovskii, L. I. Murin, J. Coutinho, V. J. B. Torres, P. R. Briddon, L. Dobaczewski, E. V. Monakhov, and B. G. Svensson, "Trivacancy and trivacancy-oxygen complexes in silicon: Experiments and ab initio modeling," *PHYSICAL REVIEW B*, vol. 80, DEC 2009.

[106] S. L. Dudarev, G. A. Botton, S. Y. Savrasov, C. J. Humphreys, and A. P. Sutton, "Electron-energy-loss spectra and the structural stability of nickel oxide: An LSDA+U study," *Phys. Rev. B*, vol. 57, pp. 1505–1509, Jan 1998.

[107] G. Brocks, P. J. Kelly, and R. Car, "The energetics of adatoms on the Si(100) surface," *Surf. Sci*, vol. 269-270, pp. 860 – 866, 1992.

[108] G. Brocks, P. J. Kelly, and R. Car, "Binding and diffusion of a Si adatom on the Si(100) surface," *Phys. Rev. Lett.*, vol. 66, pp. 1729–1732, Apr 1991.

[109] K. Iwaya, D. R. Bowler, V. Brázdová, A. Ferreira da Silva, C. Renner, W. Wu, A. J. Fisher, A. M. Stoneham, and G. Aeppli, "Half-filled orbital and unconventional geometry of a common dopant in Si(001)," *Phys. Rev. B*, vol. 88, p. 035440, Jul 2013.

[110] M. Duerr and U. Hoefer, "Hydrogen diffusion on silicon surfaces," *PROGRESS IN SURFACE SCIENCE*, vol. 88, pp. 61–101, FEB 2013.

[111] J. Wieferink, P. Krueger, and J. Pollmann, "Ab initio study of atomic hydrogen diffusion on the clean and hydrogen-terminated Si(001) surface," *PHYSICAL REVIEW B*, vol. 82, AUG 23 2010.

[112] J. Owen, K. Miki, and D. Bowler, "Interaction between electronic structure and strain in Bi nanolines on Si(001)," *SURFACE SCIENCE*, vol. 527, pp. L177–L183, MAR 10 2003.

[113] L. Gross, N. Moll, F. Mohn, A. Curioni, G. Meyer, F. Hanke, and M. Persson, "High-Resolution Molecular Orbital Imaging Using a p-Wave STM Tip," *Phys. Rev. Lett.*, vol. 107, p. 086101, Aug 2011.

[114] K. Sagisaka, M. Marz, D. Fujita, and D. Bowler, "Adsorption of phosphorus molecules evaporated from an InP solid source on the Si(100) surface," *PHYSICAL REVIEW B*, vol. 87, APR 30 2013.

[115] O. Kubo, J.-T. Ryu, H. Tani, T. Harada, T. Kobayashi, M. Katayama, and K. Oura, "{STM} study of structural changes on Si(100)21-Sb surface induced by atomic hydrogen," *Applied Surface Science*, vol. 169170, no. 0, pp. 93 – 99, 2001.

[116] J. Wang, H. Mizuseki, Y. Kawazoe, T. Hashizume, M. Naitoh, D. Wang, and E. Wang, "Stability of Sb line structures on Si(001)," *PHYSICAL REVIEW B*, vol. 67, MAY 15 2003.

[117] S. R. Schofield, P. Studer, C. F. Hirjibehedin, N. J. Curson, G. Aeppli, and D. R. Bowler, "Quantum engineering at the silicon surface using dangling bonds," *NATURE COMMUNICATIONS*, vol. 4, APR 2013.

[118] S. Schofield. Private communication, 2013.

[119] E. Anderson, Z. Bai, C. Bischof, S. Blackford, J. Demmel, J. Dongarra, J. Du Croz, A. Greenbaum, S. Hammarling, A. McKenney, and D. Sorensen, *LAPACK Users' Guide*. Philadelphia, PA: Society for Industrial and Applied Mathematics, third ed., 1999.

[120] H. Koga and T. Ohno, "Misoriented Bi dimers blocking Ag nanowire growth along the Bi nanoline: a first-principles study," *JOURNAL OF PHYSICS-CONDENSED MATTER*, vol. 19, OCT 3 2007. International School and Workshop on Nanoscience and Nanotechnologh, Rome, ITALY, NOV 06-09, 2006.

[121] C. J. Pickard and R. J. Needs, "Ab initio random structure searching," *Journal of Physics: Condensed Matter*, vol. 23, no. 5, p. 053201, 2011.

[122] M. Hortamani, H. Wu, P. Kratzer, and M. Scheffler, "Epitaxy of Mn on Si(001): Adsorption, surface diffusion, and magnetic properties studied by density-functional theory," *Phys. Rev. B*, vol. 74, p. 205305, Nov 2006.